Molecular and functional characterization of the quality control Valosin-containing protein VCP/p97 and of its co-factors in *Leishmania*

Thèse

Bruno Guedes Alcoforado Aguiar

Doctorat en microbiologie-immunologie
Philosophiæ doctor (Ph. D.)

Québec, Canada

Résumé

Leishmania est un parasite protozoaire eucaryote unicellulaire qui infecte plus de 1.6 millions de personnes chaque année dans plus de 98 pays. Aucun vaccin humain est actuellement disponible et peu de traitements efficaces sont utillisés pour lutter contre le large spectre de pathologies causées par *Leishmania*. Récemment, l'étude du contrôle de la qualité des protéines chez *Leishmania infantum* a révélé que DDX3, une DEAD-box hélicase à ARN dotée de multiples fonctions dans le métabolisme de l'ARN et la signalisation cellulaire, joue un rôle central dans le contrôle de qualité des protéines dans la mitochondrie. Une étude plus approfondie de ce mécanisme a révélé des interactions potentielles de DDX3 avec des composantes clés de la réponse cellulaire au stress, en particulier avec une protéine de la famille des AAA + ATPases, VCP/p97/Cdc48. Comme VCP/p97/Cdc48 participe à de multiples étapes dans le contrôle de qualité des protéines en utilisant son hydrolyse de l'ATP pour séparer les protéines ubiquitinées de leurs partenaires et les acheminer au protéasome 26S pour dégradation, nous avons émis l'hypothèse que l'homologue très conservé chez *Leishmania, Li*VCP, pourrait agir de la même façon. Cette étude a permis la caractérisation fonctionnelle de l'homologue VCP chez *Leishmania,* son rôle dans la réponse du parasite au stress et sa survie dans les macrophages, ses interactions potentielles avec d'autres partenaires dont des cofacteurs clés, ainsi que la modélisation 3D des interactions *Li*VCP-cofacteurs. En utilisant des mutants génétiquement générés ayant moins de copies du gène *Li*VCP ou des mutants dominants négatifs avec une activité VCP altérée, nous avons démontré que *Li*VCP est un gène essentiel et que les mutants VCP sont incapables de survivre sous le shock de la chaleur et présentent un déficit de croissance très marqué chez les amastigotes. De plus, nous avons montré une forte accumulation de protéines polyubiquitinées et une sensibilité accrue au stress protéotoxique chez ces mutants, soutenant la fonction de chaperone sélective de l'ubiquitine de *Li*VCP. Grâce à des analyses *in silico* et à la «protéomique en réseau» en utilisant des études de co-immunoprécipitation et de spectrométrie de masse (LC-MS / MS), nous avons établi le premier réseau protéique de VCP chez les parasites protozoaires et déterminé que p47, FAF2, UFD1, PUB1 et l'hétérodimère NPL4-UFD1 étaient les principaux cofacteurs de *Li*VCP. Enfin, nos travaux nous ont permis de faire progresser nos connaissances générales sur la protéine essentielle VCP et le contrôle de la qualité des protéines chez *Leishmania* et d'indiquer quelques perspectives intéressantes pour approfondir notre compréhension sur ces mécanismes importants non seulement chez *Leishmania* mais aussi chez d'autres trypanosomatides.

Abstract

Leishmania is a unicellular eukaryotic protozoan parasite that infects over 1.6 million people each year in more than 98 countries. No human vaccine is currently available and few effective treatments are used to combat the broad spectrum of diseases caused by *Leishmania*. Recently, studies on Protein Quality Control in *Leishmania infantum* revealed that the multifunctional DEAD-box RNA helicase DDX3 involved among others in RNA metabolism and cell signaling plays a central role in mitochondrial protein quality control. Further studies revealed potential interactions of DDX3 with key components of the cellular stress response, particularly with the conserved AAA+ ATPase VCP/ p97/Cdc48. As VCP is associated with many ubiquitin-dependent cellular pathways that are central to protein quality control in other eukaryotic systems using its ATP hydrolysis to separate ubiquitinated proteins from their partners and bring them to the 26S proteasome for degradation, we hypothesized that the *Leishmania* highly conserved counterpart, *Li*VCP, might act in similar way. This study enabled the functional characterization of the *Leishmania* VCP homolog, its role in the parasite's response to stress and survival inside macrophages, its potential interactions with other partners including key VCP cofactors, and the homology 3D modeling of *Li*VCP-cofactor interactions. Using genetically engineered mutants with fewer copies of the *LiVCP* gene or dominant negative mutants with altered VCP activity, we demonstrated that *Li*VCP is an essential gene and that VCP mutants are unable to survive under heat stress and exhibit a very marked growth defect in amastigotes. In addition, we showed a high accumulation of polyubiquitinated proteins and increased susceptibility to proteotoxic stress in these mutants, supporting that *Li*VCP has an ubiquitin selective chaperone function. Using "network proteomics" analyses by co-immunoprecipitation and mass spectrometry (LC-MS/MS) studies, we established the first VCP protein network in protozoan parasites and determined p47, FAF2, UFD1, PUB1 and the NPL4-UFD1 heterodimer as the major cofactors of *Li*VCP. Overall, our work allowed us to advance general knowledge of the essential role of VCP in *Leishmania* protein quality control and to propose some interesting perspectives to deepen our understanding of these important pathways not only in *Leishmania* but also in other trypanosomatids.

Table des matières

Liste des figures

Liste des tableaux

Liste des abréviations, sigles, acronymes

AD	associated degradation
CL	cutaneous leishmaniasis
CMA	chaperone mediated autophagy
CP	core particle
DC	dendritic cells
Doa1	degradation of alpha 1
DR	Drug Resistance
DUB	deubiquitinating enzymes
E1	ubiquitin-activating enzyme
E2	ubiquitin-conjugating enzyme
E3	ubiquitin ligase
eIFs	eukaryotic translation initiation factors
ER	Endoplasmic Reticulum (ER)
ERAD	ER-associated protein degradation
FAF	Fas-associated factor
gRNA	guide RNA
HIV	human immuno-deficiency virus
HSP	heat shock protein
HYG	hygromycin B resistance gene
IFN-γ	interferon gamma
IL	interleukin
IMS	intermembrane space
IR	intergenic region
kDNA	kinetoplast DNA
KO	knockout
LAMB	liposomal amphotericin B
LPG	lipophosphoglycan
LZ	leishmanization
MA	meglumine antimoniate
MAD	Mitochondria-associated degradation
MF	Miltefosine
MIM	mitochondrial inner membrane
mRNP	messenger ribonucleoprotein
mt	mitochondrial
NE	neutrophil elastase
NEO	neomycin phosphotransferase gene
NET	neutrophil extracellular traps
NK	natural killer cells

NO	nitric oxide
OMM	outer mitochondrial membrane
ORF	open reading frame
PABP	poly(A)-binding protein
PCR	polymerase chain reaction
PERK	pancreatic endoplasmic reticulum eIF2 kinase
PFU	PLAA family ubiquitin binding
PFU	PLAA family ubiquitin binding domain
PKDL	post-kala-azar dermal leishmaniasis
PLAA	phospholipase A-2- activating protein
PM	paramomycin
PM	peritrophic matrix
PQC	protein quality control
PUB	PNGase/UBA or UBX containing proteins
PUL	PLAP, Ufd3p, and Lub1p
PUR	puromycin
PV	parasitophorous vacuole
ROS	reactive oxygen species
RP	regulatory particle
RQC	Ribosome-bound quality control
RT-PCR	polymerase chain reaction with reverse transcribed RNA
Sb5+	pentavalent antimonial
SGs	stress granules
SSG	sodium stibogluconate
TF	Treatment Failure
TNF	tumor necrosis factor
tRNA	transfer RNA
Ub	ubiquitin
UBA	ubiquitin-associated domain
UBX	ubiquitin regulatory X
UBXD	ubiquitin X domain
UBXL	UBX-like
UFD	ubiquitin fusion degradation
UIM	ubiquitin-interacting motif
UPR	Unfolded Protein Response
UPS	ubiquitin–proteasome system
VL	visceral leishmaniasis
WT	wild-type
ZEO	zeocin
αIR	intergenic region of α-tubulin

Remerciements

Here I express some of my gratitude to many people that in many ways were important to this pathway to this PhD degree.

From the beginning and on the top of my list, I sincerely and strongly thank Dr. Barbara Papadopoulou. Since the very first skype meeting until the very end of these 5 years, I received attention, kindness, guidance, and lot of trust from you. Barbara, thank you very much for making this life changing opportunity so worthy, valuable and such an enriching experience.

Je tiens à remercier spécialement Carole Dumas, pour toutes ces agréables journées de routine! Carole, ce laboratoire fonctionne grâce à toi! Merci beaucoup pour ta générosité, ta bienveillance et ton amitié.

My dear friend Prasad, thank you for every smile, the songs during culture experiments and the best scientific discussions.

I thank Ouafa and Hiva for all scientific help and initial guidance. You were essential to my training. I very much enjoyed working with you.

With all my love and with lots of *saudades*, I address this section to unique friends that shared part of them with me. Cultures, essences, gestures, discussions, incessant help and countless moments that I recall every single day. *Saudades* – this missing feeling mixed in the same second with enormous joy from the pleasant moments lived together. Merci beaucoup to Karima, Flora, Anais, Olus and Dafni.

À mes chers collègues de laboratoire, merci d'être de si bons modèles!! Clément pour sa gentillesse, Joan sa passion pour la Nature, Jessica son travail si dur, Malika sa sympathie, Rafik son charme, Marie-Claude sa joie; Felipe, Larissa and Christopher for being my best examples of happiness/life/research balance.

I deeply appreciated having spent such good times with Zeinab, Angana, Arijit and Mansi. Thank you for every moment shared. Camila, Marine, Dominique, Raquel, José, Ana Maria, Katherina, and MOU team whom I thank for the funny moments lived inside and outside the

lab. Martin et Céline qui je remercie pour leur professionnalisme associé à leur sympathie quotidienne.

Je remercie aussi Mme Véronique Mimeault du Centre d'aide aux étudiants de l'Université Laval pour son aide professionnelle lors des moments difficiles.

I would like to express my deepest gratitude to Raf, Larissa, Alex, Sean, and Gabriel whom I was very lucky to find. It was an enormous pleasure to live in a harmonious and genuine friendship.

My previous scientific background is due and dedicated to Dr. Carlos Costa and Dr. Paulo Sarmanho. The preceding training allowed me to fly higher.

To all my friends back in Brazil, thanks for your always precious support.

I thank also the Brazilian program Science without Borders from CAPES which provided my full PhD scholarship and made this dream possible.

To my family, I dedicate this accomplishment. If I could meet, enjoy and make true friends all around the world and achieve such difficult goals it's because I had a strong base of principles, hard work and love built everyday with good examples. Francisco Guedes, Edna G Aguiar, Beatriz and Samara, obrigado! A special thank you to Samara. Not only the master, but now the doctorate thesis is also dedicated to you. Another accomplishment made together! Thank you for being my support and with whom I feel comfortable and complete. Thank you for all your love and for accepting to make a cheerful life by my side.

To all those who contributed scientifically and socially to this journey, my sincere acknowledgment for making it a better one. Thank you!

Avant-propos

This doctorate thesis presents most of the studies done to unveil features of the cellular quality control in *Leishmania*, mainly involving the valosin-containing protein VCP. The work was done under the supervision of my thesis director, Prof. Barbara Papadopoulou and the constant technical help from Dr. Prasad Padmanabhan and Carole Dumas. In this thesis you will find i) a recent litterature review in the Introduction section organized into three sub-sections, ii) the main results of my research thesis in the form of three research papers (2 chapters and Appendix 1), iii) the discussion, conclusion and general perspectives of the project, and iv) a handful of appendices with valuble additional work related to VCP characterization and function carried out during this PhD period (Appendices 2-10).

The first sub-section of the Introduction (**1.1**) presents a brief review about *Leishmania* and its biological (life cycle of L*eishmania spp.*, the parasite response to stress) and clinical aspects (diagnosis, treatment, and vacccine development).

The second sub-section of the Introduction (**1.2**) presents a general overview of how different organisms, especially eukaryotes, respond to stress. This section covers the different aspects and specific pathways of protein quality control.

The third sub-section of the Introduction (**1.3**) introduces the importance of the major protein addressed in this thesis, the VCP protein. The section covers the generalities on VCP and its structure and how it performs its multiple cellular functions with the help of several protein partners (co-factors). This part resumes the importance of VCP to the cellular quality control in orther organisms and the therapeutical potential of this protein-target for several human diseases.

Chapter 1 presents our hypothesis and objectives. Both objectives were the exact subject of the two publications presented in chapters 2 and 3.

Chapter 2 presents the work published by Aguiar, B., Padmanabhan, P. K., Dumas, C., & Papadopoulou, B. entitled **"Valosin-containing protein VCP/p97 is essential for the intracellular development of *Leishmania* and its survival under heat stress".** The paper was published in *Cellular Microbiology*, Oct;20(10):e12867 in 2018. After interesting preliminary data on the cloning and characterization of other factors participating in the antioxidant response in *Leishmania*, some of which involve RNA-binding proteins, we

succefully indentified VCP as an essential protein related to the overall cellular protein quality control and to the intracellular development of *Leishmania*.

Chapter 3 presents the work on VCP cofactors and their characterization in *Leishmania* by Aguiar, B., Padmanabhan, P. K., Maaroufi, H., Dumas, C., & Papadopoulou, B. **'Molecular and functional characterization of the AAA+ ATPase Valosin-containing protein (VCP)/p97/Cdc48 interaction network in *Leishmania'*** that was submitted for publication to '*Scientific Reports*'.

Chapter 4 is composed by the overall thesis discussion, perspectives and general conclusions. The several perspectives presented emerge from different preliminary results from this thesis, incorporated as appendices.

Appendix 1 presents the preliminary work that allowed the identification and characterization of important interactions between a key RNA-binding protein, the DEAD box RNA helicase DDX3, involved in mitochondrial homeostasis and other components of the stress response, especially the AAA+ ubiquitin chaperone VCP/p97/Cdc48. The results of my contribution in this work are shown here and were included in the published paper in *Cell Death and Disease*: **Padmanabhan PK, Zghidi-Abouzid O, Samant M, Aguiar B, Dumas C, Estaquier J. and Papadopoulou B. (2016) DDX3 DEAD-box RNA helicase plays a central role in mitochondrial protein quality control in *Leishmania*. *Cell Death Dis.* Oct13;7(10):e2406.**

Appendix 2 presents the generation of *Li*Ufd1 knockout using CRISPR-Cas9. *Li*UFD1 is one of the main *Li*VCP co-factors, and our work shows that this gene is essential for *Leishmania* growth.

Appendix 3 shows the generation of knockouts using CRISPR-Cas9 for key VCP cofactors such as *Li*Faf, *Li*NPL4 and *Li*Pub1. Our data suggest that these genes are essential for *Leishmania* growth.

Appendix 4 introduces the putative link of *Li*VCP with the *Li*PLAA/Doa1/Lub1 protein whose homolog in yeast was shown to play a role in mitochondria associated degradation. Its putative role in mitochondria associated degradation is also highilighted in the general discussion section.

Appendix 5 shows the *Li*VCP localization in *Leishmania infantum* by different approaches using a HA-tagged VCP integrated into the VCP genomic locus or overexpressed as part of an episomal vector and or by fusing the VCP protein with GFP.

Appendix 6 presents immunofluorescence data supporting *Li*VCP co-localization with DHH1 (a stress granule associated protein) protein in *Leishmania infantum*.

Appendix 7 presents immunofluorescence data with PABP2, a stress granule associated protein, in *Leishmania infantum* and *Trypanosoma brucei*.

Appendix 8 presents immunofluorescence data supporting *Li*VCP partial co-localization with PABP2 protein in *Leishmania infantum.*

Appendix 9 shows data on the accumulation of mitochondrial ROS in mutant parasites with impaired VCP activity.

Appendix 10 presents preliminary data on the effect of drugs known to target VCP in other eukaryotes, such as DBeQ, NMS874 and ML240, on *Leishmania infantum* growth.

Introduction

1.1 General aspects of *Leishmania* biology and control

1.1.1 The order of Kinetoplastidae

Kinetoplastids are characterized by the presence of the Kinetoplast wich contains the structurally complex mitochondrial genome (1). Best know as kDNA it is shared by different unicellular eukaryotic organisms. Kinetoplastidae have adapted to survive as free-living marine non-parasitic organisms such as *Bodo saltans*, as well as parasites of diverse invertebrate, vertebrate, and plant species such as *Leptomonas* spp, *Trypanosoma* spp. and *Phytomonas* spp. (Figure 1). The kDNA is formed by minicircles and maxicircles. Maxicircles encode for mitochondrial genes such as cytochrome b, cytochrome oxidase subunits and NADH dehydrogenase subunits. kDNA minicircles encode for guide RNAs (gRNAs) that play a lead role in RNA editing. This process alters DNA-encoded sequences and can repair or generate different transcripts by nucleoside insertions and deletions (mostly an uracil) (2). This way to correct errors and modulate genetic sequences at the RNA level appears to have arisen in evolution several times in different organisms (3) as they are also organized differently (1). Recent evidences detail how gene gain and loss associated with evolutionary innovations in kDNA allowed free-living phagotrophs to become adapted to exploiting hostile host environments (1,4). Among those kinetoplastids adapted to stress environment and in contrast to the majority of trypanosomatids, members of the *Leishmania* genus are not monoxenous and can be transmitted to sandflies and to invade mammals (5).

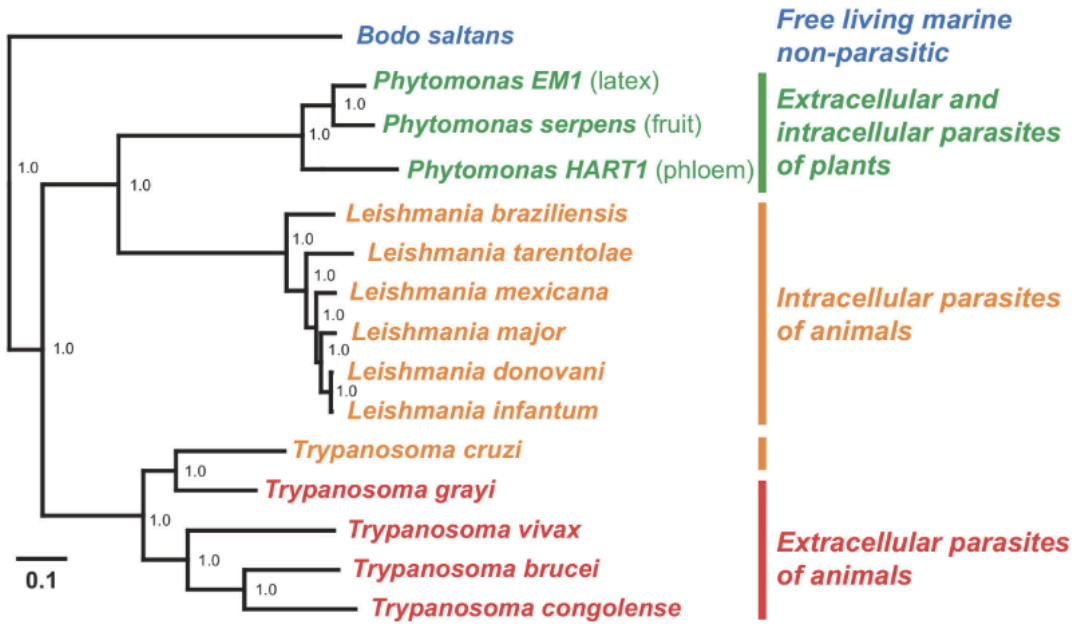

Figure 1 - Close trypanosomatid relatives.
From (6).

1.1.2 *Leishmania* and Leishmaniasis

Leishmania, one of the kDNA containing organisms, is a single celled eukaryotic protozoan parasite transmitted by a sandfly vector to humans, non-human primates (7), dogs (8), cats (9), silvatic mammals (10), marsupials (7), and much more. In humans, it causes a diverse group of diseases due to different *Leishmania* species that are classified into two major groups based on their clinical manifestations: visceral leishmaniasis (VL) and cutaneous leishmaniasis (CL) that includes the muco-cutaneous subgroup. All *Leishmania* species together have the potential to affect about 556 million people for VL and 399 million for CL in more than 98 countries (11). Every year, 0.2 to 0.4 million VL cases and 0.7 to 1.2 million CL cases, respectively, occur (12). Global burden and tools such as the Disability-adjusted life-years – DALYs – that represent the sum of the years lived with disability and years of life lost, have the potential to inform public health policy and priority-setting (13). Countries with the higher incidence for CL are within Africa and the Middle East (13) and another 13 contries is considered as high-burden for VL. Only Brazil has a high burden for both types of leishmaniasis (Figure 2) (11) and yet no efficacy control is in progress or under

development as public health policy to eradicate those preventable and debilitating diseases.

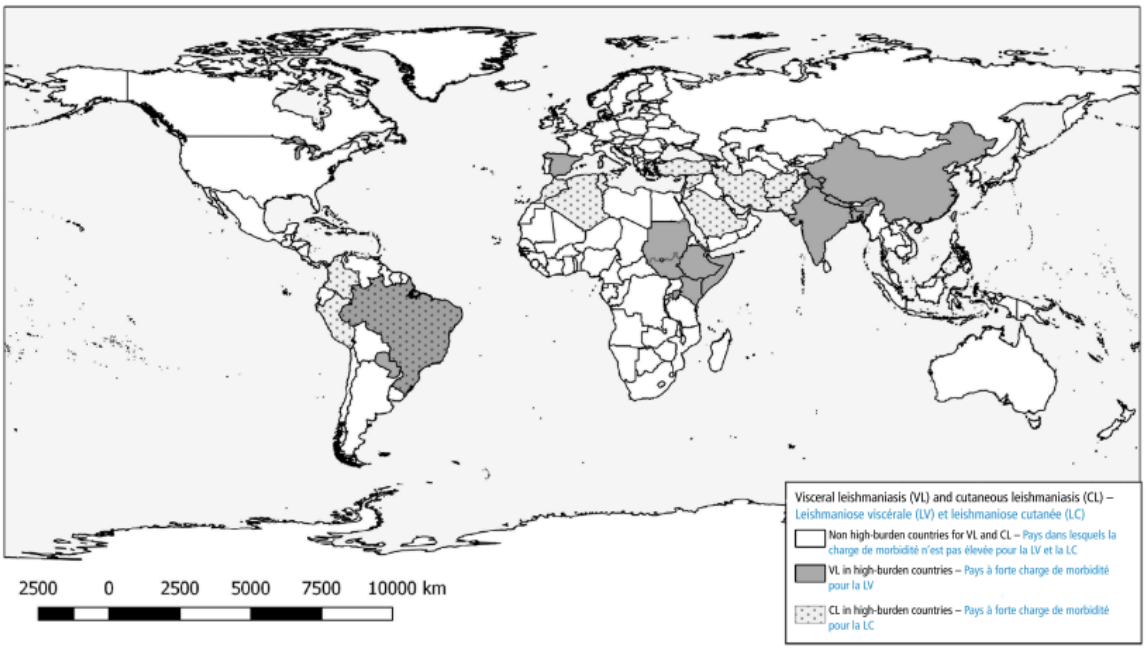

Figure 2 - Leishmaniasis in high-burden countries.
From (11).

Different *Leishmania* species can cause asypmtomatic infection (14) as well as mild and severe clinical manifestations. The outcome is determined depending on the species, vector biology, and host factors (15). VL is the most severe form of leishmaniasis and is lethal, if left untreated. It is characterized by persistent fever and splenomegaly. Moreover, VL patients can present weight loss, anemia, hepatomegaly and, as laboratorial findings, pancytopenia and hypergammaglobulinaemia (16). CL, otherwise, is a self-healing disease in most cases that is characterized by skin lesions with different patterns (dry lesions to wet or ulcerating sores) depending on the species, location of bite and host immunicity (17). In some cases, CL can evolve to oronasal mucocutaneous leishmaniasis and diffuse and recidivan forms of cutaneous leishmaniasis. Immunosupression is a major risk factor for the development of CL variants (17). Another clinical feature of leishamiasis is the post-kala-azar dermal leishmaniasis (PKDL). PKDL occurs after an episode of treated VL in which parasites can persist in the skin and reemerge, in an immunodeficient episode and more frequently in immunocompromised patients, in a form of erythematous maculopapular rash around the body. HIV-patients are among those immunocompromised individuals. In fact,

Leishmania might accelerate HIV progression wich renders the co-infection by these two pathogens a major public health problem (18).

1.1.3 Diagnosis

Historically, the diagnosis of leishmaniasis is based extrinsically on clinical signs combined with geographic localization and epidemiological data. Unfortunantely, clinical pathology of the disease is complicated. CL lesions vary in number, size, clinical appearance (dry or wet lesion) duration of spontaneous cure and have similar characteristics with bacterial tropical ulcers, Hansen's disease, and others (19). On its turn, many symptoms of VL are also indicative for several other diseases (also present in endemic areas) such as chonic myeloid leukemia and liver cirrhosis (19,20). Furthermore, some species can cause different clinical outcomes and can be associated with different treatment regimens (see treatment section). Moreover, two or more *Leishmania* species can be present in half of endemic countries (Figure 3) and distinguishing them is important not only for molecular epidemiology purposes but also for medical purposes.

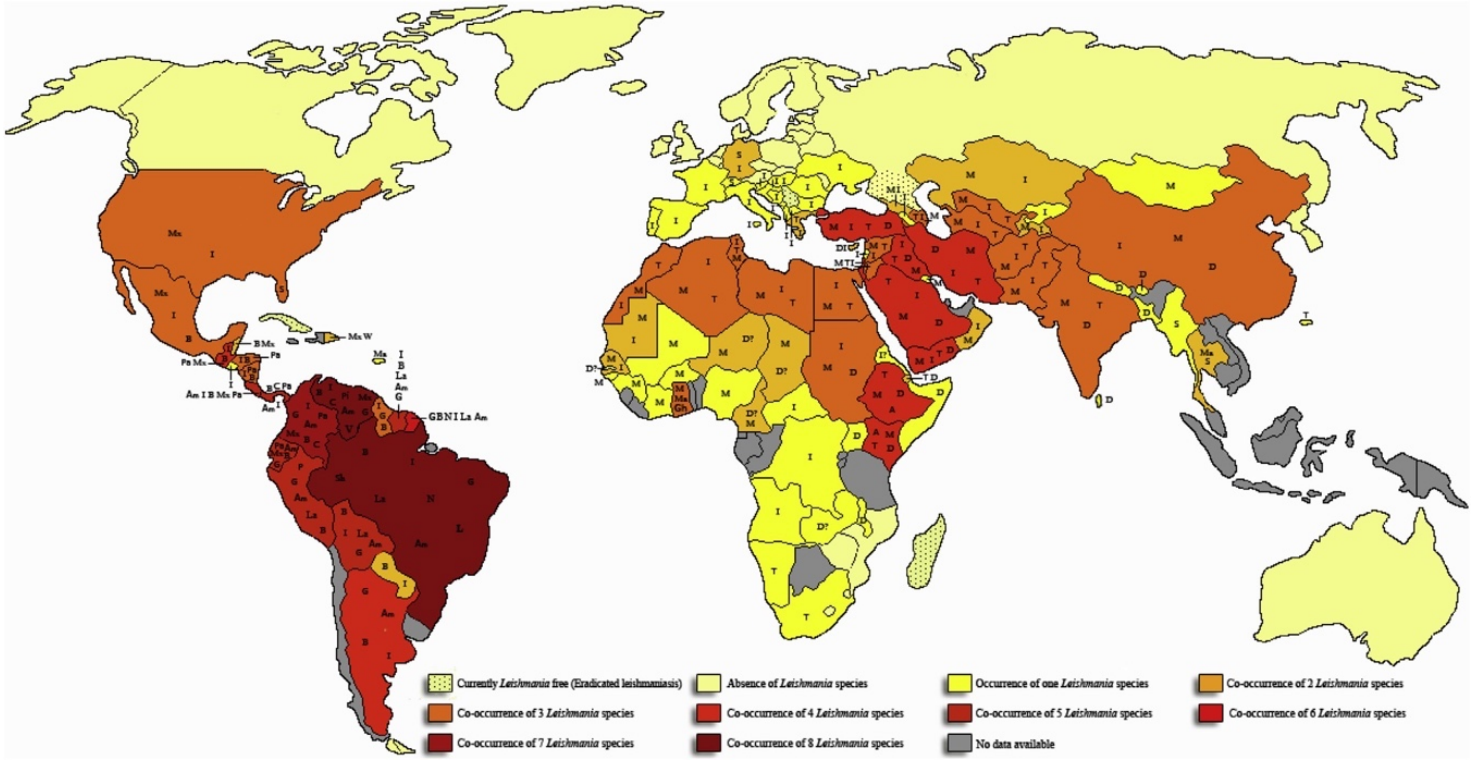

Figure 3 - Global distribution of 21 *Leishmania* species pathogenic for humans.

A: *L. aethiopica;* Am: *L. amazonensis*; B: *L. braziliensis*; C: *L. colombiensis*; D: *L. donovani*; G: *L. guyanensis*; Gh: *'Ghana strain'*; I: *L. infantum*; La: *L. lainsoni*; L: *L. lindenbergi*; M: *L. major*; Ma: *L. martiniquensis*; Mx: *L. mexicana*; N: *L. naiffi*; Pa: *L. panamensis*; P: *L. peruviana*; S: *L. 'siamensis'*; Sh: *L. shawi*; T: *L. tropica*; V: *L. venezuelensis* and W: *L. waltoni*. From (19).

Leishmania can be detected in infections by microscopic examination of lesion biopsy smears for CL and aspirates of the spleen, bone marrow and lymph nodes for VL, which are then examined under the microscope following Giemsa-staining. This useful, rapid and cheap diagnostic approach is invasive, can be painful and does not allow discrimination between *Leishmania* species. Microscopic examination can be followed by parasite culturing *in vitro*, which can prolongate diagnosis for 7, 14, 21 days or more. Other methods with higher sensitivity and specificity are the conventional PCR and real time quantitative PCR (qPCR). In addition to diagnosis, in which kDNA target is more recommended (21), qPCR can be applied for monitoring disease progression (22), defining parasite virulence or drug resistance markers (23) and species discrimination (24). A handful of other methods are described and can be useful for detection, species identification and discrimination, parasite load quantification and molecular typing (Figure 4).

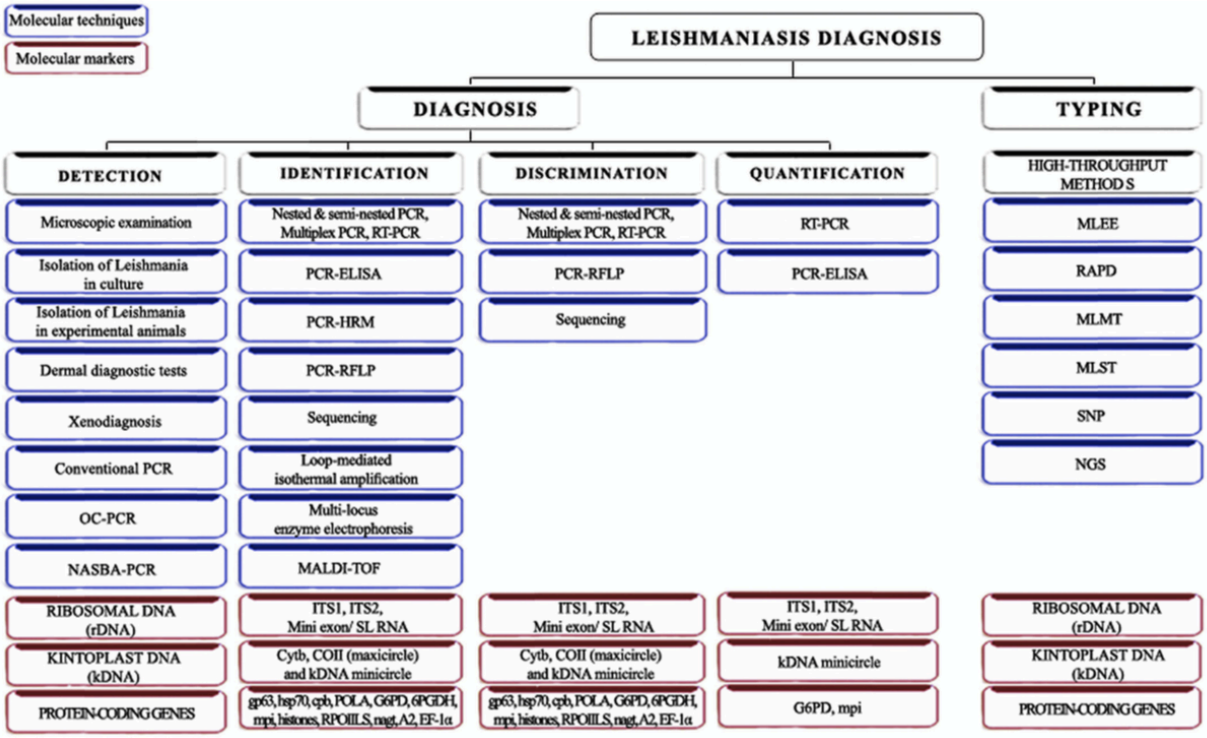

Figure 4 - Molecular markers and tools proposed for the diagnosis of leishmaniasis. (19)

1.1.4 Treatment of Leishmaniasis

The treatment of leishmaniais is still challenging and limitating. The current therapeutic approaches are effective only against specific *Leishmania* strains and some medications or dosage regimens have insufficient evidence to support their recommendation (25). Furthermore, special groups such as children under 3 years old and immunocompromised patients need different therapeutic regimens. Still, drug resistant parasites contribute to treatment failure (26).

The treatment for visceral leishmaniasis (VL) caused by *Leishmania infantum* is based on pentavalent antimonials, amphotericin B deoxycholate or liposomal amphotericin B (LAMB) (Table 1) (25). For VL patients infected with *Leishmania donovani*, in some parts of East Africa a combination of pentavalent antimonials and paramomycin is used and in the India subcontinent a combination of LAMB/Miltefosine (MF), LAMB/paramomycin(PM) or MF/PM can be used (Table 1). The difference of regimens and the doses as well as the combination of drugs is also a response to Treatment Failure (TF) and Drug Resistance (DR) (26). For cutaneous leishmaniasis, the treatment can include the use of pentamidine, LAMP, PM, MF in combination or not with local thermotherapy or cryotherapy, and the systemic use of azoles such as fluconazole, ketoconazole or allopurinol – each of them with different level of evidence (Table 2).

Table 1 - Recommended treatments for visceral leishmaniasis

		LAMB	Pentavalent antimonials	Amphotericin B deoxycholate	Combination treatment
Leishmania infantum	All regions	10 mg/kg per daily dose by infusion given over 2 days, up to a total dose of 20 mg/kg	20 mg Sb5+* per kg per day intramuscularly or intravenously for 28 days	0·75–1·0 mg/kg per day by infusion, daily or on alternate days for 20–30 doses, for a total dose of 2–3 g	--
		3–5 mg/kg per daily dose by infusion given over 3–6 days, up to a total dose of 18–21 mg/kg	--	--	--
Leishmania donovani	East Africa	3–5 mg/kg per daily dose by infusion given over 6–10 days up to a total dose of 30 mg/kg.	20 mg Sb5+* per kg per day intramuscularly or intravenously for 30 days	--	Pentavalent antimonials (20 mg Sb5+* per kg per day of intramuscularly [preferably]) or intravenously plus PM (15 mg [11 mg base] per kg bodyweight per day intramuscularly) for 17 days
	Indian subcontinent	10 mg/kg as a single dose, or 3–5 mg/kg per daily dose up to a total dose of 15 mg/kg over 3–5 days	--	0·75–1 mg/kg per day by infusion, daily or on alternate days for 15–20 doses	LAMB (5 mg/kg single dose) plus MF (daily for 7 days, as per below) 9
		--	--	--	LAMB (5 mg/kg single dose) plus PM (daily for 10 days, as per above)
		--	--	--	MF (as per below) plus PM (as per above), both daily for 10 days,

Sb5+=pentavalent antimonial. PM=paromomycin. SSG=sodium stibogluconate. LAMB=liposomal amphotericin B. MF=miltefosine. NA=not available. *Sb5+ can be either sodium stibogluconate (SSG) or meglumine antimoniate (MA); the respective doses are equivalent. Adapted from (17).

Table 2 - Selected treatment regimens for cutaneous and mucocutaneous leishmaniasis

		Combination treatment				
		Local treatment regimens		Systemic treatment regimens		
Old World	*Leishmania major*	15% paromomycin plus 12% methylbenzethonium ointment for 20 days; the evidence for this regimen is graded A	Intralesional antimonials plus cryotherapy, both every 3–7 days for up to 5 sessions; the evidence for this regimen is graded A	Oral fluconazole 200 mg for 6 weeks; the evidence for this regimen is graded A	Pentavalent antimonials 20 mg/kg per day for 10–20 days; the evidence for this regimen is graded D	Pentavalent antimonials 20 mg/kg per day plus pentoxifylline, 400 mg three times daily for 1–20 days; the evidence for this regimen is graded A
	Leishmania tropica and *Leishmania infantum*	Thermotherapy, 1–2 sessions with localised heat (50°C for 30 s); the evidence for this regimen is graded A	Pentavalent antimonials 20 mg/kg per day for 10–20 days; the evidence for this regimen is graded D	Pentavalent antimonials 20 mg/kg per day for 15 days plus oral allopurinol 20 mg/kg for 30 days to treat recidivans caused by L tropica; the evidence for this regimen is graded C	--	--
New World	*Leishmania mexicana*	15% paromomycin plus 12% methylbenzethonium ointment for 20 days; the evidence for this regimen is graded B	--	Ketaconazole 600 mg once daily for 28 days (adult); the evidence for this regimen is graded B	Oral miltefosine 2·5 mg/day for 28 days; the evidence for this regimen is graded B	--
	Leishmania braziliensis	Thermotherapy, 1–2 sessions with localised heat (50°C for 30 s); the evidence for this regimen is graded A	--	Pentavalent antimonials 20 mg/kg per day for 10–20 days; the evidence for this regimen is graded C	Liposomal amphotericin B 2–3 mg/kg per day up to 20–40 mg/kg total dose; the evidence for this regimen is graded C	--
	Leishmania panamensis and *Leishmania guyanensis*	Intralesional antimonials 1–5 mL per session every 3–7 days for up to 5 sessions; the evidence for this regimen is graded B	--	Pentamidine isethionate intramuscularly on alternate days for three doses; the evidence for this regimen is graded C	Pentavalent antimonials 20 mg/kg per day for 10–20 days; the evidence for this regimen is graded C	Oral miltefosine 2·5 mg/day for 28 days; the evidence for this regimen is graded B
	Mucocutaneous leishmaniasis	--	--	Pentamidine isethionate intramuscularly on alternate days for three doses; the evidence for this regimen is graded C	Pentavalent antimonials 20 mg/kg per day plus pentoxyfylline, 400 mg three times daily for 1–20 days; the evidence for this regimen is graded A	Liposomal amphotericin B 2–3 mg/kg per day up to 40–60 mg/kg total dose; the evidence for this regimen is graded C

WHO evidence grading system: evidence obtained from at least one properly designed randomised controlled trial was graded A; evidence obtained from well designed trials without randomisation was graded B; opinions of respected authorities based on clinical experience, descriptive studies, or reports of expert committees were graded C; and expert opinion without consistent or conclusive studies was graded D. Adapted from (17).

1.1.5 Vacccine development

As part of the control of leishmaniasis, the developing of a safe, effective, and affordable vaccine for their prevention remains an urgent need and a possible milestone. Primary infection, if cured, usually leads to protection against further infection (27). Hence, the practice of injecting live virulent parasites in healthy individuals called leishmanization (LZ) is so far the only effective way of inducing immunity against leishmaniasis in humans (28, 29). For safety reasons and difficulty of standardization of injecting parasites, it is no longer widely used (28–30). Nevertherless, those experiements show that generating a vaccine against *Leishmania* is a possible achievement.

The first-generation leishmaniasis vaccines were based on killed whole-parasites. Many strategies with autoclaved lysates producing different levels of protection were tried (28–30). A meta-analysis review shows however their inability to protect vaccinated individuals against infection by the *Leishmania* parasites (30,31). In fact, autoclaving does not mimic natural infection and can lower the immunogenicity of the parasite by destroying most of its proteins (32).

Another strategy of vacctination is the use of attenuated parasites. Several attempts tried to generate parasites lacking key factors for pathogenesis by repeated in vitro culturing or by gene knockouts (32–34). Although there is no licensed vaccine against human leishmaniasis, some human vaccine candidates have reached phase I and II clinical trials (35,36). Indeed, despite solid efficacy results and impact on parasite transmission, two canine vaccines are already in the market and post-marketing data would therefore be helpful to the progress towards effective and universal vaccines (37).

A third generation of vaccines is based on the use of DNA (38). It can combine a few different genes in a DNA plasmid to be translated inside the human body. Vaccination with plasmid DNA encoding protective *Leishmania* antigens gives a promising approach to vaccination against leishmaniasis. However, none of DNA vaccines for human trial has shown promising effects in accordance with the clinical trials (32).

1.1.6 Biology and life cycle of *Leishmania spp.*

During a blood feeding, an infected phlebotominae sand fly releases *Leishmania* infective metacyclic promastigotes to the mammalian host. The parasites invade macrophages and

other cells, undergo differentiation into amastigote forms inside the phagolysosome where they replicate. Amastigote-containing macrophages are ingested by sand flies during another blood meal and restart the cycle (Figure 5).

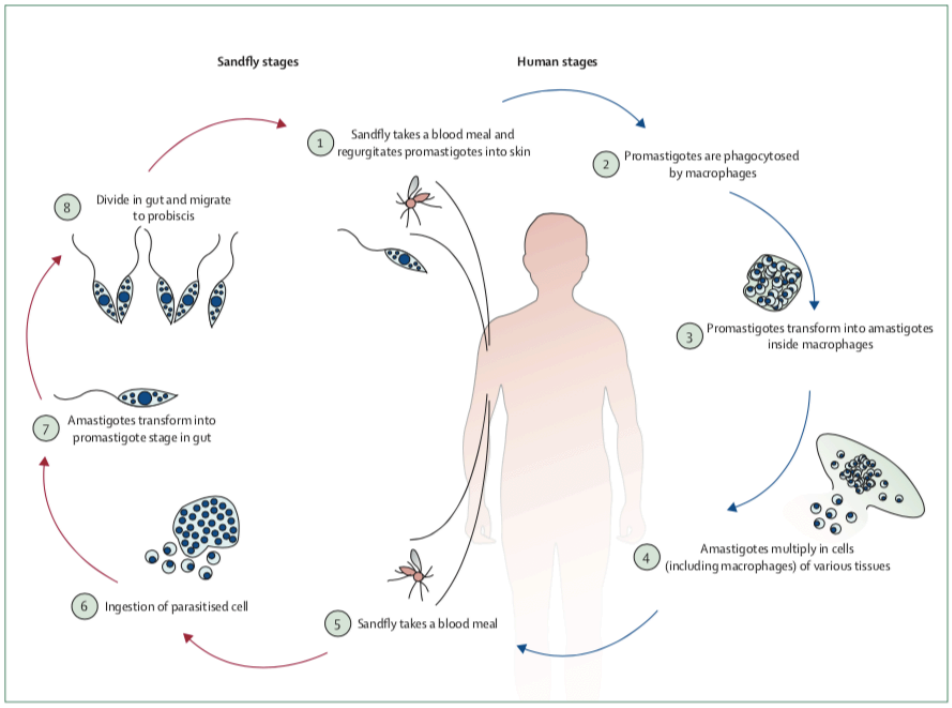

Figure 5 - Life cycle of Leishmania spp.

From (39)

1.1.7 Inside the vector

The majority of trypanosomatids are mostly commensals and parasites of insects (5). From the mammal host, *Leishmania* amastigote parasites can be ingurgitated during a sandfly blood meal. Inside the midgut of the vector, *Leishmania* will suffer the action of proteolytic enzymes and the peritrophic matrix (PM) of the insect which protect it against mechanical and chemical damage from blood meal and invaders (40). *Leishmania* developed resistance mechanisms such as the overexpression of proteophosphoglycan (PPG) on its surface that confers protection from midgut digestive enzymes (41). Furthermore, PPGs and the Promastigote Secretory Gel (PSG), a PPG-rich gel which accumulates in sand fly gut and mouthparts are important for *Leishmania* transmission and infection as they facilitate regurgitation by blocking the lumen of the insect's anterior midgut and stomodeal valve (42). Although lots of parasites are killed during the insect life cycle, the remaining ones will

undergo structural changes into different promastigote subtypes that ultimately form metacyclic promastigotes.

Exosomes are another feature of *Leishmania* associated with vector-transmitted infections. *Leishmania* exosomes are secreted within the sand fly midgut and co-egested during the insect's blood meal. They have been shown to enhance the disease pathology via overproduction of inflammatory cytokines (43) and are proposed to be an integral part of the parasite's infectious life cycle (44). As exosomes contain specific lipids, proteins and nuclear materials, all together, these parasite-derived vesicles are a very interesting natural cocktail for vaccination purposes (45).

Once the parasites undergo transformation to metacyclic promastigotes and are present in the proboscis of an infected female sandfly, the vector can release the infective *Leishmania* to the mammalian host during a blood meal. The presence of 1-2 parasites is sufficient to infect the human host (46).

1.1.8 The host immune system

Once metacyclic promastigote parasites leave the sand fly environment towards the vertebrate host, multiple parallel events occur to defeat the microbial invader.

The neutrophils, Dendritic cells (DCs) and Macrophages are the main cells that are infected by *Leishmania*. Although neutrophils are the first ones to encounter and phagocyte *Leishmania*, the macrophages are their main host for their invasion and replication. Neutrophils are the first line of defense to generate an inflammatory response. To restrain the invading pathogens, they produce extracellular traps (NETs), an extracellular fiber network of granule proteins, as they generate a potent oxidative burst and secrete granule-derived toxic compounds in the surrounding environment.

Alongside, *Leishmania* are phagocyted by immature dentritic cells and also DCs that migrate to lymphoid tissues to develop adaptive immunity. Infected DCs produce cytokine IL-12 resulting in the polarization of T cells toward Th1 subset and subsequent IFN-γ production to control the infection. IFN-γ signaling leads to activation and chemoattraction of macrophages to the site of infection and promote, on infected macrophages, expression of inducible nitric oxide (NO) synthase (iNOS, NOS2) and NO production that, together with reactive oxygen species (ROS), are essential to kill intracellular *Leishmania*. The consequent antigen-presenting process will activate a CD4+Th1 mediated immune

response to allow the total clearance of the parasites. A similar immunological response is desired in a future leishmanial vaccine and leshmanization was the only approach so far capable of inducing immunity in human subjects (28,29). Though, vaccine studies suggest that a balance between Th1 and Th2 response should be the goal to achieve (36), as antigens stimulating a Th1 response during the disease or after cure have shown no protective effect as vaccine (47, 48).

1.1.9 Silent entry of *Leishmania*

After phagocytosis by neutrophils, macrophages, and dendritic cells, *Leishmania* attempts to suppress their immune response. Neutrophils for instance, instead of generating an inflammatory response, may act as carriers that facilitate silent infection of macrophages – the so-called Trojan Horse theory (49,50). Similarly, some infected neutrophils can have their lifespan extended to be then silently phagocytized by DCs and macrophages. This may inhibit DC activation, motility and migration, delaying the development of adaptive immunity. The uptake of infected neutrophils by DCs also leads to the inhibition of $CD8^+$ T cells priming (51).

To escape from NET-mediated killing, *Leishmania* can secrete nucleases and take advantage of endonuclease (Lundep) from the vector's saliva (52). The expression of LPG on promastigotes might also be associated with *Leishmania* survival to NETs (53).

Promastigotes survive in neutrophils, but they do not differentiate into amastigotes. The inhibition of neutrophil-mediated oxidative burst as well the outcome and success of the "silent phase" of the neutrophils and DCs interaction with the parasite depends on the *Leishmania* species and the developmental stage.

Moreover, parasites modulate the pattern of cytokine secretion and inhibit the generation of NO and ROS, while extending the survival of the infected macrophages. Coupled with an anti-inflammatory response associated with TGF-β and IL-10 secretion, *Leishmania* regulates a favorable environment for its survival and division while avoiding a proper generation of the adaptive immune response. This immune response towards CD4+ T helper 2 (Th2) contributes to the development of a non-healing phenotype and grants the success of the parasite (54, 55).

1.1.10 Inside Macrophages

After silently entering the host cells, *Leishmania* take advantage of nearby neutrophil and other cells until they encounter their definitive host cell– macrophages. Once within macrophages, some *Leishmania* species may delay phagosome formation and maturation, preventing phagosome acidification and action of proteases, while securing the nutrients needed for their survival. The expression of some virulence factors, such as the glycolipid LPG, selectively modify the recruitment of phagosome maturation factors and the fusion with lysosomes (56). Inside of the so-called parasitophorous vacuole (PV), instead of being affected by NADPH oxidase, V-ATPase complexes and other anti-microbial responses, *Leishmania* is protected from oxidative damage and immune recognition (56). From this safe environment, *Leishmania* i) suppress inflammation by upregulating host PPAγ and protein tyrosine phosphatases, ii) prevents macrophage activation by interfering with the JAK/STAT pathway, iii) inhibits ROS generation by preventing NADPH oxidase assembly, iv) suppress efficient antigen presentation by MHC class II inhibition, and v) induce autophagy in macrophages. Then, inside this acidic, high-temperature, hydrolase- and ferrous-rich environment, promastigotes transform into nonmotile amastigotes.

1.1.11 PERK and Phosphorylation of the translation initiation factor eIF2α

One of the key events to preserve homeostasis inside a stressful environment is the phosphorylation of eukaryotic translation initiation factor 2 alpha (eIF2α) (57). Protein kinase R (PKR)-like endoplasmic reticulum kinase (PERK) is a protein synthesis regulator essential for the unfolded protein response (UPR) which makes it an attractive therapeutic target for the treatment of many diseases associated with ER stress and defects in proteostasis (58). The PERK-dependent phosphorylation of the alpha subunit of eukaryotic translation-initiation factor 2 (eIF2-α) leads to its inactivation and consequently to a decrease in translation initiation and a repression of global protein synthesis (59). For similar reasons, in *Leishmania*, this transmembrane protein kinase was demonstrated to be required for efficient promastigote to amastigote differentiation (60). Amastigotes have to enter in a slow growth state to adapt to the stressful conditions encountered inside macrophages (61).

Several other mechanisms and pathways must be present in *Leishmania* for helping the parasite to adapt to the rush environment and survive inside the vector and, as an amastigote form, inside the mammalian host. Several of these pathways, including those

involved in protein quality control, are well conserved in other eukaryotes and are considered in the next sections.

1.2 Stress response and quality control mechanisms

1.2.1 Protein Quality control (PQC)

Many organisms have evolved to maintain conserved the network of factors that are responsible for protein quality control (PQC) (62). To maintain protein homeostasis (proteostasis) the PQC has to continuously ensure the good conformational folding of nascent polypeptides as well as surveillance, prevention, and rescue of protein defects (63). Naturally, proteins are not always properly folded and they might need the cellular system to unfold or to degrade the misfolded and the normal proteins that needed to be recycled (64). To adapt to different unexpected challenging or stressfull situations, cells rely on chaperones, the ubiquitin-proteasome system (UPS) and autophagy (63). The immediate response to protein misfolding consists of decreasing global protein synthesis while increasing expression of chaperone-encoding genes and their availability (Figure 6). The missfolding signals also increase ubiquitination, thus proteasome degradation and the continuous stress signals can end up to an autophagy process to degrade large-molecular complexes and entire organelles (Figure 6) (63).

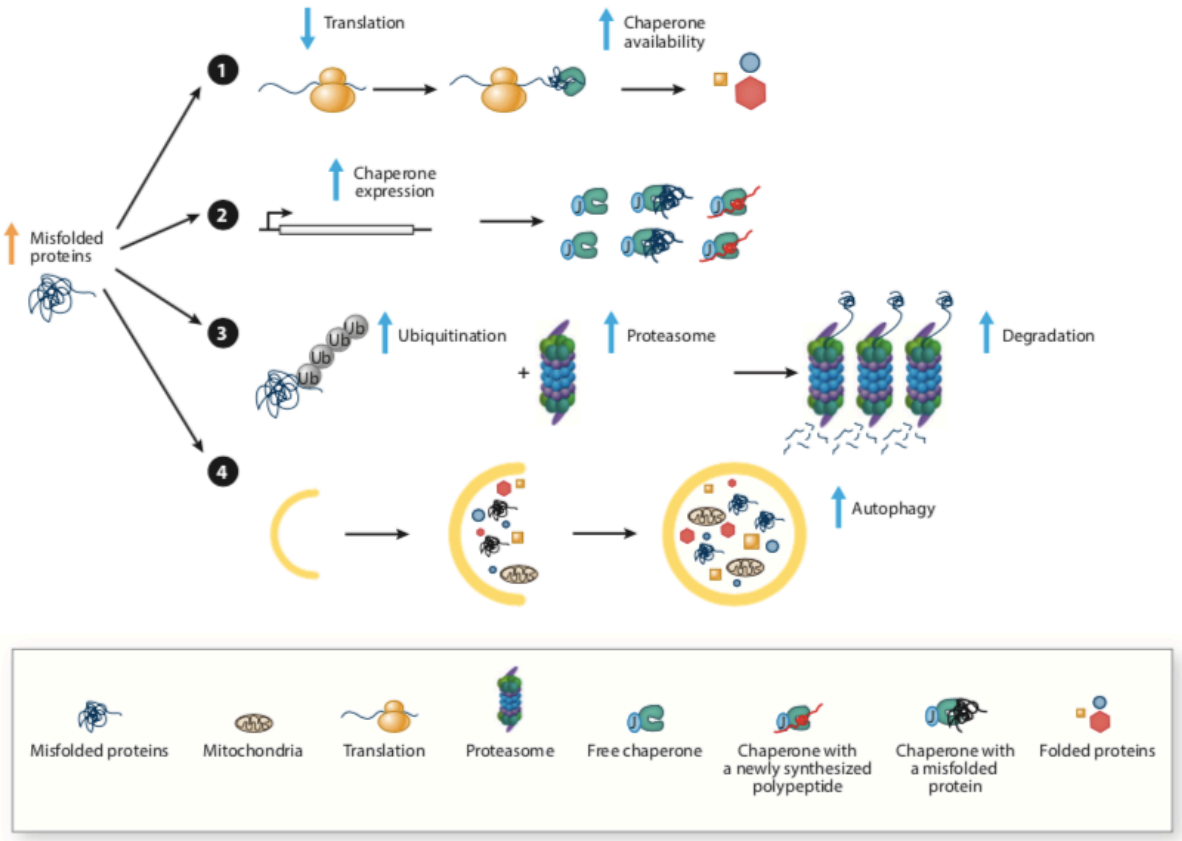

Figure 6 - Cellular responses to protein misfolding.
From (63).

1.2.2 Chaperones and chaperonins

Chaperones recognize unfolded proteins by the presence of hydrophobic surface, as that portion is generally covered in a properly folded protein (62). The majority of chaperones are induced during stress and are identified as Heat Shock Proteins (HSP) with different molecular weights. Chaperones can hold the substrate until spontaneous folding occurs, can use ATP to unfold stable misfolded proteins and can work as disaggregases using ATP hydrolysis, always with the goal of properly refolding proteins (62). This protein folding action can facilitate protein import in different subcellular compartments and can receive help from chaperonins. These cylindrical-shaped multisubunit complexes form a cavity where the folding process takes place in a protected environment (63). Specific roles of important chaperones such as ER BiP protein and mitochondrial HSP70 are covered in the following

ERAD and MAD sections. If such efforts fail, cells can rely on the ubiquitin (Ub)-proteasome system (UPS) or the autophagy-lysosome system.

1.2.3 UPS

The ubiquitin–proteasome system (UPS) is the major selective protein degradation pathway in eukaryotic cells. Proteins destined for degradation are tagged on lysine residues with the small protein ubiquitin (Ub, 8.5-kDa peptide, 76 amino acids) and subsequently degraded by the proteasome (65). The ubiquitylation of proteins is mediated by the sequential activities of the ubiquitin-activating enzymes (E1), the ubiquitin-conjugating enzymes (E2), and the ubiquitin ligases (E3), which determine substrate specificities (66). The ubiquitylation process starts with Ub activation by E1 in the presence of ATP. The ubiquitin is then transferred from E1 to E2. The E3 ligase recruits substrate and the ub-bound E2 to transfer the ubiquitin from E2 to the substrate. The successive cycles of ubiquitin conjugation form polyubiquitin chains that are the main signal for proteasomal degradation. Once in proteasome, substrates are degraded into short peptides and then by the action of aminopeptidases (APPs) are further broken down into amino acids (Figure 7) (67).

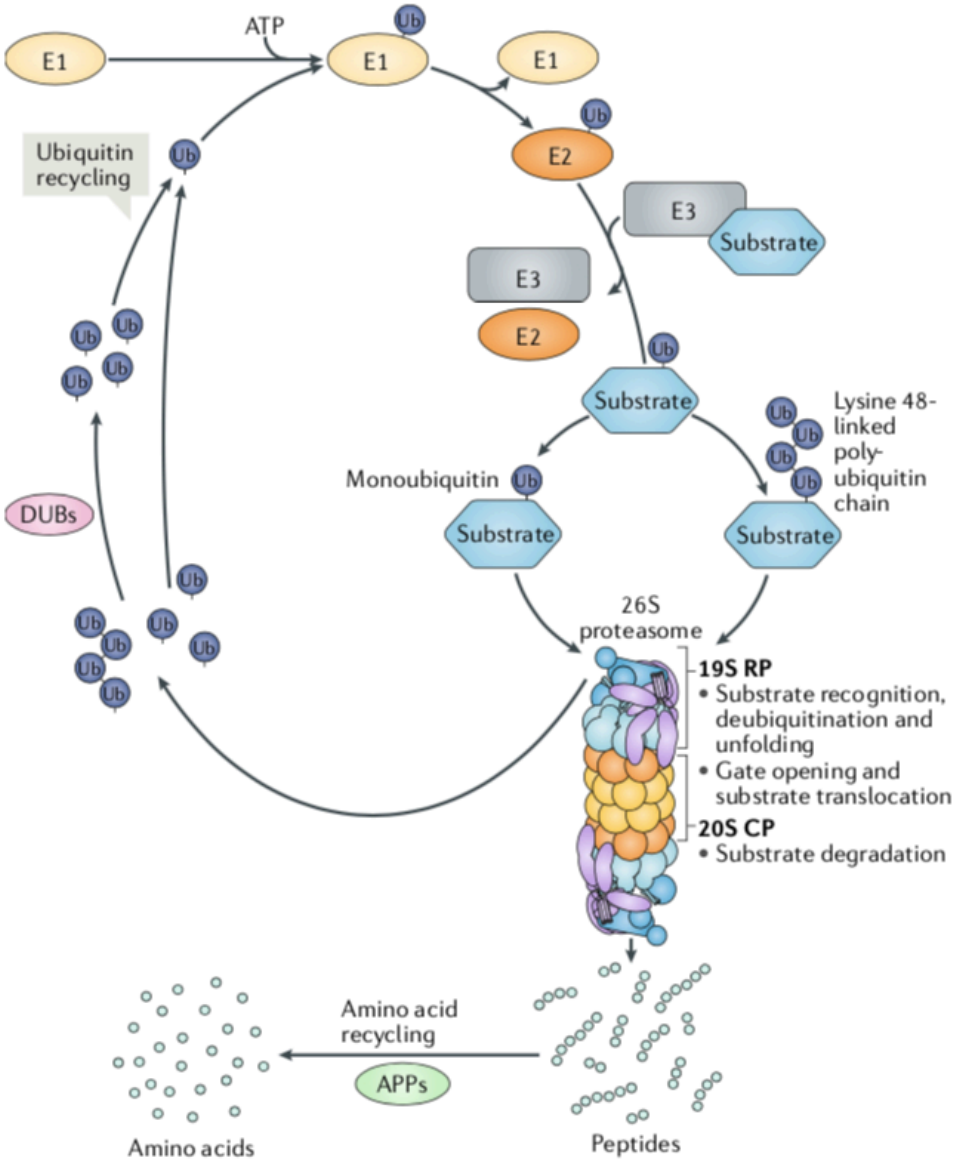

Figure 7 - The ubiquitin–proteasome system.
From (67).

The accumulation of misfolded proteins due to translation errors, misfolding, or age-induced or chemical damage can be toxic and thus the UPS has to take care of that wherever unwanted proteins are. Because of this, more specific associated degradation (AD) processes take place to control the quality of proteins before and during synthesis at the ribosome (RQC section), in the Endoplasmic Reticulum (ERAD section), mitochondria (MAD section) and other locations such as cytoplasmic stress granules to limit their cellular accumulation.

1.2.4 RQC

Protein translation with a magnitude of around 3 million ribosomes working to translate codons at a rate of close to six amino acids per second is a remarkably efficient but an expensive process that consumes up to 75% of the cell's total energy (68). To initiate translation on a given mRNA, the cap-binding factor eIF4E, the scaffold protein eIF4G and the poly(A) binding protein are first bound to the mRNA and facilitate the recruitment of the 40S ribosome subunit and the initiator methionine tRNA to form the initiation complex which will subsequently recruit the 60S subunit allowing the full assembly of translating ribosomes. As the elongation complex advances, tRNAs are charged with the correct amino acid and the translation proceeds. Then, several HSPs with the help of chaperonins assist the nascent peptide chains to fold and to form in their native protein state (68). Though, the folding and maintenance of proteins in their functional, native, 3D conformations frequently fail. A defect on mRNAs (aberrant or truncated or highly structured mRNAs) or an insufficient amino acid or tRNA numbers, or an unproper folding of nascent peptides can cause ribosome stalling and delay or stop the elongation process (Figure 8).

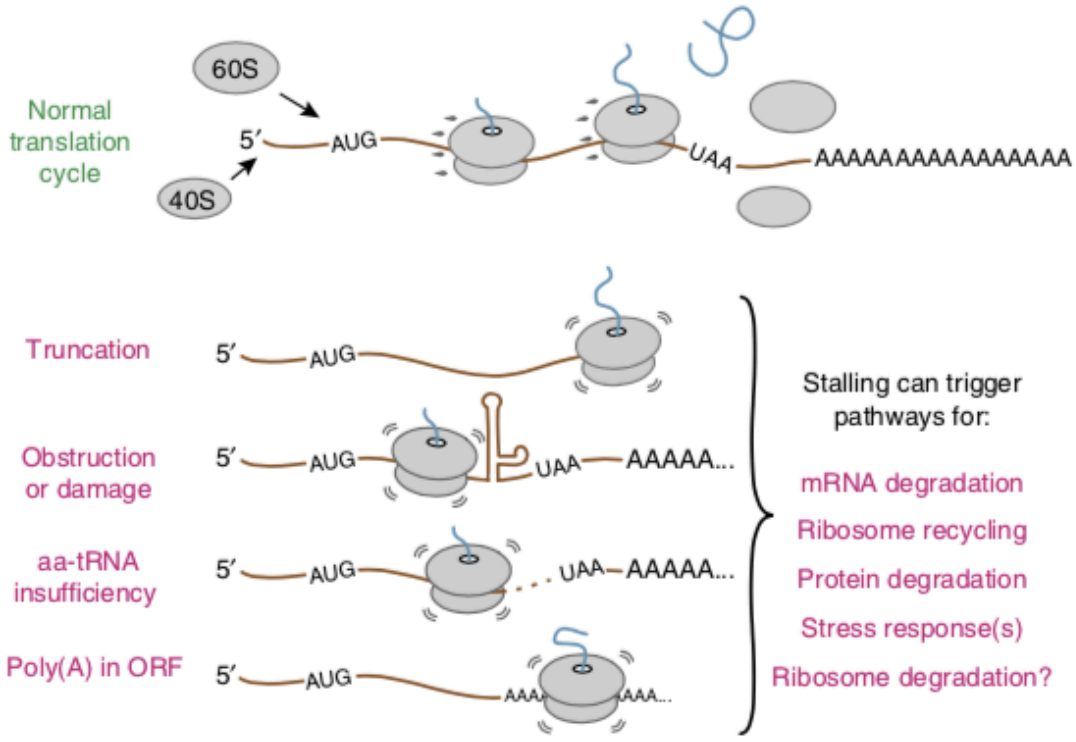

Figure 8 - Causes of aberrant translation elongation.

From (69).

In cases of ribosome stalling, the accumulation of protein aggregates can become toxic for the cell. The stalled 60S subunits of ribosomes with peptides and tRNA stops translation and can lead to protein aggregation. The Ribosome quality control (RQC) complex recognizes those aberrant peptides, extracts them from the stalled 60S subunit and delivers them to the proteasome (70). The RQC complex contains an E3 ligase (Ltn1/Listerin) and Rqc2/NEMF protein that cooperates with the ATPase Cdc48/p97 through the heterodimer formed by its co-factors Ufd1/UFD1L and Npl4/NPLOC4 (Figure 9) (70). Briefly, the first step of RQC involves subunits separation of the stalled ribosome. Then, the released 60S subunit exposes the peptidyl-tRNA that is recognized by RQC components. The NEMF protein binds to the exposed interface and prevents reassociation of the ribosome subunits. Listerin E3 ligase, through the binding of its RING domain, facilitates the ubiquitination of the nascent aberrant peptides (69). The Cdc48–Ufd1–Npl4 complex acts then downstream of Ltn1 to promote release of the peptide from the ribosome, so that it can be degraded by the proteasome (Figure 9) (71).

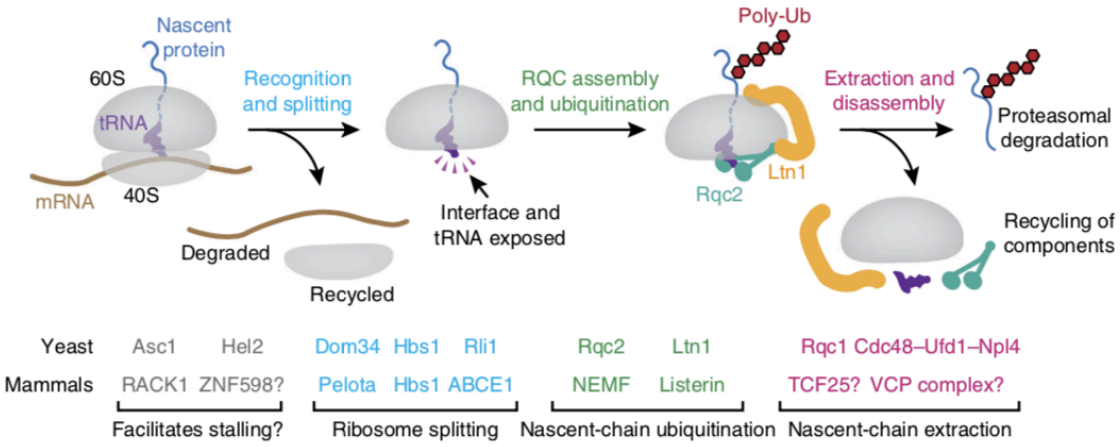

Figure 9 - Steps and factors of RQC.
From (69).

1.2.5 ERAD

The Endoplasmic Reticulum (ER)-associated protein degradation (ERAD) is one of the major quality-control machineries that monitors the biosynthesis, assembly, and trafficking of most proteins (72). It is the main site for protein folding in mammalian systems as one-third of all proteins enter the ER (64). During translation, a series of events occur to properly

fold and assemble proteins. To accomplish this objective, proteins are targeted to ER by signal peptides and there receive multiple modifications, such as disulfide bond formation, cis-trans isomerization, N-link glycosylation, and signal peptide cleavage to stabilize them and present the nascent proteins to their final destinations (73). To promote protein efficient folding, chaperones (as the HSP70 - BiP and HSP90) identify immature or aberrant proteins by hydrophobic exposed segments. This task is shared with chaperone co-factors and isomerase proteins such as the protein disulfide isomerase (PDI) (73). Some of those nascent polypeptides (e.g. Pex2p, Pex10p, Pex11p, Pex12p) can be exported as vesicles to form peroxisomes (74), as others will be delivered to Golgi and other locations (73).

While folded proteins exit the ER, the unwanted proteins have to follow retrotranslocation to the cytoplasm and then to proteasome for degradation. This coordinated process starts with recognition of the unfolded substrate by chaperones (e.g. BiP) and lectins, followed by specific proteins ER adaptors such as SEL1L and then channel retrotranslocation (e.g. HRD1, DER1) (Figure 10). Once the substrate is translocated across the ER lipid bilayer, VCP/p97 protein can proceed with extraction right after substrate polyubiquitination (Figure 10) (72,75). For this purpose, the ATPase protein acts with several co-factors as the ERAD involved protein complex NPL4-UFD1 (76).The whole process is highly conserved among eukaryotes and most of the understanding of the mammalian ERAD system comes from yeast and other organisms (77,78).

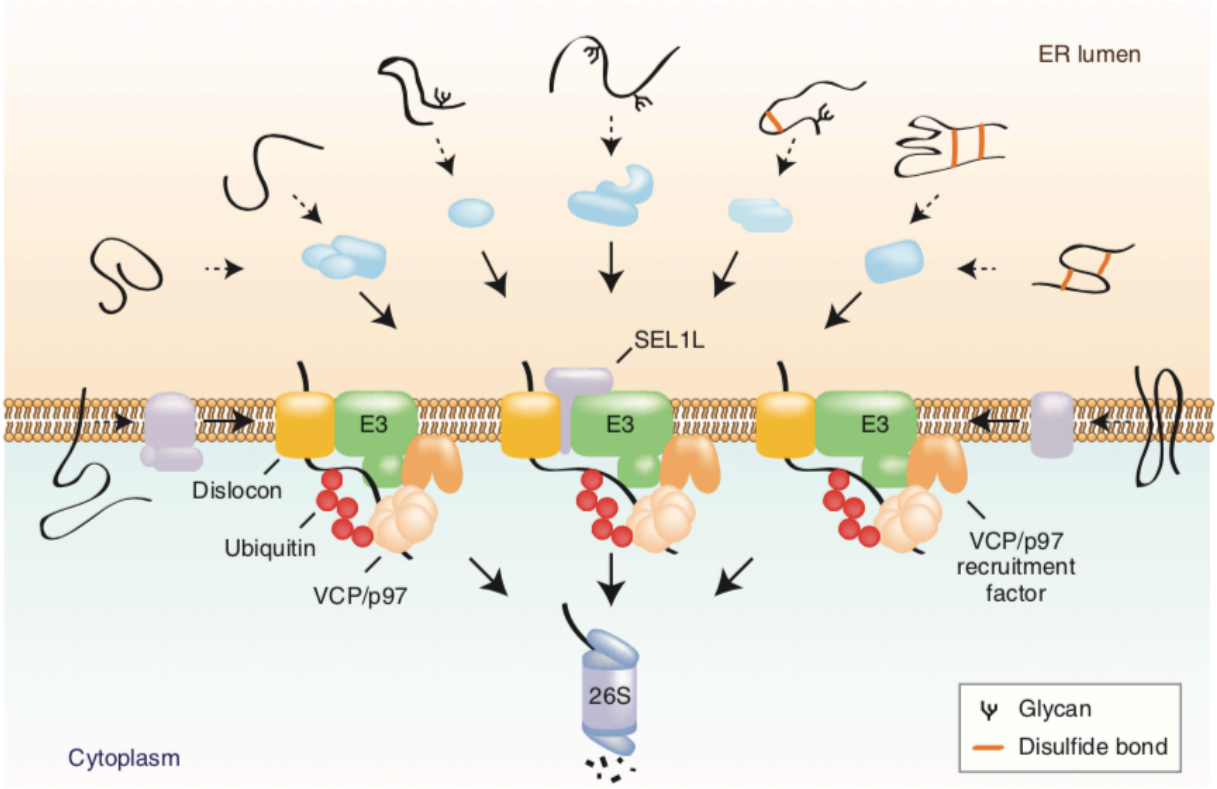

Figure 10 - ERAD system.
From (77).

1.2.6 UPR

The accumulation of misfolded proteins inside the ER can trigger the Unfolded Protein Response (UPR). This activation is a signal to ER membrane sensors such as the IRE1∝, PERK and ATF6 (63). Altogether, they increase protein fold activity and degradation while protein translation decreases. A similar inducible and acute reaction can be led by the mitochondrial UPR (UPRmt). Mitochondrial stress can communicate to the nucleus and results in the increased expression of mitochondrial-associated protein chaperones (68). Nevertheless, the specific signal and downstream effects still remain unclear (68). Furthermore, exposure to severe stress and continuous activation of the UPR could trigger autophagy (79) or drive signaling toward cell death (57).

1.2.7 Mitochondria and MAD

Beside its main role on energy production, mitochondria perform numerous essential functions for the survival of eukaryotic cells, such as calcium storage, fatty acid oxidation and ATP production (80). Mitochondrial importance is further highlighted by the number of conserved genes and pathways in different models that involve human mitochondria in health and disease (81). During cellular metabolism, the action of electrons passing through the mitochondrial electron transport chain produces Reactive Oxygen Species (ROS) as by-products, which can then damage lipids and proteins inside mitochondria (81). Several mitochondrial control pathways have evolved to maintain mitochondrial integrity ensuring that dysfunctional mitochondria proteins are either repaired or eliminated. These include DNA replication and repair; removal of reactive oxygen species (ROS); fission and fusion process to regulate mitochondrial morphology or whole organelle removal (mitophagy) (82) (Figure 11).

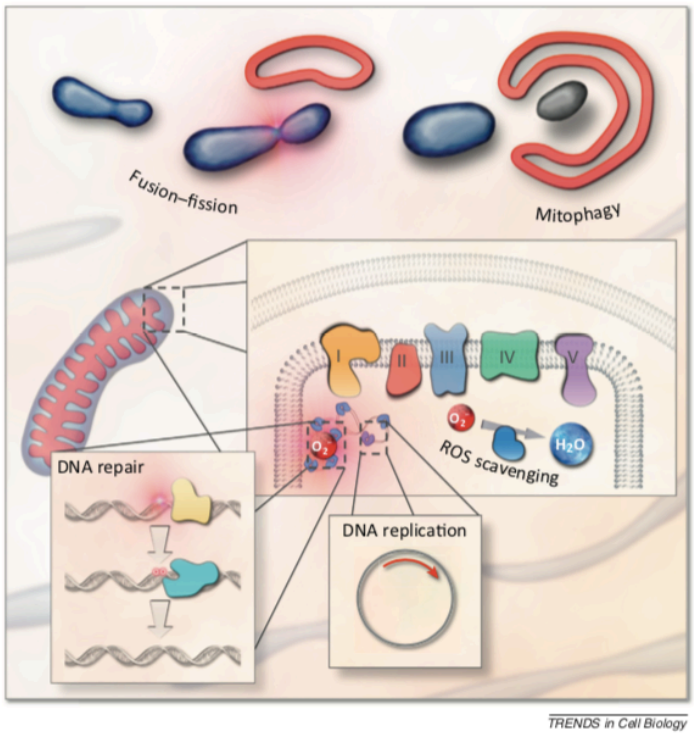

Figure 11 - Mitochondrial protein control pathways.
From (82).

As a first line of defense, ROS is converted to peroxide (H_2O_2) by the superoxide dismutase enzyme (SOD). Peroxiredoxin enzymes and peroxisome catalase can moderate the

damaging effect of H_2O_2, converting it into H_2O and O_2 (81). Nevertheless, especially under cellular stress, ROS does cause mitochondrial damage and the cell has to deal and remove the damaged components. Misfolded proteins can be refolded and mitochondrial Hsp70 might prevent denatured proteins from forming protein aggregates (81). Yet, most mitochondrial damaged proteins will be eliminated by different degradation systems, including proteases, mitophagy, and ubiquitin-dependent degradation. To remove the damaged components, a network of AAA+ ATPases selects, destroys and recycles the proteins from mitochondria. These proteins can bind and hydrolyse ATP to promote disaggregation and removal of damaged proteins. These proteases are anchored in the mitochondrial inner membrane (MIM) on the matrix side or on the intermembrane space (IMS) side (80). Still, the complete IMM retro-translocation to the cytosolic face remains under debate. Recently, the ubiquitination of intramitochondrial proteins was proposed to occur inside the matrix and intramembrane space, after which ubiquitinated proteins accumulate (65). Nevertheless, how IMM-ubiquitinated proteins reach the cytosolic proteasome, remains unknown (65).

By contrast, the turnover of outer mitochondrial membrane (OMM) proteins is more documented and appears to happen in cooperation with the ubiquitin proteasome system (UPS). The yeast Vms1 protein translocates to mitochondria, interacts with VCP and plays a role in recruiting the UPS for mitochondrial protein degradation (83). In mammals, the E3 ligase parkin is responsible for regulating the recruitment of VCP to the mitochondria (84). These studies established Cdc48/p97/VCP as a novel and essential component of the OMM-associated protein degradation pathway (85). The so-called Mitochondria-associated degradation (MAD) is thought to be mediated by the VCP complex that pulls over the ubiquitinated mitochondrial outer-membrane proteins and bring them to the proteasome for degradation. A critical mediator of the MAD process was recently unveiled - the Doa1 protein. This yeast protein composed by PUL (PLAA) VCP binding site and two ubiquitin binding sites (WD40 and PFU) was shown to recruit the ubiquitinated substrates and facilitate substrate interaction with the Cdc48-Ufd1-Npl4 complex in the mitochondria and being hence critical to the mitochondrial proteostasis (86). The MAD process has yet a lot to be unveiled as most substrates and specific co-factors are still under covered.

By contrast to the ubiquitin-dependent degradation that is a highly specific mechanism controlling numerous essential cellular functions (87), accumulation of misfiled and or aggregated proteins might induce the fusion-fission process or mitochondrial autophagy

(mitophagy), a pathway resulting in the degradation of the complete organelle in the lysosome (66). Mitophagy and proteases are mainly related to damage or stress-induced responses and exhibit low specificity (88).

1.2.8 Autophagy

Autophagy is a cellular mechanism involved in orderly degradation and recycling of cellular components. Autophagy can be identified as microautophagy, chaperone mediated autophagy (CMA) and macroautophagy lysosome (89). The first is a degradation process where the lysosome extends its membrane to invaginate other cellular contents. CMA requires a specific protein sequence KFERQ recognized by a chaperone protein (HSC70) to deliver the unwanted proteins to the lysosomal membrane. The most prevalent autophagy pathway, macroautophagy, involves the formation of the autophagosome. This spherical double membrane structure entrapes cytoplasmic components, or entire organelles, and then fuses them with the lysosome (89).

1.2.9 Proteasome complex

As mentioned, most quality control pathways end up with the ubiquitination of unwanted proteins and subsequent delivery to proteasomal degradation. However, the proteasome is not programmed for automatic protein destruction and ubiquitination alone does not necessarily lead to protein degradation. The final protein fate is actually judged by the proteasome. In fact, once in the proteasome, proteins can be deubiquitylated, escape proteolysis and be released by the 26S proteasome subunit (90). After Ub-mediated docking of the substrate at the proteasome, the 19-subunit regulatory particle (RP) removes ubiquitin and translocates the target protein into the proteolytic chamber of the core particle (CP) (91). At this step, the protein must already be unfolded and deubiquitylated, as ubiquitinated substrates can resist unfolding (91). The rate of protein degradation and its recognition patterns, processing (co)/factors and the selective degradation of some proteins are still subjects of intense studies (90). Polypeptides entering into the CP are then digested to short peptides and subsequently to amino acids by cytosolic peptidases (90).

The proteasome is the most prominent protease complex harboring AAA-ATPases in eukaryotes. In these protein degradation machineries, the proteolytically active sites are formed by either threonines or serines which are buried inside interior cavities of cylinder-shaped complexes (92). ATPases Associated with diverse cellular Activities (AAA proteins)

couple chemical energy provided by ATP hydrolysis to conformational changes which are transduced into mechanical force exerted on a macromolecular substrate. Proteins belonging to this family are involved in processes such as DNA replication, protein degradation, membrane fusion, microtubule severing, peroxisome biogenesis, signal transduction and the regulation of gene expression. A myriad of proteins is subject to AAA-ATPase coupled protein degradation by proteasomes (92). Among them, is the ubiquitous AAA+ ATPase VCP/p97/Cdc48.

No work has been done on VCP protein or its pathways in *Leishmania* and only a pair of studies in *Trypanosoma brucei* was published a decade ago (93,94). Furthermore, VCP co-factors were not studied in any trypanosomatidae. For these reasons and for introducing the work conducted during my PhD thesis on VCP/p97/Cdc48 and its co-factors in *Leishmania*, we included below a whole section reviewing the specific functions of VCP in other eukaryotic systems.

1.3 VCP

Valosin-containing protein (VCP) (p97 in mammals and Cdc48 in yeast) is a conserved AAA+ protein with ATPase-based unfoldase activity associated with several major quality control pathways. It plays a main role in protein degradation and is associated with multiple ubiquitin-dependent cell signaling pathways in different organisms.

1.3.1 VCP Structure and ATPase regulation

The VCP protein has an hexameric structure shaped like a mushroom, built up by 12 ATPase domains that make a cylindrical middle form, topped with the N-terminal domain which can change to up- and down- conformation (95) (Figure 12). D1 and D2 work together, although they have different functions. While D2 is the essential domain for ATPase activity related to unfolding process and translocation of the substrate through the VCP central pore, D1 is more relevant to deubiquitination and substrate release (96). The activity of those ATPases can change in function depending on up- or down- conformation (increase and decrease, respectively) co-factor binding (97), the class of the co-factor bound and the additional presence of K48-ubiquitinated substrate (95) or be regulated by some post-translational modifications (98).

Each monomer of the hexameric VCP protein is composed by an N-terminal domain followed by two ATPase domains and an unstructured C-terminal extension (99) (Figure 12). The N-domain can be further subdivided into Nn and Nc subdomains. This structure allows the association of a large variety of adaptors to VCP, the recruitment of different substrates and modulates the formation of different VCP/p97-cofactor complexes within different cellular localization (98,100,101).

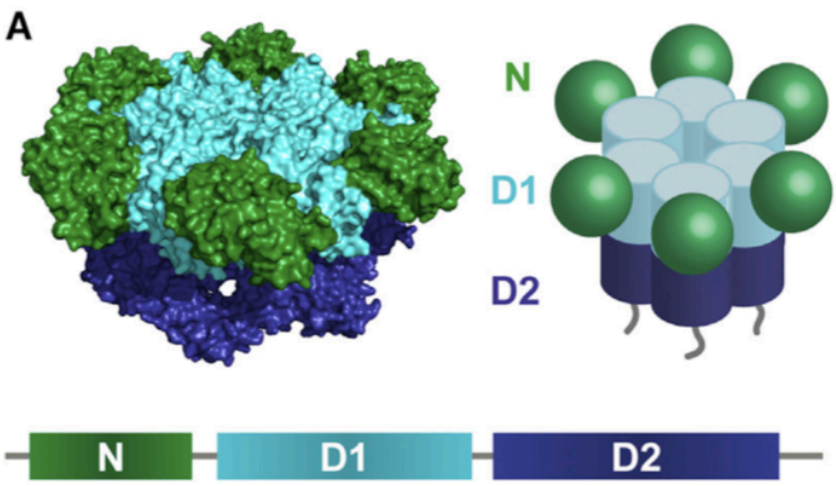

Figure 12 - Structure of human p97 hexamer.
N domain (green) and the two ATPase domains D1 (cyan) and D2 (blue). From (102).

1.3.2 General mode of VCP action

Especially under stress conditions, VCP mitigates proteotoxic and organellar stress by playing a major role in the degradation of unwanted/toxic proteins (102). Polyubiquitinated substrates are extracted from macromolecular complexes and membranes by VCP/Cdc48 in cooperation with its cofactors through a pulling force that causes protein unfolding (103). The protein is then delivered to proteasomal degradation and the polyubiquitin chains are trimmed to oligoubiquitin by deubiquitinating enzymes – DUBs (103).

Most misfolded proteins are post-translationally modified with ubiquitin by the ubiquitinating enzymes E1, E2, and E3 (Figure 13). As most VCP substrates described are ubiquitinated, their interaction is mediated by adaptor proteins/binding partners which contain both VCP-interacting and ubiquitin-interacting sites (95). Using its ATPase activity, VCP takes out the protein from the binding partner as it unfolds ubiquitinated substrates by translocation through its central pore (see section – unfoldase activity) and then hands over to the proteasome for final degradation (Figure 13).

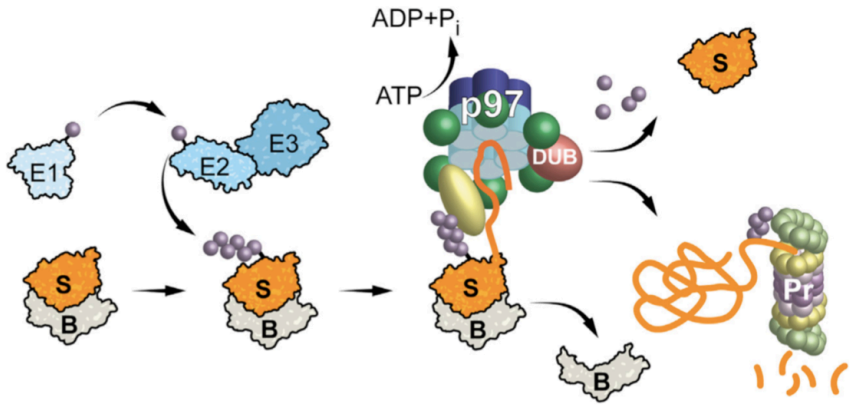

Figure 13 - General model of action of VCP.

Ubiquitin (purple), adaptor proteins (yellow), binding partners (B), deubiquitinating enzyme (DUB) and proteasome (Pr). Adapted from (102).

1.3.3 VCP unfoldase activity

VCP is an unfoldase that pulls the polypeptide substrate through its central pore (103). D1 domain, while in down conformation, binds to ATP as the substrate binds to the VCP complex with, e.g., the UN cofactor. The pulling force exerted by the D2 ATPase domain results in the unfolding of the substrate that passes through the central pore and then released with ubiquitin moieties in the D2 side of the central pore (103). Meanwhile, part of the ubiquitin chain is released from the substrate D1 side in cooperation with deubiquitinating enzymes - DUBs like OTU1 (Figure 14).

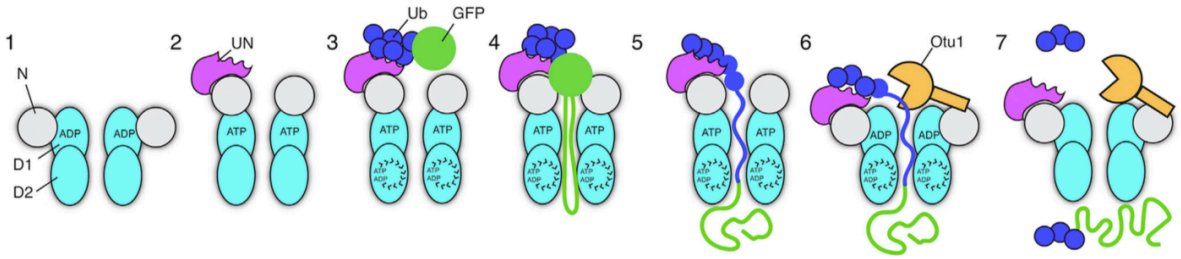

Figure 14 - Model for VCP unfolding activity.

Adapted from (103). 1) Cdc48 starts out with the D1 ATPases in the ADP-bound state. The N domains are in the down-conformation, co-planar with the D1 ring. 2) When the D1 domain binds ATP, the N domains move upward. 3) Substrate is initially bound to the Cdc48 complex exclusively through an interaction of the attached K48-linked polyubiquitin chain with the UN cofactor. 4) Substrate binding

also stimulates ATP hydrolysis in the D2 domain. This activity allows pore loops in the D2 ring to move and drag the substrate polypeptide through the central pore. 5) The pulling force exerted by the D2 ATPases results in the unfolding of the substrate. During translocation, most of the polyubiquitin moiety remains on the cis side, bound to the UN cofactor. However, a portion of the ubiquitin chain can enter the central pore along with the substrate. 6) The final step is substrate release. Once D1 has hydrolyzed ATP, the N domains convert back to the down-conformation, allowing access of the polyubiquitin chain to the deubiquitinating enzyme Otu1. 7) When the ubiquitin chain has been shortened sufficiently, its affinity for the UN complex is reduced or lost, and the remaining ubiquitin moieties are unfolded and pulled through the central pore. The ubiquitin probably refolds rapidly after translocation, although this needs to be tested by future experimentation.

1.3.4 VCP functions

Central to the Ubiquitin Proteasome System (UPS), VCP plays a key role in a variety of fundamental cellular processes aiming at cellular proteostasis (102,104,105). Indeed, VCP/p97 is involved in the extraction of misfolded proteins, especially under stress conditions, from the endoplasmic reticulum (ER-associated protein degradation, ERAD) (64,106) and similarly in the translocation of damaged mitochondrial proteins from the outer mitochondrial membrane into the cytosol (OMM-associated degradation) (83, 84), the ribosome quality control (108), the removal of chromatin-bound proteins (109), genome stability (110), stress granules clearance (111) and the removal of damaged lysosomes by autophagy (112). For more details, see previous RAD, MAD and ERAD sections.

1.3.5 VCP Co-factors

In conjunction with a large number of cofactors and adaptors, VCP uses ATP hydrolysis to segregate proteins from immobile cellular structures that often results in proteasomal degradation of the extracted polypeptides (113).

1.3.6 VCP binding modules

Despite the large number of cofactors, these specifically interact with VCP via a small number of conserved binding modules (100). Overall, only three different interaction sites have been identified so far in VCP: the hydrophobic inter-subdomain Nn-Nc cleft (99), the SHP binding site in the Nc subdomain, and the unstructured tail formed by the last 7 amino acids in the C-terminus of VCP (98,100,101). Most co-factors, whether they have a substrate-recruiting, processing or regulatory function, interact with the N-terminus of VCP.

Proteins containing the UBX modules interact by the Rx(3)FPR motif within the Nn-Nc cleft of the N-domain of VCP (Figure 15). Co-factors harboring either a VIM (VCP-interacting motif) or VBM (VCP-binding motif) binding motif also interact within the same hydrophobic pocket located in the N-domain (98) (Figure 15A). Differently, but also in the N domain, cofactors with a SHP binding site, $h(x)_{1-2}F/W(x)_{0-1}GxGx_2L$ (h, hydrophobic amino acid residue; x, any amino acid), interact with the subdomain Nc of VCP (98) (Figure 15B). Otherwise, a few co-factors interact with the C-terminus of VCP. These proteins contain a PUB or PUL domain which form a hydrophobic pocket for interactions with the VCP tail associating with key amino acids such as the Leucine[804] and the aromatic side chain of the penultimate tyrosine[805] residue (98,100,101) (Figure 15C).

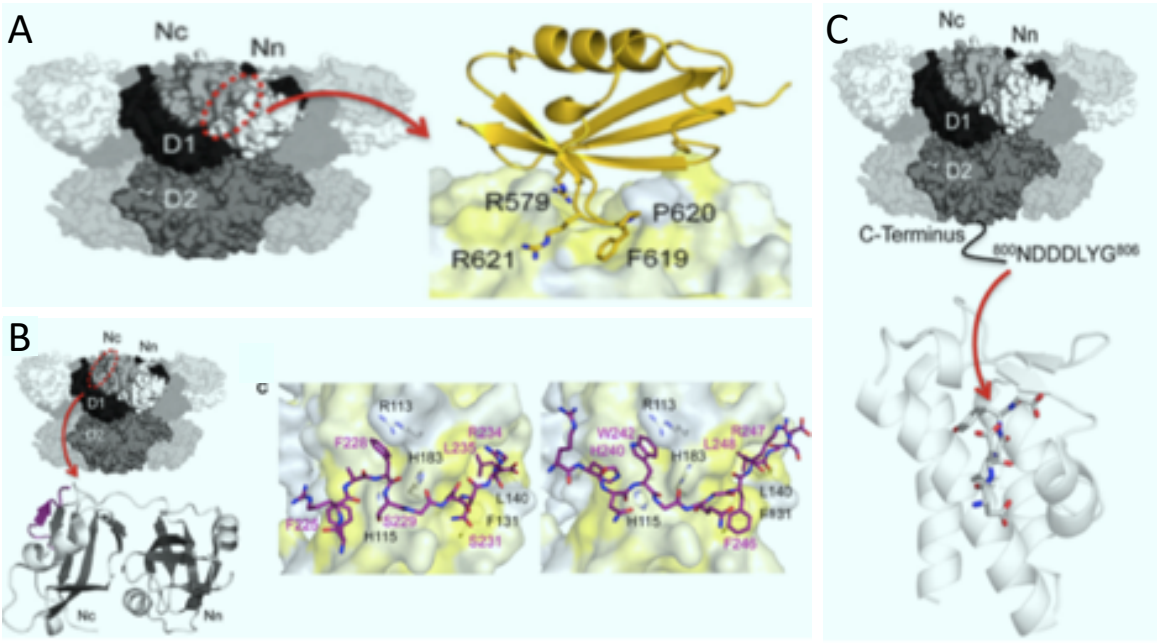

Figure 15 - Co-factor binding sites within VCP.

A) Co-factor interaction with Nn-Nc cleft of the N-domain of VCP. Molecular surface of VCP. Right, FAF1-UBX—VCP N complex. The UBX domain (colored in gold) is shown in cartoon representation and p97 N as molecular surface. The R...FPR motif is shown in stick representation. **B) Co-factor interaction with Nc subdomain of VCP.** Top left, molecular surface of VCP with the SHP binding site indicated. Bottom left, cartoon representation of the overall structure of the UFD1 SHP binding motif (colored in purple) bound to the VCP N domain (β-strands in dark gray and α-helices in light gray). Right - Stick representations of the SHP binding motifs of UFD1 and DER1. **C) Interaction of VCP with PUB and PUL**

domain-containing cofactor. Top, molecular surface of VCP with the VCP C-terminal cofactor binding site indicated. Bottom, overall structure of the VCP C-terminus (stick representation) bound to the PNGase PUB domain shown in cartoon representation. All figures are from (98).

1.3.7 Co-factor diversity

Most of VCP co-factors in mammals contain the ubiquitin X domain (UBXD) or UBXL (UBX-like) with similar three-dimensional structure described for ubiquitin. Ubiquitination per se is not required for p97 function, as protein substrates can bind directly with some co-factors, without the presence of a UBA domain (114). Proteins such as UBXD1 (UBXN6), UBXD2 (Erasin, UBXN4), UBXD3 (UBXN10), UBXD4 (UBXN2A), UBXD5 (Socius, COA-1, UBXN11), UBXD6 (Rep-8, UBXN8), UBXD9 (TUG, ASPL, ASPSCR1), and UBXD11 (P37, UBXN2B) contain only UBX domain. Other co-factors, the UBA-UBX proteins, such as UBXD7 (UBXN7), UBXD8 (FAF2), UBXD10 (P47, NSFL1C), UBXD12 (FAF1), and UBXD13 (SAKS1, and UBXN1) also accommodate an UBA domain fundamental for interacting with ubiquitinated substrates (113,115). Some proteins, such as the p47, harbor not only the UBX and the UBA domains that are important for their role in the ubiquitin proteasome system (UPS) but also contains a SHP motif as an additional binding site for VCP interaction (101). Other proteins form complexes to interact with VCP. One of the most well studied VCP co-factor, the UFD1 protein, associates with the NPL4 protein to form the complex VCP-UFD1-NPL4 involved in a series of events, including the Endoplasmic Reticulum-associated degradation (ERAD) (116). Finally, other cofactors containing PUB (PNGase/UBA or UBX containing proteins) or PUL (PLAP, Ufd3p, and Lub1p) domain can harbor the unstructured C-terminal tail of VCP (117) (Figure 16).

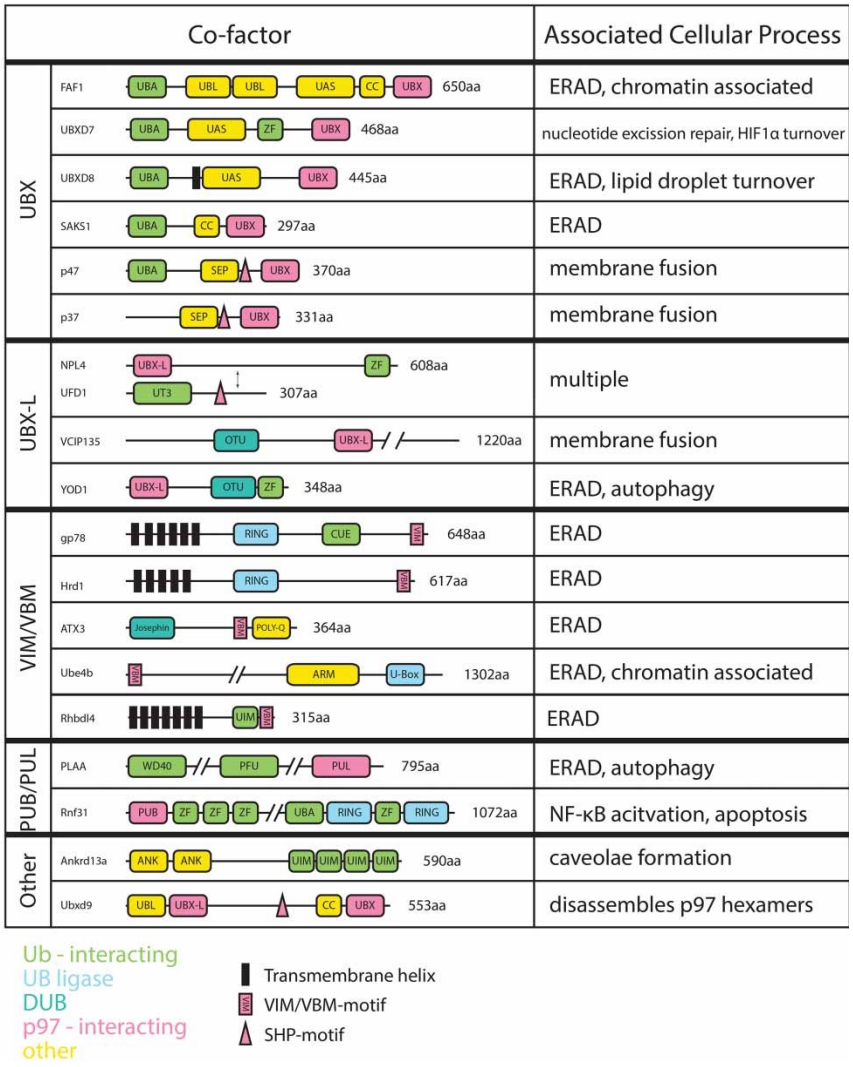

Figure 16 - Ubiquitin-associated VCP cofactors.
Adapted From (95).

1.3.7.a UFD1-NPL4

Ufd1-Npl4 (UN) is one of the most studied VCP cofactors. This heterodimer links VCP to multiple cellular processes such as the Endoplasmic Reticulum-associated degradation (ERAD) (95,113,118). A recent model proposes that UFD1 binds to the Nc portion of VCP through its two SHP sites, meanwhile the UBX-like and Zn finger domains of NPL4 help its binding to VCP (116). The heterodimer UN forms, together with VCP a structure to accommodate and interact with at least 5 ubiquitin molecules. This UN-VCP complex would serve as a universal module to recognize multiple ubiquitinated substrates and then

translocate them to the VCP central pore through ATP hydrolysis from its D2 domain. As the substrate passes through the central pore (D1 to D2 side), the D1 ATPase domain would trim the ubiquitin chain in association with deubiquitinases, as the Otu1 (103,116). The unfolded substrate would then be delivered to the proteasome system. However, the mechanics of this process still need to be better addressed.

1.3.7.b p47

p47 (UBXN2C, UBXD10, NSFL1C) is one of the first identified and most abundant VCP adapters (119). As one of the most prominent co-factors, it contains an UBA domain responsible for ubiquitin binding, a SEP (after Shp1, eyc, and p47) domain of unknown function and an UBX domain that interacts with VCP. The UBX domain along with SEP are responsible for p47 trimerization, when coupled with VCP, to form the stable complex VCP-p47 (101,120). p47 has been linked to membrane dynamics during cell division (119), Golgi membrane fusion (121) and to inflammation as it cooperates to the degradation of IκB kinase (IKK) regulator, an NF-κB essential modulator (NEMO) (122). p47 is mainly localized to the nucleus during specific cellular phases (123) and its phosphorylation interfears with membrane attachment in some organelles (123). p47 was also recently associated with ERAD as the p47 gene is rapidly increased during ERAD (124). However, complex disassembly or protein unfolding has not been demonstrated for p47 substrates (114).

1.3.7.c FAF

The Fas-associated factor-1 (FAF1) also binds to VCP in a 3:6 ratio via the UBX site (125). Although the cooperation between FAF1 protein and the UFD1-NPl4 complex was previously demonstrated to be important to the ERAD system (126), lately this protein was shown to be important to DNA replication. The FAF1 human protein and its homolog UBXN-3 in nematodes were demonstrated to avoid stalling of fork replication and thus preventing activation of the DNA damage response (127). More recently, FAF1 was shown to be important for nematode DNA replication termination and mitosis (128).

With similar structure but different functions, the FAF2 protein (UBXD8 or ETEA) interacts with VCP through its UBX site. This human protein is part of the UBX-UBA class of co-factors as it also possesses an UBA domain, as FAF1. But differently, FAF2 acts in the regulation of intracellular fatty acid storage as some fatty acid (FA) associated proteins are degraded by the ERAD system through the interaction of the VCP-FAF2 complex (129).

Indeed, the FAF2 protein can be found not only in the ER membrane, but also in lipid drops (LD) (130,131). Moreover, this membrane-bound protein is shown to bind to substrate proteins in the ER while recruiting VCP to complete protein extraction from the ER membrane to the cytoplasm for proteasomal degradation (129,130).

1.3.7.d PUB

A smaller group of proteins binds the VCP C-terminal sequence DDLYG-COOH (95). PUB (PNGase/UBA- or UBX-containing proteins) and PUL (PLAA,Ufd3p and Lub1p) domains form a hydrophobic pocket into which the VCP tail binds to. Although the physiological significance of this interaction remains to be determined, the phosphorylation at the Y805 blocks VCP-PUB interaction and hence disturbs the ERAD process (117,132). PLAA (phospholipase A-2- activating protein) proteins binds to VCP via its PUL domain and interacts with ubiquitin though its WD40 (WD-repeat) and PFU (PLAA family ubiquitin binding) domains (95). A homolog of human PLAA in yeast, the Doa1 (degradation of alpha 1) protein is essential for mitochondrial oxidative stress response, and acts in cooperation with the Cdc48-Ufd1-Npl4 complex to mediate degradation of mitochondrial substrates (86).

1.3.8 VCP relevance to human disease

Given the diversity of VCP substrates, this unfoldase protein has profound influence on cellular physiology ranging from protein homeostasis to DNA lesion sensing (113). Point mutations that cause, for example, multisystem proteinopathy 1 (MSP1) lead to destabilization of the ADP-bound, “down” conformation of the N-domain, which favors the “up” conformation. As some co-factors such as p47 bind more tightly to the ATP-bound (up) conformation, these VCP mutants have high-affinity to some co-factors and may compromise the dynamics and functions of VCP protein complexes (97,133). Mutations in VCP can also lead to protein aggregation and have been linked to several diseases, including cancer and neurodegenerative and muscular disorders (134–136).

1.3.9 Therapeutic potential of VCP inhibitors

Given that VCP mutations have been associated with a number of human diseases where protein aggregates are formed, drugs targeting VCP are being actually developed. Besides the fact that several neurodegenerative disorders are associated with VCP mutations, VCP was found up-regulated in many forms of cancer (137).

The first studies targeting VCP demonstrated that some compounds could potently inhibit cancer cell growth (138). Since then, several other molecules emerged as potential VCP inhibitors such as the DBeQ, NMS, ML240/ML241, Eerl, and others. (95). Moreover, some compounds targeting VCP and other protein quality control proteins were considered against some parasitic protozoa. As in these parasites there is less components relative to higher eukaryotes, members of trypanosomatids and the causative agents of malaria and toxoplasmosis could be more sensitive to the inhibition of protein quality control systems such as VCP (139). Harbut and colleagues reported that some compounds that target the ER quality control pathway demonstrated nanomolar activities and could therefore be used as antiparasitic therapeutics such as the DBeQ drug on *Plasmodium falciparum* (139).

1.3.9.a DBeQ

DBeQ (N2,N4-dibenzylquinazoline-2,4-diamine) is a specific inhibitor of p97 protein identified as selective, potent, reversible, and ATP-competitive p97 inhibitor (138). It prevents the degradation of ubiquitinated proteins and blocks the ERAD pathway. The DBeQ rises also as a new strategy to control other opportunistic human pathogens such as *Candida albicans* (140).

1.3.9.b NMS

High-throughput screening led to the development of new covalent and allosteric compounds that inhibit VCP. One of the major outcomes, the allosteric NMS-873 was identified as UPR activator and the most potent and specific VCP inhibitor described today (141). Later, this NMS compound was shown to modulate co-factors binding to VCP with distinct effects on the interaction of different adaptors (142) as well one mechanism to overcome such effect (143). In the presence of cytotoxicity effects produced by the VCP inhibitor NMS-873, the binding of some co-factors is increased, and a mutation in the D2 domain of the p97 sequence (A530T) was sufficient to overcome the NMS-873 drug effect and to become insensitive to it (143). This work has shown that some drug side effects can be overcome by adaptive changes without affecting the drug binding and thus raise questions on VCP drug resistance.

1.3.9.c ML240 and ML241

Using high-throughput screening coupled with structure–activity relationship (SAR) studies, researches arrived to two new potent and selective inhibitors of VCP derived from the DBeQ molecule – ML240 and ML241 (144).

1.3.9.d CB-5083

Another compound, the small-molecule inhibitor of VCP, CB-5083 - Cleave Bioscience, is emerging as an approach to treat cancer (145). From the optimization of DBeQ and ML240 compounds, the improved VCP inhibitor CB-5083 is orally bioavailable and induces a strong unfolded protein response that leads to disruption of protein homeostasis and cancer cell death. This VCP inhibitor is an ATP-competitive binding molecule that targets the D2 domain of VCP and demonstrates antitumor effects in vivo in multiple myeloma and solid tumor models (145).

1.3.9.e Disulfiram

Other drugs might target some VCP co-factors. Some studies have identified an association of the use of the alcohol-abuse drug disulfiram (tetraethylthiuram disulfide, DSF) with lower risk of death from cancer. Recently, the NPL4 cofactor was suggested as one of its molecular target (146).

As novel promising therapeutic approach, VCP, and now some co-factors, keep being suggested and tested as therapeutic targets in several diseases such as Acute Lymphoblastic Leukemia (147). Due to the evolutive conservation of those proteins and considering the drug availability and the possibility of drug repurposing, those compounds are of interesting value for testing their potentiality against *Leishmania* and leishmaniasis.

Chapter 1: Hypothesis and Objectives

1.1 Hypothesis

As is the case for its eukaryotic counterparts, the *Leishmania (Li)* VCP is a conserved AAA+ (ATPases associated with diverse cellular activities) ATPase that uses its ATP hydrolysis to segregate ubiquitinated proteins from their binding partners and deliver them to the 26S proteasome for degradation, thus playing a key role in *Leishmania* protein quality control.

1.2 Objectives

Although VCP and its cofactors have extensively been studied in yeast and higher eukaryotes, there is no work done on this important protein and its contribution to diverse cellular pathways in *Leishmania.* Only a pair of studies in *Trypanosoma brucei* was published a decade ago. Furthermore, VCP co-factors have not been studied in any trypanosomatid parasite. Given the central role of this protein in protein quality control, especially under conditions of stress, such as *Leishmania* experiences inside macrophages, we undertook a series of experiments, as part of my PhD thesis, to characterize the VCP/p97/Cdc48 protein homolog and its co-factor network, as well as to assess the role of VCP in the parasite response to stress and its intracellular development.

1.2.1 Objective 1

Study *Li*VCP expression, localization, and its role in the parasite survival during its digenetic life cycle.

1.2.2 Objective 2

Characterize the *Li*VCP protein network in *Leishmania* and identify *Li*VCP major cofactors and their interacting partners.

Chapter 2: Valosin - containing protein VCP/p97 is essential for the intracellular development of *Leishmania* and its survival under heat stress

2.1 Avant-propos

This chapter corresponds to a scientific paper entitled “Valosin-containing protein VCP/p97 is essential for the intracellular development of *Leishmania* and its survival under heat stress” by **Guedes Aguiar, B**., Padmanabhan, P. K., Dumas, C., & Papadopoulou, B. published on June 5, 2018 in *Cellular Microbiology.* This paper is presented as it was published. The study was designed by BGA and BP. All experiments were performed by BGA with help of CD and PKP. The paper was written and corrected by BGA and BP.

Valosin-containing protein VCP/p97 is essential for the intracellular development of *Leishmania* and its survival under heat stress

Bruno G. Aguiar[1,2,3], Prasad K. Padmanabhan[1,2], Carole Dumas[1,2] and Barbara Papadopoulou[1,2*]

[1]Research Center in Infectious Diseases, CHU de Quebec Research Center-University Laval
[2]Department of Microbiology-Infectious Disease and Immunology, Faculty of Medicine, University Laval, Quebec, QC. Canada G1V 4G2
[3]Department of Community Medicine, Federal University of Piauí, Teresina, Brazil

* Corresponding author:
Barbara Papadopoulou
CHU de Quebec Research Center-University Laval
2705 Laurier Blvd., Quebec (QC), Canada G1V 4G2
Phone: (418) 525-4444, ext. 47608; Fax: (418) 654-2715
Email: barbara.papadopoulou@crchudequebec.ulaval.ca

Running title: VCP/p97 and *Leishmania* intracellular survival

Key words: *Leishmania*; VCP/p97; Dominant negative mutants; Heat stress; Amastigote survival; Poly-ubiquitination

2.2 Résumé

VCP/p97/Cdc48 est l'une des AAA + ATPases cytosoliques de type II les mieux caractérisées et les plus connues pour leur rôle dans le contrôle de la qualité des protéines dépendant de l'ubiquitine. Nous fournissons ici un aperçu fonctionnel du rôle de l'homologue de VCP, VCP/p97 (*Li*VCP), chez *Leishmania* dans le développement intracellulaire du parasite. Nous démontrons que, bien que *Li*VCP soit un gène essentiel, les promastigotes de *L. infantum* peuvent se développer avec moins de VCP. En revanche, la croissance des amastigotes axéniques et intracellulaires est considérablement affectée par la diminution des taux de *Li*VCP chez les mutants *Li*VCP hétérozygotes et sensibles à la température ou chez des mutants dominants négatifs connus pour cibler spécifiquement le deuxième domaine ATPase de VCP qui contribue largement à l'activité ATPase globale. Fait intéressant, ces mutants de VCP sont également incapables de survivre le stress thermique et un mutant de VCP sensible à la température est défectueux pour sa croissance en amastigotes. Conformément à la fonction essentielle de *Li*VCP chez les amastigotes, l'expression de l'ARNm de *Li*VCP est induite à ce stade developmental via un mécanisme de régulation dépendant du 3'UTR. De plus, nous montrons que les lignées mutantes de parasites exprimant des niveaux de VCP plus faibles ou des formes de VCP aggissants comme des mutants dominant négatifs présentent une forte accumulation de protéines polyubiquitinées et une sensibilité accrue au stress protéotoxique, soutenant la fonction de chaperone sélective pour l'ubiquitine de *Li*VCP. Ensemble, ces résultats soulignent le rôle crucial que *Li*VCP joue en conditions de stress thermique et lors du développement intracellulaire du parasite.

2.3 Abstract

VCP/p97/Cdc48 is one of the best-characterized type II cytosolic AAA+ ATPases most known for their role in ubiquitin-dependent protein quality control. Here, we provide functional insights into the role of the *Leishmania* VCP/p97 homolog (*Li*VCP) in the parasite intracellular development. We demonstrate that although *LiVCP* is an essential gene, *L. infantum* promastigotes can grow with less VCP. In contrast, growth of axenic and intracellular amastigotes is dramatically affected upon decreased *Li*VCP levels in heterozygous and temperature sensitive *Li*VCP mutants or the expression of dominant negative mutants known to specifically target the second conserved VCP ATPase domain, a major contributor of the VCP overall ATPase activity. Interestingly, these VCP mutants are also unable to survive heat stress and a temperature sensitive VCP mutant is defective in amastigote growth. Consistent with *Li*VCP's essential function in amastigotes, *LiVCP* mRNA undergoes 3'UTR-mediated developmental regulation, resulting in higher VCP expression in amastigotes. Furthermore, we show that parasite mutant lines expressing lower VCP levels or dominant negative VCP forms exhibit high accumulation of polyubiquitinated proteins and increased sensitivity to proteotoxic stress, supporting the ubiquitin-selective chaperone function of *Li*VCP. Together, these results emphasize the crucial role *Li*VCP plays under heat stress and during the parasite intracellular development.

2.4 Introduction

The valosin-containing protein (VCP)/p97 (also called Cdc48 or Ter94) is one of the best-characterised type II AAA+ (ATPases associated with diverse cellular activities) superfamily of proteins involved in a variety of fundamental cellular processes that is conserved from yeast to human. It plays a key role in multiple protein quality control pathways mediated by the Ubiquitin Proteasome System and is implicated in the maintenance of cellular proteostasis (Franz, Ackermann, & Hoppe, 2014; Meyer, Bug, & Bremer, 2012; van den Boom & Meyer, 2017). In all these pathways, VCP/p97 hydrolyses adenosine triphosphate (ATP) and uses the resulting energy to extract or disassemble polyubiquitinated substrates from membranes, organelles, chromatin, or in general from large protein assemblies and deliver them to the 26S proteasome for degradation (Bodnar & Rapoport, 2017b; Christianson & Ye, 2014; Ye, Tang, Zhang, & Xia, 2017). VCP/p97 is indeed involved in the extraction of ubiquitylated proteins from the endoplasmic reticulum associated protein degradation (ERAD; Qi, Tsai, & Arvan, 2017; Wolf & Stolz, 2012) and similarly in the translocation of damaged mitochondrial proteins from the outer mitochondrial membrane into the cytosol (associated degradation; (Heo et al., 2010; Taylor & Rutter, 2011), the ribosome quality control (Brandman et al., 2012), the removal of chromatin-bound proteins (Franz, Ackermann, & Hoppe, 2016), genome stability (Vaz, Halder, & Ramadan, 2013), stress granules clearance (Buchan, Kolaitis, Taylor, & Parker, 2013), and the removal of damaged lysosomes by autophagy (Papadopoulos et al., 2017). Consistent with its central role in essential protein quality control pathways, mutations in human VCP/p97 have been linked to several diseases, including cancer and neurodegenerative and muscular disorders (Fessart, Marza, Taouji, Delom, & Chevet, 2013; Meyer & Weihl, 2014; Tang & Xia, 2016).

The functional diversity of VCP/p97 relies on its ability to associate with a large variety of regulatory cofactors which link VCP/p97 to a specific substrate in a subcellular compartment (adaptors) or recruit the substrates or mediate substrate processing (e.g., ubiquitin ligases, deubiquitinases, peptide N-glycanases) and turnover (Buchberger, Schindelin, & Hänzelmann, 2015; Hänzelmann & Schindelin, 2017). To date, more than 40 cofactors have been identified in mammals from which the majority interacts via a small number of conserved binding modules. Most of these cofactors interact with the N-terminal domain of VCP/p97, but a few cofactors bind the C-terminal tail. One of the most important cofactors is the Ufd1/Npl4 heterodimer, which recruits polyubiquitinated substrates to the VCP/p97 (Stein, Ruggiano, Carvalho, & Rapoport, 2014). The localisation to a specific subcellular compartment or substrate, enzyme activity, stability, and structure of VCP/p97

can be modulated by the formation of different VCP/p97-cofactor complexes or following VCP/p97 posttranslation modifications (Hänzelmann & Schindelin, 2017).

The VCP/p97/Cdc48 ATPase consists of three structured domains, the N-terminal and two tandem highly conserved AAA+ ATPase (D1 and D2) domains connected by a short polypeptide linker (Davies, Brunger, & Weis, 2008; DeLaBarre & Brunger, 2003). Crystal and cryo-electron microscopy structures of VCP/p97 showed that the D1 and D2 ATPase domains form two stacked hexameric rings surrounding a central pore through which polyubiquitinated substrates are translocated and released to the cytosol (Benerjee et al., 2016; Davies et al., 2008). Each ATPase domain contains a Walker A and B sites responsible for ATP binding and hydrolysis, respectively (Hänzelmann & Schindelin, 2017). Both ATPase rings hydrolyse ATP, but D2 domain seems to be the major contributor of the overall ATPase activity (Chou et al., 2014; Song, Wang, & Li, 2003). ATP binding/hydrolysis of VCP/p97 by the D2 ring results in profound conformational changes of the homohexameric, barrel-shaped VCP complex (Rouiller et al., 2002), which generate the mechanical force required for ubiquitin-directed disassembly of macromolecular complexes (Pye et al., 2006) and transfer of the polyubiquitinated substrates to the 26S proteasome for degradation (Richly et al., 2005). ATP hydrolysis by the D1 ring is proposed to be important for subsequent substrate release from the VCP/p97 complex (Bodnar & Rapoport, 2017a).

In trypanosomatids, very little is known about VCP/p97's diversified functions. In *Trypanosoma brucei*, it was shown that *Tb*VCP is an essential homohexameric cytoplasmic protein expressed preferentially in the procyclic stage (tsetse fly) (Lamb, Fu, Wirtz, & Bangs, 2001; Roggy & Bangs, 1999). In *Leishmania*, we have reported recently that VCP/p97 associates with the DDX3 DEAD-box ribonucleic acid (RNA) helicase shown to play a central role in mitochondrial protein quality control (Padmanabhan et al., 2016). In this study, we have investigated the functional role of the *Leishmania* VCP/p97 homologue (*Li*VCP/p97) in the parasite response to intracellular stress and development. We show that the *LiVCP/p97*gene is essential for *Leishmania*'s viability and undergoes 3'UTR-mediated developmental regulation, resulting in higher VCP expression in the mammalian amastigote stage. Furthermore, we demonstrate that parasite mutant lines expressing lower *Li*VCP/p97 levels or dominant negative VCP forms targeting the *Li*VCP/p97 D2 ATPase domain are unable to grow inside macrophages and to survive under heat stress. In addition, we show that impairing the *Li*VCP/p97 ubiquitin-chaperone function triggers the accumulation of high cellular levels of polyubiquitinated proteins and increases sensitivity to proteotoxic stress.

Altogether, these results emphasise the crucial role *Li*VCP/p97 plays under stress and during the parasite intracellular development.

2.5 Results

The Leishmania VCP/p97 homolog shares a high sequence identity and structural organization with its evolutionary distant eukaryotic counterparts

In general, VCP from all eukaryotes are composed by a structured N-terminal domain barrel followed by two ATPase domains (D1, 199–450 and D2, 471–750) and an unstructured but functionally important C-terminal domain (Xia, Tang, & Ye, 2016). The N domain can be further subdivided into an Nn (residues 15–95) and Nc (residues 104–175) subdomain and its intersubdomain cleft (9 amino acid [aa]) serving as a cofactor-binding site (Hänzelmann & Schindelin, 2017; Figure 1a). The *Leishmania infantum Li*VCP/p97 gene (LinJ.36.1420; TriTrypDB; http://tritrypdb.org; thereafter we will refer to it as *Li*VCP) encodes a protein of 784 aa and harbours all the characteristic domains of eukaryotic VCP homologues (Figure 1a). The nucleotide sequence of the polymerase chain reaction (PCR)-amplified *LiVCP*gene from *L. infantum* total deoxyribonucleic acid (DNA) is 99% identical (2349/2355 bp) to the annotated sequence of *Leishmania donovani* BPK282A1 (LdBPK_361420.1). However, its alignment with the reference sequence of *L. infantum* (LinJ.36.1420, annotated as a 689 aa protein; http://tritrypdb.org) revealed a missing part of 283 nucleotides (95 aa) within the ATPase D1 domain (from aa 195 to aa 290) but a 99% similarity with the remaining sequence. De novo assembly from *L. infantum* Next-generation sequencing (NGS) (kindly provided by Dr. Carlos Costa, Federal University of Piauí, Teresina, Brazil) confirmed also the wrong assembly in the reference *L. infantum* genome sequence. The multiple sequence alignment of *Li*VCP along with *L. donovani* (*Ld*VCP), *T. brucei (Tb*VCP) and *Homo sapiens* (p97) revealed that all VCP homologues share the same domain composition (Figure 1b). The phylogenetic relationship of *Li*VCP between other trypanosomatids and protozoa as well as more evolutionary distant organisms such as yeast, plants, and *Homo sapiens* is illustrated in the Neighbour-joining tree presented in Figure 1c. As expected, *Li*VCP is clustered with the other pathogenic and nonpathogenic trypanosomatids (Figure 1c). Our data indicate that the *Leishmania* VCP is evolutionary closer to *Homo sapiens* than to the unicellular eukaryote *Saccharomyces cerevisiae* (Figure 1c).

The *Leishmania* VCP/p97 homolog localizes mostly to the cytosol and is associated with organellar compartments

To determine the subcellular localisation of *Li*VCP, we carried out indirect immunofluorescence studies by confocal microscopy using an antibody directed against the *T. brucei* VCP protein (*Tb*VCP) (Roggy & Bangs, 1999) that specifically recognises the *Leishmania* VCP. Immunofluorescence studies indicate that *Li*VCP is largely distributed throughout the cytosol showing a granular pattern in both promastigote (Figure 2a,b) and amastigote (Figure S1a) life stages. As a central player to the ERAD (Qi et al., 2017; Wolf & Stolz, 2012) and the translocation of damaged mitochondrial proteins from the outer mitochondrial membrane into the cytosol (Heo et al., 2010; Taylor & Rutter, 2011), VCP/p97 has been found associated with both endoplasmic reticulum (ER) and outer mitochondrial membrane fractions. Here, we investigated organellar association of the *Leishmania* VCP protein using mitochondrial (MitoTracker) or ER (an anti-BiP chaperone antibody) markers in colocalisation studies. Our data suggest a weak association of *Li*VCP with the mitochondrion (Figures 2a and S1b). On the other hand, *Li*VCP partially colocalises with BiP as revealed by the spread orange pattern in the merge panels with anti-BiP and anti-VCP antibodies (Figure 2b). Furthermore, a digitonin permeabilisation experiment with increasing concentrations of digitonin (20 µM–10 mM) and Western blotting on the different cellular subfractions using an anti-*Tb*VCP antibody indicated some association of *Li*VCP with organellar fractions where the ER BiP protein is enriched (Figure 2c). Given that the bulk of the *Li*VCP protein is cytoplasmic, it is likely that *Li*VCP is sitting on the cytoplasmic leaflet of the ER. This is in agreement with previous studies in yeast and in mammals showing that the cytosolic VCP/p97/Cdc48 protein is translocated to the ER membrane during ERAD to extract polyubiquitinated proteins and transfer them to the proteasome for degradation (Qi et al., 2017; Wolf & Stolz, 2012).

*Li*VCP undergoes 3'UTR-mediated developmental gene regulation and exhibits higher expression in the amastigote life stage of the parasite

In the related kinetoplastid *T. brucei,* VCP was shown to be more expressed in the insect procyclic form (Roggy & Bangs, 1999). To assess VCP expression in both life stages of *L. infantum*, we carried out Western blot analysis on protein lysates from axenic promastigote and amastigote cultures using an anti-*Tb*VCP antibody. *Li*VCP expression is shown to be ~2.6-fold higher in amastigotes compared with promastigotes (Figure 3a).

Northern blot hybridisation using the *LiVCP* ORF as a probe demonstrated also a ~2.4-fold higher accumulation of *LiVCP* messenger RNA (mRNA) in amastigotes (Figure 3b), hence corroborating *Li*VCP protein levels.

To determine whether sequences within the *LiVCP* 3'UTR account for *Li*VCP developmental regulation, we used the *NEO* gene as read out by replacing one of the two endogenous VCP copies with the *NEO* marker in the heterozygous *Li*VCP$^{(NEO/+)}$ mutant (see Figure 4a below). Northern blot hybridisation using the *NEO* ORF as a probe revealed a 2.8-fold higher accumulation of the *NEO* transcript in amastigotes compared with promastigotes, similarly to the endogenous *LiVCP* mRNA expression (Figure 3c). Western blot analysis using an anti-NEO antibody indicated 3.5-fold higher NEO protein levels in amastigotes than in promastigotes, similarly to the endogenous *Li*VCP protein pattern (2.6- to 3.3-fold) in the wild type (WT; Figure 3a) and *Li*VCP$^{(NEO/+)}$ strains (Figure 3d). Altogether, these data indicate that preferential upregulation of *Li*VCP in amastigotes is most likely mediated by cis-acting sequences within the *LiVCP* 3'UTR.

*Li*VCP is an essential gene in *Leishmania*

To assess the cellular function of *Li*VCP, we used a targeted gene replacement strategy based on homologous recombination for depleting the *LiVCP* gene in *L. infantum* (Figure 4a). Although aneuploidy can occur in *Leishmania*, Chromosome 36 has a disomic organisation in members of the *L. donovani* complex (Rogers et al., 2011). Two independent drug resistant selection cassettes harbouring either the hygromycin phosphotransferase gene (*HYG*) or *NEO* drug resistance genes flanked by the *Li*VCP 5′- and 3'-UTR regions were made to sequentially target the *LiVCP* locus as detailed in Section 4. We have replaced successfully one of the two *LiVCP* alleles by the *NEO* targeting cassette, generating a heterozygous *Li*VCP$^{(NEO/+)}$ mutant (Figure 4b, Lane 2). However, all our attempts to generate a homozygous knockout mutant by introducing the *HYG* targeting cassette into *Li*VCP$^{(NEO/+)}$ (or *NEO*targeting cassette into *Li*VCP$^{(HYG/+)}$; data not shown) failed. Instead, we have obtained mutants harbouring the *NEO* (2.8 kb) and *HYG* (3.0 kb) gene replacement cassettes but also an additional WT *VCP* copy (4.3 kb) as shown by Southern blot hybridisation using the 3'flank VCP region as a probe (Figure 4b, Lane 3). Genetic inactivation of *LiVCP* was only possible by ectopically expressing into *LiVCP*$^{(NEO/+)}$ a hemagglutinin (HA) epitope-tagged *Li*VCP^{HA} or ^{HA}*Li*VCP (Figure 4c; upper right panel) or a nontagged version of *Li*VCP (Figure 4a). This led to the generation of three facilitated VCP homozygous knockout (dKO) mutants, *LiVCP*$^{(NEO/HYG)}$ + VCP^{HA}, *LiVCP*$^{(NEO/HYG)}$ + ^{HA}VCP,

and *LiVCP*$^{(NEO/HYG)}$ + VCP (Figure 4b; Lanes 4–6), all grown similarly to the WT as promastigotes (Figure 5a). Altogether, these results demonstrate that VCP is an essential gene in *L. infantum*.

*Li*VCP expression in the heterozygous *Li*VCP$^{(NEO/+)}$ and the facilitated VCP dKO mutants was analysed by Western blot using an anti-*Tb*VCP specific antibody (Figure 4c). A ~50% reduction in VCP levels was observed in the heterozygous *LiVCP*$^{(NEO/+)}$ and *LiVCP*$^{(NEO/HYG/+)}$ mutants (Figure 4c; Lanes 2 and 3) whereas VCP levels were on average 2-fold higher in the facilitated VCP dKO strains as compared with the WT (Figure 4c; Lanes 4–6). A similar expression pattern was observed in the *Li*VCP$^{(NEO/+)}$ mutant strain (vs. WT) grown as axenic amastigotes (Figure S2).

Decreased *Li*VCP protein expression results in *Leishmania* amastigote growth inhibition

We next assessed the growth phenotype of the heterozygous *Li*VCP$^{(NEO/+)}$ and the facilitated VCP dKO mutants under axenic amastigote conditions. The *Li*VCP$^{(NEO/+)}$ mutant (50% less VCP, Figures 4c and S2) grew as amastigotes in the first passage, but it was unable to survive in subsequent passages (Figure S3), even after several attempts (not shown). In contrary to the facilitated VCP dKO mutants *LiVCP*$^{(NEO/HYG)}$ + ^{HA}VCP and *LiVCP*$^{(NEO/HYG)}$ + VCP, the *LiVCP*$^{(NEO/HYG)}$ + VCP^{HA} mutant was unable to grow as axenic amastigotes (Figure 5b). The severe growth defect observed in *LiVCP*$^{(NEO/HYG)}$ + VCP^{HA} was rescued when ectopically expressing *Li*VCP without any epitope tag (pSPαZEOα-VCP; Figure S4a,b). These results suggest that tagging *Li*VCP at the C-terminus may alter its function specifically under conditions of amastigote growth (e.g., high temperature and acidic pH), as no effect was seen in promastigotes (Figure 5a). To explain this intriguing effect of *Li*VCP C-terminal tagging on endogenous VCP function in amastigotes, we replaced one *VCP* genomic copy by VCP^{HA} (Figure S5a,b) and evaluated VCP protein expression by Western blotting using an anti-HA antibody. Remarkably, there was a dramatic reduction of VCP^{HA} in initial amastigote passages (P1 and P2) and onwards VCP^{HA} was completely degraded, whereas no changes were observed in promastigote passages (Figure S5c). These data indicate that C-terminal tagging of *Li*VCP greatly affects protein stability, possibly due to conformational changes triggered by amastigote growth signals such as heat stress. These findings also explain the inability of VCP^{HA} to rescue the *LiVCP*$^{(NEO/HYG)}$ dKO strain under axenic amastigote growth (Figure 5b).

Impairing *Li*VCP function by dominant negative mutants targeting the *Li*VCP ATPase D2 domain has a dramatic effect on both axenic and intracellular amastigote *Leishmania* growth

To further explore the role VCP plays in *Leishmania* amastigote survival, we opted for a dominant negative approach aiming at altering the ATPase activity of *Li*VCP. Similar approaches have been used successfully in other organisms (Chou et al., 2014; Kitami et al., 2006; Piccirillo & Goldberg, 2012) including the related trypanosomatid *T. brucei* (Lamb et al., 2001). Like all VCP homologues, *Li*VCP has two tandem AAA ATPase domains (D1 and D2) harbouring Walker A and B motifs, which are responsible for ATP binding and hydrolysis, respectively (Xia et al., 2016; Figure 6a). It has been reported previously that mutating the essential glutamic acid residue in each Walker B motif to a glutamine (neutral charge) blocks ATP hydrolysis but does not affect ATP binding (Chou et al., 2014). Therefore, using a PCR-based site-directed mutagenesis strategy, we replaced the glutamate residue within each *Li*VCP ATP hydrolysis motif to a glutamine to generate two single ATPase mutants VCP^{Q1}(E295Q in ATPase D1 domain) and VCP^{Q2} (E568Q in ATPase D2), as well as a double VCP^{QQ}mutant (E295Q/E568Q; Figure 6a) (see Section 4). Ectopic expression of these *Li*VCP mutated proteins into either *L. infantum* WT or *Li*$VCP^{(NEO/+)}$ (sKO) background was confirmed by Western blot using an anti-HA antibody (Figure 6b,c). Although the $VCP^{Q1,}$ VCP^{Q2} and VCP^{QQ}mutant proteins were episomally expressed, total VCP levels did not increase over WT as shown by Western blot using an anti-VCP antibody (Figure 6d). In the *Li*$VCP^{(NEO/+)}$ strain where basal VCP protein levels are lower, ectopic expression of the VCP^{Q2} mutant or the double VCP^{QQ} mutant, but not of VCP^{Q1}, did not alter significantly endogenous VCP levels (Figure 6e).

VCP^{Q1} or VCP^{Q2} or VCP^{QQ} expression in the WT background did not affect axenic promastigote (Figure 6f) or amastigote growth (Figure 6g). However, expression of the VCP^{Q2}or the VCP^{QQ} mutant, but not of VCP^{Q1}, into the *Li*$VCP^{(NEO/+)}$ sKO background dramatically decreased axenic amastigote growth (Figure 6i) without affecting promastigote survival (Figure 6h). Considering there were no differences in amastigote growth between the $VCP^{Q2}$and VCP^{QQ} mutants (Figure 6i), we conclude that the single E568Q mutation in the ATPase D2 domain, presumably acting as a dominant negative mutant, can severely alter endogenous *Li*VCP function.

Next, we investigated the role of *Li*VCP in the parasite infectivity and intracellular survival. *L. infantum* late-stationary promastigotes from WT, *Li*$VCP^{(NEO/+)}$, *Li*$VCP^{(NEO/+)}VCP^{QQ}$, and the facilitated dKO mutant *Li*$VCP^{(NEO/HYG)}$ + VCP^{HA} were used for

infection of Phorbol 12-Myristate 13-Acetate (PMA)-treated THP1 macrophages (MØ). Prior to infection, we evaluated the ability of the VCP mutant lines to develop into metacyclic forms. No significant differences in the percentage of metacyclics (20% in average) were observed between the WT, *Li*VCP$^{(NEO/+)}$, *Li*VCP$^{(NEO/+)}$VCP^{QQ}, and the *Li*VCP$^{(NEO/HYG)}$ + VCP^{HA} strains as determined by the peanut-mediated agglutination assay (Alcolea et al., 2014; Figure S6). The percentage of infected THP1 MØ at 6 hr postinfection was evaluated at 35%–50% depending on the experiment for all strains tested (Figures S7 and S8a). No differences in the average number of parasites per MØ were also detected at 6-hr postinfection between the different strains (Figures 7 and S8b), suggesting that parasite mutant lines expressing lower VCP levels or dominant negative VCP forms showed no defect in macrophage infectivity. While the number of amastigotes per MØ was steadily increasing with time for the WT strain reaching 13 parasites at 48-hr postinfection and 37 parasites in average after 96 hr following infection, the number of *Leishmania* amastigotes per MØ for the *Li*VCP$^{(NEO/+)}$, *Li*VCP$^{(NEO/+)}$VCP^{QQ}, and *Li*VCP$^{(NEO/HYG)}$ + VCP^{HA} strains remained stable at 5–8 in average over the same period (Figure 7). This phenotype was specifically associated to an altered *Li*VCP function as rescuing the facilitated dKO mutant *Li*VCP$^{(NEO/HYG)}$ with VCP (nonepitope tagged) restored MØ infection to WT levels (Figure S8c). Similarly, although MØ infection rates increased up to 90% at 96-hr postinfection for WT parasites, the percentage of infection remained practically unchanged over time (around 30%–40%) for the mutant lines expressing lower VCP levels or dominant negative VCP forms (Figure S7). Taken together, these data indicate that when *Li*VCP expression and/or function are impaired, amastigotes stop replicating inside macrophages. Our findings with intracellular parasites corroborate the results obtained with the same mutant strains under conditions of axenic amastigote growth (Figures 5b and 6i). Globally, these results demonstrate the essential role *Li*VCP plays in *Leishmania* amastigote growth within macrophages.

_Li_VCP is essential for the parasite survival under heat stress

Our results indicate that *Li*VCP is required for both axenic and intracellular amastigote growth. *L. infantum* axenic amastigote differentiation and growth in MAA medium requires a temperature shift from 25 to 37 °C and acidic pH (5.5; Sereno, Roy, Lemesre, Papadopoulou, & Ouellette, 2001). It is well established that heat stress and acidic pH trigger amastigote differentiation (Barak et al., 2005). We therefore evaluated the effect of heat stress or acidic pH on growth of *Leishmania* parasites with decreased VCP

expression and or altered function in the presence of dominant negative mutants. Neither heat stress nor acidic pH seems to regulate *Li*VCP protein expression (Figure S9). Interestingly, we found that the dominant negative mutant VCP^{QQ} expressed in *Li*$VCP^{(NEO/+)}$ and the facilitated dKO mutant *LiVCP*$^{(NEO/HYG)}$ + VCP^{HA} both failed to grow as axenic and intracellular amastigotes (Figures 6i and 7 and S8b), were also unable to survive under heat stress or combined heat and acidic pH stress but not in acidic pH alone (Figure 8a). The dramatic decrease in VCP^{HA} protein levels seen in the *LiVCP*$^{(NEO/HYG)}$ + VCP^{HA} mutant grown as amastigotes (Figure S5c) renders this strain highly sensitive to heat stress. This temperature sensitive (ts) phenotype was fully restored by rescuing the facilitated dKO mutant *LiVCP*$^{(NEO/HYG)}$ with a nontagged VCP protein (Figure 8a).

To assess whether parasite mutant lines expressing lower VCP levels or dominant negative VCP forms were dying upon heat stress, we used the Fixable Viability Dye eFluor™ 780 which can irreversibly label dead cells detected by fluorescence-activated cell sorting. Our results demonstrate a 2-fold higher percentage of dead cells in *Leishmania* mutants with decreased or altered *Li*VCP function than in WT cells upon increasing exposure to heat stress (Figure 8b, see also Supporting File 1 for detailed results). Together, these data emphasise the essential role VCP plays for the parasite survival under heat stress.

Impairing *Li*VCP expression/function results in the accumulation of high cellular levels of polyubiquitinated proteins and increased sensitivity to proteotoxic stress

VCP/p97 is an ubiquitin-selective chaperone that uses energy through ATP hydrolysis to extract or “segregate” ubiquitylated target proteins from membranes or stable protein assemblies and present them for proteasomal degradation (Pye et al., 2006; Richly et al., 2005). Here, we investigated whether decreased *Li*VCP expression in the heterozygous *Li*$VCP^{(NEO/+)}$ mutant or impaired *Li*VCP function in the presence of dominant negative mutants targeting the ATPase D2 domain (VCP^{Q2} or VCP^{QQ}) has an effect on cellular levels of polyubiquitinated proteins. Western blot analysis using a FK2 antibody recognising K29-, K48-, and K63-linked monoubiquitilated and polyubiquitilated proteins showed that the dominant negative VCP^{Q2} or VCP^{QQ} forms expressed into the WT or *Li*$VCP^{(NEO/+)}$ background led to an increased accumulation of polyubiquitinated proteins (Figures 9 and S10, Lanes 3 and 4) in comparison with the WT (Figures 9 and S10, Lane 1). Interestingly, deletion of a single *Li*VCP allele was sufficient to increase accumulation of polyubiquitinated proteins (Figure 9a,b, Lanes 1) albeit to a lesser extent than the VCP^{Q2} or

VCP^{QQ} dominant negative mutants (Figure 9b, compare Lanes 1 with 3 and 4). Ectopic expression of VCP or VCP^{Q1} (not acting as a dominant negative mutant) into the *Li*VCP sKO background partly rescued the polyubiquitination phenotype (Figure 9b, Lanes 2 and 5). Altogether, these data suggest a direct link between *Li*VCP function and the removal of polyubiquitinated substrates for subsequent proteosomal degradation as is the case for other eukaryotic VCP homologues (Meyer et al., 2012).

Furthermore, we tested whether parasite mutant lines with a significant decrease in VCP expression levels are more sensitive to proteasome inhibitors or to other stresses inducing proteotoxicity. Proteosome inhibition by MG-132 is known to increase accumulation of polyubiquitinated proteins, also in *Leishmania* (Padmanabhan et al., 2016). Both the *Li*$VCP^{(NEO/+)}$ and the *Li*$VCP^{(NEO/HYG)}$ + VCP^{HA} strains showed ~2-fold higher sensitivity to MG-132 than the WT strain (Figure S11a,c). Inducing proteotoxicity by L-azetidine-2-carboxylic acid, a toxic proline analogue incorporated into proteins competitively with proline (Fowden, Lewis, & Tristram, 1967) and causing protein misfolding, led to >2-fold sensitivity to L-azetidine-2-carboxylic acid in the *Li*$VCP^{(NEO/HYG)}$ + VCP^{HA} strain compared with the WT (Figure S11b,c). These results suggest that *Li*VCP is important for the *Leishmania* response to proteotoxic stress.

2.6 Discussion

In this study, we provide functional insights into the crucial role the *Leishmania* VCP/p97 homologue plays in the parasite intracellular development. We show that although *VCP* is an essential gene in *Leishmania*, consistent with previous findings in other eukaryotes (Fröhlich et al., 1991; Lamb et al., 2001; Müller, Deinhardt, Rosewell, Warren, & Shima, 2007), promastigote forms can grow normally with less VCP (50% less) or impaired VCP activity by a dominant negative approach. In contrast, parasites exposed to heat stress and amastigote forms grown axenically or inside macrophages strictly depend on VCP for growth. Indeed, decreasing *Li*VCP expression by heterozygous gene replacement or by overexpressing a ts VCP mutant or impairing VCP's function using dominant negative mutants specifically targeting the putative *Li*VCP ATPase D2 domain has a dramatic effect on intracellular amastigote growth and the parasite ability to survive under heat stress. The increased need for VCP in *Leishmania* amastigotes is further supported by our results that *LiVCP* mRNA undergoes 3'UTR-mediated developmental regulation, leading to higher protein levels in the amastigote life stage of the parasite.

An interesting finding here is the demonstration that altering VCP function by ectopically expressing in the heterozygous *Li*VCP$^{NEO/+}$ strain (50% less VCP) dominant negative VCP mutant forms (VCP^{Q2} and also VCP^{QQ}) with the essential glutamic acid residue in the D2 ATPase Walker B motif mutated to a glutamine specifically inhibits amastigote but not promastigote growth. No effect on parasite survival was seen with the dominant negative VCP^{Q1} mutant interfering with the D1 ATPase motif, hence emphasising the importance of the D2 domain in VCP function under conditions of amastigote growth or exposure to heat stress. Previous studies have shown that the two ATPase domains of VCP/p97 are not functionally equivalent. Both ATPase rings hydrolyse ATP, but the D2 domain seems to be the major contributor of the overall ATPase activity (Chou et al., 2014; Song et al., 2003). Studies using D2 specific inhibitors demonstrated that D1 contributes to the overall ATPase activity by ~30% (Chou et al., 2014). ATP binding/hydrolysis of VCP/p97 by the D2 ring is central to VCP's function as it results in important conformational changes of the homohexameric VCP complex (Beuron et al., 2006; Rouiller et al., 2002), which provide the energy required for ubiquitin-directed disassembly of macromolecular complexes (Pye et al., 2006) and transfer of the polyubiquitinated substrates to the 26S proteasome for degradation (Richly et al., 2005). Moreover, the conserved glutamic acid residue in Walker B of D2 domain acts as a switch from an active to an inactive conformation upon ATP binding (Stach & Freemont, 2017).

Our finding that VCP^{Q2} or VCP^{QQ} act presumably as dominant negative mutants specifically in amastigotes is intriguing given that no significant differences in the expression ratio *Li*VCP WT versus *Li*VCP^{Q2} or *Li*VCP^{QQ} mutant proteins were observed between promastigotes and amastigotes. In *T. brucei*, constitutive overexpression of *Tb*VCP harbouring a single mutation in the second ATP hydrolysis motif (Q2) or mutations in both hydrolysis motifs (QQ) directly resulted in cell death but in the procyclic forms (Lamb et al., 2001). It has been reported that the VCP ATPase activity could be influenced by physical parameters such as temperature (Song et al., 2003). *Leishmania* amastigotes grow at elevated temperature (37 °C) as opposed to promastigotes (25 °C). It is therefore possible that conformational changes within the hexameric VCP structure triggered by temperature stress contribute to the differential dominant negative effect seen between promastigote and amastigote forms. While attempting to generate a *Li*VCP homozygous mutant by episomally expressing VCP^{HA}, we obtained a facilitated double knockout mutant with no growth defect in promastigotes (25 °C) but a lethal phenotype in the amastigote stage (37 °C). In fact, we showed that C-terminal tagging of *Li*VCP renders the protein highly unstable only in

amastigotes and promotes its degradation. These data suggest that the C-terminus of *Li*VCP is critical for the stability of the protein under heat stress as also hypothesised in the yeast model (Marinova et al., 2015). It was shown previously that the unstructured VCP C-terminal tail plays possibly a role in maintaining the conformation of the D2 module during the ATPase cycle (Niwa et al., 2012). As a result of the *Li*VCP^{HA} protein instability at 37 °C, this facilitated VCP dKO mutant exhibits a ts phenotype being thus unable to grow under heat stress. This ts phenotype prevents also growth as amastigotes, emphasising the crucial role VCP plays for the *Leishmania* survival under heat stress. A ts phenotype has been described previously in Cdc48 (VCP) mutants in yeast (Marinova et al., 2015). Noteworthy, while in *Leishmania* the *Li*VCP$^{NEO/HYG}$ + VCP^{HA} ts phenotype can be reversed only by expressing a nontagged WT VCP protein in this mutant, in yeast even the introduction of different spontaneous mutations inside the Cdc48 sequence could suppress the ts phenotype (Marinova et al., 2015).

Here, we also show that a ~50% decrease in the expression of *Li*VCP (*Li*VCP$^{NEO/+}$) or an alteration of its function using a dominant negative approach triggers the accumulation of high cellular levels of polyubiquitinated proteins. Increased polyubiquitination has no significant effect on promastigote growth. However, in amastigotes where heat stress further induces proteotoxicity, the requirement for VCP is more critical in ensuring cellular proteostasis. This is also in agreement with VCP being more expressed (~3-fold) in *Leishmania* amastigotes. VCP functions as an ubiquitin-selective chaperone in other eukaryotes and is central to multiple protein quality control pathways mediated by the Ubiquitin Proteasome System (Meyer et al., 2012; van den Boom & Meyer, 2017). Polypeptides modified with K48-linked polyubiquitin chains, which also serve as a major targeting signal for the proteasome (Chau et al., 1989), are physiological substrates for VCP. Our previous studies revealed *Li*VCP association with several proteasome subunits (Padmanabhan et al., 2016). The partial colocalisation of *Li*VCP with the ER and its weaker association with the mitochondrion, as suggested by indirect immunofluorescence studies, are in line with *Li*VCP being involved in the extraction of polyubiquitinated proteins from cellular organelles for subsequent proteasomal degradation, as described in other eukaryotes (Qi et al., 2017; Taylor & Rutter, 2011). Although the function of Cdc48/p97 is best understood in ERAD (Stein et al., 2014), how this process is regulated remains still unclear. Ubx2, an integral ER membrane protein, recruits Cdc48 to the ER and mediates binding of Cdc48 to ER ubiquitin ligases and to ERAD substrates (Schuberth & Buchberger, 2005). After polyubiquitylation of the protein substrates, Cdc48 together with

its cofactor complex Ufd1-Npl4 pulls the misfolded proteins out and away from the ER membrane and delivers them to degradation by the proteasome (Wolf & Stolz, 2012; Ye, Meyer, & Rapoport, 2003). The higher sensitivity of the *Li*VCP$^{NEO/+}$ and the *Li*VCP$^{(NEO/HYG)}$ + VCP^{HA} mutant strains to the proteasome inhibitor MG-132 further supports a similar role for *Li*VCP. Accumulation of polyubiquitinated proteins was even higher upon expression of the VCP^{Q2} or VCP^{QQ}dominant negative mutants, especially into the *Li*VCP$^{NEO/+}$ background, suggesting that the presumably impaired ATPase D2 domain-mediated ATP hydrolysis is very important for the ubiquitin-selective chaperone function of *Li*VCP.

In summary, this study provides the first characterisation of the essential ubiquitin selective chaperone VCP/p97 in *Leishmania*. Our results emphasise the crucial role *Li*VCP plays in the parasite intracellular development and its survival particularly under heat stress. VCP is central to multiple essential protein quality control pathways and VCP-associated mutations in humans have been implicated in a multitude of diseases, including cancer and neurodegeneration (Fessart et al., 2013; Meyer & Weihl, 2014; Tang & Xia, 2016). Thus, VCP/p97 has emerged as an important therapeutic target not only for cancer and neurodegeneration (Anderson et al., 2015; Chapman, Maksim, de la Cruz, & Clair, 2015; Vekaria, Home, Weir, Schoenen, & Rao, 2016) but also for parasitic diseases (Harbut et al., 2012). A more comprehensive understanding of the function and regulation of VCP in maintaining protein homeostasis in *Leishmania,* especially under conditions of intracellular stress, would not only increase knowledge of how this parasite responds to stress but also lead to novel therapeutic interventions.

2.7 Experimental procedures

Parasite strains and cell culture

Leishmania infantum MHOM/MA/67/ITMAP-263 was used in this study. L. infantumpromastigotes were cultured in SDM-79 medium supplemented with 10% heat-inactivated Fetal calf serum (FCS) (Multicell Wisent Inc., Canada) and 5 µg/ml hemin at pH 7.0 and 25 °C. L. infantum axenic amastigotes were grown in MAA-20 medium supplemented with 20% FCS in 5% CO_2 atmosphere at pH 5.5 and 37 °C (Sereno et al., 2001). THP1 Human Acute Monocytic Leukaemia Cell Line was seeded in a 16-well chamber and infected with L. infantum stationary promastigotes as described previously (Chow, Cloutier, Dumas, Chou, & Papadopoulou, 2011).

Sequence alignments

Protein sequence alignments of the *L. donovani* transitional ER ATPase (LdVCP), putative (NCBI, CBZ38580.1), the *Homo sapiens* p97 (NCBI, P55072.4), and *T. brucei* TbVCP (NCBI, AAC02215.1) VCP homologues were carried out by ClustalW (Larkin et al., 2007) multiple alignment using Bioedit sequence Alignment Editor (Hall, 1999). The evolutionary history including *L. donovani* (CBZ38580.1), *Leishmania major* (XP_001686709.1), *Leptomonas pyrrhocoris* (XP_015658481.1), *Phytomonas* sp. (CCW67021.1), *T. brucei* (AAC02215.1) *Plasmodium vivax* (XP_001616207.1), *Mus musculus* (BAE40919.1), *Homo sapiens* (P55072.4), *Danio rerio* (BAC87740.1), *Arabidopsis thaliana* (OAO95421.1), *Glycine max* (NP_001235099.1) and *S cerevisiae (NP_010157.1)* was inferred using the neighbour-joining method (Saito & Nei, 1987). The optimal tree with the sum of branch length = 1.17841600 is shown. The percentage of replicate trees in which the associated taxa clustered together in the bootstrap test (1,000 replicates) are shown next to the branches (Felsenstein, 1985). The tree is drawn to scale, with branch lengths in the same units as those of the evolutionary distances used to infer the phylogenetic tree. The evolutionary distances were computed using the Poisson correction method (Zuckerkandl & Pauling, 1965) and are in the units of the number of aa substitutions per site. The analysis involved 12 aa sequences. All positions containing gaps and missing data were eliminated. There were a total of 771 positions in the final dataset. Evolutionary analyses were conducted in MEGA7 (Kumar, Stecher, & Tamura, 2016).

Plasmid constructs and transfections

The *VCP* gene from *L. infantum* genomic DNA (LinJ.36.1420; TriTrypDB; http://tritrypdb.org) was amplified by PCR using specific primers (see Table S1). The amplified product was cloned into HindIII and XbaI sites of pSP72αZEOα (Richard, Leprohon, Drummelsmith, & Ouellette, 2004) to generate plasmid pSP-αZEOα-*Li*VCP. ZEO represents the zeocin resistance gene and the symbol α represents the intergenic region of the *Leishmania enriettii* α-tubulin gene necessary for trans-splicing and polyadenylation. To generate a heterozygous mutant (*Li*VCP$^{(NEO/+)}$) where one of the two *L. infantum VCP* genomic copies was replaced by the neomycin phosphotransferase (*NEO*) gene, VCP 5′- and 3′-flanking regions were amplified from genomic DNA and fused to the *NEO* gene as shown in Figure 4a. The fused fragment was cloned into pGEM-T-Easy (Promega) and released by NotI and NdeI for transfection and integration into the *L. infantum* wild type

strain. The same strategy was applied to delete the second *VCP* genomic allele using the *HYG* targeting cassette (5'flank VCP-HYG-3'flank VCP). *VCP* amplified products containing an HA epitope tag either at the VCP C-terminus (VCP^{HA}) or N-terminus (^{HA}VCP) or without HA-tag (VCP) were cloned into HindIII and XbaI sites of pSPαBLASTα (Coelho, Leprohon, & Ouellette, 2012). BLAST stands for blasticidin resistance gene. The generated plasmids were then transfected into the *L. infantum* wild type or the *Li*$VCP^{(NEO/+)}$ sKO strain. Facilitated double knockout mutants (*Li*$VCP^{(NEO/HYG)}$ + VCP^{HA}, *Li*$VCP^{(NEO/HYG)}$ + ^{HA}VCP and *Li*$VCP^{(NEO/HYG)}$ + VCP) were generated using the 5'flankVCP-HYG-3'flankVCP cassette in the presence of one of the above VCP-tagged proteins in *Li*$VCP^{(NEO/+)}$background. To generate the *Li*VCP ATPase domain mutants, we used a Phusion DNA polymerase (NEB)-based PCR combined with a modified megaprimer PCR method (Ke, 1997). We used two round of PCR reactions to introduce a specific point mutation G883C (E295Q) in the Walker B site of ATPase D1 domain (mutation Q1) or a G1701C (E568Q) in ATPase D2 (mutation Q2) or in both sites (mutation QQ) using specific set of primers (see strategy in Table S1). The three VCP mutated products (*V*CP^{Q1}, VCP^{Q2}, and VCP^{QQ}) were initially cloned into pGEM-T-Easy and then into XbaI and HindIII sites of pSPαZEOα vector and next transfected into WT (*Li*$VCP^{(+/+)}$) and sKO (*Li*$VCP^{(NEO/+)}$) *L. infantum* promastigotes. A nonmutated VCP was used as a control. Purified plasmid DNA (10–20 µg, Qiagen Plasmid Mini Prep Kit, Toronto, Ontario, Canada) or linearised fragments (10–20 µg) were transfected into *Leishmania* by electroporation as described (Lamontagne & Papadopoulou, 1999). Stable transfectants were selected and cultivated with either 0.025 mg/ml G418 (Sigma) or 0.16 mg/ml Hygromycin-B (Sigma) or 0.6 mg/ml zeomycin (Sigma) or 0.045 mg/ml blasticidin (Sigma).

Protein lysate preparations and Western blots

Western blots were performed following standard procedures. The antimouse alpha-tubulin antibody (1:10000 dilution; Sigma), the antimouse HA tag monoclonal antibody (1:3000; ABM), the antimouse monoubiquitinated and polyubiquitinated conjugates monoclonal antibody (FK2; 1:5000 and blocking in 1% BSA, Enzo), the antimouse HSP60 (mitochondrial) antibody (1:400, Acris), the antimouse *T brucei* VCP antibody (1:5000; Roggy & Bangs, 1999) kindly provided by Dr. James D. Bangs (Department of Microbiology & Immunology, Jacobs School of Medicine & Biomedical Sciences, University at Buffalo, USA), and the rabbit polyclonal anti-*T. brucei* BiP (kindly provided by Dr. J.D. Bangs) were

used in this study. As a secondary antibody, we used the antimouse Horseradish peroxidase (HRP) (Cell Signalling) or the anti-rabbit-HRP antibody (GE Healthcare). Blots were visualised by chemoluminescence with Pierce ECL2 Western blotting kit (Thermo Scientific). Protein levels were quantified by densitometric analyses using the ImageJ 1.38x software (Schneider, Rasband, & Eliceiri, 2012). Fractionation of total proteins of *L. infantum* was undertaken in the presence of increasing concentrations of digitonin (20 µM to 10 mM) as described previously (Foucher, Papadopoulou, & Ouellette, 2006), and each fraction was analysed by Western blot.

DNA and RNA analysis and hybridizations

DNA and RNA analysis and hybridisations studies were done as described previously (Padmanabhan, Samant, Cloutier, Simard, & Papadopoulou, 2012). Genomic DNA and total RNA of *L. infantum* were extracted using DNAzol (Life Technologies Inc., Toronto, Ontario, Canada) and Trizol (Invitrogen) following the manufacturer's instructions. Southern and Northern blot hybridisations were performed following standard procedures (Rio, 2015). Double-stranded DNA probes were radiolabelled with [α-32P] dCTP using random oligonucleotides and Klenow fragment DNA polymerase I (New England Biolabs). Hybridisation intensity signals of *Li*VCP or NEO were normalised to the 18S rRNA or to the α-tubulin mRNA by densitometric analyses using the ImageJ 1.38x software.

Immunofluorescence studies

Immunofluorescence microscopy studies were done as described previously (Padmanabhan et al., 2016). Briefly, 2−4 × 10^7/ml *L. infantum* parasites were spotted on a slide (spread 5 µl), air dried at Room temperature (RT) and fixed in 2% paraformaldehyde for 10 min. Following washings in 1xPBS, cells were permeabilised in 1xPBS, 0.2% Triton X-100, and 5% FCS at RT for 30 min and blocked in 1xPBS, 2% milk, 0.02% Tween 20, and 0.1% Triton X-100 for 1 hr at RT. The anti-*T. brucei* VCP antibody was used as primary antibody followed by Alexa Fluor® 488 antimouse as secondary antibody. Nucleus and kinetoplast DNA was stained with DAPI (blue). Images are maximal Z-projections of 20 to 30 contiguous sections separated by 0.15 µm and acquired with a 63x objective using a Quorum WaveFX spinning disk confocal system (Quorum Technologies, Guelph, Ontario). Image acquisition and processing was performed using Volocity 4.2.1 analysis software.

Flow cytometry analysis

To monitor cellular death, *L. infantum* parasites (10^7) grown in SDM-79 medium were stained for 30 min with eBioscience™ Fixable Viability Dye eFluor™ 780 (eBiosciences, San Diego, CA), which can irreversibly label dead cells prior to detection by fluorescence-activated cell sorting. Cells were then washed with PBS1x, fixed with paraformaldehyde 4% and stored at 4 °C protected from light prior to their analysis by FACS Canto flow cytometer (BD Biosciences). Data were processed using the BD FACSDiva™ Software v. 6.1.3 (BD Biosciences). The entire raw data can be accessed in Supporting File 1.

Statistical analyses

All analyses were performed using GraphPad Prism software (version 5.01; GraphPad, La Jolla, CA, USA). Statistical significance was assessed by two-tailed unpaired *t*-test. Statistical significance was set at $P \leq 0.05$ ($^{**}P \leq 0.01$ and $^{***}P \leq 0.001$).

2.8 Acknowledgements

We thank Dr. James D. Bangs for having kindly provided the anti *Trypanosoma brucei* VCP antibody.

BA is a recipient of doctoral fellowships from the CAPES 'Frontiers without Borders' program. This work was supported by the Canadian Institutes of Health Research (CIHR) operating grant MOP-12182 and the Natural Sciences and Engineering Research Council of Canada (NSERC) Discovery Grant GC100741 (418444) awarded to BP.

2.9 Conflict of interest

The authors declare no conflicts of interest.

2.10 Rereferences

Alcolea, P. J., Alonso, A., Garcia-Tabares, F., Toraño, A., & Larraga, V. (2014). An insight into the proteome of *Crithidia*fasciculate choanoamastigotes as a comparative approach to axenic growth, peanut lectin agglutination and differentiation of *Leismania* spp. promastigotes. *PLoS one*, **9**(12), e113837.

Anderson, D. J., Le Moigne, R., Djakovic, S., Kumar, B., Rice, J., Wong, S., … Rolfe, M.(2015). Targeting the AAA ATPase p97 as an approach to treat cancer through disruption of protein homeostasis. *Cancer Cell*, **28**(5), 653–665.

Barak, E., Amin-Spector, S., Gerliak, E., Goyard, S., Holland, N., & Zilberstein, D.(2005). Differentiation of *Leishmania donovani* in host-free system: Analysis of signal perception and response. *Molecular and Biochemical Parasitology*, **141**(1), 99–108.

Benerjee, S., Bartesaghi, A., Merk, A., Rao, P., Bulfer, S. L., Yan, Y., … Subramaniam, S.(2016). 2.3 Å resolution cryo-EM structure of human p97 and mechanism of allosteric inhibition. *Science*, **351**(6275), 871–875.

Beuron, F., Dreveny, I., Yuan, X., Pye, V. E., Mckeown, C., Briggs, L. C., … Freemont, P. S. (2006). Conformational changes in the AAA ATPase p97–p47 adaptor complex. *The EMBO Journal*, **25**(9), 1967–1976.

Bodnar, N. O., & Rapoport, T. A. (2017a). Molecular mechanism of substrate processing by the Cdc48 ATPase complex. *Cell*, **169**(4), 722–735.e9.

Bodnar, N. O., & Rapoport, T. A. (2017b). Toward an understanding of the Cdc48/p97 ATPase. *F1000Research*, **6**(0), 1318.

Brandman, O., Stewart-Ornstein, J., Wong, D., Larson, A., Williams, C. C. C., Li, G.-W., … Weissman, J. S. S. (2012). A ribosome-bound quality control complex triggers degradation of nascent peptides and signals translation stress. *Cell*, **151**(5), 1042–1054.

Buchan, J. R., Kolaitis, R.-M., Taylor, J. P., & Parker, R. (2013). Eukaryotic stress granules are cleared by autophagy and Cdc48/VCP function. *Cell*, **153**(7), 1461–1474.

Buchberger, A., Schindelin, H., & Hänzelmann, P. (2015). Control of p97 function by cofactor binding. *FEBS Letters*, **589**(19PartA), 2578–2589.

Chapman, E., Maksim, N., de la Cruz, F., & Clair, J. (2015). Inhibitors of the AAA+ Chaperone p97. *Molecules*, **20**(2), 3027–3049.

Chau, V., Tobias, J. W., Bachmair, A., Marriott, D., Ecker, D. J., Gonda, D. K., & Varshavsky, A. (1989). A multiubiquitin chain is confined to specific lysine in a targeted short-lived protein. *Science, New Series*, **243**(4898), 1576–1583.

Chou, T.-F., Bulfer, S. L., Weihl, C. C., Li, K., Lis, L. G., Walters, M. A., … Arkin, M. R.(2014). Specific inhibition of p97/VCP ATPase and kinetic analysis demonstrate interaction between D1 and D2 ATPase domains. *Journal of Molecular Biology*, **426**(15), 2886–2899.

Chow, C., Cloutier, S., Dumas, C., Chou, M.-N., & Papadopoulou, B. (2011). Promastigote to amastigote differentiation of *Leishmania* is markedly delayed in the absence of PERK eIF2alpha kinase-dependent eIF2alpha phosphorylation. *Cellular Microbiology*, **13**(7), 1059–1077.

Christianson, J. C., & Ye, Y. (2014). Cleaning up in the endoplasmic reticulum: Ubiquitin in charge. *Nature Structural & Molecular Biology*, **21**(4), 325–335.

Coelho, A. C., Leprohon, P., & Ouellette, M. (2012). Generation of *Leishmania*hybrids by whole genomic DNA transformation. *PLoS Neglected Tropical Diseases*, **6**(9), e1817.

Davies, J. M., Brunger, A. T., & Weis, W. I.(2008). Improved structures of full-length p97, an AAA ATPase: Implications for mechanisms of nucleotide-dependent conformational change. *Structure*, **16**(5), 715–726.

DeLaBarre, B., & Brunger, A. T. (2003). Complete structure of p97/valosin-containing protein reveals communication between nucleotide domains. *Nature Structural Biology*, **10**(10), 856–863.

Felsenstein, J. (1985). Confidence limits on phylogenies: An approach using the bootstrap. *Evolution*, **39**(4), 783.

Fessart, D., Marza, E., Taouji, S., Delom, F., & Chevet, E. (2013). P97/CDC-48: Proteostasis control in tumor cell biology. *Cancer Letters*, **337**(1), 26–34.

Foucher, A. L., Papadopoulou, B., & Ouellette, M. (2006). Prefractionation by digitonin extraction increases representation of the cytosolic and intracellular proteome of *Leishmania infantum*. *Journal of Proteome Research*, **5**(7), 1741–1750.

Fowden, L., Lewis, D., & Tristram, H.(1967). Toxic amino acids: Their action as antimetabolites. *Advances in Enzymology and Related Areas of Molecular Biology*, **29**, 89–163. PMID: 4881886

Franz, A., Ackermann, L., & Hoppe, T.(2014). Create and preserve: Proteostasis in development and aging is governed by Cdc48/p97/VCP. *Biochimica et Biophysica Acta (BBA) - Molecular Cell Research*, **1843**(1), 205–215.

Franz, A., Ackermann, L., & Hoppe, T.(2016). Ring of change: CDC48/p97 drives protein dynamics at chromatin. *Frontiers in Genetics*, **7**(MAY), 1–14.

Fröhlich, K. U., Fries, H. W., Rüdiger, M., Erdmann, R., Botstein, D., & Mecke, D.(1991). Yeast cell cycle protein CDC48p shows full-length homology to the mammalian protein VCP and is a member of a protein family involved in secretion, peroxisome formation, and gene expression. *The Journal of Cell Biology*, **114**(3), 443–453.

Hall, T. A. (1999). BioEdit: A user-friendly biological sequence alignment editor and analysis program for Windows 95/98/NT. *Nucleic Acids Symposium Series*, **41**, 95–98.

Hänzelmann, P., & Schindelin, H. (2017). The interplay of cofactor interactions and post-translational modifications in the regulation of the AAA+ ATPase p97. *Frontiers in Molecular Biosciences*, **4**(April), 1–22.

Harbut, M. B., Patel, B. A., Yeung, B. K. S., McNamara, C. W., Bright, A. T., Ballard, J., … Greenbaum, D. C. (2012). Targeting the ERAD pathway via inhibition of signal peptide peptidase for antiparasitic therapeutic design. *Proceedings of the National Academy of Sciences*, **109**(52), 21486–21491.

Heo, J.-M., Livnat-Levanon, N., Taylor, E. B., Jones, K. T., Dephoure, N., Ring, J., … Rutter, J. (2010). A stress-responsive system for mitochondrial protein degradation. *Molecular Cell*, **40**(3), 465–480.

Ke, S. (1997). Rapid and efficient site-directed mutagenesis by single-tube “megaprimer” PCR method. *Nucleic Acids Research*, **25**(16), 3371–3372.

Kitami, M.-I. I., Kitami, T., Nagahama, M., Tagaya, M., Hori, S., Kakizuka, A., … Hattori, N. (2006). Dominant-negative effect of mutant valosin-containing protein in aggresome formation. *FEBS Letters*, **580**(2), 474–478.

Kumar, S., Stecher, G., & Tamura, K.(2016). MEGA7: Molecular evolutionary genetics analysis version 7.0 for bigger datasets. *Molecular Biology and Evolution*, **33**(7), 1870–1874.

Lamb, J. R., Fu, V., Wirtz, E., & Bangs, J. D.(2001). Functional analysis of the trypanosomal AAA protein Tb VCP with trans-dominant ATP hydrolysis mutants. *Journal of Biological Chemistry*, **276**(24), 21512–21520.

Lamontagne, J., & Papadopoulou, B.(1999). Developmental regulation of spliced leader RNA gene in *Leishmania donovani* amastigotes is mediated by specific polyadenylation. *Journal of Biological Chemistry*, **274**(10), 6602–6609.

Larkin, M. A. A., Blackshields, G., Brown, N. P. P., Chenna, R., McGettigan, P. A. A., McWilliam, H., … Higgins, D. G. G. (2007). Clustal W and Clustal X version 2.0. *Bioinformatics*, **23**(21), 2947–2948.

Marinova, I. N., Engelbrecht, J., Ewald, A., Langholm, L. L., Holmberg, C., Kragelund, B. B., … Hartmann-Petersen, R. (2015). Single site suppressors of a fission yeast temperature-sensitive mutant in Cdc48 identified by whole genome sequencing. *PLoS one*, **10**(2), e0117779.

Meyer, H., Bug, M., & Bremer, S. (2012). Emerging functions of the VCP/p97 AAA-ATPase in the ubiquitin system. *Nature Cell Biology*, **14**(2), 117–123.

Meyer, H., & Weihl, C. C. (2014). The VCP/p97 system at a glance: Connecting cellular function to disease pathogenesis. *Journal of Cell Science*, **127**(18), 3877–3883.

Müller, J. M. M., Deinhardt, K., Rosewell, I., Warren, G., & Shima, D. T. (2007). Targeted deletion of p97 (VCP/CDC48) in mouse results in early embryonic lethality. *Biochemical and Biophysical Research Communications*, **354**(2), 459–465.

Niwa, H., Ewens, C. A., Tsang, C., Yeung, H. O., Zhang, X., & Freemont, P. S. (2012). The role of the N-domain in the ATPase activity of the mammalian AAA ATPase p97/VCP. *Journal of Biological Chemistry*, **287**(11), 8561–8570.

Padmanabhan, P. K., Samant, M., Cloutier, S., Simard, M. J., & Papadopoulou, B.(2012). Apoptosis-like programmed cell death induces antisense ribosomal RNA (rRNA) fragmentation and rRNA degradation in *Leishmania*. *Cell Death and Differentiation*, **19**(12), 1972–1982.

Padmanabhan, P. K., Zghidi-Abouzid, O., Samant, M., Dumas, C., Aguiar, B. G., Estaquier, J., & Papadopoulou, B. (2016). DDX3 DEAD-box RNA helicase plays a central role in mitochondrial protein quality control in *Leishmania*. *Cell Death and Disease*, **7**(10), e2406.

Papadopoulos, C., Kirchner, P., Bug, M., Grum, D., Koerver, L., Schulze, N., … Meyer, H. (2017). VCP/p97 cooperates with YOD1, UBXD1 and PLAA to drive clearance of ruptured lysosomes by autophagy. *The EMBO Journal*, **36**(2), 135–150.

Piccirillo, R., & Goldberg, A. L. (2012). The p97/VCP ATPase is critical in muscle atrophy and the accelerated degradation of muscle proteins. *EMBO Journal*, **31**(15), 3334–3350.

Pye, V. E., Dreveny, I., Briggs, L. C., Sands, C., Beuron, F., Zhang, X., & Freemont, P. S.(2006). Going through the motions: The ATPase cycle of p97. *Journal of Structural Biology*, **156**(1), 12–28.

Qi, L., Tsai, B., & Arvan, P. (2017). New insights into the physiological role of endoplasmic reticulum-associated degradation. *Trends in Cell Biology*, **27**(6), 430–440.

Richard, D., Leprohon, P., Drummelsmith, J., & Ouellette, M. (2004). Growth phase regulation of the main folate transporter of *Leishmania infantum* and its role in methotrexate resistance. *Journal of Biological Chemistry*, **279**(52), 54494–54501.

Richly, H., Rape, M., Braun, S., Rumpf, S., Hoege, C., & Jentsch, S. (2005). A series of ubiquitin binding factors connects CDC48/p97 to substrate multiubiquitylation and proteasomal targeting. *Cell*, **120**(1), 73–84.

Rio, D. C. (2015). Northern blots: Capillary transfer of RNA from agarose gels and filter hybridization using standard stringency conditions. *Cold Spring Harbor Protocols*, **2015**(3), 306–313.

Rogers, M. B., Hilley, J. D., Dickens, N. J., Wilkes, J., Bates, P. A., Depledge, D. P., … Mottram, J. C. (2011). Chromosome and gene copy number variation allow major structural change between species and strains of *Leishmania*. *Genome Research*, **21**(12), 2129–2142.

Roggy, J. L., & Bangs, J. D. (1999). Molecular cloning and biochemical characterization of a VCP homolog in African trypanosomes. *Molecular and Biochemical Parasitology*, **98**(1), 1–15.

Rouiller, I., DeLaBarre, B., May, A. P., Weis, W. I., Brunger, A. T., Milligan, R. A., & Wilson-Kubalek, E. M. (2002). Conformational changes of the multifunction p97 AAA ATPase during its ATPase cycle. *Nature Structural Biology*, **9**(12), 950–957.

Saito, N., & Nei, M. (1987). The neighbor-joining method: A new method for reconstructing phylogenetic trees. *Molecular Biology and Evolution*, **4**(4), 406–425.

Schneider, C. A., Rasband, W. S., & Eliceiri, K. W. (2012). NIH Image to ImageJ: 25 years of image analysis HISTORICAL commentary. *Nature Methods*, **9**(7), 671–675.

Schuberth, C., & Buchberger, A. (2005). Membrane-bound Ubx2 recruits Cdc48 to ubiquitin ligases and their substrates to ensure efficient ER-associated protein degradation. *Nature Cell Biology*, **7**(10), 999–1006.

Sereno, D., Roy, G., Lemesre, J. L., Papadopoulou, B., & Ouellette, M. (2001). DNA transformation of *Leishmania infantum* axenic amastigotes and their use in drug screening. *Antimicrobial Agents and Chemotherapy*, **45**(4), 1168–1173.

Song, C., Wang, Q., & Li, C.-C. H. (2003). ATPase activity of p97-valosin-containing protein (VCP). *Journal of Biological Chemistry*, **278**(6), 3648–3655.

Stach, L., & Freemont, P. S. (2017). The AAA+ ATPase p97, a cellular multitool. *Biochemical Journal*, **474**(17), 2953–2976.

Stein, A., Ruggiano, A., Carvalho, P., & Rapoport, T. A. (2014). Key steps in ERAD of luminal ER Proteins reconstituted with purified components. *Cell*, **158**(6), 1375–1388.

Tang, W. K., & Xia, D. (2016). Mutations in the human AAA+ chaperone p97 and related diseases. *Frontiers in Molecular Biosciences*, **3**(December), 1–12.

Taylor, E. B., & Rutter, J. (2011). Mitochondrial quality control by the ubiquitin–proteasome system: Figure 1. *Biochemical Society Transactions*, **39**(5), 1509–1513.

van den Boom, J., & Meyer, H. (2017). VCP/p97-mediated unfolding as a principle in protein homeostasis and signaling. *Molecular Cell*, **69**, 1–13.

Vaz, B., Halder, S., & Ramadan, K. (2013). Role of p97/VCP (Cdc48) in genome stability. *Frontiers in Genetics*, **4**(April), 60.

Vekaria, P. H., Home, T., Weir, S., Schoenen, F. J., & Rao, R. (2016). Targeting p97 to disrupt protein homeostasis in cancer. *Frontiers in Oncology*, **6**(August), 181.

Wolf, D. H., & Stolz, A. (2012). The Cdc48 machine in endoplasmic reticulum associated protein degradation. *Biochimica et Biophysica Acta - Molecular Cell Research*, **1823**(1), 117–124.

Xia, D., Tang, W. K., & Ye, Y. (2016). Structure and function of the AAA+ ATPase p97/Cdc48p. *Gene*, **583**(1), 64–77.

Ye, Y., Meyer, H. H., & Rapoport, T. A.(2003). Function of the p97–Ufd1–Npl4 complex in retrotranslocation from the ER to the cytosol. *The Journal of Cell Biology*, **162**(1), 71–84.

Ye, Y., Tang, W. K., Zhang, T., & Xia, D.(2017). A mighty “protein extractor” of the cell: Structure and function of the p97/CDC48 ATPase. *Frontiers in Molecular Biosciences*, **4**(June), 1–20.

Zuckerkandl, E., & Pauling, L. (1965). Evolutionary divergence and convergence in proteins. In V. Bryson, & H. J. Vogel(Eds.), *Evolving Genes and Proteins* (pp. 97–166). New York: Academic Press.

2.11 Figures

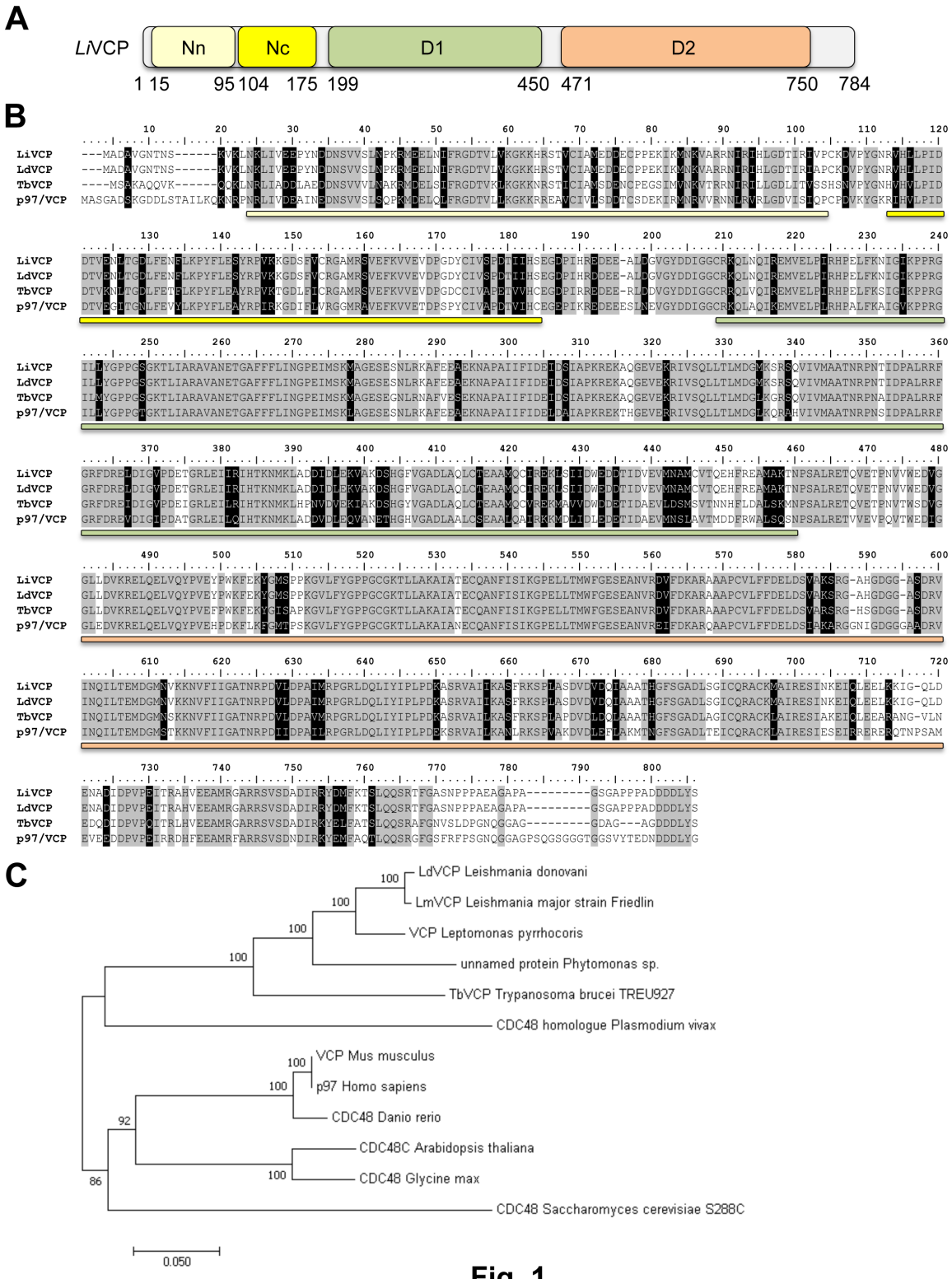

Fig. 1

FIGURE 1 The *Leishmania infantum Li*VCP/p97 homolog is highly conserved among its eukaryotic counterparts. (A) Schematic representation of the *L. infantum* VCP/p97 homolog (*Li*VCP) and its conserved domains, including the N-terminal (Nn and Nc subdomains) region and the two ATPase domains D1 and D2. (B) Sequence alignments of the PCR-amplified *VCP* sequence from *L. infantum* translated into protein along with the *L. donovani* valosin-containing protein (LdBPK_361420.1, http://tritrypdb.org), the *Trypanosoma brucei Tb*VCP (Tb927.10.5770, http://tritrypdb.org) and the *Homo sapiens* p97 homolog (NCBI, NP_009057.1) by ClustalW multiple alignment using Bioedit sequence Alignment Editor. Identical amino acid residues are in gray background and similar amino acids (aa) are in black. Conserved domains of the *Li*VCP protein are indicated with color bars under the aa sequence as illustrated in A. (C) Neighbor-joining tree showing the phylogenetic relationship between VCP homologs from different organisms including, in addition to those presented in panel B, *Leishmania major* (XP_001686709.1), *Leptomonas pyrrhocoris* (XP_015658481.1), *Phytomonas* sp. (CCW67021.1), *Plasmodium vivax* (XP_001616207.1), *Mus musculus* (BAE40919.1), *Danio rerio* (BAC87740.1), *Arabidopsis thaliana* (OAO95421.1), *Glycine max* (NP_001235099.1) and *Saccharomyces cerevisiae (NP_010157.1)* The optimal tree with the sum of branch length = 1.17841600 is shown. The percentage of replicate trees in which the associated taxa clustered together in the bootstrap test (1000 replicates) is shown next to the branches. Evolutionary analyses were conducted in MEGA7.

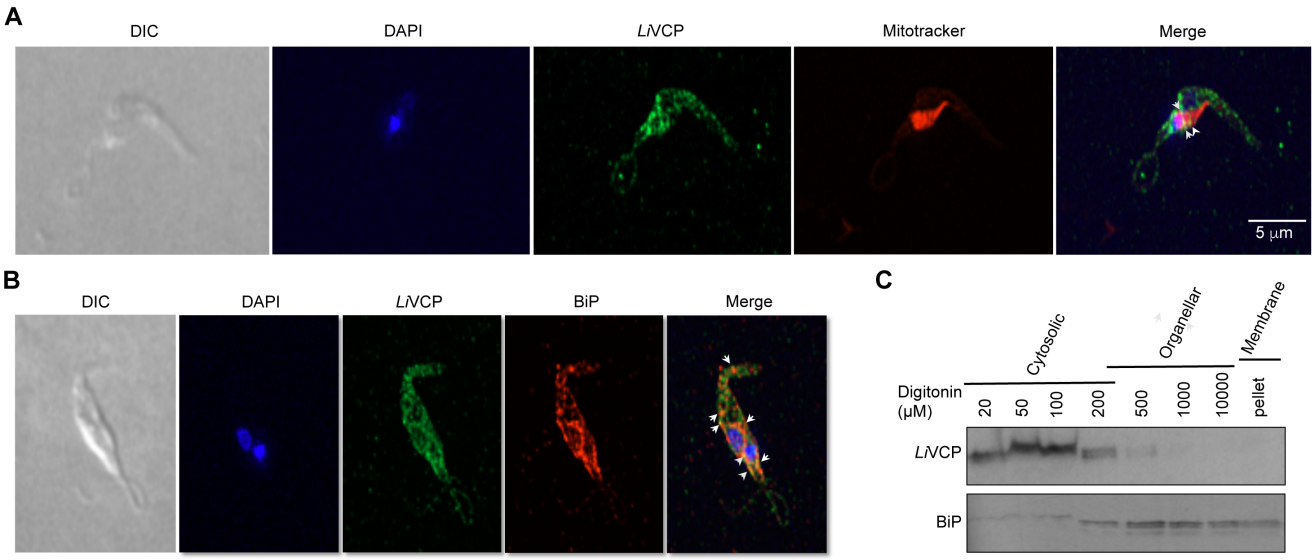

Fig. 2

FIGURE 2 *Li*VCP is localized mainly to the cytosol and is associated with organellar compartments. (A) Immunofluorescence studies showing *Li*VCP (green) localization in *L. infantum* promastigotes. An anti-*Trypanosoma brucei* VCP antibody was used as primary antibody followed by Alexa Fluor® 488 anti-mouse as secondary antibody. Nucleus and kinetoplast DNA were stained with DAPI (blue). Mitochondrial (A) or endoplasmic reticulum (B) *Li*VCP putative co-localization was assessed using MitoTracker™ (red in A) to define the *Leishmania* single mitochondrion or an anti-BiP antibody (red in B) as an ER marker, respectively. An Alexa Fluor® 555 anti-rabbit was used as secondary antibody for MitoTracker and BiP. On merge panels, overlapping signals of *Li*VCP with the mitochondrion or the ER are indicated with arrows. All images are maximal Z-projections of 20 to 30 contiguous sections separated by 0.15 μm and were acquired with a 63x objective, using a Quorum WaveFX spinning disk confocal system (Quorum Technologies, Guelph, Ontario). Image acquisition and processing was done using Volocity 4.2.1 analysis software. (C) Western blot of *L. infantum* promastigote digitonin-fractionated samples (20 μM-10 mM) using the anti-*Tb*VCP antibody to detect the *Li*VCP protein and the anti-BiP antibody for detecting endoplasmic reticulum-enriched fractions. The 20 μM to 200 μM digitonin fractions are enriched with cytosolic proteins, the 500 μM, 1 mM and 10 mM fractions contain mostly organellar proteins and the pellet fraction contains membrane-associated proteins.

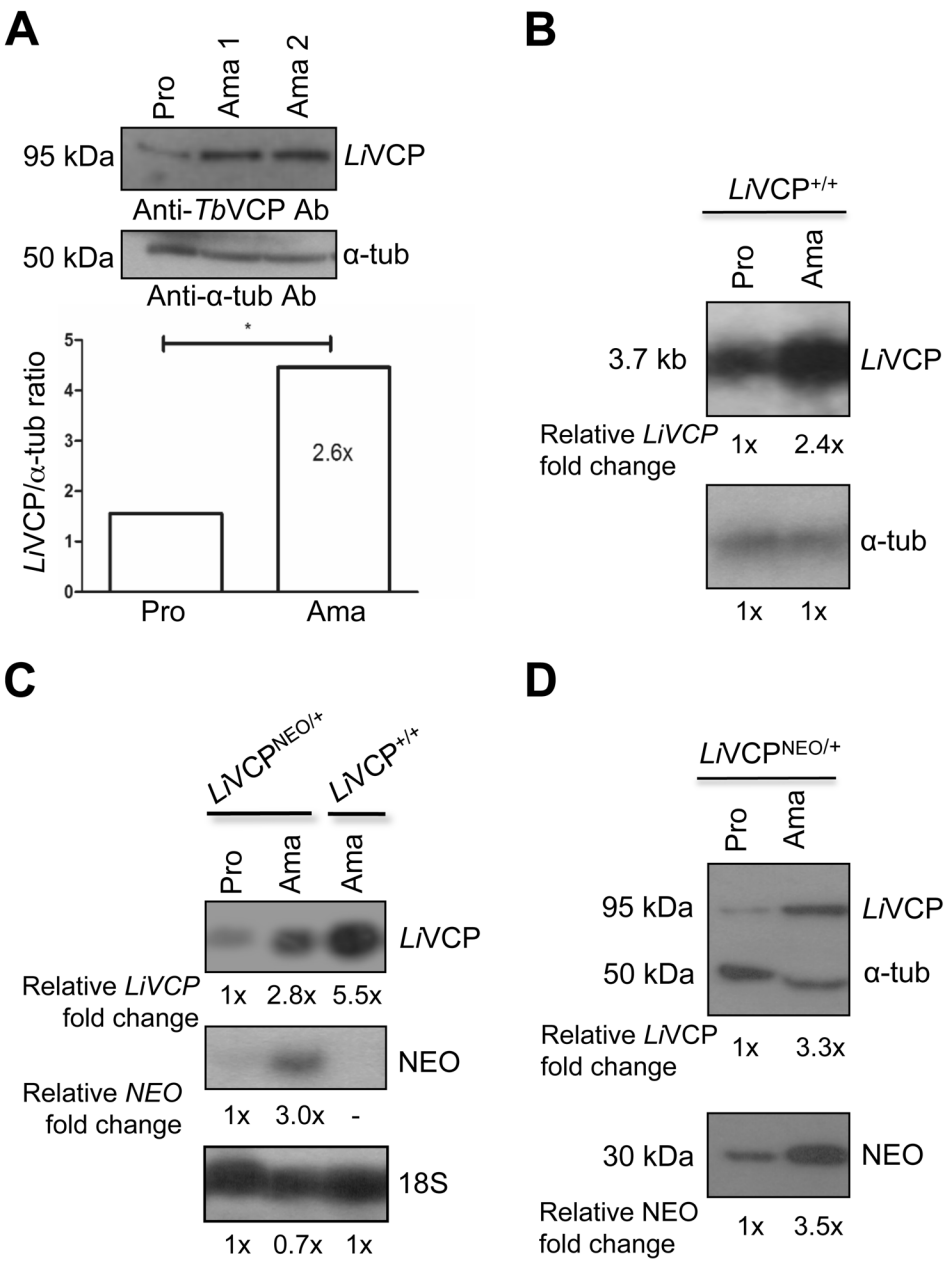

Fig. 3

FIGURE 3 *Li*VCP is developmentally regulated with higher mRNA and protein levels in *L. infantum* axenic amastigotes. (A) Western blot analysis of *Li*VCP$^{+/+}$ (WT) *L. infantum* promastigote (Pro) and axenic amastigote (Ama; passages 1 and 2) whole cell extracts using an anti-*T. brucei* (*Tb*) VCP antibody. The membrane was blotted with an anti-α-tubulin antibody as protein loading control. Quantification, expressed in *Li*VCP protein/ α -tubulin

ratio is presented (lower panel). Two-tailed unpaired t-test was performed: statistical significance $p < 0.05$. Northern blot hybridization to evaluate expression of the *LiVCP* (B and C) and *NEO* (C) transcripts in WT and *Li*VCP$^{NEO/+}$ (sKO) exponentially grown Pro and Ama. The α -tubulin or 18S rRNA probes were used as RNA loading controls. (D) Western blot analysis of *Li*VCP$^{NEO/+}$ Pro and Ama total lysates using anti-*Tb*VCP and anti-NEO antibodies. *Li*VCP and NEO mRNA and protein levels were normalized to the 18S rRNA or to the α-tubulin mRNA or protein controls by densitometric analyses using the ImageJ 1.38x software. The fold change values of normalized *Li*VCP or NEO mRNA and protein levels in axenic amastigotes relative to the levels seen in promastigotes are shown below the blots.

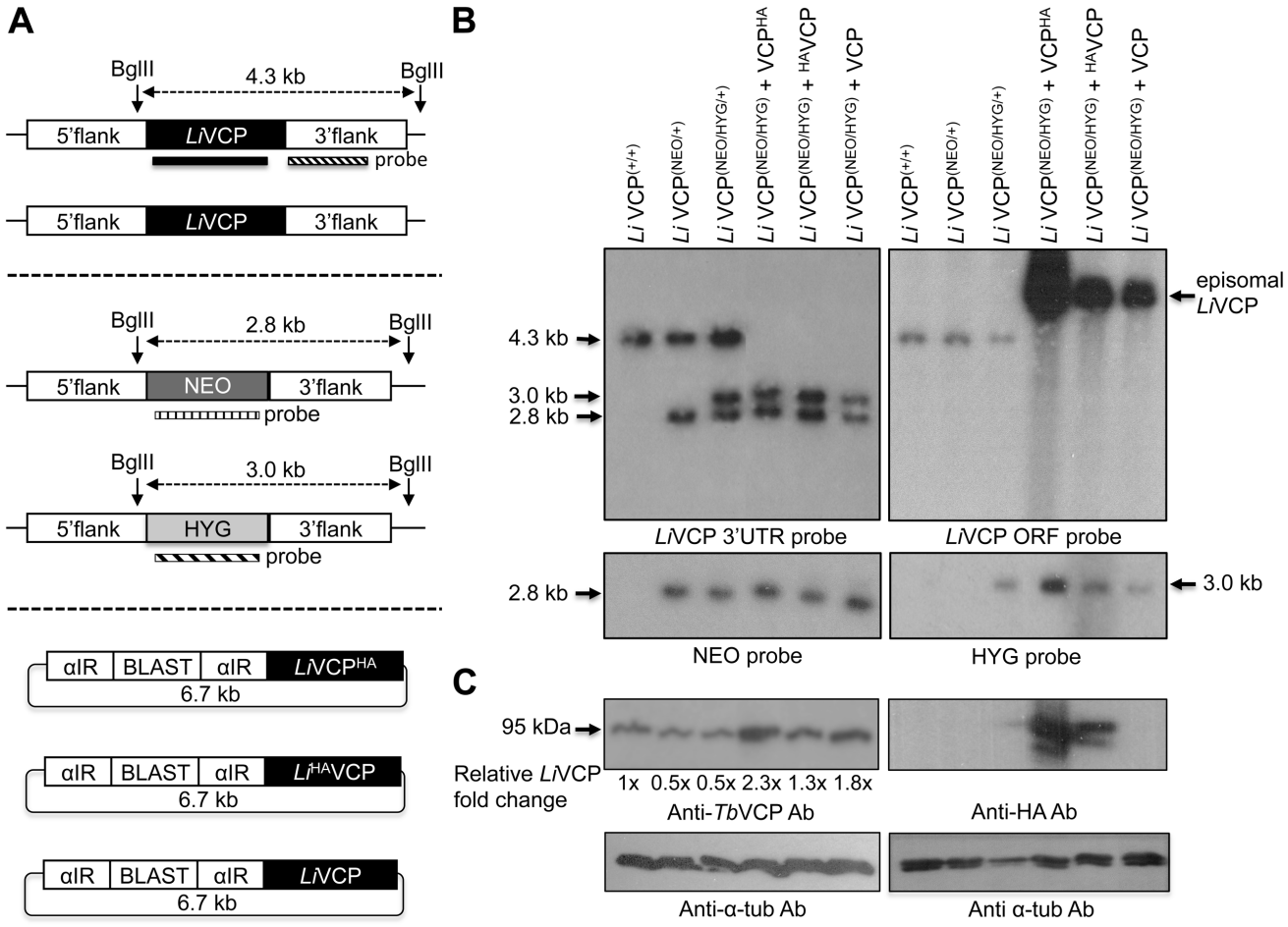

Fig. 4

FIGURE 4 *Li*VCP is an essential gene for *Leishmania infantum* promastigote growth. (A) Schematic draw of the *L. infantum VCP* genomic locus and the neomycin phosphotransferase gene (*NEO*) and hygromycin phosphotransferase gene (*HYG*) targeting cassettes used for replacing both endogenous *VCP* gene copies (LinJ.36.1420; http://tritrypdb.org) through homologous recombination at the 5'- and 3'-flank sequences of *VCP*. The two *LiVCP* alleles in the wild type (WT) strain (*Li*VCP$^{(+/+)}$) were subsequently replaced by the *NEO* and *HYG* targeting cassettes to generate the *Li*VCP$^{(NEO/+)}$ and *Li*VCP$^{(NEO/HYG)}$ mutants, respectively. Following *NEO* gene replacement, double inactivation in *Li*VCP$^{(NEO/+)}$ was only possible by ectopically providing a pSPαBLASTα vector expressing VCP tagged with an HA epitope either at the C-terminus (VCP^{HA}) or at N-terminus (^{HA}VCP) or a non-tagged VCP. The blasticidin (BLAST) expression vectors harboring either *Li*VCP or *Li*^{HA}VCP or *Li*VCP^{HA} are illustrated here. (B) Southern blot of total genomic DNA digested with BglII hybridized with the *Li*VCP 3'flank sequence or the *VCP* or the *NEO* and or the

HYG ORF probes. (C) Western blot analysis of WT and VCP mutant strains using an anti-*Tb*VCP antibody or an anti-HA antibody. An anti-α-tubulin antibody was used as protein loading control.

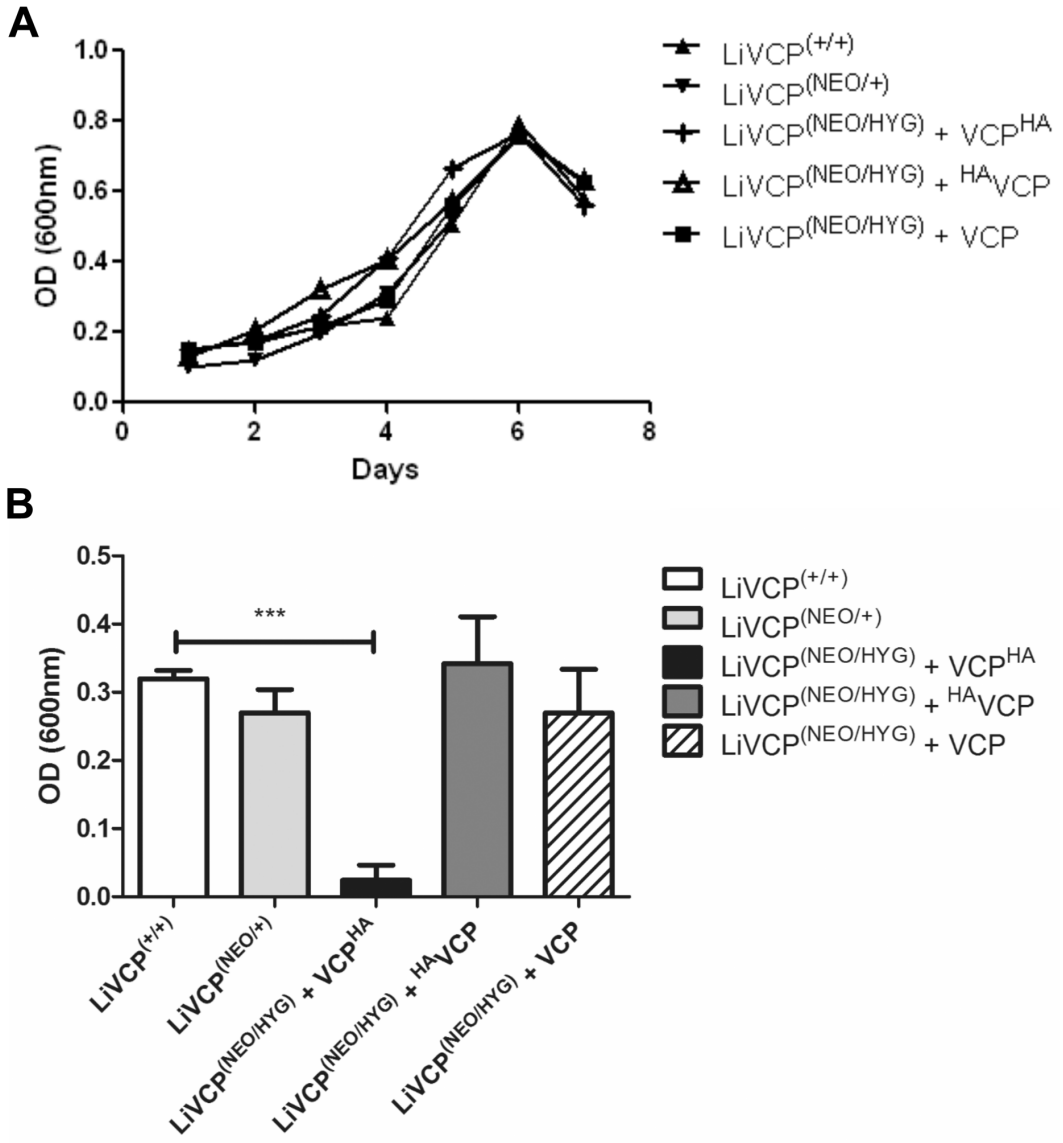

Fig. 5

FIGURE 5 *Li*VCP is required for *Leishmania* axenic amastigote growth. (A) Promastigote growth of *L. infantum* WT, *Li*VCP$^{(NEO/+)}$ and the facilitated dKO *Li*VCP$^{(NEO/HYG)}$ strains episomally expressing *Li*VCP tagged with an HA epitope either at the C-terminus (*Li*VCP$^{(NEO/HYG)}$+VCP^{HA}) or at the N-terminus (*Li*VCP$^{(NEO/HYG)}$+^{HA}VCP) or non-tagged (*Li*VCP$^{(NEO/HYG)}$+VCP) in SDM-79 medium. (B) Axenic amastigote growth of *L. infantum* lines as in (A) cultured in MAA medium at 37°C and acidic pH for 72 hours. The results shown here are the mean and standard deviation of three independent experiments. Statistical significance was assessed by two-tailed unpaired *t* test (***$P \leq 0.001$). Asterisks indicate significant difference between the WT and the facilitated dKO mutant *Li*VCP$^{(NEO/HYG)}$+VCP^{HA}.

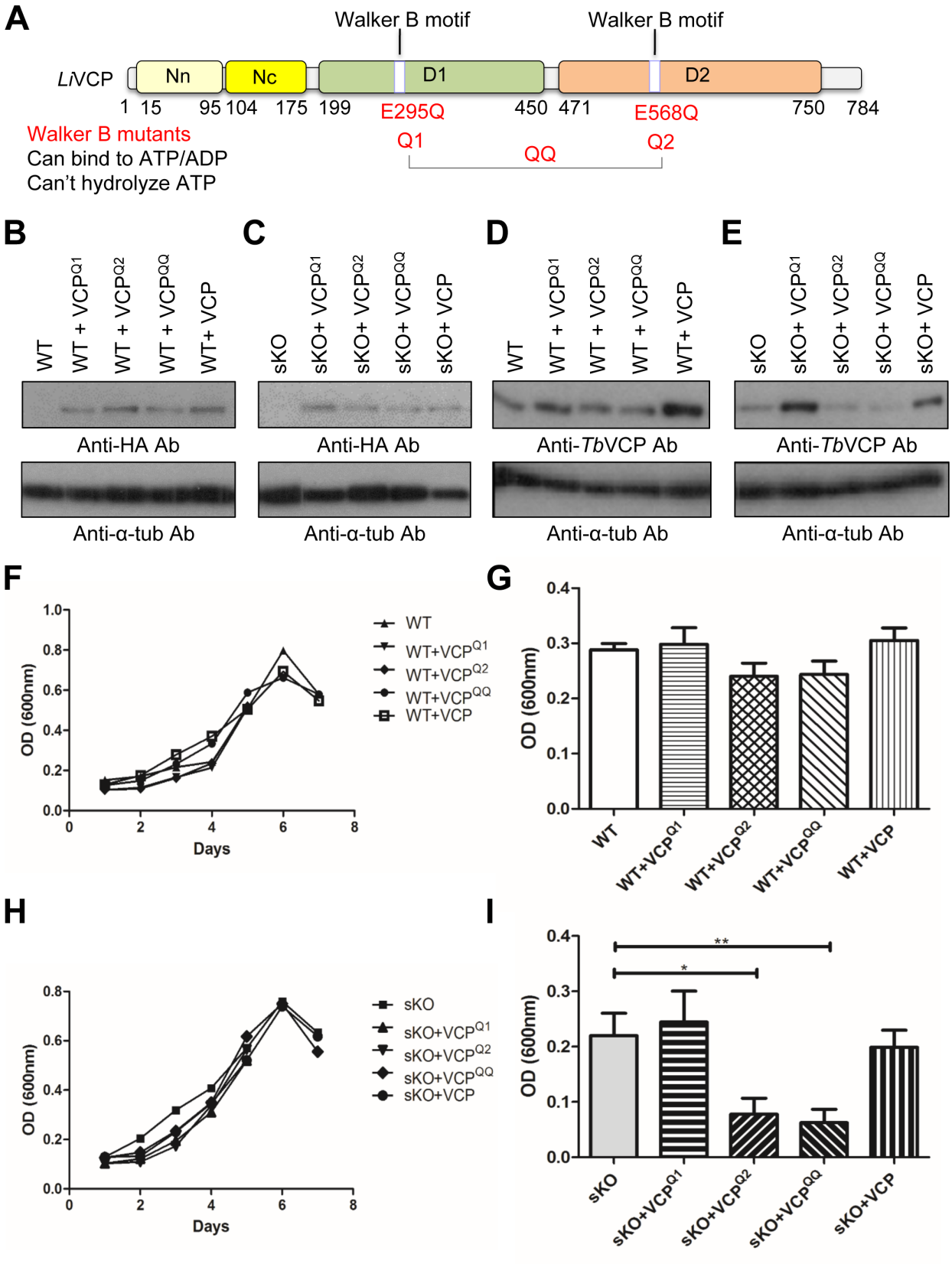
A
Walker B motif
Walker B motif
LiVCP
Nn
Nc
D1
D2
1 15 95 104 175 199 E295Q 450 471 E568Q 750 784
Walker B mutants
Can bind to ATP/ADP
Can't hydrolyze ATP
Q1
QQ
Q2
B
WT
WT + VCPQ1
WT + VCPQ2
WT + VCPQQ
WT+ VCP
Anti-HA Ab
Anti-α-tub Ab
C
sKO
sKO+ VCPQ1
sKO+ VCPQ2
sKO+ VCPQQ
sKO+ VCP
Anti-HA Ab
Anti-α-tub Ab
D
WT
WT + VCPQ1
WT + VCPQ2
WT + VCPQQ
WT+ VCP
Anti-TbVCP Ab
Anti-α-tub Ab
E
sKO
sKO+ VCPQ1
sKO+ VCPQ2
sKO+ VCPQQ
sKO+ VCP
Anti-TbVCP Ab
Anti-α-tub Ab
F
OD (600nm)
Days
WT
WT+VCPQ1
WT+VCPQ2
WT+VCPQQ
WT+VCP
G
OD (600nm)
WT
WT+VCPQ1
WT+VCPQ2
WT+VCPQQ
WT+VCP
H
OD (600nm)
Days
sKO
sKO+VCPQ1
sKO+VCPQ2
sKO+VCPQQ
sKO+VCP
I
OD (600nm)
**
*
sKO
sKO+VCPQ1
sKO+VCPQ2
sKO+VCPQQ
sKO+VCP

Fig. 6

FIGURE 6 Impairing *Li*VCP function by targeting the *Li*VCP D2 ATPase domain using a dominant negative approach leads to a dramatic decrease in *Leishmania* axenic amastigote growth. (A) Schematic representation of *Li*VCP mutant proteins with a point mutation in the Walker B site (involved in ATP hydrolysis) of the ATPase D1 domain (E295Q, VCP^{Q1}) or the ATPase D2 domain (E568Q, VCP^{Q2}) or in both sites (E295Q and E568Q, VCP^{QQ}). (B-E) Western blot analysis of whole protein lysates from *L. infantum* WT or sKO (*Li*$VCP^{(NEO/+)}$) expressing or not the dominant negative mutants VCP^{Q1} or VCP^{Q2} or VCP^{QQ} tagged with an HA epitope using an anti-HA antibody or an anti-*Tb*VCP antibody. A non-mutated *Li*VCP-HA was used as a control. The anti-α-tubulin antibody was used as protein loading control (lower panels). (F) Growth of *L. infantum* promastigotes expressing either VCP^{Q1} or VCP^{Q2} and or VCP^{QQ} mutants in the WT background. (G) As in F but grown as axenic amastigotes for 72 hours in MAA medium. (H) Growth of *L. infantum* promastigotes expressing either VCP^{Q1}, or VCP^{Q2} and or VCP^{QQ} mutants in the sKO background. (I) As in H but grown as axenic amastigotes. The results shown here are the mean and standard deviation of three independent experiments. Statistical significance was assessed by two-tailed unpaired *t*-test (*$P<0.05$ and **$P\leq0.01$). Asterisks indicate significant differences between sKO and sKO+VCP^{Q2} and between sKO and sKO+VCP^{QQ}.

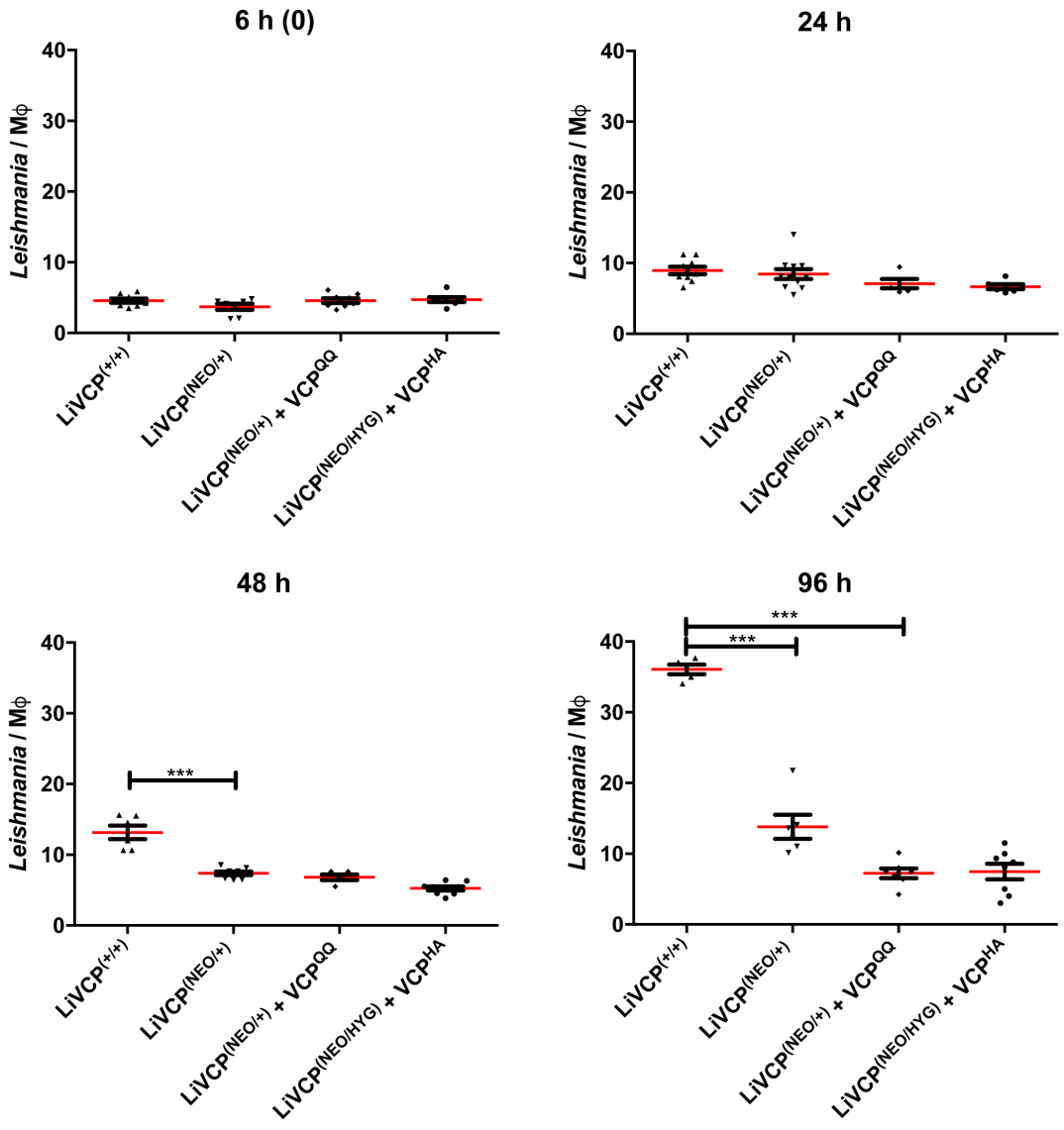

Fig. 7

FIGURE 7 *Li*VCP is essential for *Leishmania* intracellular growth. Late-stationary *L. infantum* promastigotes from WT, *Li*VCP$^{(NEO/+)}$, *Li*VCP$^{(NEO/+)}$+VCP^{QQ} and the facilitated dKO mutant *Li*VCP$^{(NEO/HYG)}$+VCP^{HA} were used for *in vitro* infection of PMA-treated THP1 macrophages. An average of *Leishmani*a per macrophage (MØ) at 6 hours (time point 0), 24, 48 and 96 hours post-infection was determined microscopically by Giemsa staining. Each dot represents count of 500 MØ. Statistical significance was assessed by the two-tailed

unpaired *t*-test (***$P \leqslant 0.001$). Asterisks indicate significant differences between the WT and VCP mutant strains.

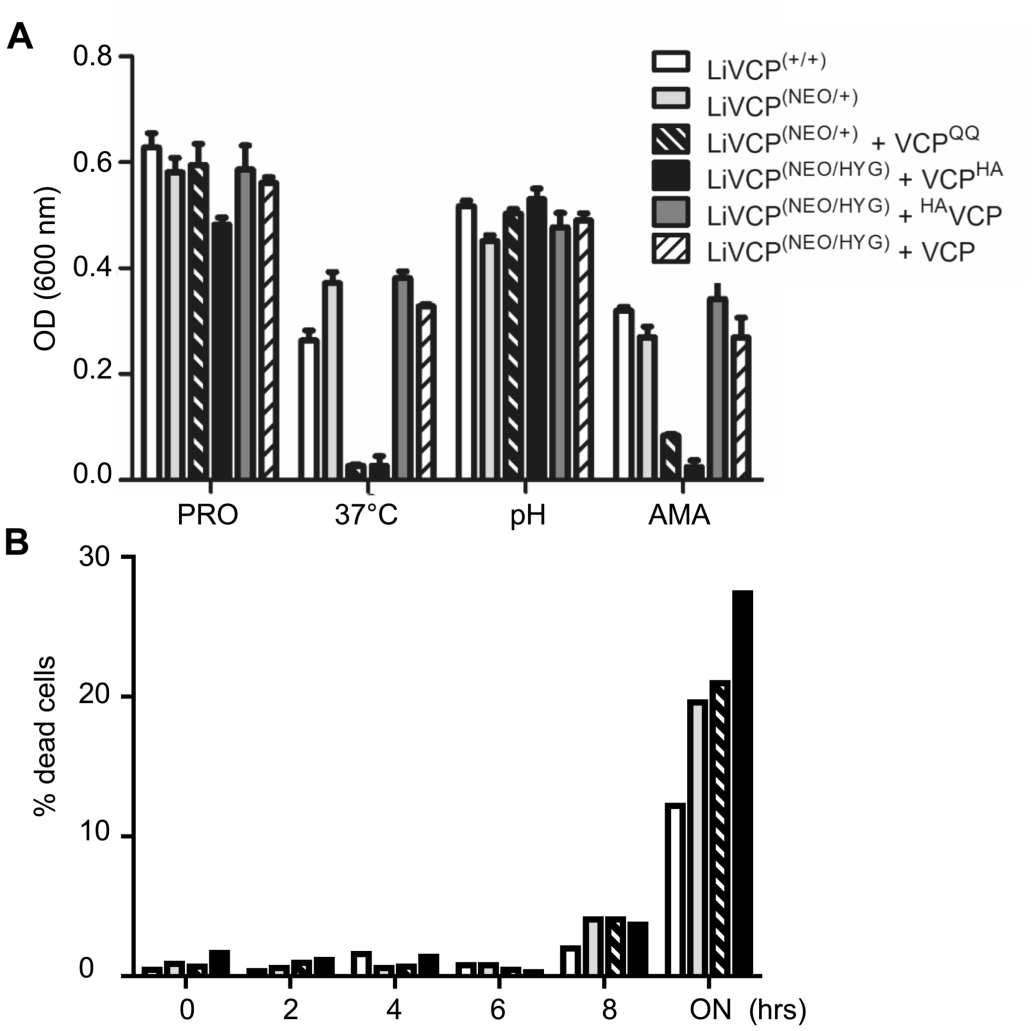

Fig. 8

FIGURE 8 *Li*VCP is essential for *Leishmania* survival under heat stress. (A) Effect of heat or pH stress on the growth of *Leishmania* VCP mutants. *L. infantum Li*VCP$^{(+/+)}$, *LiVCP*$^{(NEO/+)}$, *Li*VCP$^{(NEO/+)}$+VCP^{QQ} and the facilitated dKO mutants *LiVCP*$^{(NEO/HYG)}$+VCP^{HA}, *LiVCP*$^{(NEO/HYG)}$+^{HA}VCP and *LiVCP*$^{(NEO/HYG)}$+VCP were cultured in SDM-79 medium (PRO; pH 7.0 and 25°C) or in SDM-79 combined to heat stress (37°C) or in MAA medium (pH 5.5) at 25°C or in MAA medium at 37°C (combined temperature and acidic pH stress) (AMA). The results shown here are the mean and standard deviation of two experiments performed in triplicates. (B) Evaluation of the percentage of dead cells in the VCP mutant lines cultured under conditions of combined temperature and acidic pH stress (MAA medium at 37°C) for selected time points up to 24 hrs by fluorescence-activated cell sorting using the eBioscience™ Fixable Viability Dye eFluor™ 780, which can irreversibly label dead cells.

Cells were analyzed with a FACS Canto flow cytometer (BD Bioscences) and data were processed using BD FACSDiva™ Software v. 6.1.3.

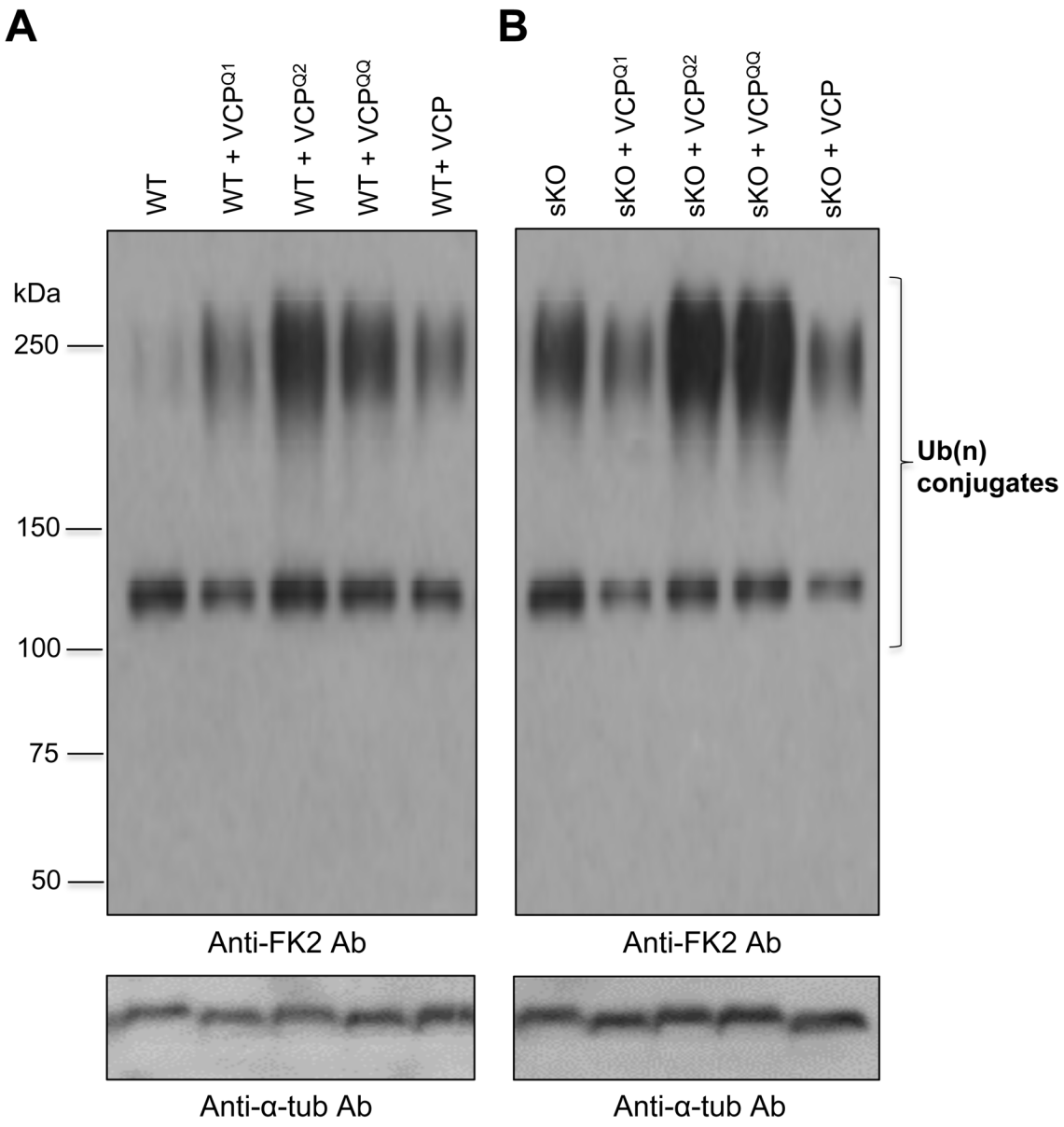

Fig. 9

FIGURE 9 Decreasing expression of *Li*VCP or impairing its function using dominant negative mutants leads to high accumulation of polyubiquitinated proteins. Western blot analysis of *L. infantum* WT (A) and sKO (*Li*VCP$^{(NEO/+)}$) lines (B) using the FK2 antibody recognizing K29-, K48-, and K63-linked mono- and polyubiquitinated proteins. Equal amount of proteins was loaded on the gel. An anti-α-tubulin antibody (lower panels) was used as protein loading control. The data shown here are representative of four independent experiments yielding similar results.

2.12 Supplementary Table S1. Primers used in this study.

	Primer sequence	Restriction sites, epitope tag and other details		
***Li*VCP (LinJ.36.1420)-HA**				
LiVCP gene amplification				
*Li*VCP forward (V1)	5'-GC**TCTAGA**ATGGCGGACGCTGTTGGG-3'	XbaI		
*Li*VCP reverse (V2)	5'-CCCAAGCTTTTAGCTGTAGAGGTCGTCGTCGT	HindIII		
LiVCP gene amplification including an HA epitope at the C-terminus (VCP^{HA})		XbaI	HA-tag sequence	
*Li*VCP forward (V1)	5'-GC**TCTAGA**ATGGCGGACGCTGTTGGG-3'	HindIII		
*Li*VCP reverse with HA-tag (V3)	5'-CCC**AAGCTT**TTA**AGCGTAGTCTGGCACGTCGT AGGGTA**GCTGTAGAGGTCGTCGTCG-3'			
LiVCP gene amplification including an HA epitope at the N-terminus (^{HA}VCP)				
*Li*VCP forward with HA-tag (V4)	5'-GCTCTAGAATG**TACCCTTACGACGTGCCAGA CGCT**GCGGACGCTGTTGGGAACACA-3'		HA-tag sequence	
*Li*VCP reverse (V2)	5'-CCC**AAGCTT**TTAGCTGTAGAGGTCGTCGTCGT	HindIII		
Neomycin *(NEO)* targeting cassette				
Amplification of the 5'flank region of the LiVCP gene				
5'flank *Li*VCP forward	5'-**GCGGCCGC**GCTCTCTTCTCCTTTTCTCTCT-3'	NotI		
5'flank *Li*VCP reverse	5'-**AATCCATCTTGTTCAATCATG**GTTGCTTCTGC TGTCTT-3'	NEO complemen		
NEO gene amplification				
NEO forward	5'-**AAGACACGGCAGAAGCAACC**ATGATTGAACA ATGGATT-3'	5'flank complement		
NEO reverse	5'-**ACATCCGCCACCTCCTCCTC**TCAGAAGAACTC CAAGAA-3'	3'flank complement		
3' flank region of the LiVCP gene				
3'flank *LiVCP* forward	5'- **TTCTTGACGAGTTCTTCTGA**GAGGAGGAGGT CGGATGT -3'	NEO complemen		
3'flank *LiVCP* reverse	5'- **CATATG**GAGACAACAACCCCTCTCGCC-3'	NdeI		
Hygromycin *(HYG)* targeting cassette				
Amplification of the 5'flank region of the				

LiVCP gene 5'flank *LiVCP* forward 5'flank *LiVCP* reverse	5'-**GCGGCCGC**GCTCTCTTCTCCTTTTCTCTCT-3' 5'-**AAGCTTAAGCTTGTTAACGTTAAC**TGGTTGCTTC TGCCGTGTCTTTG-3'	NotI HindIII	HpaI	3'flank complement
Hygromycin *(HYG) gene amplification* *HYG* forward *HYG* reverse	5'-**GTTAAC**ATGAAAAAGCCTGAACTCAC-3' 5'-**AAGCTT**CTATTCCTTTGCCCTCGGACGAG-3'	HpaI HindIII		
Amplification of the 3' flank region of the LiVCP gene 3'flank *LiVCP* forward 3'flank *LiVCP* reverse	5'- **GTTAACGTTAACAAGCTTAAGCTT**GAGGAGG GGTGGCGGATGTGA -3' 5'-**CATATG**GAGACAACAACCCCTCTCGCC-3'	HpaI NdeI	HindIII	5'flank complement
LiVCP ATP hydrolysis dominant negativemutants* ***LiVCP gene amplification containing mutations in domain D1 (Q1 mutation)*** *LiVCP* forward (V1) Internal mutagenic reverse (M1R)	5'-GC**TCTAGA**ATGGCGGACGCTGTTGGG-3' 5'-TCG GGG CGA TGG AGT CGA TTT GAT CGA T AGA TGA TCG C-3'	XbaI Containing M1		
LiVCP gene amplification containing mutations in domain D2 (Q2 mutation) Internal mutagenic forward (M2F) *LiVCP* Reverse with HA-tag (V3)	5'-TGC GTG CTC TTT TTT GAT CAA CTG GAC TC GTG GCC AAG-3' 5'-CCC**AAGCTT**TTA**AGCGTAGTCTGGCACGTCGT** **AGGGTA**GCTGTAGAGGTCGTCGTCG-3'	Containing M2 HindIII	HA-tag sequence	

*** *LiVCP* ATP hydrolysis dominant negative mutants.** The first PCR reaction was carried out using forward VCP primer (V1) and internal mutagenic reverse primer (M1R) for Q1 mutation. For Q2 mutation, internal mutagenic forward (M2F) and reverse VCP primer (V3) were used. The second-round PCR was done using the amplified-PCR product containing Q1 mutation as megaprimer forward (Mega1) and VCP reverse primer (V3) to generate a VCP product containing Q1 mutation (VCP^{Q1}). VCP forward (V1) and amplified-PCR product containing Q2 as megaprimer reverse (Mega2) were used to generate a VCP product containing Q2 mutation (VCP^{Q2}). Lastly, Mega1 as forward and Mega2 as reverse primers were combined to generate a VCP product containing both mutations Q1 and Q2 (VCP^{QQ})

2.13 Supplementary Figures

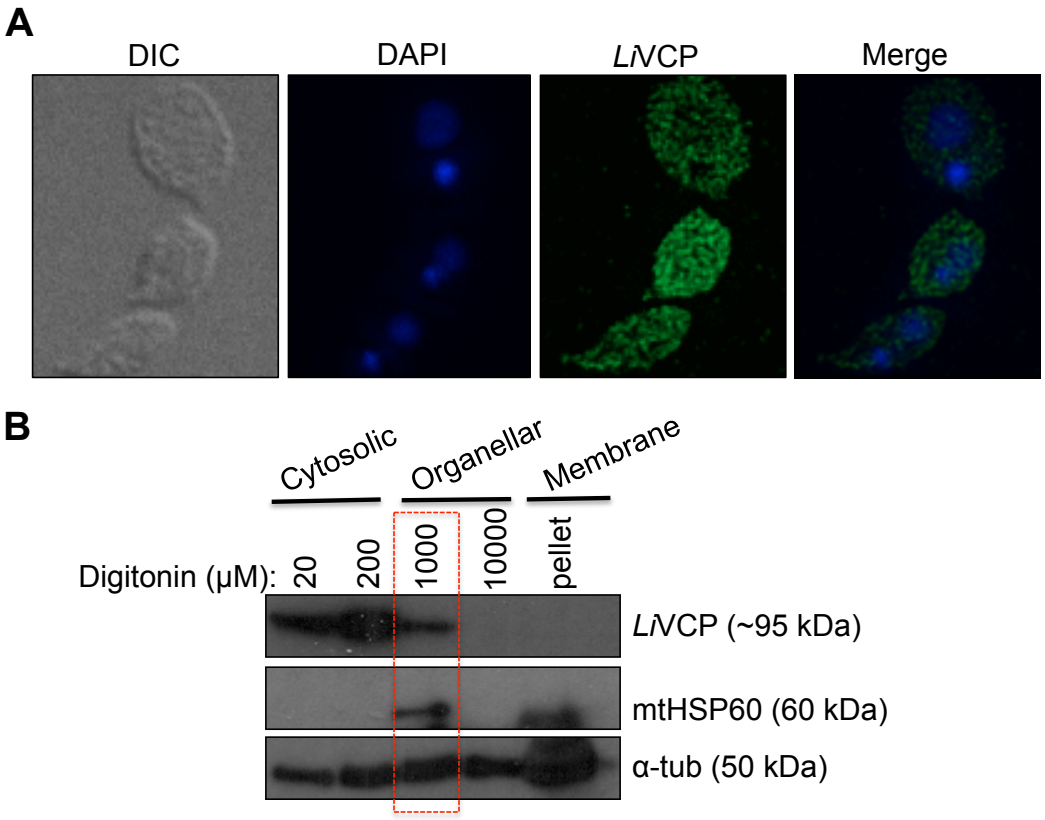

Fig. S1

FIGURE S1 *Li*VCP localization in *L. infantum* amastigotes. (A) Immunofluorescence studies showing *Li*VCP (green) localization in *L. infantum* axenic amastigotes. An anti-*Trypanosoma brucei* VCP antibody was used as primary antibody followed by Alexa Fluor® 488 anti-mouse as secondary antibody. Nucleus and kinetoplast DNA were stained with DAPI (blue). All images are maximal Z-projections of 20 to 30 contiguous sections separated by 0.15 μm and were acquired with a 63x objective, using a Quorum WaveFX spinning disk confocal system (Quorum Technologies, Guelph, Ontario). Image acquisition and processing was done using Volocity 4.2.1 analysis software. (B) Western blot of *L. infantum* promastigote digitonin-fractionated samples (20 μM-10 mM) using the anti-*Tb*VCP antibody to detect the *Li*VCP protein. The anti-HSP60 (mitochondrial) antibody was used as a control for organellar fraction enrichment. The anti-α-tubulin antibody was used as a control for membrane-associated proteins. The 20 μM and 200 μM digitonin lanes correspond to cytosolic fractions and the 1 mM and 10 mM lanes correspond

to organellar fractions. The pellet fraction contains membrane-associated proteins.

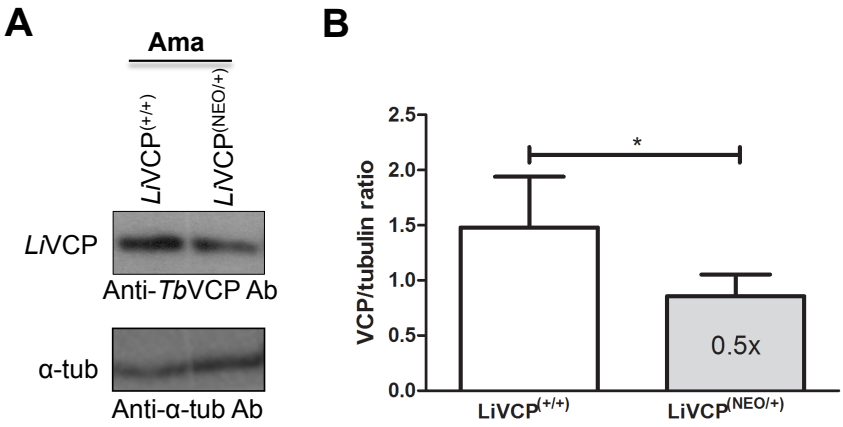

Fig. S2

FIGURE S2 VCP protein expression in the heterozygous *L. infantum* *Li*VCP$^{(NEO/+)}$ mutant. (A) Western blot analysis on protein lysates from *L. infantum* WT (*Li*VCP$^{(+/+)}$) and the heterozygous *Li*VCP$^{(NEO/+)}$ mutant axenic amastigotes (Ama) using an anti-*T. brucei* VCP antibody. An anti-α-tubulin antibody was used as protein loading control. (B) VCP protein expression ratio in *Li*VCP$^{(NEO/+)}$ vs. *Li*VCP$^{(+/+)}$. Statistical significance was assessed by two-tailed unpaired t-test ($p < 0.05$).

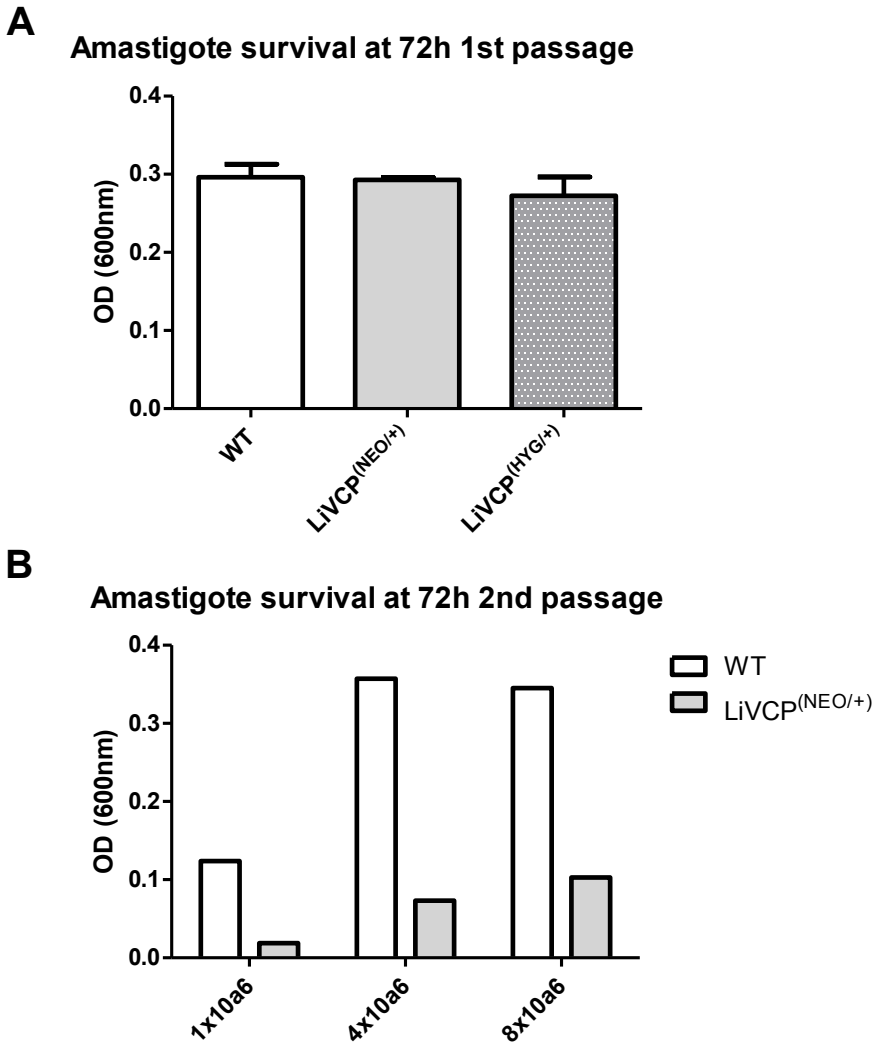

Fig. S3

FIGURE S3 Axenic amastigote growth of *L. infantum Li*VCP$^{(NEO/+)}$ and *Li*VCP$^{(HYG/+)}$ heterozygous mutants. Parasites were cultured in MAA medium (pH 5.5) at 37°C. (A) 1st passage as axenic amastigotes. (B) 2nd passage as axenic amastigotes.

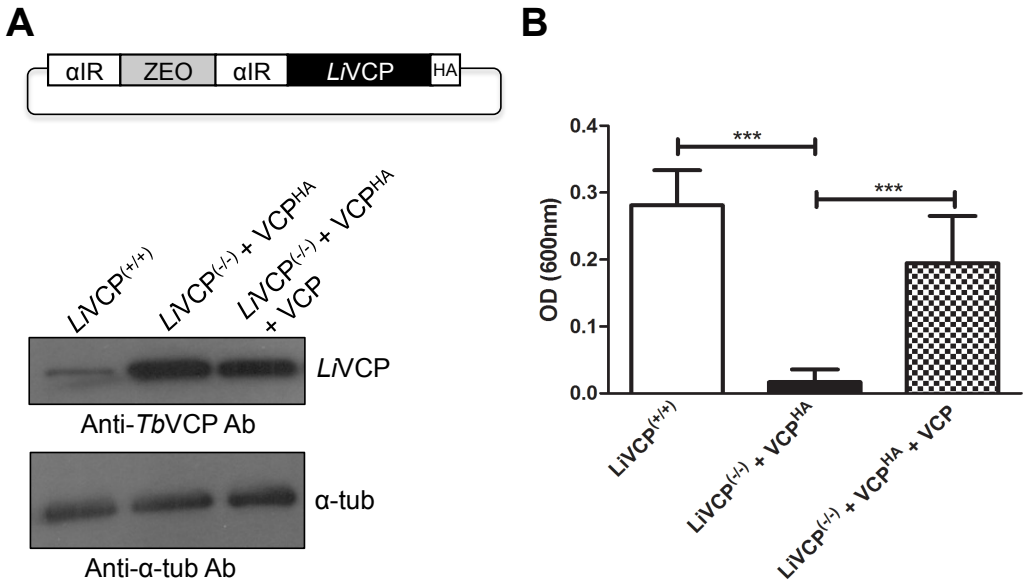

Fig. S4

FIGURE S4 C-terminal epitope tagging of *Li*VCP inhibits VCP function in *L. infantum* axenic amastigotes but not in promastigotes. (A) Schematic representation of the *Li*VCP-expressing vector pSPaZEOa-VCP^{HA} transfected into the facilitated dKO *Li*VCP$^{(-/-)}$ mutant (upper panel). ZEO, zeomycin resistance gene; aIR stands for the intergenic region of the *L. enriettii* a-tubulin gene providing the processing signals. Western blot analysis to evaluate *Li*VCP expression (promastigote lysates) using an anti-*T. brucei* VCP antibody. An anti-α-tubulin antibody was used as protein loading control (lower panel). (B) Ectopic expression of *Li*VCP^{HA} into the *Li*VCP$^{(-/-)}$ dKO mutant failed to restore growth in axenic amastigotes. *L. infantum* amastigote growth of wild type (*Li*VCP$^{+/+}$), facilitated dKO mutant *Li*VCP$^{(-/-)}$ +VCP^{HA} episomally expressing *Li*VCP^{HA} and the above facilitated mutant rescued with a non-tagged VCP version.

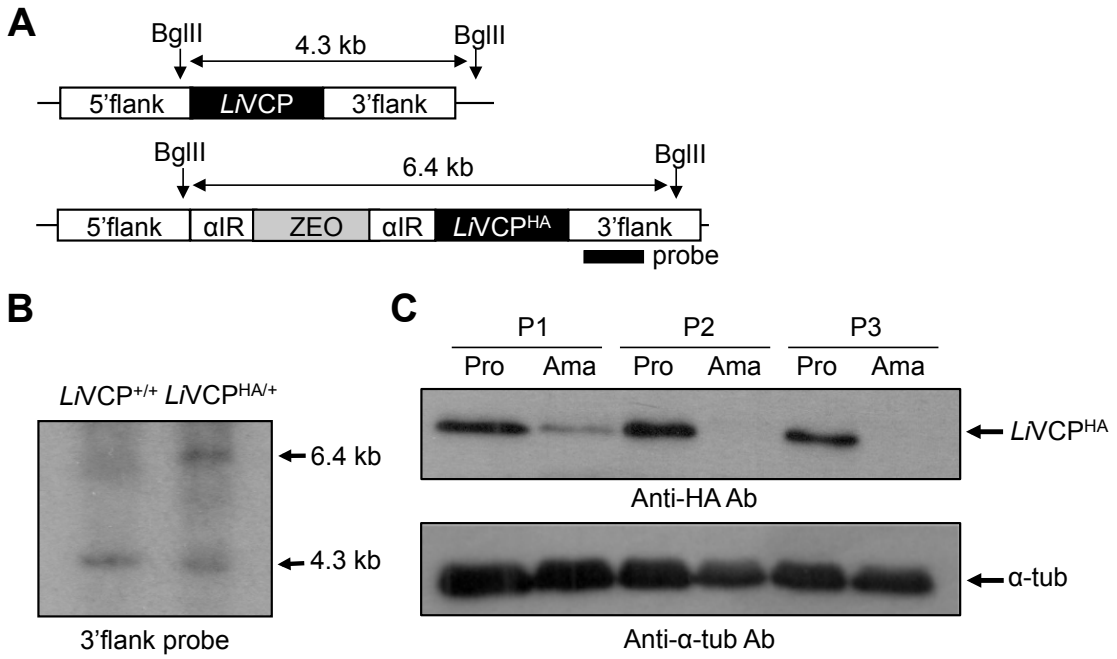

Fig. S5

FIGURE S5 C-terminal epitope tagging of *Li*VCP causes *Li*VCP protein instability specifically in *L. infantum* amastigotes. (A) Schematic representation of the targeting cassette 5'flank-αZEOα-VCP^{HA}-3'flank to replace one of the two *L. infantum LiVCP* endogenous gene copies by a *Li*VCP^{HA} copy. (B) Southern blot hybridization using the 3'flank *VCP* region as a probe confirming genomic replacement of one *VCP* copy by the *VCP^{HA}* copy. (C) Expression of *Li*VCP^{HA} integrated into the *VCP* endogenous locus as evaluated by Western blot using an anti-HA antibody (upper panel). Different passages (P1 to P3) of axenic promastigote and amastigote cultures were tested. The same membrane was blotted with an anti-α-tubulin antibody as protein loading control (lower panel).

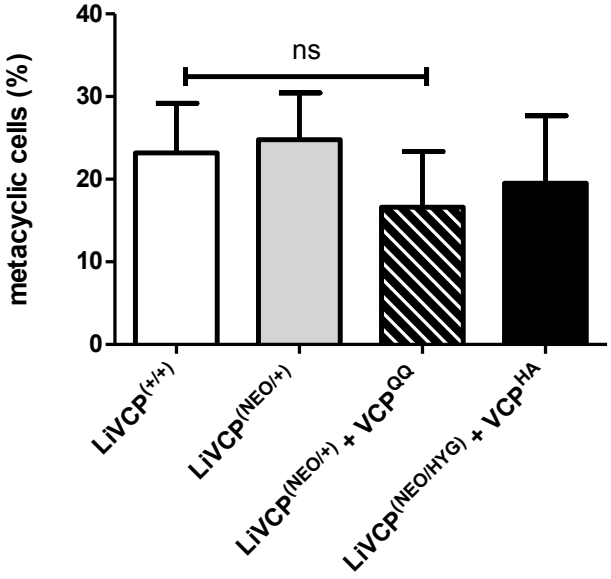

Fig. S6

FIGURE S6 Percentage of metacyclic *L. infantum* forms collected from stationary promastigote cultures of different VCP mutants. To evaluate the percentage of metacyclic promastigotes in *Li*VCP$^{(+/+)}$, *LiVCP*$^{(NEO/+)}$, *Li*VCP$^{(NEO/+)}$+VCP^{QQ} and the facilitated dKO mutant *LiVCP*$^{(NEO/HYG)}$+VCP^{HA}, a suspension of 10^8/ml stationary phase promastigote cells grown in SDM-79 medium without serum was supplemented with 50 µg/ml peanut agglutinin lectin (PNA) (Vector Laboratories) and incubated at 26^0 C with agitation for 30 min as described by Alcolea et al. (2014). The cells were harvested at 700-800 rpm for 5 min to remove the agglutinated promastigotes (PNA$^+$) and the metacyclic parasites (PNA$^-$) in the supernatant were recuperated by centrifugation at 3000 rpm during 10 min and resuspended for quantification. The results shown here are the mean and standard deviation of three independent experiments. Statistical analysis was done by the two-tailed unpaired *t*-test.

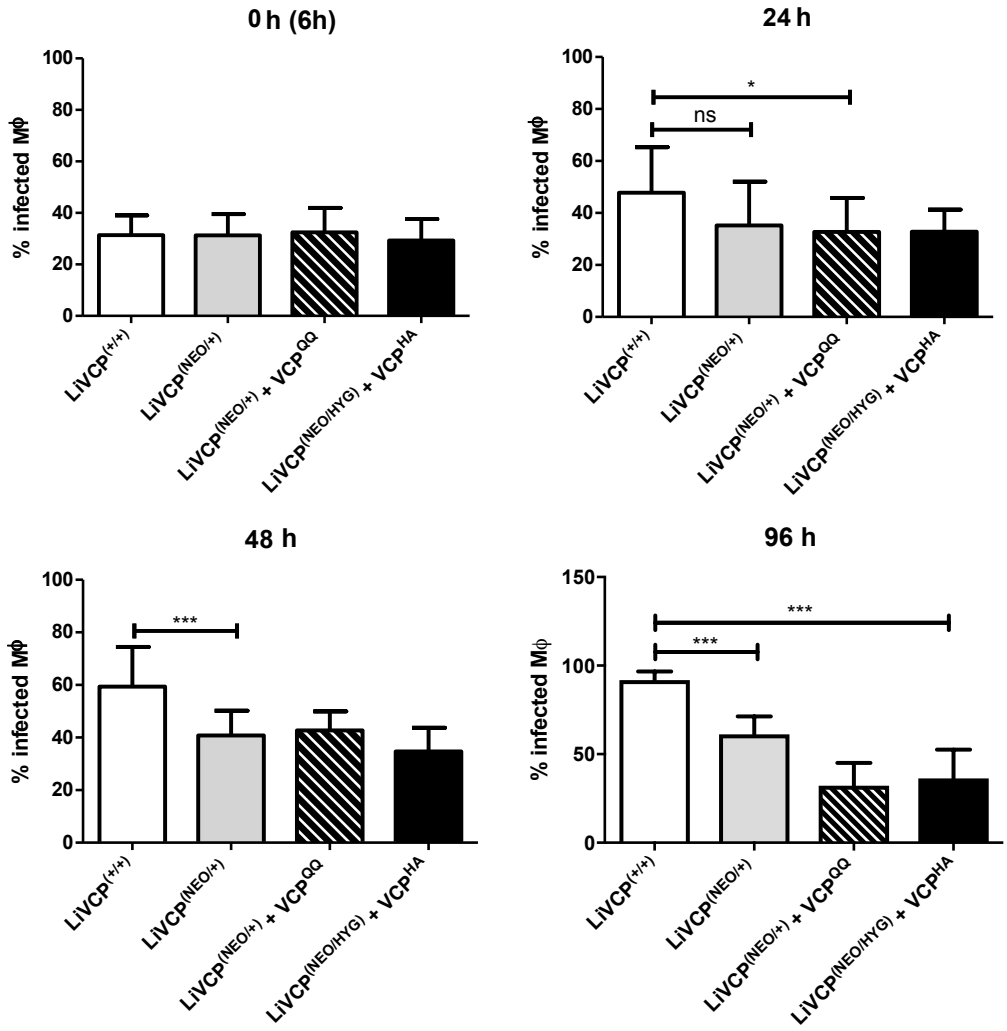

Fig. S7

FIGURE S7 Percentage of infected macrophages by *L. infantum* VCP mutant lines. The percentage of THP1 macrophages (MØ) infected with (*Li*VCP$^{+/+}$) or *Li*VCP$^{(NEO/+)}$ or *Li*VCP$^{(NEO/+)}$+VCP^{QQ} or the facilitated dKO *Li*VCP$^{(NEO/HYG)}$+VCP^{HA} mutant at 6 (time 0), 24, 48 and 96 hours post-infection was determined microscopically by Giemsa staining. Mean and standard deviation derived from several (5-9) counting of ~500 macrophages for each strain at each time point. Statistical significance was assessed by the two-tailed unpaired *t*-test ($*P \leqslant 0.01$, $***P \leqslant 0.001$).

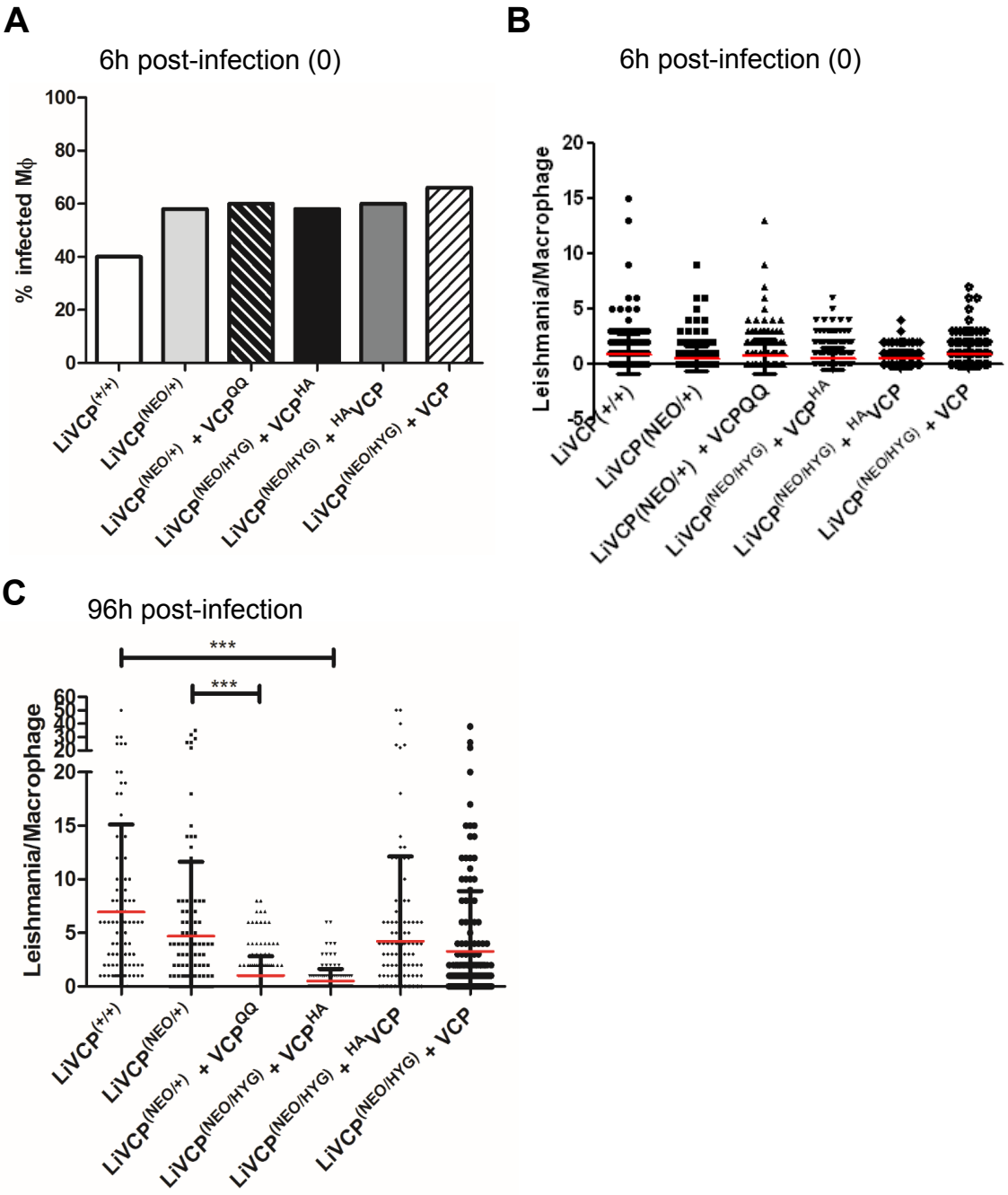

Fig. S8

FIGURE S8 *Li*VCP is essential for *Leishmania* intracellular amastigote growth. Stationary-phase *L. infantum* promastigotes from *Li*VCP$^{+/+}$ or *Li*VCP$^{(NEO/+)}$ or *Li*VCP$^{(NEO/+)}$+VCP^{QQ} and or the facilitated dKO mutants *Li*VCP$^{(NEO/HYG)}$+VCP^{HA}, *Li*VCP$^{(NEO/HYG)}$+^{HA}VCP and *Li*VCP$^{(NEO/HYG)}$+VCP were used for *in vitro* infection of PMA-treated THP1 macrophages (MØ). The percentage of infected MØ with the above strains at 6 hours post-infection is shown in (A). The average number

of *L. infantum* intracellular amastigotes per THP1 MØ immediately after infection (6 hours) (B) and at 96 hours post-infection (C) as determined microscopically by Giemsa staining. The results shown here are the mean and standard deviation of two experiments performed in triplicates. Statistical significance was assessed by the two-tailed unpaired *t*-test ($***P \leqslant 0.001$). Asterisks indicate significant difference between the *L. infantum* VCP mutant cell lines.

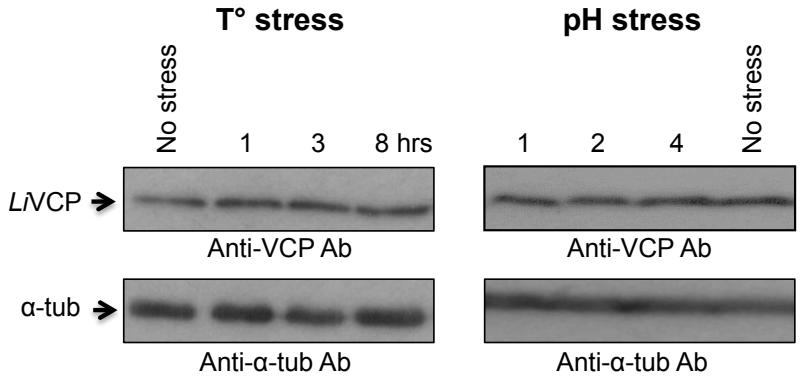

Fig. S9

FIGURE S9 *Li*VCP protein expression under heat or acidic pH stress. Western blot analysis of *L. infantum* total lysates from parasites cultured either in SDM-79 medium at pH 7.0 and 25°C (no stress) or in SDM-79 combined to heat stress (37°C) or in MAA medium (pH 5.5) at 25°C (acidic pH stress) at different time points using an anti-*Tb*VCP antibody. The same membrane was blotted with an anti-α-tubulin antibody as protein loading control (lower panel).

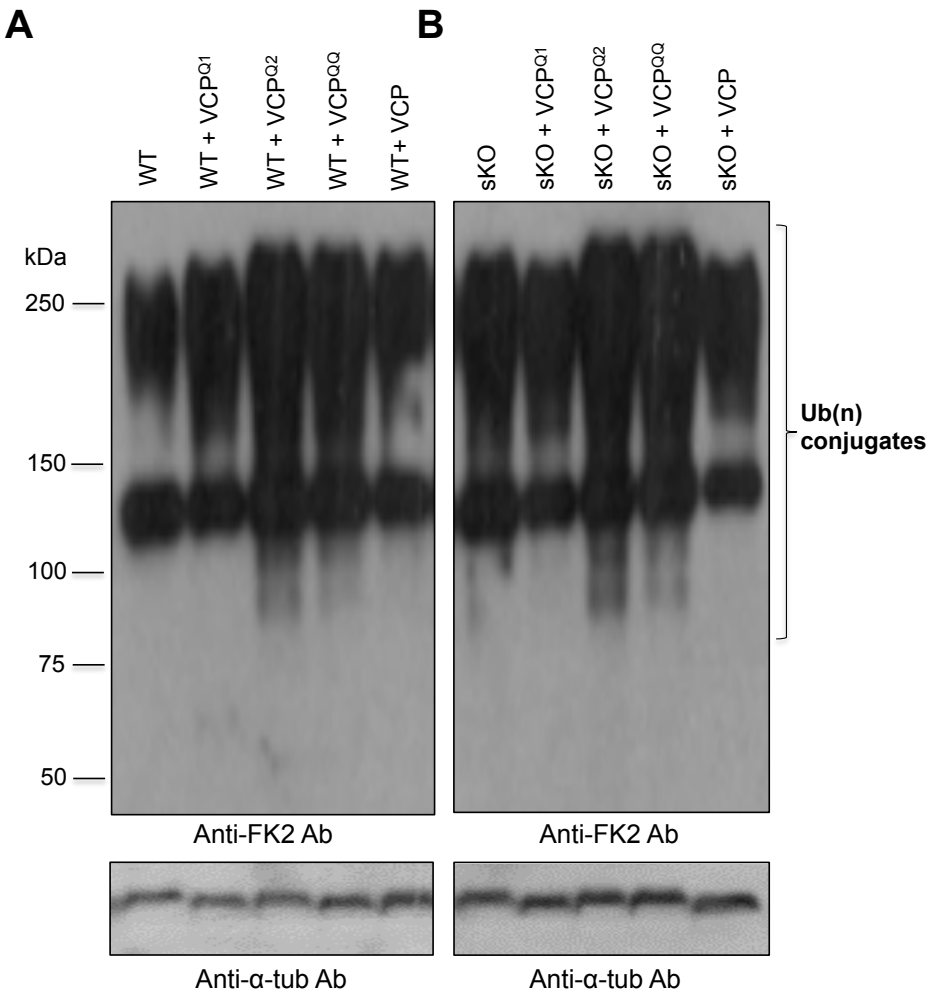

Fig. S10

FIGURE S10 Decreasing expression of *Li*VCP or impairing its function using dominant negative mutants leads to high accumulation of polyubiquitinated proteins. This figure is a longer exposure of Figure 9. Western blot analysis of *L. infantum* WT (A) and sKO (*Li*VCP$^{(NEO/+)}$) lines (B) using the FK2 antibody recognizing K29-, K48-, and K63-linked mono- and polyubiquitinated proteins. Equal amount of proteins was loaded on the gel. An anti-α-tubulin antibody (lower panels) was used as loading control. The data shown here are representative of four independent experiments yielding similar results.

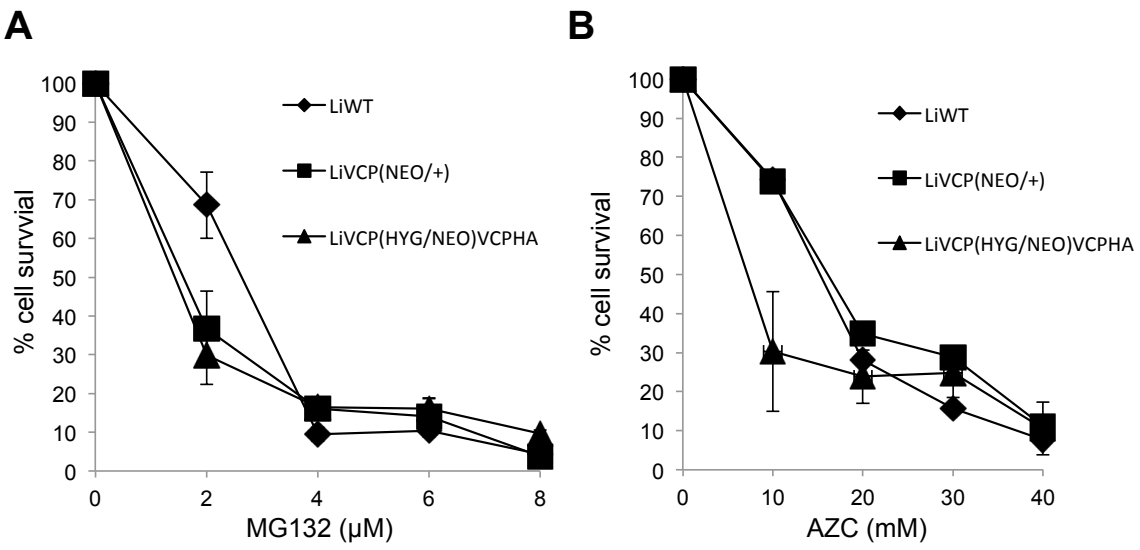

C

IC_{50}:	MG-132 (μM)	AZC (mM)
*Li*WT	2.6±0.22	15±1.7
*Li*VCP$^{(NEO/+)}$	1.5±0.25	16±2.0
*Li*VCP$^{(HYG/NEO)}$VCP^{HA}	1.3±0.15	7.3±1.5

Fig. S11

FIGURE S11 Sensitivity of *L. infantum* VCP mutants to proteasome inhibitors or to drugs inducing proteotoxicity. *Li*WT, *Li*VCP$^{(NEO/+)}$ and *Li*VCP$^{(HYG/NEO)}$+VCP^{HA} strains were treated with various concentrations of the proteasome inhibitor MG-132 (Enzo; 0 to 8 μg/ml) (A) or L-Azetidine-2-carboxylic acid (AZC) (Santa Cruz) (0 to 40 mM) (B) for 96 h. The drug sensitivity was evaluated by measuring the OD at 600 nm in 24 well plates. (C) The IC_{50} values for MG-132 and AZC are expressed as mean ± SD.

Chapter 3: Molecular and functional characterization of the AAA+ ATPase Valosin-containing protein (VCP)/p97/Cdc48 interaction network in *Leishmania*

3.1 Avant-propos

This chapter corresponds to a scientific paper entitled “Functional characterization of the p97/valosin-containing protein (VCP) interacting network in *Leishmania*” by Guedes Aguiar, B., Maaroufi H; Padmanabhan, P. K., Dumas, C., & Papadopoulou, B. submitted for publication in *Scientific Reports* on November 2019. This paper is presented as it was submitted. The study was designed by BGA and BP. All experiments were performed by BGA with help of CD and PKP. HM was responsible for 3D structure prediction and docking studies. The paper was written and corrected by BGA and BP.

Molecular and functional characterization of the AAA+ ATPase Valosin-containing protein (VCP)/p97/Cdc48 interaction network in *Leishmania*

Bruno G. Aguiar[1,2,3], Carole Dumas[1,2], Halim Maaroufi[4], Prasad K. Padmanabhan[1,2] and Barbara Papadopoulou[1,2]*

[1]Research Center in Infectious Diseases, CHU de Quebec Research Center-University Laval

[2]Department of Microbiology-Infectious Disease and Immunology, Faculty of Medicine, University Laval, Quebec, QC. Canada G1V 4G2

[3]Department of Community Medicine, Federal University of Piauí, Teresina, Brazil

[4]Institut de Biologie Intégrative et des Systèmes (IBIS), University Laval, Quebec, QC. Canada G1V 0A6

* Corresponding author:

Barbara Papadopoulou
CHU de Quebec Research Center-Laval University
2705 Laurier Blvd., Quebec (QC), Canada G1V 4G2
Phone: (418) 525-4444, ext. 47608; Fax: (418) 654-2715
Email: barbara.papadopoulou@crchudequebec.ulaval.ca

Running title: VCP protein network in *Leishmania*

Key words: *Leishmania*; VCP/p97; VCP cofactors; Immunoprecipitation; LC-MS/MS; Network proteomics; 3D homology modeling; protein-protein docking; Gene Ontology; Immunofluorescence

List of abbreviations

AAA	ATPases Associated with diverse cellular Activities
DUB	Deubiquitinating enzyme
ER	Endoplasmic reticulum
ERAD	ER-associated degradation
EUPC	Exclusive unique peptide count
FAF	Fas-associated factor
FCS	Fetal calf serum
IP	Immunoprecipitation
*Li*VCP	*Leishmania infantum* VCP
MPN	Mpr1, Pad1 N-terminal domain
NPL4	Nuclear protein localization protein 4
OMM	Outer mitochondrial membrane
OTU1	Ovarian tumor domain-containing protein 1
PP1	Protein phosphatase type 1
PUB	PNGase/UBA or UBX-containing proteins
PUL	PLAP, Ufd3p, and Lub1p

SEP	Shp, eyes-closed, p47
SHP	BS1, binding segment 1
SPFH	Stomatin, prohibitin, flotillin, HflC/K
UBA	Ubiquitin-associated
UBL	Ubiquitin-like domain
UBX	Ubiquitin regulatory X
UBXD	Ubiquitin X domain
UBXL	UBX-like
UFD1	Ubiquitin fusion degradation protein 1
UPS	Ubiquitin Proteasome System
VBM	VCP-binding motif
VCP	Valosin-containing protein
VIM	VCP-interacting motif

3.2 Résumé

La protéine valosine (VCP)/p97/Cdc48 est une AAA + ATPase associée à de nombreuses voies cellulaires dépendantes de l'ubiquitine qui sont essentielles au contrôle de la qualité des protéines. VCP lie divers cofacteurs qui déterminent la sélectivité et la dégradation du substrat. Ici, nous avons utilisé des études de co-immunoprécipitation et de spectrométrie de masse couplées à des analyses *in silico* pour identifier l''interactome' de *Leishmania infantum* VCP (*Li*VCP) et pour prédire les interactions moléculaires entre *Li*VCP et ses principaux cofacteurs. Nos données corroborent un réseau de protéines associées à VCP qui est largement conservé chez *Leishmania*, y compris des partenaires d'interaction connus mais également nouveaux. L'analyse protéomique en réseau a confirmé les interactions *Li*VCP-cofacteurs et a fourni de nouvelles informations sur les partenaires spécifiques des cofacteurs et la diversité des complexes *Li*VCP, y compris le complexe bien caractérisé VCP-UFD1-NPL4. L'analyse de l'ontologie des gènes, associée aux études de fractionnement à la digitonine et d'immunofluorescence, supporte la compartimentation sous-cellulaire de cofacteurs avec une localisation cytoplasmique ou organellaire ou vacuolaire. En outre, des modèles *in silico* basés sur la modélisation d'homologie 3D et l'amarrage (docking) protéine-protéine ont prédit que les modules de liaison conservés chez les cofacteurs de *Li*VCP, à l'exception du NPL4, interagissaient avec des sites de liaison spécifiques dans l'hexamère *Li*VCP, de la même manière que leurs orthologues chez d'autres eucaryotes. Globalement, ces résultats nous ont permis de construire le premier réseau d'interaction de protéines liant VCP chez les parasites protozoaires grâce à l'identification de partenaires d'interaction connus et nouveaux potentiellement associés à des complexes de VCP distincts.

3.3 Abstract

Valosin-containing protein (VCP)/p97/Cdc48 is an AAA+ ATPase associated with many ubiquitin-dependent cellular pathways that are central to protein quality control. VCP binds various cofactors, which determine pathway selectivity and substrate processing. Here, we used co-immunoprecipitation and mass spectrometry studies coupled to *in silico* analyses to identify the *Leishmania infantum* VCP (*Li*VCP) interactome and to predict molecular interactions between *Li*VCP and its major cofactors. Our data support a largely conserved VCP protein network in *Leishmania* including known but also novel interaction partners. Network proteomics analysis confirmed *Li*VCP-cofactor interactions and provided novel insights into cofactor-specific partners and the diversity of *Li*VCP complexes, including the well-characterized VCP-UFD1-NPL4 complex. Gene Ontology analysis coupled with digitonin fractionation and immunofluorescence studies support cofactor subcellular compartmentalization with either cytoplasmic or organellar or vacuolar localization. Furthermore, *in silico* models based on 3D homology modeling and protein-protein docking indicated that the conserved binding modules of *Li*VCP cofactors, except for NPL4, interact with specific binding sites in the hexameric *Li*VCP protein, similarly to their eukaryotic orthologs. Altogether, these results allowed us to build the first VCP protein interaction network in parasitic protozoa through the identification of known and novel interacting partners potentially associated with distinct VCP complexes.

3.4 Introduction

Leishmania species cause a large spectrum of diseases in humans ranging from skin lesions to visceral damage, which is lethal, if left untreated. Treatment options for leishmaniasis are limited and toxic and no effective vaccine is currently available (https://www.dndi.org/diseases-projects/leishmaniasis/). Within its mammalian host, *Leishmania* replicates in the phagolysosome compartment of macrophages where it encounters various stress stimuli that trigger important changes in gene expression[1–5] and parasite metabolism[6,7]. Most of those stresses lead to DNA damage or protein misfolding that has to be corrected. As many other eukaryotes[8], *Leishmania* has evolved quality control systems that cooperate to eliminate damaged proteins[9–12].

Recently, we have undertaken studies to characterize the *Leishmania* valosin-containing protein (VCP)/p97/Cdc48 ortholog (VCP and p97 in metazoa, Cdc48 in yeast)[10], one of the key quality control components in recycling or degrading misfolded proteins or aggregates. VCP belongs to the AAA+ (Associated with diverse cellular Activities) family of ATPases that hydrolyze ATP and use the resulting energy to extract polyubiquitinated target proteins from membranes, organelles, and large protein assemblies and delivered them to proteasomal degradation[13–16]. As a central component of the Ubiquitin Proteasome System (UPS), VCP/p97 plays a critical role in cellular proteostasis[13,17,18]. Indeed, VCP/p97 is involved in the endoplasmic reticulum (ER)-associated protein degradation[15,19], the mitochondrion-associated protein degradation[20], ribosomal quality control[21], the extraction of chromatin-bound proteins[22] or of damaged lysosomes by autophagy[23], genome stability[24], and stress granules clearance[25]. Mutations in this well-conserved protein can lead to protein aggregation and have been linked to several diseases, including neurodegenerative and muscular disorders and cancer[26–28].

Each monomer of the hexameric VCP/p97 protein is composed by an N-terminal domain followed by two tandem ATPase domains (D1 and D2) separated by a short linker, and an unstructured C-terminal tail[29]. The N-terminal domain can be further subdivided into two subdomains, Nn (15-95 aa) and Nc (104-175 aa). This structure allows the association of VCP with a large variety of cofactors/adaptors which determine substrate specificity, target the ATPase to different cellular locations, or modify the ubiquitin chain attached to the substrate[30–32]. So far, about 30-40 cofactors have been identified in mammals but their exact functions are still poorly understood. Whether they have a substrate-recruiting, processing or regulatory function, most cofactors interact with the Nn or Nc subdomains of VCP via a small number of conserved binding modules, while a lower number binds to the unstructured C-terminal tail formed by the last 7 amino

acids[30–32]. In mammals, most VCP cofactors contain the ubiquitin regulatory X domain (UBX) or UBX-like (UBXL) with similar three-dimensional structure described for ubiquitin. The UBX module interacts with the Nn-Nc cleft of the VCP through the Rx(3)FPR motif. Proteins such as UBXD1 to UBXD6, UBXD9 and UBXD11 contain only a UBX domain. The UBA (ubiquitin associated)-UBX cofactors, such as UBXD7, UBXD8 (FAF2), UBXD10 (p47), UBXD12 (FAF1) and UBXD13 also accommodate an UBA domain that is fundamental for interacting with ubiquitinated substrates[16,33]. Cofactors such as p47 harbor, in addition to the UBX and UBA domains important for their function in the UPS, a SHP (BS1, binding segment 1) motif as another site for interaction with the Nc subdomain of VCP [31,32]. Cofactors harboring either a VIM (VCP-interacting motif) or VBM (VCP-binding motif) motif also interact with the same hydrophobic pocket of the N-domain[32]. One of the most studied VCP cofactor, the heterodimer UFD1-NPL4 (UN), interacts with VCP to form the VCP-UFD1-NPL4 complex which extracts polyubiquitinated proteins from membranes and macromolecular complexes and is involved in a series of biological processes, including ER-associated degradation (ERAD)[34]. Few cofactors have been reported to interact with the C-terminus of VCP. These harbor a PUB (PNGase/UBA or UBX-containing proteins) or a PUL (PLAP, Ufd3p, and Lub1p) domain which forms a hydrophobic pocket for interactions with the C-terminal tail of VCP [35] following association of key amino acids such as Leu[804] and the aromatic side chain of the penultimate tyrosine[805] residue[30–32].

Our initial studies on the ubiquitin selective chaperone VCP/p97 in *Leishmania* (*Li*VCP) demonstrated its essential role in the parasite intracellular development and survival under heat stress[10]. In this study, we provide novel insights into the *Li*VCP interaction network. A series of immunoprecipitation experiments coupled to liquid chromatography-tandem mass spectrometry analysis were used to identify the major interacting partners of *Li*VCP. These studies uncovered p47, UFD1, NPL4, FAF2 and PUB1 as the core *Li*VCP cofactors. Network proteomics for each cofactor confirmed close partnership with *Li*VCP and revealed the presence of multiple *Li*VCP complexes in *Leishmania*, including the well-characterized *Li*VCP-*Li*UFD1-*Li*NPL4 complex. Gene Ontology analysis of each cofactor proteome combined with digitonin fractionation and immunofluorescence studies support cofactor subcellular compartmentalization. Furthermore, *in silico* models based on 3D homology modeling and protein-protein docking predicted that conserved binding modules within key *Leishmania* VCP cofactors, with the exception of NPL4, interact with specific binding sites in the hexameric *Li*VCP protein, as described for their mammalian orthologs. Altogether, these results allowed us to build the *Leishmania* VCP protein network, the first characterized in parasitic protozoa.

3.5 Results

Identification of the *Leishmania* VCP/p97 cofactors and core proteome

VCP/p97 is a hexameric protein that can interact with a large number of protein cofactors through its N-terminal and C-terminal domains[27]. These interactions are key for its activity and functional diversity. This study aimed to identify the *Leishmania* VCP interactome based on the human VCP/p97 network from the BioGrid database (Supplementary Table S1) as well as on protein-protein interaction experiments. According to the e-value similarity accessed by protein BLAST (blastP), most proteins from the human VCP network have homologs in *Leishmania* (Supplementary Fig. S1).

Seeking for the identification of *Leishmania* VCP cofactors, we carried out a series of immunoprecipitation (IP) experiments with either C- or N-terminally HA-tagged *Leishmania infantum* VCP (*Li*VCP; LinJ.36.1420)[10] followed by LC-MS/MS, database searching, and peptide identification. To allow VCP expression from its endogenous locus, we replaced one *Li*VCP genomic copy by an HA-epitope tagged *Li*VCP (*Li*VCP-HA) (Fig. 1A). Both episomal and integrated *Li*VCP-HA versions were expressed at levels comparable to the endogenous VCP protein (Fig. 2B) and yielded similar IP results. From seven independent IP-MS/MS experiments (see Methods), 218 proteins were initially identified as potential *Li*VCP interacting partners (Supplementary Table S2). To decrease the number of false positives in the *Li*VCP network building, we applied a stringent filter. First, we calculated the average number of peptides for each protein in all seven IPs and then we excluded proteins also found in five independent IP-MS/MS studies conducted with HA-tagged proteins unrelated to the VCP complex (Fig. 1C and Supplementary Table S2). From this analysis, 24 proteins were selected to specifically associate with *Li*VCP. Among those, 15 proteins with an average of exclusive unique peptide count (EUPC) ≥ 2.0 were classified as the *Li*VCP core partners (Fig. 1D and Supplementary Table S2). These share conserved domains with known VCP cofactors in other eukaryotes, such as the p47 (Shp1) UBX/UBA- and SEP-containing protein (LinJ.22.0200), the UBX-containing protein FAF (Fas-associated factor) shown a higher homology to the human FAF2 protein (UBXD8 or ETEA; LinJ.35.1960), the ubiquitin fusion degradation protein 1 (UFD1; LinJ.36.6780), the nuclear protein localization 4 (NLP4; LinJ.25.1320) known to form a heterodimer with UFD1[34], an ubiquitin associated UBA/TS-N domain protein (LinJ.24.1650) with an identified ER membrane signal peptide, and two PUB (PNGase/UBA or UBX) domain containing proteins (LinJ.11.0920 and LinJ.09.1060). In addition, the *Li*VCP proteome core includes the serine/threonine phosphatase type 1 (PP1) (LinJ.34.0900), the PP1 regulator-like protein (LinJ.05.1200) whose human homolog

SDS22 is known to interact with VCP[36], three mitochondrial proteins - a stomatin-like protein (LinJ.05.1040), an ATP-dependent zinc metallopeptidase (LinJ.36.2850) and the AAA+ FtsH protease (LinJ.36.2850), a tetratricopeptide repeat protein part of the ER membrane protein complex subunit 2 (LinJ.17.0230) and three hypothetical proteins (LinJ.36.5080, LinJ.03.0250, LinJ.15.1570) (Fig. 1D) with some similarity to the yeast nuclear envelope protein Nsp1-like C-terminal region, syntaxin-like domain, and putative nuclear jumonji-like domain, respectively.

Apart from the above core partners, *Li*VCP co-immunoprecipitated heat shock proteins, chaperonins, T-complex proteins, mitochondrial integrity and stress response proteins, translation factors and ribosomal proteins, components of the trypanothione and peroxidase systems, RNA-binding proteins, and proteasome subunits (Supplementary Table S2) in line with its function in a broad array of ubiquitin-dependent protein quality control pathways[13–16].

'Network proteomics' analysis to identify interacting partners of the core *Li*VCP cofactors and associations between cofactor-bound proteins

The interaction of p47, UFD1, NPL4, FAF2 and PUB1 with the *Leishmania* VCP ortholog was further confirmed by inverse co-immunoprecipitation studies. C- or N- terminally HA-tagged *Li*p47, *Li*NPL4, *Li*UFD1, *Li*FAF2, or *Li*PUB1 proteins cloned into vector pSPαZEOα were transfected and stably expressed in *L. infantum* promastigotes (Supplementary Fig. S2). Immunoprecipitation of these HA-tagged cofactor versions using an anti-HA antibody followed by western blotting with a specific anti-*Tb*VCP antibody[10,37] confirmed their association with *Li*VCP (Fig. 2A). The co-immunoprecipitation of *Li*UFD1, *Li*NPL4, *Li*p47, *Li*FAF2 and *Li*PUB1 with *Li*VCP (Fig. 1D and Table 1) and the detection of *Li*VCP in *Li*UFD1, *Li*NPL4, *Li*p47, *Li*FAF2 and *Li*PUB1 immunoprecipitates by western blotting (Fig. 2A) and mass spectrometry (Fig. 2B, Table 1, Supplementary Table S2) confirmed their close partnership.

As done for *Li*VCP, we carried out IP-MS/MS studies with five unrelated proteins to VCP complexes (average EUPC >3.6; *Li*VCP threshold) to filter out non-specific *Li*VCP cofactor partners (Fig. 3A and Supplementary Table S2). The remaining proteins that co-immunoprecipitated with *Li*p47 (145), or *Li*FAF2 (164), or *Li*UFD1 (46) and or *Li*PUB1 (98) can be considered as putative cofactor interacting partners (Fig. 3A, Table 1 and Supplementary Table S2).

*Li*p47 co-immunoprecipitated *Li*PUB1, the serine/threonine protein phosphatase 1 (PP1) catalytic subunit beta (LinJ.28.0730), a PP1 regulator-like protein that is homologous to the yeast SDS22 protein (LinJ.05.1200), and the PP1 phosphatase inhibitor that is homologous to the yeast Ypi1 protein (LinJ.07.0840) (Table 1). In *Saccharomyces cerevisiae,* these three proteins form a

ternary complex that is important for the nuclear localization of PP1 and whose assembly and quality control requires Cdc48 and its adaptor p47[38].

As reported in other eukaryotes[34], the *Leishmania Li*UFD1 protein complexes with NPL4 to form the heterodimer cofactor UFD1-NPL4 but also associates with *Li*FAF2 (Table 1). Complex formation between VCP-NPL4-UFD1, FAF1 and polyubiquitinated proteins was shown previously to promote ER-associated degradation[39]. Other proteins only associated with the *Li*UFD1 proteome include a mitochondrial serine carboxypeptidase (CBP1; LinJ.18.0450), a phenylalanine-4-hydroxylase (LinJ.28.1390), peroxin PEX12 (LinJ.19.1240) and three hypothetical conserved proteins (LinJ.03.0250, LinJ.29.2300, LinJ.12.0550) (Table 1 and Supplementary Table S2). Interestingly, the hypothetical protein LinJ.03.0250 was also found in *Li*VCP immunoprecipitates (Fig. 1C), and some of the other *Li*UFD1 interacting proteins have homologs known to be part of the VCP network in other systems (see Discussion).

Proteins solely detected in *Li*FAF2 pull-down include a tetratricopeptide repeat containing protein of the ER membrane protein complex (LinJ.17.0230) also found in *Li*VCP immunoprecipitates (Fig. 1C), several peroxisomal/glycosomal proteins that are homologs of the peroxins PEX2 (LinJ.25.2330), PEX10 (LinJ.25.2400) and PEX11 (LinJ.35.3740), two fatty acid elongases (ELO1: LinJ.14.0680 and ELO3: LinJ.14.0760), a cell differentiation protein-like (LinJ.34.4180), and hypothetical protein LinJ.36.5360 (Table 1).

The *Li*PUB1 cofactor co-immunoprecipitated a serine palmitoyltransferase 1-like protein (LinJ.34.3530; SPT1), also found in the *Li*UFD1 proteome (Table 1). Serine palmitoyltransferase catalyzes the first and rate-limiting step in sphingolipid (ceramide) biosynthesis and has been associated with the resistance to heat stress and apoptosis[40,41].

Interestingly, several *Li*VCP cofactor-associated proteins are common to more than two cofactors (see Table 1). For example, *Li*p47, *Li*FAF2 and *Li*PUB1 co-immunoprecipitated the tubulin polymerization-promoting protein TPPP/p25-alpha (LinJ.34.1620) that stabilizes microtubules[42] and also protects against abnormal forms of prion proteins[43], as well as the root hair defective 3 GTP-binding protein (RHD3) (LinJ.32.0380) that is analogous to the mammalian atlastin GTPases involved in shaping ER tubules[44]. An ADF/cofilin factor (LinJ.29.0520) of the family of actin remodeling proteins[45] co-immunoprecipitated with both *Li*p47 and *Li*FAF2. The ribosomal protein S33 (LinJ.26.1610) and the hypothetical protein LinJ.33.1130 co-immunoprecipitated with *Li*FAF2 and *Li*PUB1. The V-type proton ATPase subunit D (LinJ.05.1140), a multi-subunit membrane protein complex that is evolutionarily related to F-type adenosine triphosphate synthases and A-ATP synthases[46], co-immunoprecipitated with *Li*p47 and *Li*UFD1. The *Li*UFD1, *Li*FAF2 and *Li*PUB1 cofactors co-immunoprecipitated the

trypanosomatid functional analog of Tom40 (ATOM40; LinJ.35.4920), which is the central pore of the TOM complex involved in the import of mitochondrial proteins[47]. Finally, all *Li*VCP core cofactors co-immunoprecipitated a fatty acid elongase (ELO2) (LinJ.14.0700).

General features of the *Li*VCP core cofactors

Proteins specifically co-immunoprecipitated with *Li*UFD1, *Li*p47, *Li*FAF2, or *Li*PUB1 were submitted to Gene Ontology – cellular component (GO-CC) enrichment analysis using the tool provided by TriTrypDB (Fig. 3B and Supplementary Table S3). An enrichment of a 19-fold for vacuolar proteins was seen in the *Li*UFD1 proteome. Nuclear proteins were exclusively enriched within the *Li*p47 proteome and endoplasmic reticulum-related proteins were enriched only within the *Li*FAF2 and *Li*PUB1 proteomes.

Molecular function (MF) and biological process (BP) analyses were also done aside comparison with the *Li*VCP proteome (Supplementary Table S3). Globally, the molecular function analysis predicted proteins with translation factor activity and structural constituents of the ribosome, RNA-binding activity, structural molecule activity and peptidase activity. ATPase and ligase activities were exclusively enriched within the *Li*FAF2 proteome while transmembrane transporter activity was only associated with the *Li*UFD1 proteome.

The biological process analysis showed that cofactor-associated proteins were mostly involved in translation, protein targeting and folding, and several metabolic processes. Protein folding and tRNA metabolic processes were found only associated with the *Li*FAF2 proteome while protein targeting and mitotic cell cycle were enriched in the *Li*PUB1 proteome (Supplementary Table S3). Overall, Gene Ontology analysis of each proteome indicated specific compartment-association for each cofactor.

Subcellular localization of the *Li*VCP core cofactors

To determine the subcellular localization of the core *Li*VCP cofactors, we carried out digitonin fractionation and indirect immunofluorescence studies. As a central player to the endoplasmic reticulum (ER)-associated protein degradation[19,48] and the translocation of damaged mitochondrial proteins from the outer mitochondrial membrane (OMM) into the cytosol [20,49], VCP has been found associated with both ER and OMM fractions, similarly to what we have described previously for the *Leishmania Li*VCP[10].

First, we treated *Leishmania* parasites with increasing concentrations of digitonin (20 µM-10 mM) and carried out western blotting on the different cellular sub-fractions using an anti-HA antibody (all cofactors were HA-epitope tagged). Our results indicate an association of *Li*FAF2

and partly of *Li*PUB1 proteins with the organellar fraction and an enrichment of *Li*UFD1, *Li*p47 and *Li*NPL4 proteins with the cytosolic fractions (Fig. 4A). Immunofluorescence studies using an antibody directed against the ER BiP protein confirmed that *Li*FAF2 and partly *Li*PUB1 co-localize to endoplasmic reticulum (Fig. 4B, 4C). No co-localization was found with the mitochondrion (data not shown). Immunofluorescence studies to detect *Li*p47 demonstrated a partial co-localization with the histone H3 nuclear marker (Fig. 4D), as also suggested by GO analysis (Fig. 3B).

Predicted molecular interactions between the conserved domains of *Li*VCP cofactors and the *Leishmania* VCP protein based on 3D homology modeling and protein-protein docking

It has been shown previously that the VCP/p97/Cdc48 hexamer can bind to its various cofactors through the UBX or PUB domains or a ubiquitin-like fold or through one of the linear binding motifs such as SHP [32]. The *L. infantum Li*VCP encodes a protein of 784 amino acids that is highly conserved among its eukaryotic orthologs (75% aa identity with the human VCP/p97 protein)[10] and harbors all the characteristic domains of VCP orthologs (Fig. 5A, top). Based on sequence similarity and conservation to mammalian VCP cofactor orthologs (Supplementary Fig. S1) and on the EUPC for each cofactor in *Li*VCP immunoprecipitates (Fig. 1), we selected *Li*p47, *Li*UFD1, *Li*NPL4, *Li*FAF2, and *Li*PUB1 as the core *Li*VCP cofactors for further investigation. Multiple sequence alignments of these *Li*VCP cofactors along with mammalian, yeast, trypanosomatid and non-trypanosomatid species helped us to generate phylogenetic trees revealing that *Li*p47, *Li*FAF2, *Li*UFD1, *Li*NPL4 and *Li*PUB1 are evolutionary distant from other eukaryotes but they harbor binding modules/motifs that are conserved and could represent specific domains for interaction with *Li*VCP (Supplementary Figs. S3-S7).

To investigate whether *Li*VCP-cofactor interactions identified by immunoprecipitation studies take place within the predicted binding sites in the hexameric *Li*VCP [30,32] and the conserved binding modules in *Li*p47, *Li*FAF2, *Li*UFD1, *Li*NPL4 and *Li*PUB1, we constructed 3D models by homology modeling and a protein-protein docking approach. 3D homology models are helpful in refining protein-protein interaction predictions that have been based on a sequence match alone as interface binding is more directly determined by the structure of the binding site rather than its sequence. The *Li*VCP homohexamer 3D molecular structure was obtained through homology modeling by superposition with the *H. sapiens* p97 homohexamer (PDBid: 5C18) template (Fig. 5A, bottom).

The *Li*p47 protein presents the same domain composition (UBA, SEP and UBX) than its human ortholog (Fig. 5B, upper). Similarly to the human p47, *Li*p47 harbors the sequence GMPP in the UBX domain (Supplementary Fig. S8) that docks *in silico* into the Nn-Nc pocket of *Li*VCP

(Fig. 5B and Supplementary Fig. S9)[50]. Although *Li*p47 shares only 25% amino acid identity with its human ortholog, it has 41% sequence similarity and 73% sequence coverage and contains the two SHP motifs (SHP1 and SHP2) (Supplementary Fig. S8) that together with the UBX domain are known to be key for the interaction with VCP[31]. The SHP site is typically characterized by the consensus sequence FxGxGx$_2$h that was recently summarized as h(x)$_{1-2}$F/W(x)$_{0-1}$GxGx$_2$L (h, hydrophobic residue; x, any amino acid)[32] and in *Li*p47, SHP1 and SHP2 sites, FYGRGQRL and FQGHGHRL, respectively are conserved (Supplementary Fig. S8). In addition, the Ramachandran plot showed that the amino acid residues of the *Li*p47 3D homology model are found in most favoured (87%) and additional allowed regions (8.7%) (Supplementary Table S4), which makes structure predictions reliable.

The *Li*FAF2 protein interacts with *Li*VCP through the GFPP motif in its UBX C-terminal domain as predicted by 3D homology modeling (Fig. 5C, Supplementary Fig. S10) and protein-protein docking upon superposition of the available structure of the human ^{40}GYPP^{43} motif in the ovarian tumor domain-containing protein 1 (OTU1) and the homologous part within the *Leishmania* FAF2 protein (Supplementary Fig. S11). Surprisingly, *Li*FAF2 lacks the ubiquitin-associated (UBA) domain that is present in the human FAF1 and FAF2 proteins and is fundamental for interacting with ubiquitinated substrates [51].

UFD1 is known to assemble with NPL4 to form the heterodimer UFD1/NPL4 (U/N), one of the most important p97/VCP cofactors, that recognizes polyubiquitinated substrates and together with VCP extracts them from organellar membranes or macromolecular complexes [52,53]. U/N binds to the N-terminal domain of VCP via the ubiquitin-like domain (UBL) of NPL4 and the SHP box of UFD1 [32]. The *Leishmania Li*UFD1 protein also contains the UBA domain and an UT6 region that accommodates the sequences QPTFAGAGRTL and RLKALGGGGRS corresponding to the SHP1 and SHP2 sites, respectively (Fig. 5D, top and Supplementary Fig. S12). 3D homology modeling predicts binding of *Li*UFD1 to *Li*VCP via its SHP1 site (Fig. 5D, bottom). Furthermore, docking essays propose that the SHP1 motif of *Li*UFD1 (reversed comparatively to the human SHP1) interacts with the same surface as in its human ortholog using amino acid residues Phe273, Arg278 and Leu280 (Phe228, Arg234 and Leu235 in human Ufd1) (Fig. 5D bottom and Supplementary Fig. S13).

In contrast to its eukaryotic orthologs, the *Leishmania* NPL4 lacks the N-terminal ubiquitin regulatory X (UBX)-like domain bound to the N-domain of Cdc48 hexamer, as well as the two Zn^{2+}-finger domains important for anchoring the adjacent Mpr1/Pad1 N-terminal (MPN) domain to the top of the D1 ATPase ring[34]. Interestingly, protein-protein docking simulations showed that despite the absence of the UBX-like domain, *Li*NPL4 seems to interact with the N-terminus of

*Li*VCP through its C-terminal GMPP motif (aa 350-353) (Supplementary Figs. S14, S15). Similarly to other eukaryotes[34], the U/N heterodimer in *Leishmania* also recognizes polyubiquitinated substrates as shown by *Li*NPL4 and *Li*UFD1 IPs followed by western blotting (Supplementary Fig. S16).

A representative member of the PUB (PNGase/UBA or UBX-containing) domain proteins in *Leishmania*, *Li*PUB1, which has no homolog in humans, contains a conserved region (Supplementary Fig. S17) that is predicted by 3D homology modeling (Fig. 5E) and protein docking (Supplementary Fig. S18) to interact with the last five amino acids ^{780}DDLYS^{784} of the *Li*VCP C-terminus, similarly to other PUB domain proteins [54].

Altogether, despite the evolutionary distance of *Li*VCP cofactors from their mammalian orthologs, *in silico* models based on structural data from the human orthologs using 3D homology modeling and protein-protein docking indicated that the conserved binding modules of *Leishmania* VCP core cofactors (except *Li*NPL4) interact with specific binding sites in the hexameric *Li*VCP, similarly to their mammalian orthologs.

The first trypanosomatid VCP interaction network

The resulting datasets from *Li*VCP, *Li*p47, *Li*UFD1, *Li*FAF2 and *Li*PUB1 IP-MS/MS studies were mined to identify interacting partners that are specific to each *Li*VCP cofactor as well as partners that are shared among multiple cofactors and *Li*VCP complexes (Fig. 6A) and allowed us to build the first *Li*VCP interaction network (Fig. 6B). To decrease the number of false positives, we excluded proteins that were co-immunoprecipitated with unrelated HA-tagged proteins (average of EUPC=0.0). From the total number of proteins co-immunoprecipitated with *Li*p47, *Li*UFD1, *Li*FAF2, and *Li*PUB1 (Fig. 3A) only 10, 17, 23 and 9, respectively together with 24 proteins specifically associated to *Li*VCP (Fig. 1, Table 1 and Supplementary Table S2) were considered to build the topology of *Li*VCP network (83 proteins in total, 47 shown in Fig. 6B). The list of proteins and their intersections are detailed in Supplementary Table S5 whereas the complete list of interacting proteins is presented in Supplementary Table S2.

In addition to the known cofactors, eight proteins were exclusively associated with the *Li*VCP proteome and might also be considered as cofactors of the *Leishmania* VCP protein. These include another PUB domain protein (PUB2) (LinJ.11.0920), an OTU1 (ovarian tumor domain-containing protein 1)-like cysteine protease (LinJ.36.6280) that is homologous to the *S. cerevisiae* deubiquitylation enzyme OTU1 shown to interact with VCP[55], a protein present in the outer mitochondrial membrane (LinJ.29.2220), a P-type H+-ATPase (LinJ.18.1510), a microtubule-associated protein (LinJ.26.1950), a member of the FYVE zinc finger proteins

(LinJ.36.2570) that serve as regulators of endocytic membrane trafficking and receptor signaling[56], a type 1 protein serine/threonine phosphatase (PP1) (LinJ.34.0900) and a *Leishmania* specific hypothetical protein (LinJ.36.5080) (Fig. 6B and Supplementary Table S5).

Our analysis revealed that the *Li*UFD1 and *Li*FAF2 proteomes share five proteins in common with *Li*VCP. These include the mitochondrial stomatin-like protein 2 (SPL-2) (EUPC>20), the membrane-integrated mitochondrial AAA/FtsH protease[57], an UBA domain containing protein (LinJ.24.1650), and hypothetical conserved proteins LinJ.15.1570 and LinJ.36.4740 (Table 1, Fig. 6B). *Li*VCP and *Li*p47 mutually associate with the serine/threonine protein PP1 phosphatase catalytic subunit, the PP1 phosphatase inhibitor Ypi1, and the SDS22 (EUPC=20) PP1 regulator-like protein (Table 1, Fig. 6B and Supplementary Table S5). *Li*VCP and *Li*FAF2 mutually co-immunoprecipitate the tetratricopeptide repeat protein (LinJ.17.0230) and an uncharacterized protein family (LinJ.07.0450), both subunits of the ER membrane protein complex (Table 1, Fig. 6B and Supplementary Table S5). *Li*VCP and *Li*UFD1 mutually interact with the hypothetical protein LinJ.03.0250 (Table 1, Fig. 6B and Supplementary Table S5). Specific interactions between cofactor-associated partners that do not involve an association with *Li*VCP are described in detail in the 'network proteomics' section (see also Table 1 and Fig. 6B).

Overall, using combined datasets from multiple IP/MS-MS studies for *Li*VCP and its main cofactors, we unveiled the first *Leishmania Li*VCP interactome. Many of the *Li*VCP interactors have homologs that are known to interact with VCP in other eukaryotic systems but others do not and may be relevant to study further as part of distinct *Leishmania* VCP complexes.

3.6 Discussion

In this study, we have characterized the valosin-containing protein (VCP) interaction network, the first in parasitic protozoa. We have employed a series of co-immunoprecipitation and mass spectrometry analyses coupled with *in silico* models that allowed us to identify the *Leishmania* VCP proteome with its major cofactors and their interacting partners, as well as, to predict molecular interactions between conserved domains within these cofactors and specific binding sites in the hexameric *Li*VCP. Our data support several similarities but also important differences between the *Leishmania* VCP protein network and VCP complexes characterized in other eukaryotes.

Most of the known classes of VCP cofactors in other eukaryotes have orthologs in *Leishmania*. However, cofactors harboring the VIM (VCP-interacting motif)/VBM (VCP-binding motif) motifs[58] were not found in any of our immunoprecipitation experiments, and with the exception of the ERAD-associated E3 ubiquitin-protein ligase HRD1 (LinJ.15.1460) no homologs

of this class of proteins were depicted in the *Leishmania* genome. While *Li*VCP is highly conserved among different eukaryotic organisms and harbors all the characteristic domains of the human p97/VCP ortholog[10], most of the major *Li*VCP cofactors are phylogenetically distant from their eukaryotic orthologs. However, despite their evolutionary distance from yeast and mammalian orthologs, *in silico* models based on 3D homology modeling and protein-protein docking indicated that the conserved binding modules of *Leishmania* VCP cofactors interact with specific binding sites in the hexameric *Li*VCP, similarly to their eukaryotic orthologs. This is the case for *Li*p47 and *Li*FAF2 that bind the Nn-Nc pocket of *Li*VCP through the sequence GMPP/GFPP in their UBX domain. Surprisingly, *Li*FAF2 lacks the UBA domain and theoretically should have lost the ability of binding ubiquitinated substrates[59]. Similarly to its yeast ortrholog[34], *Li*UFD1 interacts with the N-terminus of *Li*VCP through its conserved SHP motif. *Li*PUB1 while has no human homolog yet interacts with the C-terminal region of *Li*VCP, as described for the human VCP-PUB complex.

One of the important differences unveiled by our study concerns *Li*NPL4, which lacks the UBX-like domain and the two Zn^{2+}-finger motifs shown to bind VCP. Indeed, recent studies on the structure of the Cdc48-Ufd1-Npl4 complex from the thermophilic fungus *Chaetomium thermophilum* demonstrated that Npl4 interacts with the Cdc48 N-terminal region through its UBX-like domain and uses the Zn^{2+}-finger motifs to anchor its MPN domain to the top of the D1 ATPase ring[34]. On the other hand, Ufd1 interacts with Npl4 to form the Ufd1-Npl4 heterodimer through a short segment of its UT6 domain[34] which is also conserved in the *Leishmania* Ufd1 ortholog. Our 3D homology modeling and docking experiments predicted binding of *Li*NPL4 to *Li*VCP through its C-terminus GMPP motif. All NPL4 orthologs of the genus *Leishmania*, *Leptomonas* and *Phytomonas* harbor the GMPP motif and a variant of this motif, GM-[EDS]-PP, is present in *Trypanosoma* species. This unique feature in Trypanosomatidae paves the way for the design of inhibitors specifically targeting NPL4 binding to VCP. Ufd1-Npl4 and p47 are substrate-recruiting cofactors shown to bind VCP in a mutually exclusive manner as they compete for the same binding modules[30,31]. This seems also to be the case in *Leishmania*. *Li*p47 was neither found in the *Li*UFD1 proteome nor *Li*UFD1 in the *Li*p47 pull-down. Moreover, they do not share common interacting partners, except for the V-type proton ATPase subunit D.

Our analysis led us to identify the first PUB domain proteins in *Leishmania* and to unveil *Li*PUB1 as one of the major *Li*VCP cofactors interacting with the C-terminal region of *Li*VCP. Furthermore, new prospects were opened with the yet non-studied PUB domain protein *Li*PUB2 identified here as a putative *Li*VCP cofactor. In addition, a third UBX- and PUB domain-containing protein (LinJ.36.0140; *Li*PUB3) was retrieved by searching the *L. infantum* genome database.

PUB domain proteins known to bind to the C-terminus of the VCP hexamer have been associated with autophagy of damaged lysosomes[23] but the physiological significance of these interactions remains to be determined. Here, we found that a serine palmitoyltransferase-like protein was associated solely with the *Li*PUB1 proteome. Interestingly, a homolog of this protein in yeast is required for resistance to heat shock and plays an essential role in the removal or refolding of denatured or aggregated cytoplasmic proteins[60]. We have reported recently that *Li*VCP is essential for the parasite survival under heat stress[10], and PUB proteins with the help of a serine palmitoyltransferase may contribute to this process.

Interestingly, our study revealed new *Li*VCP interacting partners exclusively associated with the *Li*VCP proteome that might function as *Li*VCP cofactors. These include a PUB domain protein (*Li*PUB2), an outer mitochondrial membrane protein, a P-type H+-ATPase with homology to fungal and plant proton pumps[61], a FYVE zinc-finger protein known to bind phosphatidylinositol 3-phosphate in membranes of endocytic vesicles that regulate membrane trafficking and receptor signaling[56], a microtubule-associated protein, and several hypothetical conserved proteins that may be part of distinct VCP-complexes. *Li*VCP, and also *Li*p47, associates with the type 1 protein serine/threonine phosphatase (PP1) complex consisting of the PP1 catalytic subunit Glc7/PP1-B, the SDS22 regulator-like protein and the protein phosphatase PP1 inhibitor YPI1. In *S. cerevisiae,* nuclear localization of Glc7 requires Sds22 and Ypi1[62]. It has been shown recently that nuclear PP1 activity is positively regulated by the AAA-ATPase Cdc48 and its cofactor Shp1 (p47)[63] to promote the assembly of the Glc7-Sds22-Ypi1 PP1 complex and to ensure its quality control[38]. Interestingly, here we found that *Li*p47 interacts with a large number of nuclear proteins and that is partly localized to the nucleus. From an evolutionary point of view, it is interesting that the interaction of *Li*VCP with *Li*p47 may regulate the assembly of the Glc7-Sds22-Ypi1 complex like is the case in yeast. *Li*VCP was found also associated, although not in all immunoprecipitates, with substrate-processing cofactors like the thioesterase ovarian tumor domain-containing protein 1 (OTU1), a deubiquitinating enzyme involved in ERAD through the interaction of its UBX-like (UBXL) domain with the N-terminus of Cdc48[64]. Although it is yet unclear how the polyubiquitinated substrates are released from the p97/VCP/Cdc48 complex and passed on to the proteasome[65], OTU1 can be the deubiquitinase involved in this process as its UBXL domain interacts with VCP[55]. Although the *Leishmania* OTU1 ortholog does not harbor a well-defined UBXL domain, interestingly the ^{39}GYPP^{42} loop of UBXL in *S. cerevisiae* shown not only to be critical for the interaction with VCP but also for its role in the ERAD pathway[55] it is conserved in *Leishmania* (^{49}G<u>F</u>PP^{52}).

Another novel finding here is the association of the *Leishmania* VCP and also of its cofactors *Li*FAF2 and *Li*UFD1 with a stomatin-like protein 2 (SLP-2). Stomatins are members of the SPFH (stomatin, prohibitin, flotillin, HflC/K) superfamily that localize to the mitochondrial inner membrane scaffolding for the spatial organization of inner membrane proteases regulating mitochondrial dynamics, quality control, and cell survival[66]. Accordingly, our data support the association of *Li*UFD1 with transmembrane transport and peptidase activity proteins. It is possible that *Li*VCP associates with SLP-2 through UFD1, which also interacts with FAF2. Also present in the *Li*VCP proteome and associated with both *Li*FAF2 and *Li*UFD1 cofactors is the mitochondrial ATP-dependent AAA+ protease FtsH whose proteolytic and chaperone-like activity is crucial to the protein degradation protein quality control of mitochondrial and chloroplast membranes[67]. This suggests a new model for membrane protein degradation mediated by ATP-dependent proteolytic systems[57].

Our data support a subcellular compartmentalization for the key *Li*VCP cofactors. *Li*FAF2 and *Li*PUB1 are associated with organelles, *Li*FAF2 most likely with endoplasmic reticulum (ER), *Li*p47 is partially localized to the nucleus, *Li*UFD1 is possibly associated with cytosolic vacuoles, and NPL4 is enriched in the cytoplasm. Interestingly, *Li*FAF2 is associated with the peroxisomal biogenesis factors PEX2, PEX10 and PEX11. Similarly to other eukaryotes[68], recent data in trypanosomatids support *de novo* biogenesis of peroxisomes (glycosomes) from the ER[69]. In higher eukaryotes PEX2, PEX10 and PEX12 are part of the peroxisomal E3 ubiquitin ligase complex required for pexophagy, a pathway to degrade ubiquitinated peroxisomes that involves an AAA ATPase complex with a striking similarity to p97[70]. Glycosome turnover in *Leishmania* is mediated by autophagy[71] and the VCP/p97 quality control system, possibly through its FAF2 cofactor, may contribute to the control of glycosome homeostasis and turnover in these parasites. *Li*FAF2 also associates with two fatty acid elongases of the ELO GNS1/SUR4 family involved in the membrane-bound fatty acid chain elongation[72]. Interestingly, an ELO2 fatty acid elongase was found in the proteome of all four *Li*VCP cofactors (p47, UFD1 FAF2, PUB1). In trypanosomatids, the fatty acid elongation pathway occurs in the membrane of the ER[73] and this could explain its association with components of the ERAD pathway.

In summary, this study allowed us to build the first VCP protein interaction network in trypanosomatids through the identification of known and novel interacting partners potentially associated with distinct VCP complexes. Our proteomics datasets identified biologically relevant functions for the *Leishmania* VCP cofactors and provided an important resource for further investigation of VCP function in several cellular processes related to protein quality control in these parasites.

3.7 Methods

Parasite strains, plasmid constructs and transfections

Leishmania infantum MHOM/MA/67/ITMAP-263 was used in this study. *L. infantum* promastigotes were cultured in SDM-79 medium supplemented with 10% heat-inactivated FCS (Multicell Wisent Inc., Canada) and 5 µg/ml hemin at pH 7.0 and 25° C. The *Lip47* (LinJ.22.0200/LINF_220008200), *LiFAF2* (LinJ.35.1960/LINF_350024700), *LiUFD1* (LinJ.36.6780/LINF_360076400), *LiNPL4* (LinJ.25.1320/ LINF_250019000), and *LiPUB1* (LinJ.09.1060/LINF_090016300) genes were amplified and cloned into pSP72αZEOα. An HA epitope tag was added either at their N-or C-terminus. Primers used in this study are shown in Supplementary Table S6. The generated plasmids were independently transfected into *L. infantum* promastigotes. Purified plasmid DNA (10–20 µg, Qiagen Plasmid Mini Prep Kit, Toronto, Ontario, Canada) or linearized fragments (10–20 µg for the targeting cassette 5'flank-αZEOα-VCP^{HA}-3'flank from[10]) were transfected into *Leishmania* by electroporation as described previously[74]. Stable transfectants were selected and cultured with 0.6 mg/ml zeocin (Sigma).

Protein lysate preparations and western blots

Western blots were performed following standard procedures. The anti-mouse HA tag monoclonal antibody (1:3000; ABM), the anti-mouse HSP70 (cytosolic) antibody (1:400, Acris), the anti-rabbit HSP70 (mitochondrial) antibody (1:2000, kindly provided by Dr Osvaldo de Melo Neto, Recife, Brazil), and the anti-mouse *T. brucei* (*Tb*)VCP antibody (1:5000; [37]) kindly provided by Dr. James D. Bangs (Department of Microbiology & Immunology, Jacobs School of Medicine & Biomedical Sciences, University at Buffalo, USA) were used in this study. As a secondary antibody, we used the anti-mouse Horseradish peroxidase (HRP) (Cell Signalling) or the anti-rabbit-HRP antibody (GE Healthcare). Blots were visualized by chemoluminescence with Pierce ECL2 western blotting kit (Thermo Scientific). Digitonin fractionation was carried out in the presence of increasing concentrations of digitonin (20 µM to 10 mM) as described previously [75] and each fraction was analysed by western blot.

Immunofluorescence studies

Immunofluorescence studies were done as described previously[9,10]. The anti-mouse HA tag monoclonal antibody (1:1000; ABM), the anti-mouse H3 Histone 3 antibody (1:500; ABM) and the rabbit polyclonal anti-*T. brucei* BiP (kindly provided by Dr. JD Bangs) were used as a primary antibody followed by Alexa Fluor® 488 anti-mouse and Alexa Fluor® 555 anti-rabbit as secondary

antibodies. Nucleus and kinetoplast DNA was stained with DAPI (blue). The cells were observed under a Nikon epifluorescence microscope with a 100X objective and oil immersion. Images acquisition was performed with ImagePro Plus software and ImageJ.

Immunoprecipitation studies

Immunoprecipitation (IP) studies and mass spectrometry analysis were carried out as described previously[9]. Briefly, *L. infantum* promastigotes expressing HA-tagged protein were lysed, mixed with Pierce anti-HA magnetic beads (Thermo Scientific, Canada) and kept at -20° C and subjected to mass spectrometry analysis or alternatively resolved in SDS PAGE, excised, trypsin-digested, and analyzed by mass spectrometry.

Sample preparation and LC-MS/MS analysis

Protein digestion and mass spectrometry analyses were performed by the Proteomics Platform of the CHU de Québec Research Center (Quebec, Qc, Canada) as described previously[76]. Briefly, bands of interest were extracted from gels, placed in 96-well plates and then washed with water. Tryptic digestion was performed on a liquid handling robot (MultiProbe, Perkin Elmer) according to manufacturer's instructions using the protocol detailed in [77] with some modifications as suggested in [78]. Proteins were reduced with 10 mM DTT and alkylated with 55 mM iodoacetamide. Iodoacetamide derivative of cysteine was specified as a fixed modification and oxidation of methionine and deamidation of Asparagine and Glutamine were specified as a variable modification. Two missed cleavages were allowed. Trypsin digestion was performed using 126 nM of modified porcine trypsin (Sequencing grade, Promega, Madison, WI) at 37° C for 18 hrs. Digestion products were extracted using 1% formic acid, 2% acetonitrile followed by 1% formic acid and 50% acetonitrile. The recovered peptides were pooled, vacuum-centrifuged, dried and then resuspended into 12 µl of 0.1% formic acid, and 5 µl were analyzed by mass spectrometry. Peptide samples were separated by online reversed-phase (RP) nanoscale capillary liquid chromatography (nanoLC) and analyzed by electrospray mass spectrometry (ES MS/MS). The experiments were performed with an Ekspert NanoLC425 (Eksigent) coupled to a 5600+ mass spectrometer (Sciex, Framingham, MA, USA) equipped with a nanoelectrospray ion source. Peptide separation took place on a self-packed picofrit column (New Objective) with reprosil 3u, 120A C18, 15 cm x 0.075 mm internal diameter, (Dr Maisch). Peptides were eluted with a linear gradient from 5-35% solvent B (acetonitrile, 0.1% formic acid) for 35 minutes at a flow rate of 300 nL/min. Mass spectra were acquired by a data dependent acquisition mode using Analyst software version 1.7. Each full scan mass spectrum (400 to 1250 m/z) was followed by collision-

induced dissociation of the twenty most intense ions. Dynamic exclusion was set for a period of 12 sec and a mass tolerance of 100 ppm.

Database searching

MGF peak list files were created using Protein Pilot version 4.5 software (Sciex). MGF sample files were then analyzed using Mascot (Matrix Science, London, UK; version 2.5.1). Mascot was searched with a fragment ion mass tolerance of 1.0 Da and a parent ion tolerance of 1.0 Da. Scaffold (version Scaffold_4.8.4, Proteome Software Inc., Portland, OR) was used to validate MS/MS based peptide and protein identifications based on the *Leishmania Infantum* TriTrypDB (version 9.0 released April 2016, 8589 entries). Peptide identifications were accepted if they could be established at greater than 5.0% probability to achieve an FDR less than 1.0% by the Scaffold Local FDR algorithm. Protein identifications were accepted if they could be established at greater than 99.0% probability to achieve a FDR less than 1.0% and contained at least 2 identified peptides. Protein probabilities were assigned by the Protein Prophet algorithm [79]. Proteins that contained similar peptides and could not be differentiated based on MS/MS analysis alone were grouped to satisfy the principles of parsimony.

3D homology modeling and protein-protein docking

To construct 3D models of *L. infantum* JPCM5 proteins *Li*UFD1 (LinJ.36.6780), *Li*p47 (SEP domain, LinJ.22.0200), *Li*FAF2 (UBX domain, LinJ.35.1960), *Li*PUB1 domain (LinJ.09.1060), *Li*NPL4 (LinJ.25.1320) and *Li*VCP proteins, we searched for their orthologs in PDB database using BlastP and Delta-Blast. Then, 3D structure models were built using the modelling software MODELLER[80] based on their homologous structure, PDBid : 5C1B_V, 1S3S_H, 2MX2_A, 2HPL_B, 6CDD_ A and 5C18_D, respectively. The QPTFAGAGRTL SHP1 peptide of *Li*UFD1 and the DDLYS peptide of *Li*VCP were modeled using as templates PDBid: 5C1B_V and 2HPL, respectively. The *Li*VCP hexamer was obtained by superposition with the *H. sapiens* p97 hexamer (PDBid: 5C18). The quality of the models was assessed by Ramachandran plot analysis through PROCHECK[81]. Proteins and peptides of *L. infantum* were docked into *Li*VCP using HDOCK[82] and HPEPDOCK[83], respectively. The electrostatic potential surfaces of 3D models and images were generated with PyMOL software (http://pymol.org/).

Multiple alignments and phylogeny

We used the amino acid sequence of each *L. infantum* JPCM5 protein to search by BlastP and Delta-Blast for close homologs in bacteria, archaea, fungi, plants and animals. The sequences

extracted from databases were aligned with Clustal Omega[84]. To establish the phylogenetic relationships between *L. infantum* proteins and those of prokaryotic and other eukaryotic organisms, the sequences were aligned with Clustal Omega[84] and a phylogenetic tree was constructed using PhyML[85]. The gene ontology (GO) term enrichment analysis was performed using the tool provided by TriTrypDB (http://tritrypdb.org) with Fisher exact test filtering for false discovery rate (FDR) lower than 0.05. Cellular Component, Molecular Function and Biological Process were carried out separately.

Experimental design and statistical rationale

Filter for LiVCP IP-MS/MS: Seven IP-MS/MS studies were considered for *Li*VCP (Supplementary Table S2). To select proteins that specifically associate with *Li*VCP, we calculated the average number of peptides for each protein in all seven experiments, and then excluded all proteins also found in five independent IP-MS/MS studies conducted with HA-tagged proteins unrelated to the VCP complex. From the selected 24 *Li*VCP specific interacting proteins, 15 with an average of exclusive unique peptide count (EUPC) ≥ 2.0 were classified as the *Li*VCP core and are presented in Figure 1C and Supplementary Table S2.

Filter for LiVCP cofactors IP-MS/MS: Two independent experiments were performed for each *Li*VCP cofactor (*Li*p47, *Li*FAF2, *Li*UFD1 and *Li*PUB1) and only proteins with an average of exclusive unique peptide count EUPC ≥ 2.0 in both experiments for each cofactor were considered (Supplementary Table S2). To exclude non-specific partners, IP-MS/MS studies with proteins unrelated to *Li*VCP complexes were carried out and proteins with an average of EUPC > 3.6 (*Li*VCP threshold) were used to filter out non-specific *Li*VCP cofactor associated proteins. The remaining proteins co-immunoprecipitated with *Li*p47, or *Li*FAF2, or *Li*UFD1 and or *Li*PUB1 were considered as putative *Li*VCP cofactors. Cytoscape v 3.5.1[86] was used to plot network analyses of all new interactions for *Li*VCP, *Li*p47, *Li*FAF2, *Li*UFD1 and *Li*PUB1.

Filter for network plotting: To decrease the number of false positive results in the *Li*VCP network building, we only show proteins that were not co-immunoprecipitated with all unrelated HA-tagged proteins (average of EUPC=0.0). From the total number of proteins co-immunoprecipitated with *Li*p47, or *Li*UFD1 or *Li*FAF2 and or *Li*PUB1, only 10, 17, 23 and 9, respectively were considered together with the 24 *Li*VCP specific interactors (Fig. 1, Table 1 and Supplementary Table S2) to build the topology of *Li*VCP network. No statistical analysis was needed.

3.8 Acknowledgements

We are grateful to the Proteomics platform of the CHU de Quebec Research Center-Université Laval. We also thank Dr. James D. Bangs for having kindly provided the anti-*Trypanosoma brucei* VCP antibody. BA is a recipient of doctoral fellowships from the CAPES 'Frontiers without Borders' program. This work was supported by the Natural Sciences and Engineering Research Council of Canada (NSERC) Discovery Grant GC100741 (418444) and the Canadian Institutes of Health Research (CIHR) operating grant MOP-12182 awarded to BP.

3.9 Data availability

The mass spectrometry proteomics data have been deposited to the ProteomeXchange Consortium via the PRIDE[87] partner repository with the dataset identifier PXD013731. The Reviewer account details are Username: reviewer11708@ebi.ac.uk, Password: Zm5uR3hc.

3.10 Author contributions

B.G.A. generated all constructs and performed transfections, IP experiments and western blots, sample preparations for mass spectrometry analysis, and processed all data. H.M. did the 3D homology modeling, docking and phylogeny. C.D. and P.K.P. helped with cell cultures, digitonin fractionation, and immunofluorescence studies. Conceptualization and design of the experiments was done by B.G.A. with the help of B.P. B.G.A. and B.P. wrote the manuscript. B.P. supervised the project and provided funding.

3.11 Conflict of interest

The authors declare no conflicts of interest.

3.12 References

1. Cloutier, S., Laverdière, M., Chou, M-N., Boilard, N., Chow, C. & Papadopoulou, B. Translational Control through eIF2alpha Phosphorylation during the *Leishmania* Differentiation Process. *PLoS One* **7**, e35085 (2012).
2. Chow, C., Cloutier, S., Dumas, C., Chou, M-N. & Papadopoulou, B. Promastigote to amastigote differentiation of *Leishmania* is markedly delayed in the absence of PERK eIF2alpha kinase-dependent eIF2alpha phosphorylation. *Cell. Microbiol.* **13**, 1059–1077 (2011).
3. Rochette, A., Raymond, F., Corbeil, J., Ouellette, M. & Papadopoulou, B. Whole-genome comparative RNA expression profiling of axenic and intracellular amastigote forms of *Leishmania infantum*. *Mol. Biochem. Parasitol.* **165**, 32–47 (2009).
4. Späth, G. F., Drini, S. & Rachidi, N. A touch of Zen: Post-translational regulation of the *Leishmania* stress response. *Cell. Microbiol.* **17**, 632–638 (2015).
5. Haile, S. & Papadopoulou, B. Developmental regulation of gene expression in trypanosomatid parasitic protozoa. *Curr. Opin. Microbiol.* **10**, 569–577 (2007).
6. McConville, M. J. & Naderer, T. Metabolic Pathways Required for the Intracellular Survival of *Leishmania*. *Annu. Rev. Microbiol.* **65**, 543–561 (2011).
7. Naderer, T. & McConville, M. J. Intracellular growth and pathogenesis of *Leishmania* parasites. *Essays Biochem.* **51**, 81–95 (2011).
8. Pilla, E., Schneider, K. & Bertolotti, A. Coping with Protein Quality Control Failure. *Annu. Rev. Cell Dev. Biol.* **33**, 439–465 (2017).
9. Padmanabhan, P. K. *et al.* DDX3 DEAD-box RNA helicase plays a central role in mitochondrial protein quality control in *Leishmania*. *Cell Death Dis.* **7**, e2406 (2016).
10. Aguiar, B. G., Padmanabhan, P. K., Dumas, C. & Papadopoulou, B. Valosin-containing protein VCP/p97 is essential for the intracellular development of *Leishmania* and its survival under heat stress. *Cell. Microbiol.* **20**, e12867 (2018).
11. Muñoz, C., San Francisco, J., Gutiérrez, B. & González, J. Role of the Ubiquitin-Proteasome Systems in the Biology and Virulence of Protozoan Parasites. *Biomed Res. Int.* **2015**, 1–13 (2015).
12. Dolai, S. & Adak, S. Endoplasmic reticulum stress responses in *Leishmania*. *Mol.*

Biochem. Parasitol. **197**, 1–8 (2014).

13. van den Boom, J. & Meyer, H. VCP/p97-Mediated Unfolding as a Principle in Protein Homeostasis and Signaling. *Mol. Cell* **69**, 182–194 (2018).
14. Bodnar, N. O. & Rapoport, T. A. Molecular Mechanism of Substrate Processing by the Cdc48 ATPase Complex. *Cell* **169**, 722-735.e9 (2017).
15. Christianson, J. C. & Ye, Y. Cleaning up in the endoplasmic reticulum: ubiquitin in charge. *Nat. Struct. Mol. Biol.* **21**, 325–335 (2014).
16. Ye, Y., Tang, W. K., Zhang, T. & Xia, D. A Mighty "Protein Extractor" of the Cell: Structure and Function of the p97/CDC48 ATPase. *Front. Mol. Biosci.* **4**, 1–20 (2017).
17. Meyer, H., Bug, M. & Bremer, S. Emerging functions of the VCP/p97 AAA-ATPase in the ubiquitin system. *Nat. Cell Biol.* **14**, 117–123 (2012).
18. Franz, A., Ackermann, L. & Hoppe, T. Create and preserve: Proteostasis in development and aging is governed by Cdc48/p97/VCP. *Biochimica et Biophysica Acta - Molecular Cell Research* **1843**, 205–215 (2014).
19. Qi, L., Tsai, B. & Arvan, P. New Insights into the Physiological Role of Endoplasmic Reticulum-Associated Degradation. *Trends Cell Biol.* **27**, 430–440 (2017).
20. Taylor, E. B. & Rutter, J. Mitochondrial quality control by the ubiquitin–proteasome system. *Biochem. Soc. Trans.* **39**, 1509–1513 (2011).
21. Brandman, O. *et al.* A Ribosome-Bound Quality Control Complex Triggers Degradation of Nascent Peptides and Signals Translation Stress. *Cell* **151**, 1042–1054 (2012).
22. Franz, A., Ackermann, L. & Hoppe, T. Ring of Change: CDC48/p97 Drives Protein Dynamics at Chromatin. *Front. Genet.* **7**, 1–14 (2016).
23. Papadopoulos, C. *et al.* VCP/p97 cooperates with YOD1, UBXD1 and PLAA to drive clearance of ruptured lysosomes by autophagy. *EMBO J.* **36**, 135–150 (2017).
24. Vaz, B., Halder, S. & Ramadan, K. Role of p97/VCP (Cdc48) in genome stability. *Front. Genet.* **4**, 60 (2013).
25. Buchan, J. R., Kolaitis, R.-M., Taylor, J. P. & Parker, R. Eukaryotic Stress Granules Are Cleared by Autophagy and Cdc48/VCP Function. *Cell* **153**, 1461–1474 (2013).
26. Fessart, D., Marza, E., Taouji, S., Delom, F. & Chevet, E. P97/CDC-48: Proteostasis control in tumor cell biology. *Cancer Lett.* **337**, 26–34 (2013).
27. Meyer, H. & Weihl, C. C. The VCP/p97 system at a glance: connecting cellular function

to disease pathogenesis. *J. Cell Sci.* **127**, 3877–3883 (2014).

28. Tang, W. K. & Xia, D. Mutations in the Human AAA+ Chaperone p97 and Related Diseases. *Front. Mol. Biosci.* **3**, 1–12 (2016).
29. Xia, D., Tang, W. K. & Ye, Y. Structure and function of the AAA+ ATPase p97/Cdc48p. *Gene* **583**, 64–77 (2016).
30. Buchberger, A., Schindelin, H. & Hänzelmann, P. Control of p97 function by cofactor binding. *FEBS Lett.* **589**, 2578–2589 (2015).
31. Hänzelmann, P. & Schindelin, H. Characterization of an Additional Binding Surface on the p97 N-Terminal Domain Involved in Bipartite Cofactor Interactions. *Structure* **24**, 140–147 (2016).
32. Hänzelmann, P. & Schindelin, H. The Interplay of Cofactor Interactions and Post-translational Modifications in the Regulation of the AAA+ ATPase p97. *Front. Mol. Biosci.* **4**, 1–22 (2017).
33. Rezvani, K. UBXD Proteins: A Family of Proteins with Diverse Functions in Cancer. *Int. J. Mol. Sci.* **17**, 1724 (2016).
34. Bodnar, N. O. *et al.* Structure of the Cdc48 ATPase with its ubiquitin-binding cofactor Ufd1–Npl4. *Nat. Struct. Mol. Biol.* **25**, 616–622 (2018).
35. Zhao, G. *et al.* Studies on peptide:N-glycanase-p97 interaction suggest that p97 phosphorylation modulates endoplasmic reticulum-associated degradation. *Proc. Natl. Acad. Sci.* **104**, 8785–8790 (2007).
36. Weith, M. *et al.* Ubiquitin-Independent Disassembly by a p97 AAA-ATPase Complex Drives PP1 Holoenzyme Formation. *Mol. Cell* **72**, 766-777.e6 (2018).
37. Roggy, J. L. & Bangs, J. D. Molecular cloning and biochemical characterization of a VCP homolog in African trypanosomes. *Mol. Biochem. Parasitol.* **98**, 1–15 (1999).
38. Cheng, Y.-L. & Chen, R.-H. Assembly and quality control of the protein phosphatase 1 holoenzyme involves the Cdc48-Shp1 chaperone. *J. Cell Sci.* **128**, 1180–1192 (2015).
39. Lee, J.-J. *et al.* Complex of Fas-associated Factor 1 (FAF1) with Valosin-containing Protein (VCP)-Npl4-Ufd1 and Polyubiquitinated Proteins Promotes Endoplasmic Reticulum-associated Degradation (ERAD). *J. Biol. Chem.* **288**, 6998–7011 (2013).
40. Mullen, T. D. & Obeid, L. M. Ceramide and Apoptosis: Exploring the Enigmatic Connections between Sphingolipid Metabolism and Programmed Cell Death. *Anticancer.*

Agents Med. Chem. **12**, 340–363 (2012).

41. Nikolova-Karakashian, M. N. & Rozenova, K. A. Ceramide in Stress Response. in *Advances in experimental medicine and biology* **688**, 86–108 (2010).
42. Oláh, J. *et al.* Tubulin Binding and Polymerization Promoting Properties of Tubulin Polymerization Promoting Proteins Are Evolutionarily Conserved. *Biochemistry* **56**, 1017–1024 (2017).
43. Zou, W.-Q., Zhou, X., Yuan, J. & Xiao, X. Insoluble cellular prion protein and its association with prion and Alzheimer diseases. *Prion* **5**, 172–178 (2011).
44. Qi, X., Sun, J. & Zheng, H. A GTPase-Dependent Fine ER Is Required for Localized Secretion in Polarized Growth of Root Hairs 1. *Plant Physiol.* **171**, 1996–2007 (2016).
45. Maciver, S. K. & Hussey, P. J. The ADF/cofilin family: actin-remodeling proteins. *Genome Biol.* **3**, reviews3007 (2002).
46. Marshansky, V., Rubinstein, J. L. & Grüber, G. Eukaryotic V-ATPase: Novel structural findings and functional insights. *Biochim. Biophys. Acta - Bioenerg.* **1837**, 857–879 (2014).
47. Mani, J. *et al.* Mitochondrial protein import receptors in Kinetoplastids reveal convergent evolution over large phylogenetic distances. *Nat. Commun.* **6**, 6646 (2015).
48. Wolf, D. H. & Stolz, A. The Cdc48 machine in endoplasmic reticulum associated protein degradation. *Biochim. Biophys. Acta - Mol. Cell Res.* **1823**, 117–124 (2012).
49. Heo, J.-M. *et al.* A Stress-Responsive System for Mitochondrial Protein Degradation. *Mol. Cell* **40**, 465–480 (2010).
50. Dreveny, I. *et al.* Structural basis of the interaction between the AAA ATPase p97/VCP and its adaptor protein p47. *EMBO J.* **23**, 1030–1039 (2004).
51. Song, E. J., Yim, S.-H., Kim, E., Kim, N.-S. & Lee, K.-J. Human Fas-Associated Factor 1, Interacting with Ubiquitinated Proteins and Valosin-Containing Protein, Is Involved in the Ubiquitin-Proteasome Pathway. *Mol. Cell. Biol.* **25**, 2511–2524 (2005).
52. Ye, Y., Shibata, Y., Yun, C., Ron, D. & Rapoport, T. A. A membrane protein complex mediates retro-translocation from the ER lumen into the cytosol. *Nature* **429**, 841–847 (2004).
53. Pye, V. E. *et al.* Structural insights into the p97-Ufd1-Npl4 complex. *Proc. Natl. Acad. Sci.* **104**, 467–472 (2007).

54. Zhao, G., Li, G., Schindelin, H. & Lennarz, W. J. An Armadillo motif in Ufd3 interacts with Cdc48 and is involved in ubiquitin homeostasis and protein degradation. *Proc. Natl. Acad. Sci.* **106**, 16197–16202 (2009).
55. Kim, S. J. *et al.* Structural Basis for Ovarian Tumor Domain-containing Protein 1 (OTU1) Binding to p97/Valosin-containing Protein (VCP). *J. Biol. Chem.* **289**, 12264–12274 (2014).
56. Stenmark, H., Aasland, R. & Driscoll, P. C. The phosphatidylinositol 3-phosphate-binding FYVE finger. *FEBS Lett.* **513**, 77–84 (2002).
57. Yang, Y. *et al.* Folding-Degradation Relationship of a Membrane Protein Mediated by the Universally Conserved ATP-Dependent Protease FtsH. *J. Am. Chem. Soc.* **140**, 4656–4665 (2018).
58. Stach, L. & Freemont, P. S. The AAA+ ATPase p97, a cellular multitool. *Biochem. J.* **474**, 2953–2976 (2017).
59. Alexandru, G. *et al.* UBXD7 Binds Multiple Ubiquitin Ligases and Implicates p97 in HIF1α Turnover. *Cell* **134**, 804–816 (2008).
60. Friant, S. Increased ubiquitin-dependent degradation can replace the essential requirement for heat shock protein induction. *EMBO J.* **22**, 3783–3791 (2003).
61. Meade, J. C., Shaw, J., Lemaster, S., Gallagher, G. & Stringer, J. R. Structure and expression of a tandem gene pair in Leishmania donovani that encodes a protein structurally homologous to eucaryotic cation-transporting ATPases. *Mol. Cell. Biol.* **7**, 3937–3946 (1987).
62. Bharucha, J. P., Larson, J. R., Gao, L., Daves, L. K. & Tatchell, K. Ypi1, a Positive Regulator of Nuclear Protein Phosphatase Type 1 Activity in *Saccharomyces cerevisiae*. *Mol. Biol. Cell* **19**, 1032–1045 (2008).
63. Cheng, Y.-L. & Chen, R.-H. The AAA-ATPase Cdc48 and cofactor Shp1 promote chromosome bi-orientation by balancing Aurora B activity. *J. Cell Sci.* **123**, 2025–2034 (2010).
64. Rumpf, S. & Jentsch, S. Functional Division of Substrate Processing Cofactors of the Ubiquitin-Selective Cdc48 Chaperone. *Mol. Cell* **21**, 261–269 (2006).
65. Liu, Y. & Ye, Y. Roles of p97-Associated Deubiquitinases in Protein Quality Control at the Endoplasmic Reticulum. *Curr. Protein Pept. Sci.* **13**, 436–446 (2012).

66. Wai, T. *et al.* The membrane scaffold SLP2 anchors a proteolytic hub in mitochondria containing PARL and the i -AAA protease YME1L. *EMBO Rep.* **17**, 1844–1856 (2016).
67. Janska, H., Kwasniak, M. & Szczepanowska, J. Protein quality control in organelles — AAA/FtsH story. *Biochim. Biophys. Acta - Mol. Cell Res.* **1833**, 381–387 (2013).
68. Farré, J., Mahalingam, S. S., Proietto, M. & Subramani, S. Peroxisome biogenesis, membrane contact sites, and quality control. *EMBO Rep.* **20**, e46864 (2019).
69. Bauer, S. & Morris, M. T. Glycosome biogenesis in trypanosomes and the de novo dilemma. *PLoS Negl. Trop. Dis.* **11**, e0005333 (2017).
70. Cho, D.-H., Kim, Y. S., Jo, D. S., Choe, S.-K. & Jo, E.-K. Pexophagy: Molecular Mechanisms and Implications for Health and Diseases. *Mol. Cells* **41**, 55–64 (2018).
71. Cull, B. *et al.* Glycosome turnover in *Leishmania major* is mediated by autophagy. *Autophagy* **10**, 2143–2157 (2014).
72. Oh, C.-S., Toke, D. A., Mandala, S. & Martin, C. E. ELO2 and ELO3 , Homologues of the Saccharomyces cerevisiae ELO1 Gene, Function in Fatty Acid Elongation and Are Required for Sphingolipid Formation. *J. Biol. Chem.* **272**, 17376–17384 (1997).
73. Lee, S. H., Stephens, J. L., Paul, K. S. & Englund, P. T. Fatty Acid Synthesis by Elongases in Trypanosomes. *Cell* **126**, 691–699 (2006).
74. Papadopoulou, B., Roy, G. & Ouellette, M. A novel antifolate resistance gene on the amplified H circle of *Leishmania*. *EMBO J.* **11**, 3601–3608 (1992).
75. Padmanabhan, P. K. *et al.* Novel Features of a PIWI-Like Protein Homolog in the Parasitic Protozoan *Leishmania*. *PLoS One* **7**, e52612 (2012).
76. Dupé, A., Dumas, C. & Papadopoulou, B. Differential Subcellular Localization of *Leishmania* Alba-Domain Proteins throughout the Parasite Development. *PLoS One* **10**, e0137243 (2015).
77. Shevchenko, A., Wilm, M., Vorm, O. & Mann, M. Mass Spectrometric Sequencing of Proteins from Silver-Stained Polyacrylamide Gels. *Anal. Chem.* **68**, 850–858 (1996).
78. Havliš, J., Thomas, H., Šebela, M. & Shevchenko, A. Fast-Response Proteomics by Accelerated In-Gel Digestion of Proteins. *Anal. Chem.* **75**, 1300–1306 (2003).
79. Nesvizhskii, A. I., Keller, A., Kolker, E. & Aebersold, R. A Statistical Model for Identifying Proteins by Tandem Mass Spectrometry. *Anal. Chem.* **75**, 4646–4658 (2003).
80. Eswar, N. *et al.* Comparative Protein Structure Modeling Using MODELLER. *Curr.*

Protoc. Protein Sci. **50**, 2.9.1-2.9.31 (2007).

81. Laskowski, R., Rullmann, J. A., MacArthur, M., Kaptein, R. & Thornton, J. AQUA and PROCHECK-NMR: Programs for checking the quality of protein structures solved by NMR. *J. Biomol. NMR* **8**, 477–86 (1996).
82. Yan, Y., Zhang, D., Zhou, P., Li, B. & Huang, S.-Y. HDOCK: a web server for protein–protein and protein–DNA/RNA docking based on a hybrid strategy. *Nucleic Acids Res.* **45**, W365–W373 (2017).
83. Zhou, P., Jin, B., Li, H. & Huang, S.-Y. HPEPDOCK: a web server for blind peptide–protein docking based on a hierarchical algorithm. *Nucleic Acids Res.* **46**, W443–W450 (2018).
84. Sievers, F. & Higgins, D. G. Clustal Omega for making accurate alignments of many protein sequences. *Protein Sci.* **27**, 135–145 (2018).
85. Guindon, S. *et al.* New Algorithms and Methods to Estimate Maximum-Likelihood Phylogenies: Assessing the Performance of PhyML 3.0. *Syst. Biol.* **59**, 307–321 (2010).
86. Shannon, P. Cytoscape: A Software Environment for Integrated Models of Biomolecular Interaction Networks. *Genome Res.* **13**, 2498–2504 (2003).
87. Perez-Riverol, Y. *et al.* The PRIDE database and related tools and resources in 2019: improving support for quantification data. *Nucleic Acids Res.* **47**, D442–D450 (2019).

3.13 Tables

Table 1. Proteins specifically associated with one or more *Leishmania Li*VCP cofactors as determined by immunoprecipitation and LC-MS/MS studies.

TriTrypDB ID	TriTrypDB Description	Average EUPC ≥2
	***Li*p47**	
LinJ.36.1420	**Valosin-containing protein, putative**	38.5
LinJ.05.1200	protein phosphatase type 1 (PP1) regulator-like protein (SDS22)*	19.5
LinJ.22.0200	**SEP domain containing protein, putative (p47/Shp1)**	18.0
LinJ.28.0730	serine/threonine protein phosphatase catalytic subunit, putative (Glc7/PP1-B)*	8.0
LinJ.09.1060	PUB domain containing protein, putative (PUB1)*	7.5
LinJ.14.0700	fatty acid elongase, putative (ELO2 GNS1/SUR4 family; 5 TMs)	4.5
LinJ.29.0520	ADF (actin depolymerization factor)/Cofilin	4.0
LinJ.32.0380	root hair defective 3 GTP-binding protein (RHD3), putative	3.5
LinJ.07.0840	protein phosphatase inhibitor (Ypi1, PP1 Protein phosphatase inhibitor)*	3.0
LinJ.27.2660	hypothetical protein, conserved (2 TMs)	3.0
LinJ.34.1620	TPPP/p25-alpha, putative (Tubulin Polymerization-Promoting Protein)	2.0
	***Li*UFD1**	
LinJ.36.1420	**Valosin-containing protein, putative**	50.5
LinJ.05.1040	stomatin-like protein 2 (SLP-2, mitochondrial)*	25.5
LinJ.36.2850	mitochondrial ATP-dependent zinc metallopeptidase, putative (AAA domain ATPase family; FtsH protease) (1 TM)*	22.5
LinJ.36.4740	hypothetical protein, conserved*	16.5
LinJ.24.1650	UBA/TS-N domain containing protein, putative*	15.5
LinJ.35.1960	UBX domain containing protein, putative (FAS-associated factor 2; FAF2)*	14.5
LinJ.36.6780	**ubiquitin fusion degradation protein, putative (UFD1)***	14.5
LinJ.15.1570	hypothetical protein, conserved*	12.5
LinJ.19.1240	peroxin 12 (PEX12), putative (RING/U-box)	9.0
LinJ.25.1320	**NPL4 family, putative***	8.5
LinJ.03.0250	hypothetical protein, conserved (1 TM)*	4.5
LinJ.05.1140	V-type proton ATPase subunit D, putative	4.5
LinJ.28.1390	phenylalanine-4-hydroxylase (signal peptide)	3.5
LinJ.35.4920	mitochondrial import receptor subunit ATOM40, putative	3.0
LinJ.14.0700	fatty acid elongase, putative (ELO2 GNS1/SUR4 family; 5 TMs)	2.5
LinJ.29.2300	hypothetical protein-conserved (signal peptide, 1 TM)	2.5
LinJ.18.0450	serine carboxypeptidase (CBP1)-putative (mitochondrial, 1 TM)	2.5
LinJ.12.0550	hypothetical protein-conserved (alkaline phosphatase like superfamily, 1 TM)	2.5
	***Li*FAF2**	
LinJ.36.1420	**Valosin-containing protein, putative**	19
LinJ.05.1040	stomatin-like protein 2 (SLP-2, mitochondrial)*	25
LinJ.36.2850	mitochondrial ATP-dependent zinc metallopeptidase, putative (AAA domain ATPase family; FtsH protease) (1 TM)*	19
LinJ.35.1960	**UBX domain containing protein, putative (FAF2)***	17.5
LinJ.24.1650	UBA/TS-N domain containing protein, putative*	13.5

LinJ.15.1570	hypothetical protein, conserved*	11
LinJ.36.4740	hypothetical protein, conserved*	8.0
LinJ.05.1140	V-type proton ATPase subunit D, putative	8.0
LinJ.17.0230	tetratricopeptide repeat, putative (ER membrane protein complex subunit 2)*	7.5
LinJ.07.0450	uncharacterized protein family (UPF0172) (ER membrane protein complex	5.0
LinJ.14.0700	sub. 8)*	5.0
LinJ.25.2330	fatty acid elongase, putative (ELO2 GNS1/SUR4 family; 5 TMs)	5.0
LinJ.14.0680	glycosome import protein, putative (E3 ubiquitin-protein ligase, PEX2)	3.5
LinJ.32.0380	fatty acid elongase, putative (ELO1 GNS1/SUR4 family; 6 TMs)	3.0
LinJ.14.0760	root hair defective 3 GTP-binding protein (RHD3), putative	3.0
LinJ.33.1130	fatty acid elongase, putative (ELO3 GNS1/SUR4 family; 5 TMs)	3.0
LinJ.36.5360	hypothetical protein-conserved (1 TM)	2.5
LinJ.35.4920	hypothetical protein-conserved	2.5
LinJ.29.0520	mitochondrial import receptor subunit ATOM40, putative	2.5
LinJ.34.4180	ADF (actin depolymerization factor)/Cofilin	2.5
LinJ.35.3740	cell differentiation protein-like protein (Rcd1 homolog)	2.5
LinJ.26.1610	peroxisomal biogenesis factor 11 (PEX11), putative	2.0
LinJ.34.1620	40S ribosomal protein S33, putative	2.0
LinJ.25.2400	TPPP/p25-alpha, putative (Tubulin Polymerization-Promoting Protein)	2.0
	PEX10, PEX2 / PEX12 amino terminal region/ RING/U-box containing protein	
	***Li*PUB1**	
LinJ.36.1420	**Valosin-containing protein, putative**	24.5
LinJ.09.1060	**PUB domain containing protein, putative (PUB1)***	14.5
LinJ.32.0380	root hair defective 3 GTP-binding protein (RHD3), putative	3.0
LinJ.14.0700	fatty acid elongase, putative (ELO2 GNS1/SUR4 family; 5 TMs)	3.0
LinJ.33.1130	hypothetical protein, unknown function	3.0
LinJ.36.6780	ubiquitin fusion degradation protein, putative (UFD1)*	2.0
LinJ.35.4920	mitochondrial import receptor subunit ATOM40, putative	2.0
LinJ.34.3530	serine palmitoyltransferase-like protein (long chain base biosynthesis protein)	2.0
LinJ.26.1610	40S ribosomal protein S33, putative	2.0
LinJ.34.1620	TPPP/p25-alpha, putative (Tubulin Polymerization-Promoting Protein)	2.0

Proteins in bold represent the core *Li*VCP cofactors. Proteins highlighted in grey are shared between two *Li*VCP cofactors. Proteins highlighted in yellow are shared between three or four *Li*VCP cofactors. Proteins indicated with an asterisk (*) are also found in *Li*VCP immunoprecipitates. The remaining proteins are specific to each *Li*VCP cofactor (see also Fig. 6B). TM: transmembrane helix. Average of exclusive unique peptide count (EUPC) is from seven independent IP experiments.

3.14 Figures

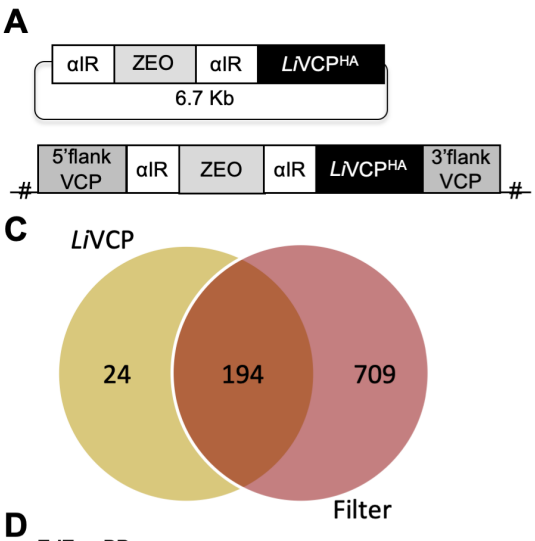

D

TriTrypDB ID	TriTrypDB Description	MW (kDa)	Peptide count	Sequence coverage
LinJ.36.1420	Valosin-containing protein, putative	76	75	70%
LinJ.05.1040	stomatin-like protein 2 (SLP-2)	40	16	46%
LinJ.22.0200	**SEP domain containing protein (p47 cofactor), putative**	38	9	37%
LinJ.05.1200	protein phosphatase type 1 (PP1) regulator-like protein (SDS22)	45	12	33%
LinJ.35.1960	**UBX domain containing protein (FAF2), putative**	37	11	33%
LinJ.36.2850	mitochondrial ATP-dependent zinc metallopeptidase, putative (FtsH)	62	14	33%
LinJ.24.1650	Ubiquitin associated (UBA)/TS-N domain containing protein	43	7	24%
LinJ.36.6780	**ubiquitin fusion degradation protein (UFD1), putative**	35	6	24%
LinJ.25.1320	**NPL4 family, putative**	47	3	17%
LinJ.36.5080	hypothetical protein, conserved, Nsp1-like C-terminal region	67	7	17%
LinJ.03.0250	hypothetical protein, conserved, Syntaxin-like domain	33	3	14%
LinJ.09.1060	**PUB domain containing protein, putative (PUB1)**	35	2	12%
LinJ.15.1570	hypothetical protein, conserved, jumonji-like domain	34	3	11%
LinJ.17.0230	tetratricopeptide repeat, putative	36	2	7%
LinJ.11.0920	PUB domain containing protein, putative (PUB2)	67	2	6%
LinJ.34.0900	serine/threonine-protein phosphatase PP1, putative	34	2	8%

Fig. 1

Figure 1. The *Leishmania LiVCP* core partners identified by co-immunoprecipitation and mass spectrometry studies. (**A**) Schematic draw of the construct used to express the *L. infantum* valosin-containing protein (*Li*VCP) tagged with an HA epitope at the C-terminus (VCP^{HA}) either episomally or integrated into the *L. infantum* VCP endogenous locus. (**B**) Western blotting to evaluate *Li*VCP-HA expression levels using anti-*Tb*VCP and anti-HA antibodies. The alpha-tubulin antibody was used as protein loading control. (**C**) Venn diagram demonstrating the number of proteins identified by mass spectrometry in *Li*VCP-HA immunoprecipitates of seven independent experiments that were filtered against 5

unrelated HA-tagged proteins (see Methods and Supplementary Table S2 for details). (**D**) *Li*VCP core partners identified in (C) with an average of exclusive unique peptide count (EUPC) of ≥ 2. The five *Li*VCP core cofactors studied here (*Li*p47, *Li*UFD1, *Li*NPL4, *Li*FAF2 and *Li*PUB1) are indicated in bold. For the complete list, see Supplementary Table S2.

A

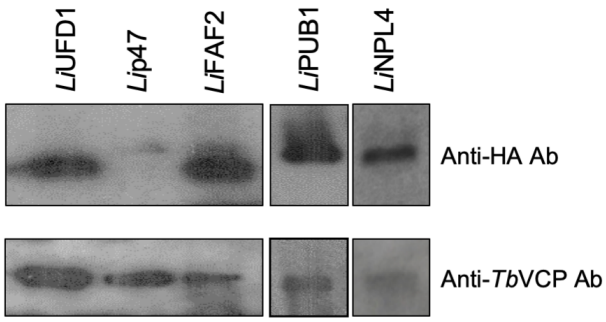

B

	*Li*UFD1	*Li*p47	*Li*FAF2	*Li*PUB1
*Li*UFD1	15	1	4	2
*Li*p47	0	18	0	4
*Li*FAF2	15	0	18	7
*Li*PUB1	0	8	0	15
*Li*VCP	51	39	19	25

Fig. 2

Figure 2. Reciprocal interactions between the *Leishmania* *Li*VCP and its key cofactors. (**A**) *Li*VCP detection by western blotting with an anti-*Tb*VCP antibody following immunoprecipitation of C- or N- terminally HA-tagged *Li*UFD1, *Li*p47, *Li*FAF2, *Li*NPL4 and *Li*PUB1 proteins ectopically expressed in *Leishmania*. (**B**) Detection of *Li*VCP and its cofactors *Li*UFD1, *Li*p47, *Li*FAF2, *Li*NPL4 and *Li*PUB1 by mass spectrometry after co-immunoprecipitation using anti-HA magnetic beads for recombinant *Leishmania* expressing C- or N- terminally HA-tagged cofactor proteins. The average of EUPC for two independent experiments for each cofactor is shown here.

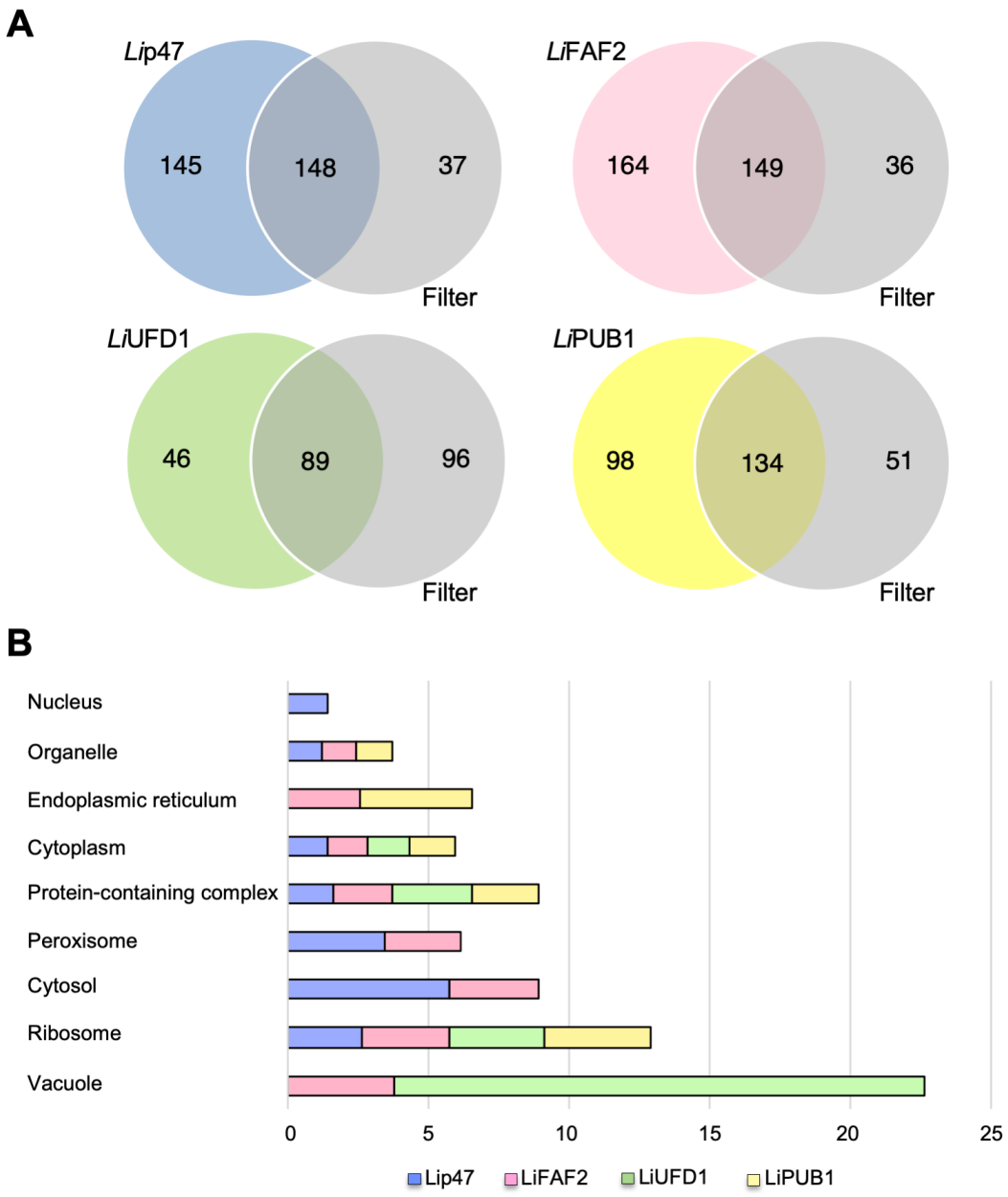

Fig. 3

Figure 3. Network proteomics to gain novel insights into *Li*VCP cofactor complexes. (**A**) Venn diagrams demonstrating the number of proteins identified by mass spectrometry in *Li*p47, *Li*FAF2, *Li*UFD1 and *Li*PUB1 co-immunoprecipitates of two independent experiments for each cofactor (see Experimental Procedures) after applying a filter of five unrelated HA-tagged proteins (average of EUPC = 3.6 on 5 unrelated proteins; see Supplementary Table S2 for details) to reduce non-specific interactions. (**B**) Gene ontology–cellular component (GO-CC) analysis of proteins identified in (A) for each *Li*VCP cofactor:

*Li*p47 (145), *Li*FAF2 (164), *Li*UFD1 (46), and *Li*PUB1 (98) according to their terms listed on TriTrypDB. The same stringent filter (grey in A) was applied for each cofactor (see Supplementary Figure S2 for details). Gene Ontology biological process and molecular function can be seen in Supplementary Figure S19.

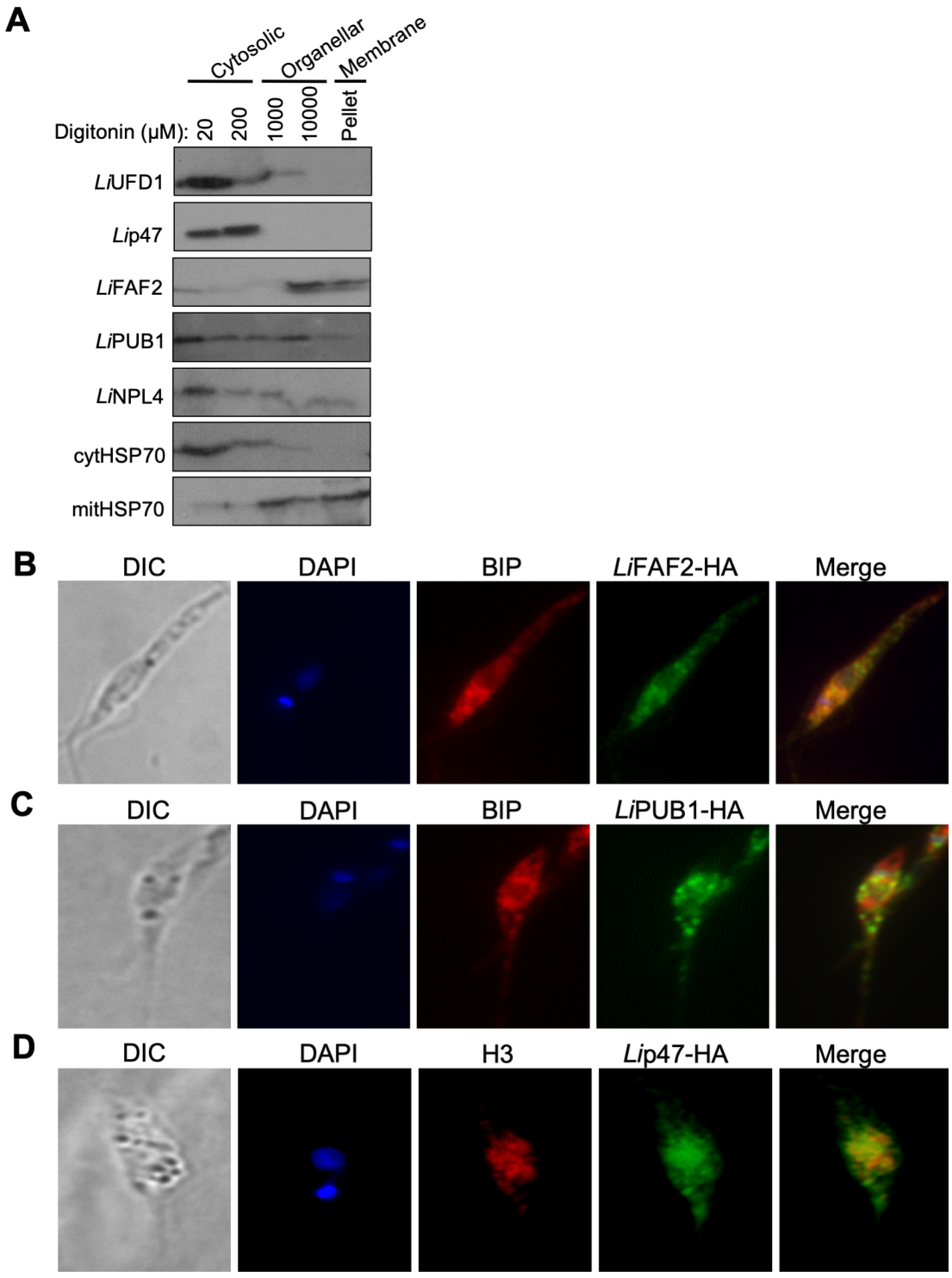

Fig. 4

Figure 4. Subcellular localization of *Li*VCP cofactors. (**A**) Western blot of *L. infantum* digitonin-fractionated promastigotes (20 µM-10 mM) using the anti-HA antibody to detect the C- or N-terminally HA-tagged *Li*UFD1, *Li*NPL4, *Lip*47, *Li*FAF2 and *Li*PUB1 proteins

ectopically expressed in *Leishmania*. The 20 µM to 200 µM digitonin fractions are enriched with cytosolic proteins, the 1 mM and 10 mM fractions contain mostly organellar proteins, and the pellet fraction contains membrane-associated proteins. Antibodies against the cytosolic or mitochondrial HSP70 were used as controls. Immunofluorescence studies showing the localization of C- or N-terminally HA-tagged *Li*FAF2 (**B**), *Li*PUB1 (**C**) and *Li*p47 (**D**) (in green). An anti-HA antibody was used as primary antibody followed by Alexa Fluor® 488 anti-mouse as secondary antibody. Nuclear and kinetoplast DNA was stained with DAPI (blue). Endoplasmic reticulum (ER) putative co-localization was assessed using an anti-BiP antibody (red in B and C) as an ER marker. An Alexa Fluor® 555 anti-rabbit was used as secondary antibody for BiP. Putative nuclear co-localization for *Li*p47 was assessed using an anti-histone H3 (H3) antibody (red in D).

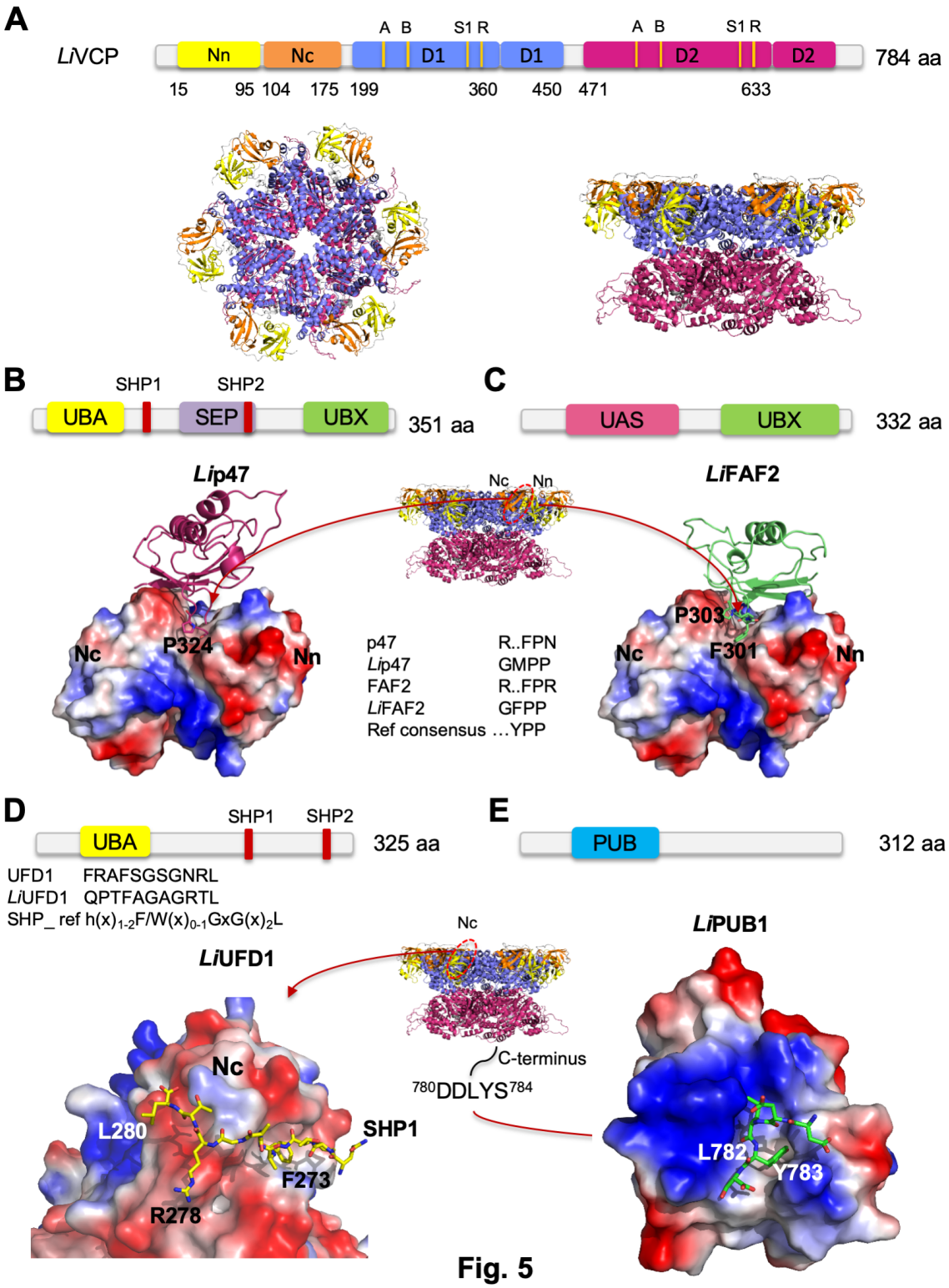

Figure 5. 3D homology modeling of the major *Li*VCP cofactors and their docking prediction into the *L. infantum Li*VCP protein. (**A**) Top, domain architecture of *Li*VCP. The N-domain is subdivided into an N- (Nn, colored in yellow) and a C-terminal (Nc, colored

in orange) subdomains and the two ATPase domains are in blue (D1) and red (D2), respectively. The Walker A (A) and Walker B (B) motifs as well as the Sensor 1 (S1) residues and arginine (R) fingers are indicated. Bottom, top (left) and side views (right) of the *Li*VCP hexamer 3D structure model built by homology with the *H. sapiens* p97 hexamer (PDBid entry 5C18). (**B**) Top, domain composition of *Li*p47. Bottom, electrostatic potential surface of *Li*VCP (colored according to hydrophobicity) with stick representation of the UBX GMPP binding motif of *Li*p47. Key interactions are shown. (**C**) Top, domain composition of *Li*FAF2. Bottom, electrostatic potential surface of *Li*VCP with stick representation of the UBX GFPP binding motif of *Li*FAF2. Middle panel between B and C shows molecular surface of *Li*VCP with the UBX binding site indicated (Nn-Nc pocket). (**D**) Top, domain composition of *Li*UFD1. Bottom, electrostatic potential surface of *Li*VCP with stick representation of the SHP1 binding site QPTFAGAGRTL. (**E**) Top, domain composition of *Li*PUB1. Bottom, electrostatic potential surface of *Li*PUB1 with a stick representation of the C-terminus of *Li*VCP ^{780}DDLYS^{784}. Middle panel between D and E shows molecular surface of *Li*VCP with the SHP binding site (Nc) and C-terminus tail indicated. 3D homology models of *Li*UFD1, *Li*p47, *Li*FAF2 and *Li*PUB1 were respectively built by homology based on the templates with pdb entries: 5C1B_V, 1S3S_H, 2MX2 and 2HPL, respectively using the modeling software MODELLER[80]. For further details, see Supplementary Figures S9, S11, S13 and S18. UBA (ubiquitin-associated); SEP (Shp, eyes-closed, p47); SHP (BS1, binding segment 1); UBX (ubiquitin regulatory X); UAS, domain of unknown function found in FAF2 and other proteins; PUB (PNGase/UBA or UBX) containing proteins. Further information about the respective domains can be found at http://www.ebi.ac.uk/interpro/.

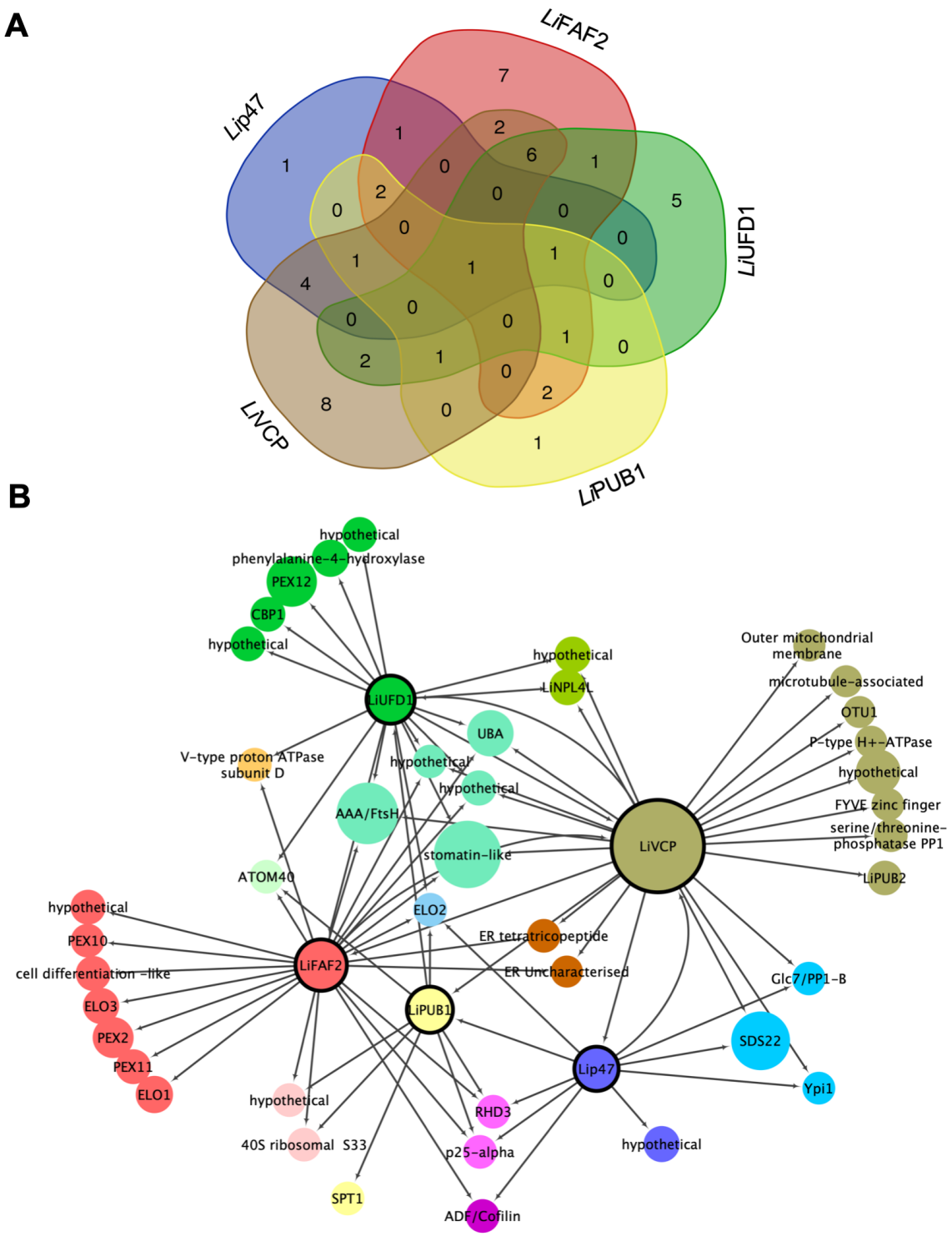

Fig. 6

Figure 6. The *Leishmania* VCP protein interaction network. (A) A Venn diagram representing the number of proteins identified by mass spectrometry in independent immunoprecipitates of *Li*VCP and its key cofactors *Li*UFD1, *Lip*47, *Li*FAF2 and *Li*PUB1. For

high stringency filtering and network clarity, only proteins absent in IPs with HA-tagged unrelated proteins (EUPC = 0.0 on five unrelated experiments) were considered for this analysis. The intersections of list of elements were calculated with the Venn tool at http://bioinformatics.psb.ugent.be/webtools/Venn/. For the list of proteins used and their intersection, see Supplementary Table S5. **(B)** Integrated interaction map of the *Li*VCP network using the data generated in this work showed as in (A). For clarity, protein names were simplified. Filled color circles for *Li*VCP and its cofactors are represented as in (A). Bigger circles represent higher average of EUPC in *Li*VCP IP experiments. The proteins *Li*UFD1, *Li*p47, *Li*FAF2, *Li*PUB1 and *Li*VCP were used as bait (see Methods) and are represented with bold border circles. The direction of interactions is represented with a target arrow shape. Spring-embedded layout was applied on Cytoscape 3.5.1

3.15 List of the Supplementary material included

Supplementary Tables*

Supplementary Table S1. Overlap between the BioGRID VCP interactors and *Leishmania* homologs. This spreadsheet presents the analysis of the overlap between interactors reported for the *H. sapiens* VCP from the Biogrid interaction dataset 3.4 and their similarities with *Leishmania* homologous proteins.

Supplementary Table S2. Proteins potentially interacting with the *Leishmania Li*VCP and its main cofactors as determined by immunoprecipitation and LC-MS/MS studies. This spreadsheet contains data from all IP-MS/MS experiments reported in this study for *Li*VCP, its cofactors and unrelated proteins used as filters.

Supplementary Table S3. GO-term analysis (cellular component, molecular function and biological process) of the *Li*p47, *Li*FAF2, *Li*UFD1 and *Li*PUB1 proteomes using the tool provided by TriTrypDB. Only proteins co-immunoprecipitated either with *Li*p47 or *Li*FAF2 or *Li*UFD1 and or *Li*PUB1 but not found in the IPs of the unrelated control proteins as described in Figure 3A were considered for these analyses. Raw data are presented.

Supplementary Table S4. Ramachandran plot analysis of all the modeled proteins. The quality of the 3D models for *Li*VCP and its main cofactors was assessed by Ramachandran plot analysis through the PROCHECK software module.

Supplementary Table S5. Proteins used for constructing the *Li*VCP interaction network classified based on their intersection. This spreadsheet contains the list of proteins used for the *Li*VCP network construction considering the presence/absence of different proteins on our multiple co-IP-MS/MS experiments.

Supplementary Table S6. Primers used in this study.

**** Supplementary Tables, 1, 2, 3, 5, and 6 are all Excel files (.xlsx) and are supplied separately.***

Supplementary figures:

Supplementary Figure S1. Known interacting partners of the *H. sapiens* VCP/p97 identified as putative cofactors of the *L. infantum Li*VCP protein.

Supplementary Figure S2. Ectopic expression of HA-tagged *Li*UFD1, *Li*p47, *Li*FAF2, *Li*NPL4 and *Li*PUB1 cofactors of the *Leishmania Li*VCP.

Supplementary Figure S3. Phylogenetic analysis of p47 homologs from different eukaryotes.

Supplementary Figure S4. Phylogenetic relationships between FAF2 homologs from different eukaryotes.

Supplementary Figure S5. Phylogenetic relationships between UFD1 homologs from different eukaryotes.

Supplementary Figure S6. Phylogenetic relationships between different NPL4 eukaryotic homologs.

Supplementary Figure S7. Phylogenetic relationships between PUB homologs from different eukaryotes.

Supplementary Figure S8. Sequence alignment of the *L. infantum Li*p47 with homologs from other eukaryotes.

Supplementary Figure S9. 3D homology modeling and docking predictions for *Li*p47 into *Li*VCP.

Supplementary Figure S10. Sequence alignment of the *L. infantum Li*FAF2 with homologs from other eukaryotes.

Supplementary Figure S11. 3D homology modeling and docking predictions for *Li*FAF2 into *Li*VCP.

Supplementary Figure S12. Sequence alignment of the *L. infantum Li*UFD1 with homologs from other eukaryotes.

Supplementary Figure S13. 3D homology modeling and docking predictions for *Li*UFD1 into *Li*VCP.

Supplementary Figure S14. Sequence alignment of the *L. infantum Li*NPL4 with homologs from other eukaryotes.

Supplementary Figure S15. 3D homology modeling and docking predictions for *Li*NPL4 into *Li*VCP.

Supplementary Figure S16. The *Leishmania* VCP cofactors *L*iUFD1 and *Li*NPL4 associate with poly-ubuquitinated chains.

Supplementary Figure S17. Sequence alignment of the *L. infantum Li*PUB1 protein with homologs from other eukaryotes.

Supplementary Figure S18. 3D homology modeling and docking predictions for *Li*PUB1 into *Li*VCP.

Supplementary Figure S19. Gene Ontology (GO) analysis.

3.16 Supplementary Tables

All Supplementary Tables* from chapter 3: “Molecular and functional characterization of the AAA+ ATPase Valosin-containing protein (VCP)/p97/Cdc48 interaction network in *Leishmania*” are included as “*Fichiers multimédia complémentaires*” presented together with this thesis.

**** Supplementary Tables, 1, 2, 3, 5, and 6 are all Excel files (.xlsx) and are supplied separately.***

Supplementary Table S4. Ramachandran plot analysis of all the modeled proteins.

Modeled proteins	Residues in most favoured regions (%)	Residues in additional allowed regions (%)	Residues in generously allowed regions (%)	Residues in disallowed regions (%)
*Li*VCP	94.3	4.8	0.6	0.3
*Li*PUB1	88.9	9.9	1.2	0.0
*Li*p47	87.0	8.7	4.3	0.0
*Li*FAF2	90.0	10.0	0.0	0.0
*Li*UFD1	87.1	11.2	1.2	0.6
*Li*NPL4	84.1	15.1	0.5	0.3

The quality of the models was assessed by Ramachandran plot analysis through the PROCHECK software module. The results of the Ramachandran plot showed that 95.7% to 100% of the amino acid residues of the constructed 3D homology models using alignments in Supplementary Figures S8, S10, S12, S14 and S17 are found in most favoured and additional allowed regions. These results indicate that the predicted structures are reliable. Moreover, Ramachandran plot also showed that in our 3D homology models the amino acid residues implicated in interactions are in most favoured regions.

3.17 Supplementary Figures

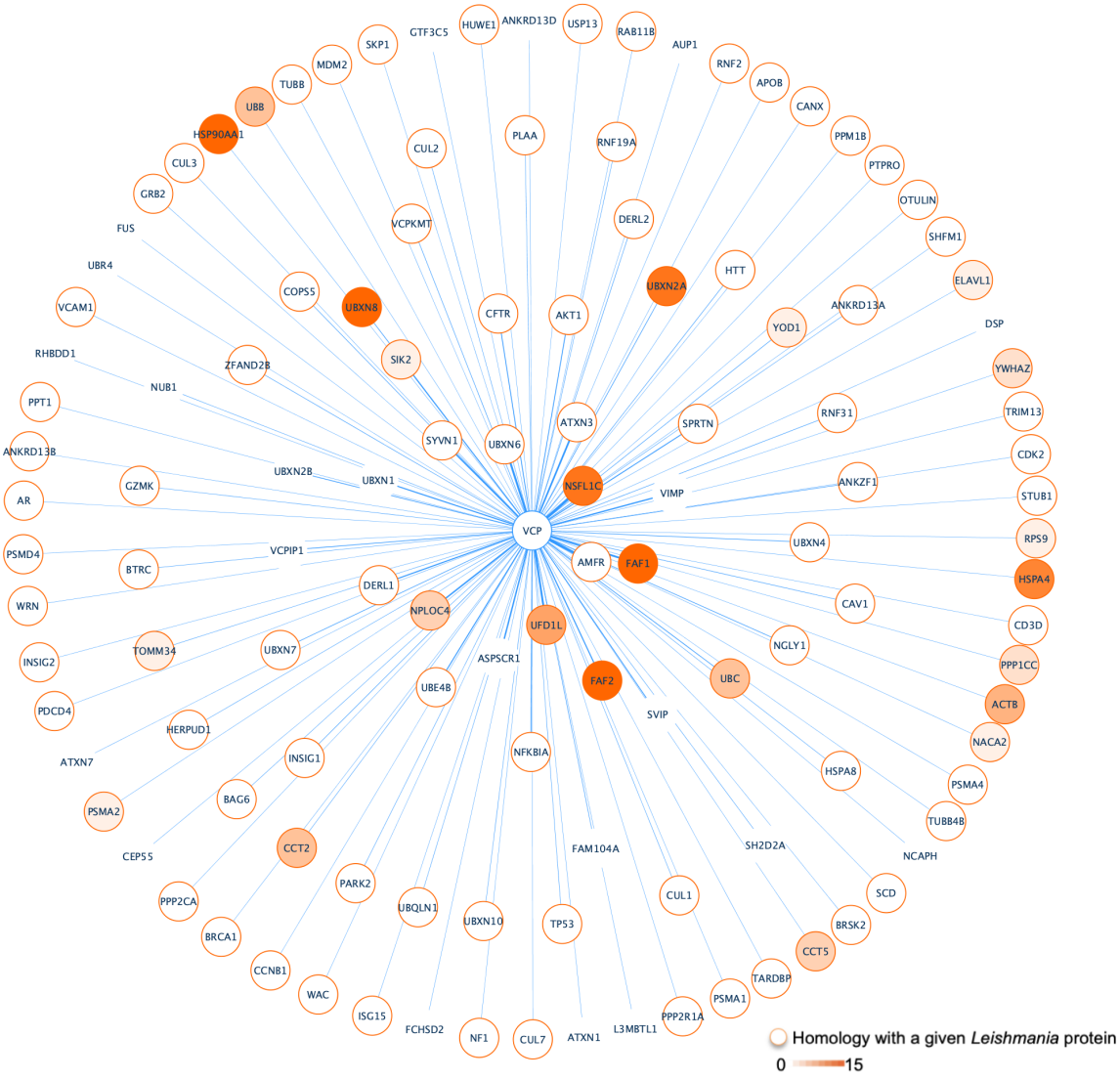

Supplementary Figure S1. Known interacting partners of the *H. sapiens* VCP/p97 identified as putative cofactors of the *L. infantum LiVCP* protein. Network analyses of the known physical (1091) and genetic (2) interactions of the human VCP ortholog from the Biogrid interaction dataset 3.4 (thebiogrid.org) plotted on Cytoscape version 3.5.1 (Shannon *et al.,* 2003). Edge length and thickness represents interaction with VCP/p97. The thicker the edge the more experimental evidence has been reported on Biogrid and closer they were placed to the center. Orange circles represent homology with any protein of the

Leishmania infantum genome (see Supplementary Table S1). Orange filled circles represent *Li*VCP interactions reported in this work. Darker shades of orange represent higher average of peptides identified by mass spectrometry in our *Li*VCP-HA co-immunoprecipitates (see Supplementary Table S2 for more details). 0-15: Average of exclusive unique peptides identified in *Li*VCP-HA immunoprecipitates followed by mass spectrometry.

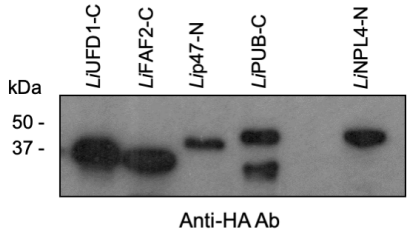

Supplementary Figure S2

Supplementary Figure S2. Ectopic expression of HA-tagged *Li*UFD1, *Li*p47, *Li*FAF2, *Li*NPL4 and *Li*PUB1 cofactors of the *Leishmania Li*VCP. Western blotting with an anti-HA antibody to detect C- or N- terminally HA-tagged *Li*UFD1, *Li*p47, *Li*FAF2, *Li*PUB1 and *Li*NPL4 cofactor proteins cloned in pSPαZEOα vector and transfected into *L. infantum* promastigotes. The *L. infantum* strains expressing these vectors were used for co-IP/LC-MS/MS analysis. Shown here are the most representative results from 3-5 similar experiments.

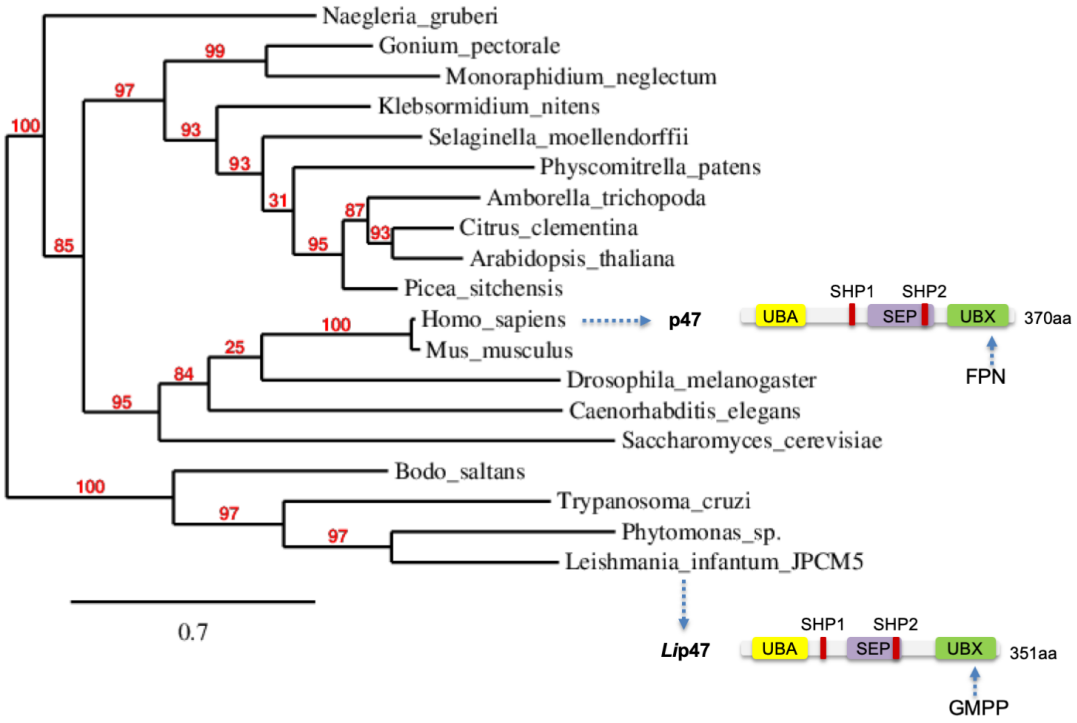

Supplementary Figure S3

Supplementary Figure S3. Phylogenetic analysis of p47 homologs from different eukaryotes. Sequence alignment of Supplementary Figure S8 was used to construct a maximum likelihood phylogenetic tree. The UBX binding site FPN in the human p47 protein and the UBX binding MPN (Mpr1/Pad1 N-terminal) domain in the *Leishmania Lip*47 protein are indicated by arrow. The analysis used a WAG substitution model and the statistical confidence of the nodes was calculated using the aLRT test.

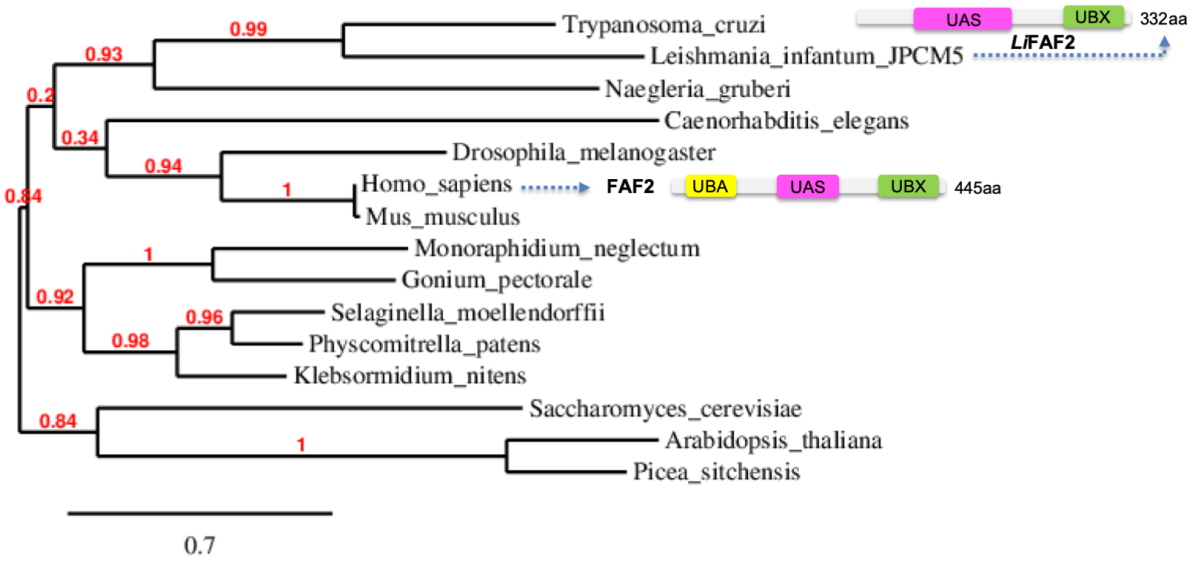

Supplementary Figure S4

Supplementary Figure S4. Phylogenetic relationships between FAF2 homologs from different eukaryotes. Sequence alignment of Supplementary Figure S10 was used to construct a maximum likelihood phylogenetic tree. The *Leishmania Li*FAF2 protein lacks the ubiquitin associated (UBA) domain. The analysis used a WAG substitution model, and the statistical confidence of the nodes was calculated using the aLRT test.

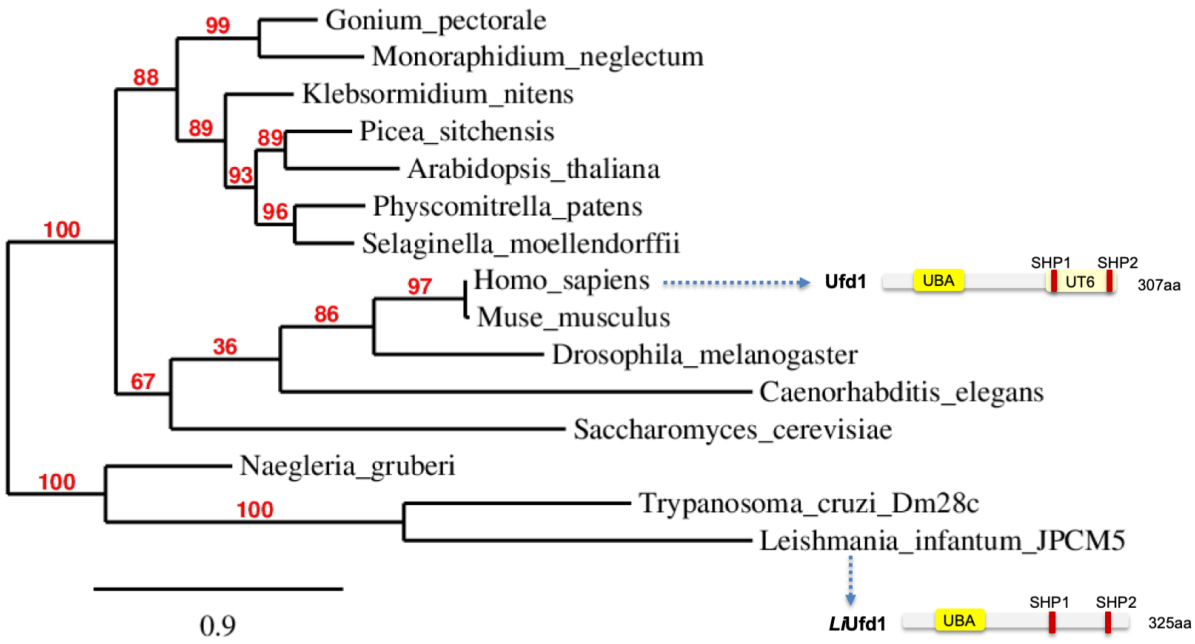

Supplementary Figure S5

Supplementary Figure S5. Phylogenetic relationships between UFD1 homologs from different eukaryotes. Sequence alignment of Supplementary Figure S12 was used to construct a maximum likelihood phylogenetic tree. The analysis used a WAG substitution model, and the statistical confidence of the nodes was calculated using the aLRT test.

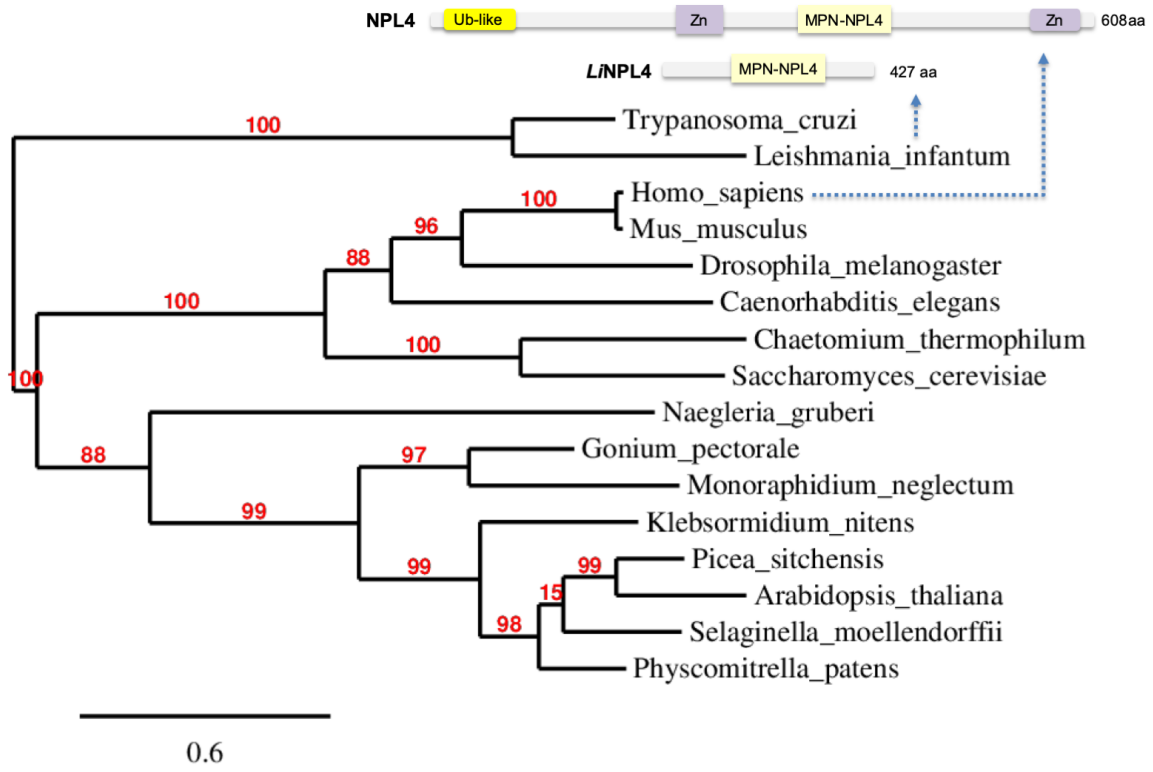

Supplementary Figure S6

Supplementary Figure S6. Phylogenetic relationships between different NPL4 eukaryotic homologs. Sequence alignment of Supplementary Figure S14 was used to construct a maximum likelihood phylogenetic tree. The *Leishmania Li*NPL4 homolog lacks the ubiquitin regulatory domain (UBX)-like and the two zinc finger motifs. The analysis used a WAG substitution model, and the statistical confidence of the nodes was calculated using the aLRT test.

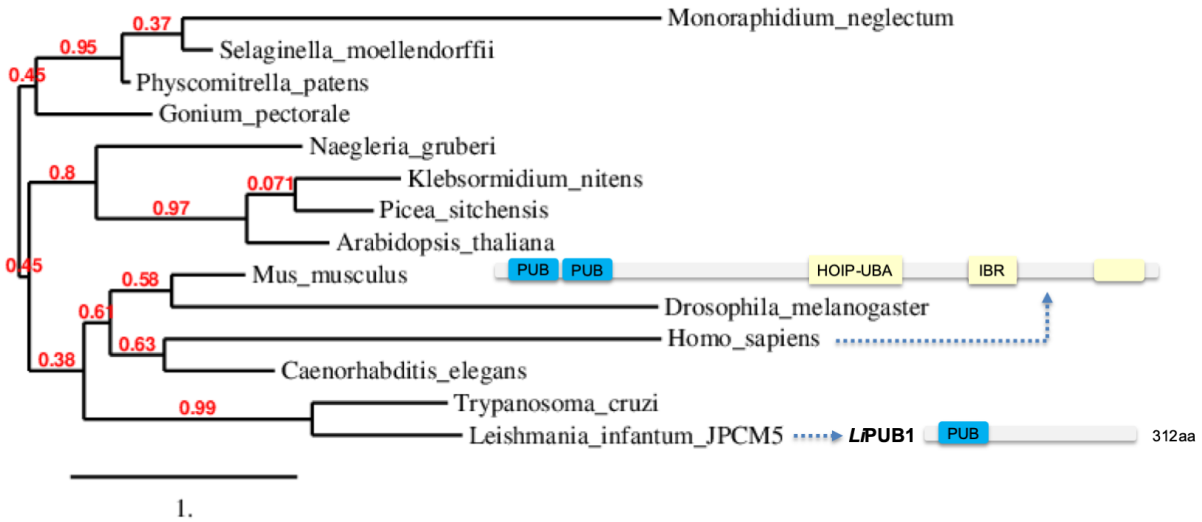

Supplementary Figure S7

Supplementary Figure S7. Phylogenetic relationships between PUB homologs from different eukaryotes. Sequence alignment of Supplementary Figure S17 was used to construct a maximum likelihood phylogenetic tree. The *Leishmania*, *Li*PUB1, protein which has no homolog in human. The analysis used a WAG substitution model, and the statistical confidence of the nodes was calculated using the aLRT test.

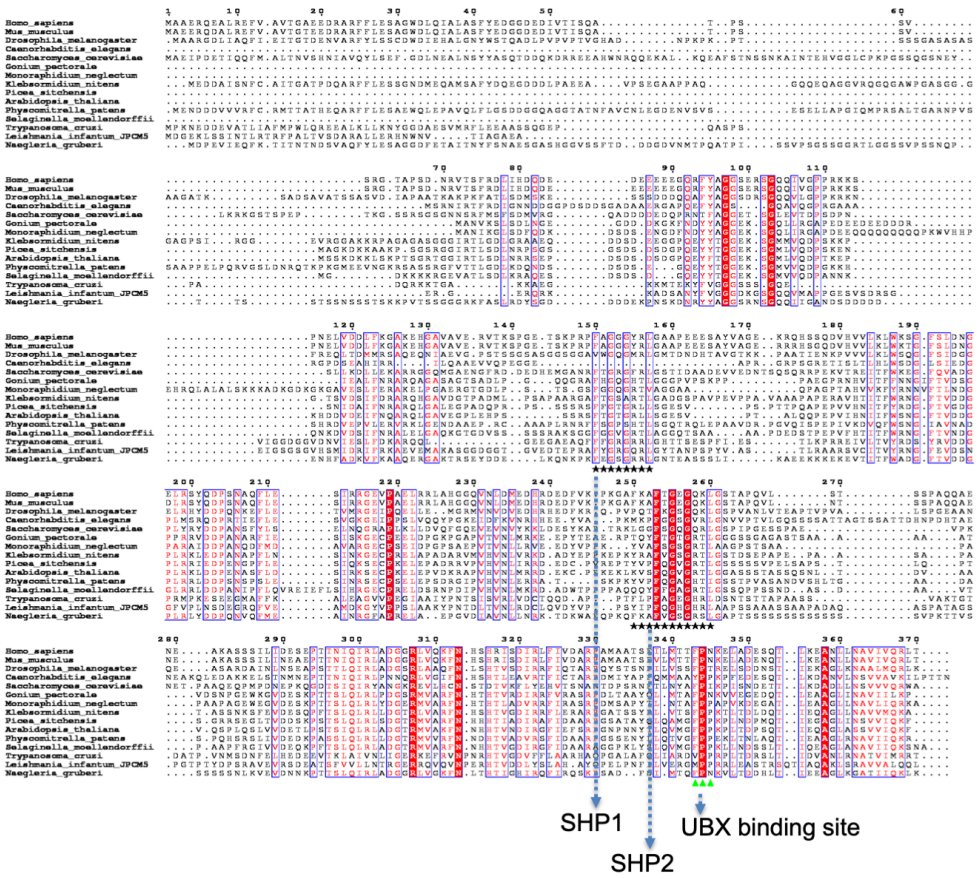

Supplementary Figure S8

Supplementary Figure S8. Sequence alignment of the *L. infantum Li*p47 with homologs from other eukaryotes. Sequence alignment was done using Clustal Omega. Highly conserved amino acid residues are shown in red and boxed in blue. Black asterisks represent residues of SHP1 and SHP2 motifs and green triangles indicate the UBX binding site. The figure was prepared with ESPript (http://espript.ibcp.fr).

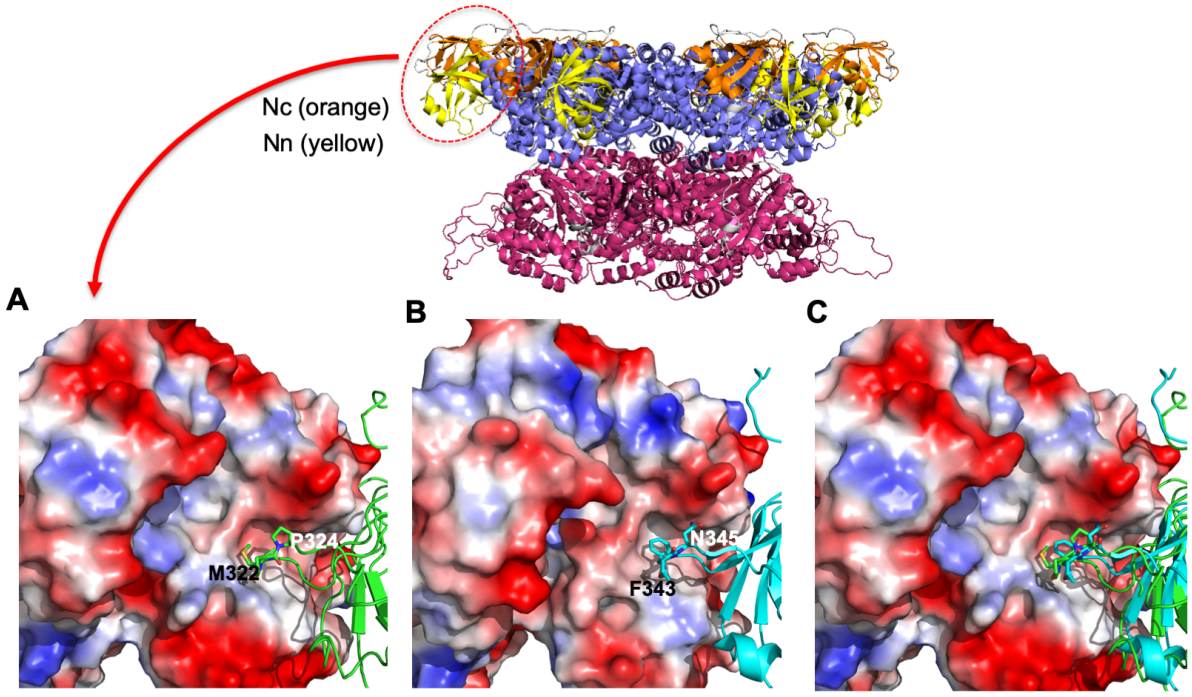

Supplementary Figure S9

Supplementary Figure S9. 3D homology modeling and docking predictions for *Li*p47 into *Li*VCP. (**A**) 3D model of interactions between the N-terminus of *Li*VCP (electrostatic potential) and the GMPP motif of *Li*p47 UBX domain (in green). (**B**) PDBid 1S3S structure representing the interactions between the N-terminus of VCP and the FPN motif within the UBX binding site of p47 (in cyan). (**C**) Superposition of structures represented in (A) and (B).

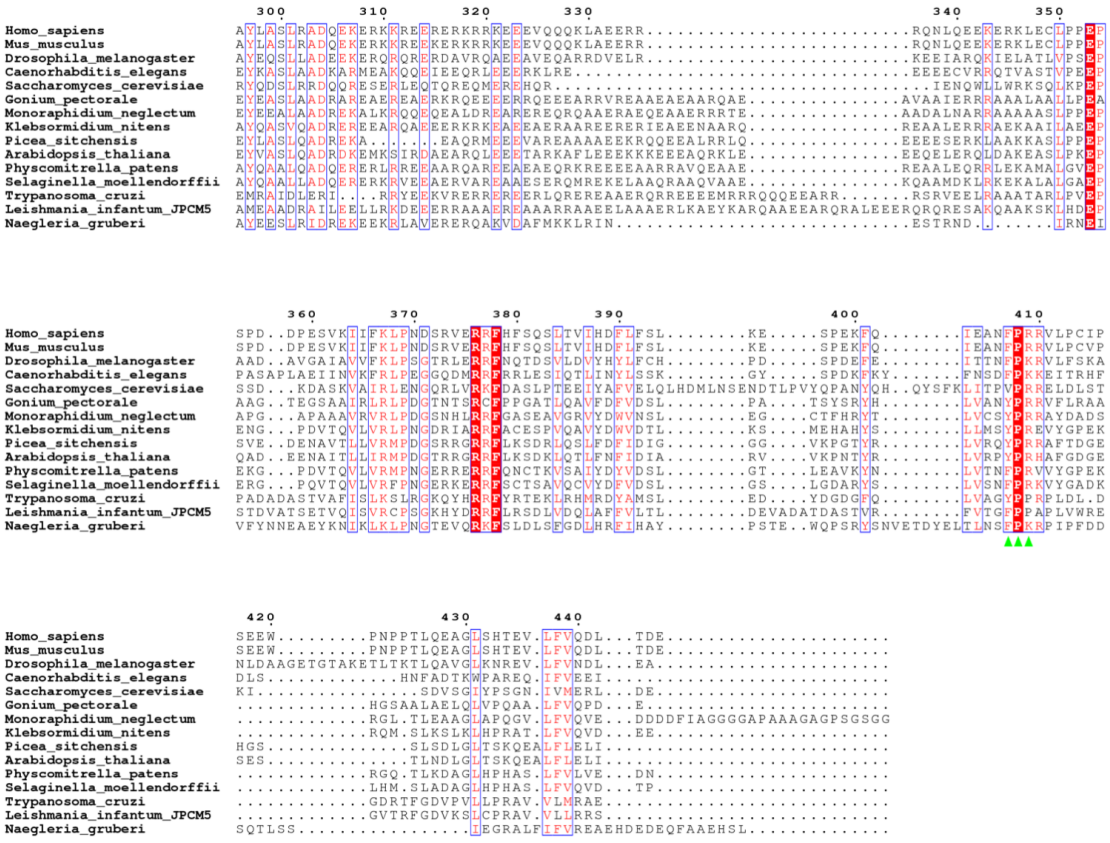

Supplementary Figure S10

Supplementary Figure S10. Sequence alignment of the *L. infantum Li*FAF2 with homologs from other eukaryotes. Sequence alignment was done using Clustal Omega. Highly conserved amino acid residues are shown in red and boxed in blue. Green triangles represent the UBX binding site FPP in *L. infantum*. The figure was prepared with ESPript (http://espript.ibcp.fr). Here, only the conserved region from aa 300 to 440 is shown, the rest of the protein sequence being more divergent between the different eukaryotic FAF proteins.

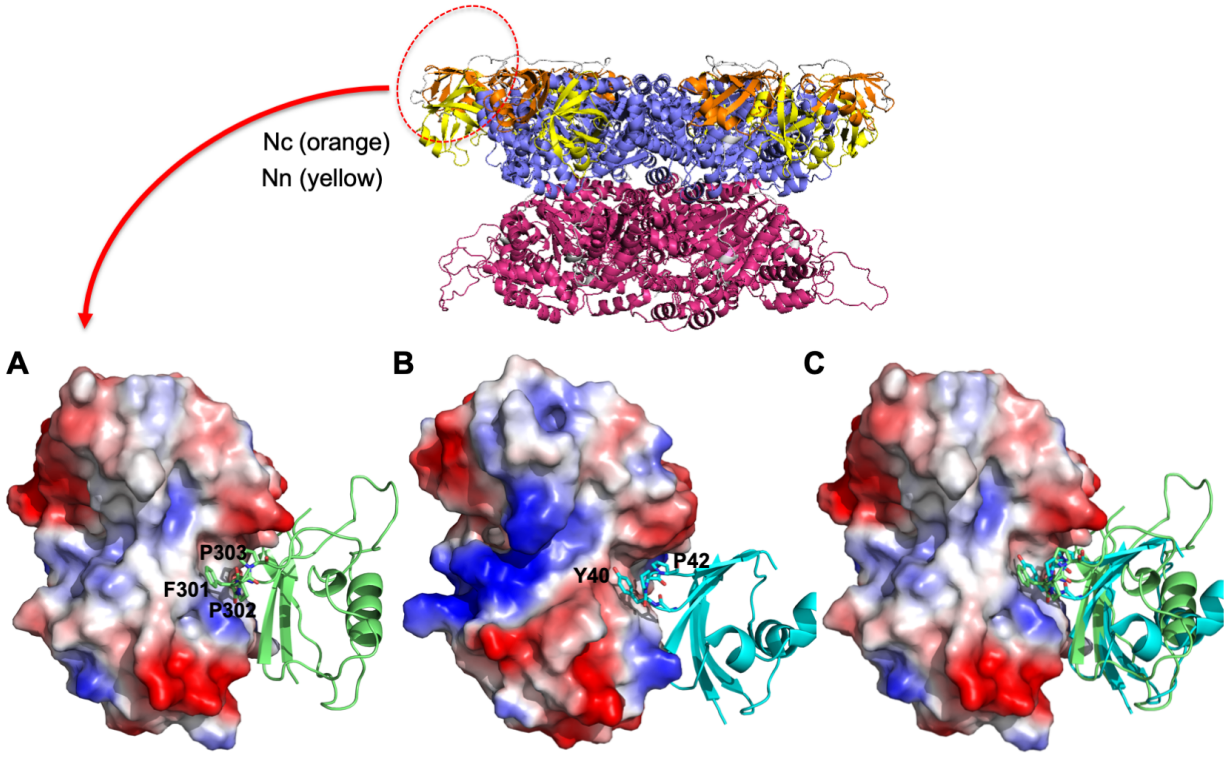

Supplementary Figure S11

Supplementary Figure S11. 3D homology modeling and docking predictions for *Li*FAF2 into *Li*VCP. (**A**) 3D model of interactions between the N-terminus of *Li*VCP (electrostatic potential) and the GFPP motif of the UBX *Li*FAF2 domain (in green). (**B**) PDBid 4KDL structure representing the interactions between the N-terminus of VCP and the ^{40}GYPP^{43} motif of ovarian tumor domain-containing protein 1 (OTU1) (in cyan). (**C**) Superposition of structures represented in (A) and (B). For details, see www.rcsb.org/structure/4KDL.

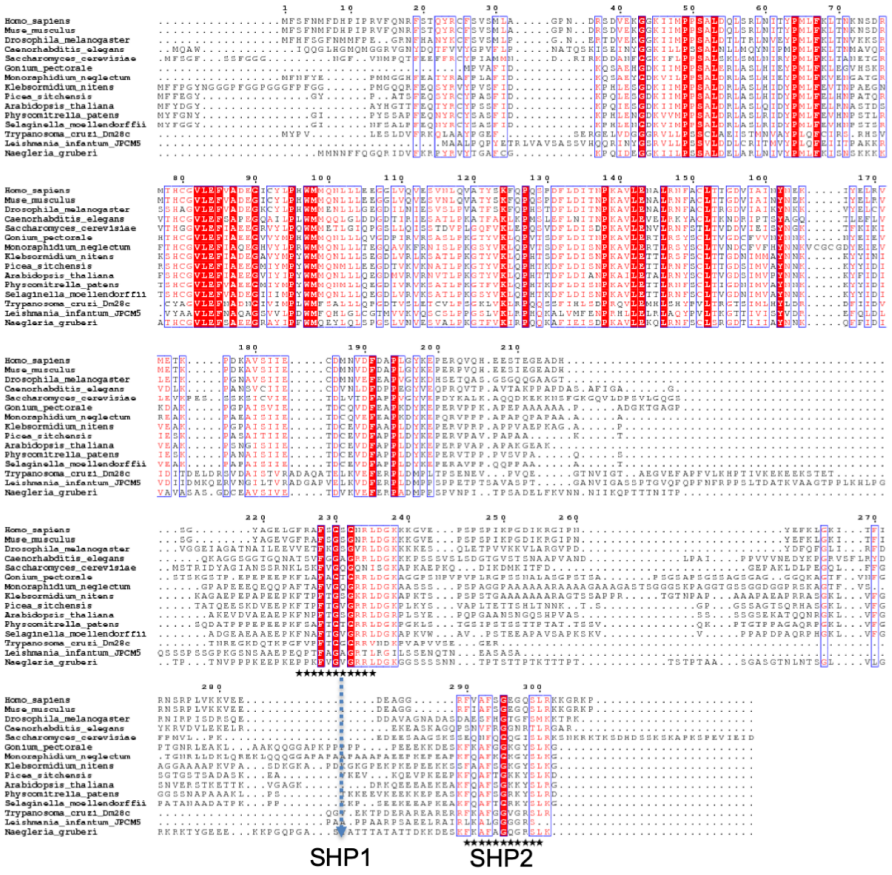

Supplementary Figure S12

Supplementary Figure S12. Sequence alignment of the *L. infantum Li*UFD1 with homologs from other eukaryotes. Sequence alignment was done using Clustal Omega. Highly conserved amino acid residues are shown in red and boxed in blue. Black asterisks represent residues of SHP1 and SHP2 motifs. The figure was prepared with ESPript (http://espript.ibcp.fr).

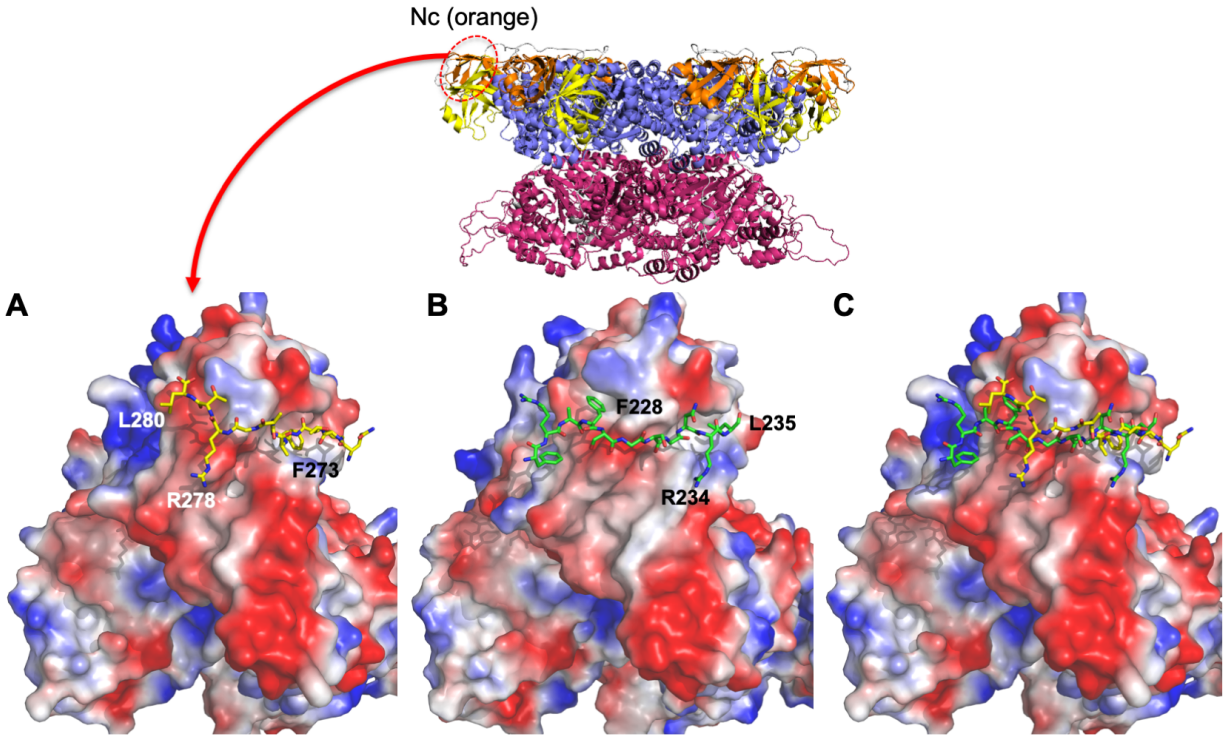

Supplementary Figure S13

Supplementary Figure S13. 3D homology modeling and docking predictions for *Li*UFD1 into *Li*VCP. (**A**) 3D model of interactions between the N-terminus of *Li*VCP (electrostatic potential) and the QPTFAGAGRTL SHP1 motif of *Li*UFD1 (in yellow). (**B**) PDBid 5C1B structure representing the interactions between the N-terminus of VCP and the SHP1 domain of UFD1 (in green). (**C**) Superposition of structures represented in (A) and (B).

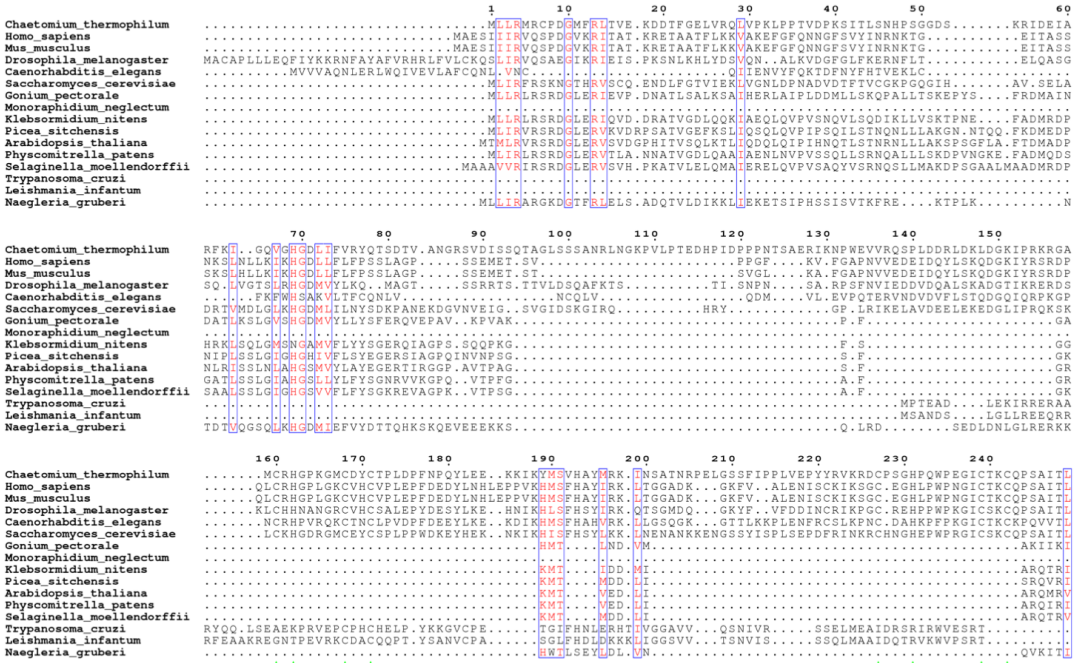

Supplementary Figure S14 1/3

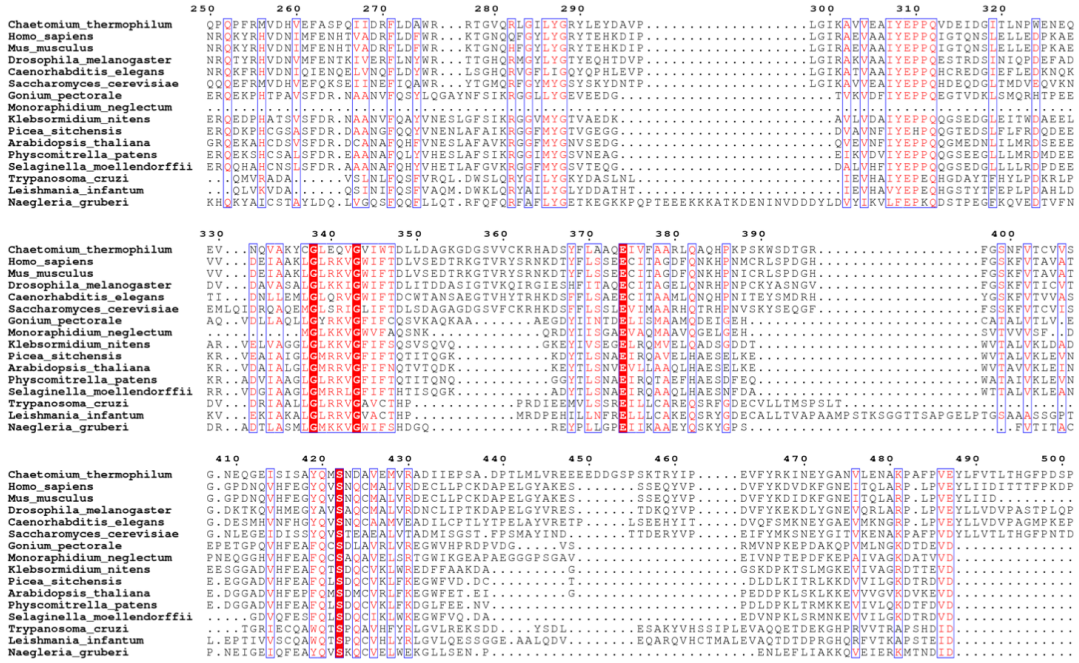

Supplementary Figure S14 2/3

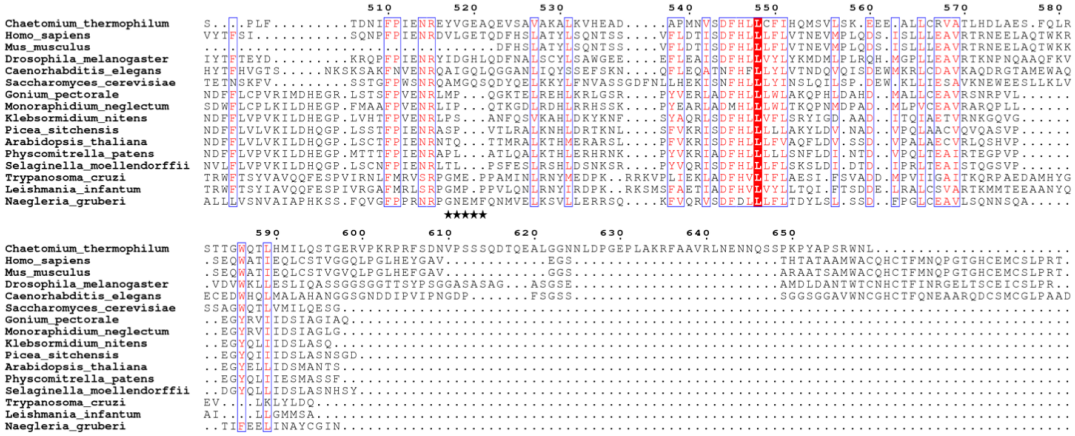

Supplementary Figure S14 3/3

Supplementary Figure S14. Sequence alignment of the *L. infantum Li*NPL4 with homologs from other eukaryotes. Sequence alignment was done using Clustal Omega. Highly conserved amino acid residues are shown in red and boxed in blue. Green triangles indicate the UBX binding site in other eukaryotic orthologs (the *Leishmania* NPL4 homolog lacks the UBX-like domain). Black asterisks represent the GMPP motif within the C-terminus of *Li*NPL4. The figure was prepared with ESPript (http://espript.ibcp.fr).

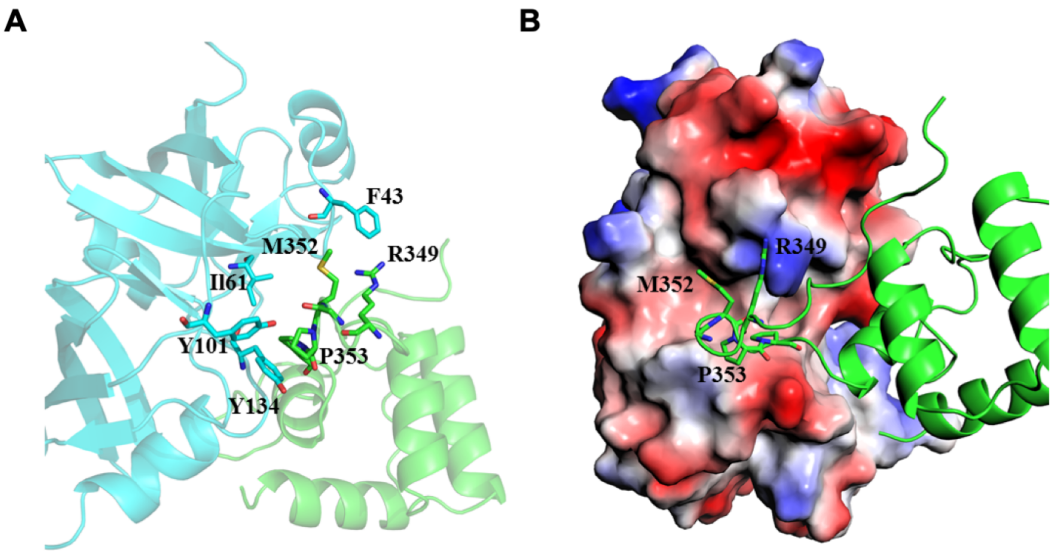

Supplementary Figure S15

Supplementary Figure S15. 3D homology modeling and docking predictions for *Li*NPL4 into *Li*VCP. (**A**) Cartoon view of the interactions between the N-terminus of *Li*VCP (cyan) and the GMPP motif located at the C-terminus of *Li*NPL4 (green). (**B**) 3D model with the electrostatic potential surface representation of the *Li*VCP N-terminus. Negative and positive charges are shown in red and blue, respectively.

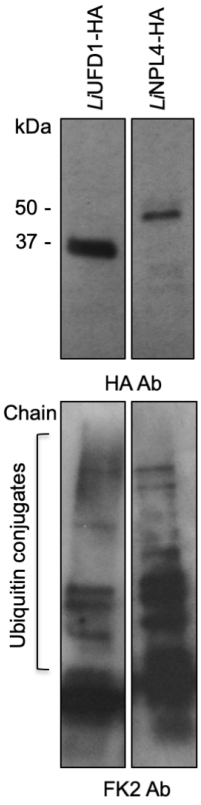

Supplementary Figure S16

Supplementary Figure S16. Immunoprecipitation from *L. infantum* parasites expressing *L*iUFD1-HA or *Li*NPL4-HA followed by western blotting using an anti-HA antibody (top panel). Western blotting of the *L*iUFD1-HA or *Li*NPL4-HA immunoprecipitates using the FK2 antibody recognizing K^{29}-, K^{48}-, and K^{63}-linked mono- and poly-ubiquitin chains.

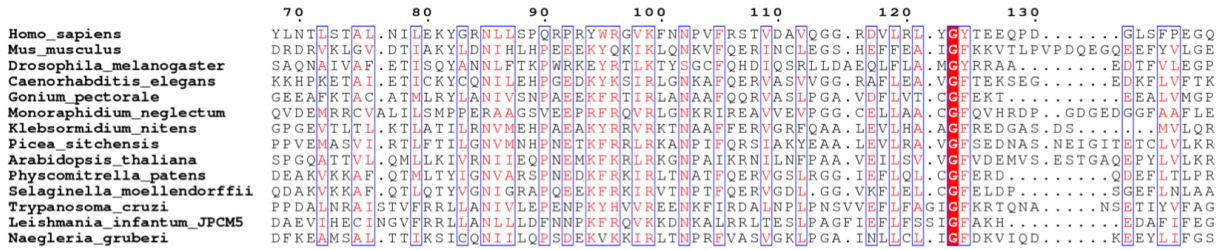

Supplementary Figure S17

Supplementary Figure S17. Sequence alignment of the *L. infantum Li*PUB1 protein with homologs from other eukaryotes. Sequence alignment was done using Clustal Omega. Highly conserved amino acid residues are shown in red and boxed in blue. The figure was prepared with ESPript (http://espript.ibcp.fr). Here, only the conserved region from PUB domain is shown, the rest of the protein sequence being more divergent between different eukaryotic organisms.

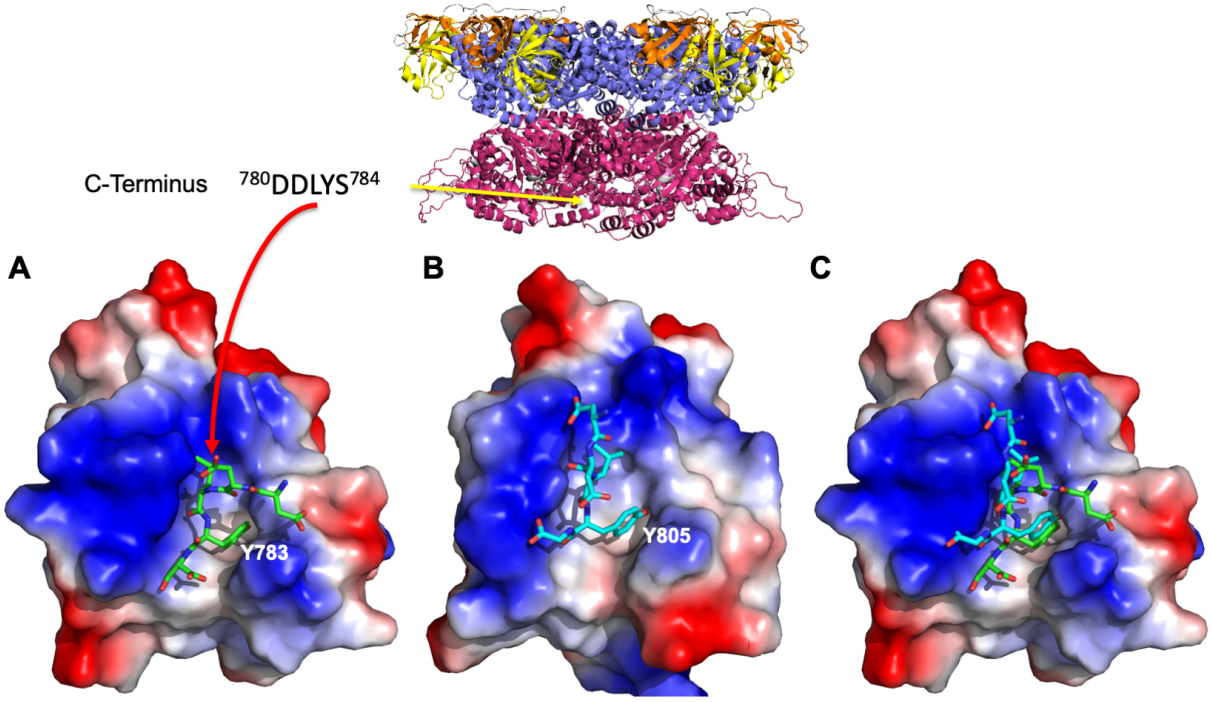

Supplementary Figure S18

Supplementary Figure S18. 3D homology modeling and docking predictions for *Li*PUB1 into *Li*VCP. (**A**) 3D model of interactions between the *Li*PUB1 protein (electrostatic potential) and the C-terminal DDLYS motif of *Li*VCP (in green). (**B**) PDBid 2HPL structure representing the interactions between the PUB domain (electrostatic potential) and the C-terminal DDLYG motif of VCP (in cyan). (**C**) Superposition of structures represented in (A) and (B).

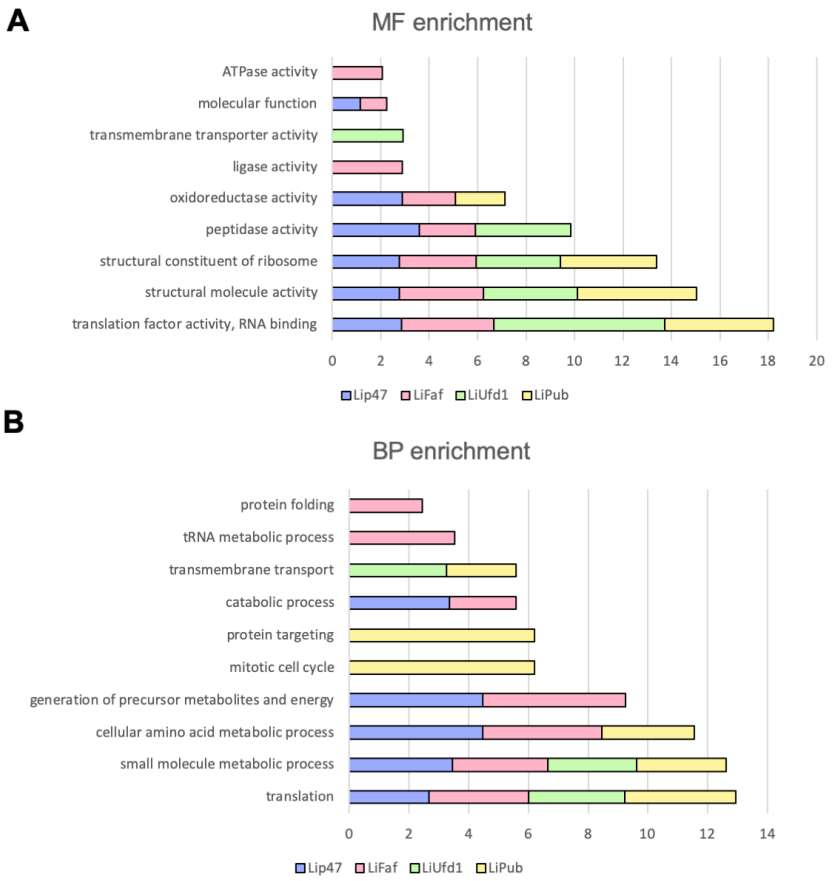

Supplementary Figure S19

Supplementary Figure S19. Gene Ontology (GO) analysis. Biological process (**A**) and molecular function (**B**) analyses for proteins identified by mass spectrometry in *Li*p47 (145), *Li*FAF2 (164), *Li*UFD1 (46) and *Li*PUB1 (98) immunoprecipitates as show in Figure 3.

Chapter 4: Discussion

The characterization of the valosin-containing protein VCP/p97/Cdc48 and its co-factors in many organisms has been of great significance for understanding protein quality control pathways (102). More recently, special attention has been given to understand how those diverse co-factors can act together with VCP (95) and how they acquire their specificity (98) to display multiple functions (113) in order to respond to stress and maintain proteostasis. The understanding of how VCP works extends to the cancer field (148), neurodegenerative disorders (136) and the discovery and repurposing of drugs to the treatment of many human pathologies (146) as well some parasitic diseases (139).

This thesis began with the demonstration that the Dde1/DDX3 DEAD-box RNA helicase ortholog in *Leishmania* plays a central role in mitochondrial homeostasis (149). Immunoprecipitation and mass-spectrometry studies revealed potential interaction of DDX3 with several components of the stress cellular response and protein quality control, including the AAA+ ATPase p97/VCP/Cdc48. VCP/p97 is a key component of the Ubiquitin Proteasome System (UPS) playing a central role in cellular proteostasis as it is involved in the endoplasmic reticulum (ER)-associated protein degradation the mitochondrion-associated protein degradation, ribosomal quality control, and stress granules clearance, among others (84,102,104,108,111). In all these pathways, VCP/p97 hydrolyzes ATP and uses the resulting energy to extract or disassemble polyubiquitinated substrates from membranes, or organelles, or in general from large protein assemblies and deliver them to the 26S proteasome for degradation (103). Given that *Leishmania* intracellular amastigotes have to adapt to different environmental stress/stimuli (e.g., oxidative and nitrosative stress, heat stress, low pH, nutrient deprivation, and osmotic pressure) most of which lead to DNA damage or protein misfolding, the parasite depends on quality control systems that cooperate to eliminate damaged proteins. However, protein quality control in these parasites, as well as in other trypanosomatids is largely understudied. The *Leishmania* VCP/p97 homolog shares a high sequence identity and structural organization with its evolutionary distant eukaryotic counterparts and thus we hypothesized that it should fulfill similar functions in protein quality control. This prompted us to initiate studies aiming at characterizing p97/VCP/Cdc48 and its key co-factors and interacting partners in

Leishmania. First, we have investigated the functional role of the *Leishmania* VCP/p97 homolog (*Li*VCP) in the parasite response to intracellular stress and development.

LiVCP is essential for the intracellular development of _Leishmania_ and its ability to respond to heat stress

Attempts to generate a null mutant for the *VCP* gene in *Leishmania* failed, suggesting that it is essential for the parasite growth, consistent with previous reports in other eukaryotes. While promastigote forms can grow normally with 50% less VCP (a heterozygous mutant is viable), they are unable to differentiate into axenic amastigotes and or to grow as intracellular amastigotes. Parasites with decreased *Li*VCP expression by heterozygous gene replacement or overexpressing a temperature sensitive VCP mutant or with impaired VCP activity using dominant negative mutants exhibit a dramatic effect on intracellular amastigote growth and the parasite ability to survive under stress, particularly heat stress. Heat stress is known to induce proteotoxicity, which explains why the requirement for VCP is more critical in amastigotes in ensuring cellular proteostasis. The fact that both VCP mRNA and protein are increased in *Leishmania* amastigotes (by ~3-fold) further supports the key role VCP may play for the parasite intracellular development.

The use of dominant negative mutants VCP^{Q2} and also VCP^{QQ} where the essential glutamic acid residue in the D2 ATPase Walker B motif was mutated to a glutamine, but not the VCP^{Q1} mutant interfering with the D1 ATPase motif, seems to impair *Li*VCP activity in amastigotes but not in promastigotes. *Leishmania* amastigotes grow at elevated temperature (37°C) as opposed to promastigotes (25°C). It is therefore possible that the hexameric VCP structure undergoes conformational changes triggered by temperature stress, which may contribute to the differential dominant negative effect seen between promastigote and amastigote forms. Our data support that ATP binding/hydrolysis of VCP/p97 by the D2 ring is central to VCP's function. It has been reported that the D2 ATPase ring allows important conformational changes of the homohexameric VCP complex (150,151), which provide the energy required for ubiquitin-directed disassembly of macromolecular complexes (152) and transfer of the polyubiquitinated substrates to the 26S proteasome for degradation (153).

Furthermore, we showed that the C-terminal region of *Li*VCP is essential for VCP protein stability and its function under heat stress. While the facilitated double knockout mutant VCP^{HA} has no growth defect in promastigotes (25°C) it is unable to grow in the amastigote

stage (37°C), hence exhibiting a temperature sensitive (ts) phenotype. In fact, we showed that C-terminal tagging of *Li*VCP renders the protein highly unstable and promotes its degradation only in amastigotes. These data suggest that the C-terminus of *Li*VCP is critical for the stability of the protein under heat stress as also hypothesized in the yeast model (154). It was reported previously that the unstructured C-terminal tail of VCP plays a role in maintaining the conformation of the D2 module during the ATPase cycle (155).

We have shown previously by co-immunoprecipitation and mass spectrometry experiments that *Li*VCP associates with the DEAD-box RNA helicase DDX3 and that inactivation of DDX3 leads to mitochondrial ROS accumulation (149). Given a possible interaction of *Li*VCP with DDX3, we further assessed the putative role of *Li*VCP in protecting the parasite from ROS production. We first measured peroxyl radicals and peroxides in parasites with decreased or altered VCP activity using the dye 2′,7′-dichlorodihydrofluorescein diacetate (H_2DCFDA), which once oxidized, emits fluorescence directly proportional to the amount of ROS. In addition, we measured mitochondrial superoxide accumulation by MitoSOX. Our results indicate that ROS levels were significantly higher in the *Li*VCP mutants, especially in the dominant negative mutant VCP^{QQ}. This effect was even more prominent when treating the cells with miltefosine (Appendix 9), a drug known to induce ROS production. We have shown that VCP impaired mutants were more sensitive to stress caused by miltefosine (156). Other stress such as increased temperature or acidic pH stress did not induce significantly higher ROS production in the different *Li*VCP mutants (data not shown). However, these are preliminary observations and additional optimized experiments should be performed to consolidate those results.

_Li_VCP is mostly localized to the cytoplasm but it is also found associated with organellar fractions and RNA granules

Immunofluorescence studies in *Li*VCP-HA or *Li*VCP-GFP overexpressing cells using an anti-HA or an anti-GFP antibody localized *Li*VCP protein predominantly to the cytoplasm (Appendix 5). To increase resolution and also specificity, we used confocal microscopy in wild type parasites with an antibody directed against the *T. brucei* VCP protein (*Tb*VCP) (93) that specifically recognizes the *Leishmania* VCP (156). These experiments also pointed out a cytoplasmic localization for *Li*VCP with a clearly granular pattern. VCP has been found associated with both ER and OMM fractions given its central role in the endoplasmic reticulum (ER)-associated protein degradation (64,106) and the translocation of damaged

mitochondrial proteins from the outer mitochondrial membrane into the cytosol (83,84). We therefore investigated if the *Leishmania* VCP protein shows any organellar association using either an antibody against the BiP ER chaperone or a mitochondrial marker (MitoTracker). Our results indicate indeed a partial co-localization of *Li*VCP with the ER and a weak association with the mitochondrion (156). Organellar association of *Li*VCP was further supported by digitonin (20 µM-10 mM) fractionation experiments and Western blotting using an anti-*Tb*VCP antibody (156). The association of *Li*VCP with the ER and to a lesser extent the mitochondrion is in line with *Li*VCP being involved in the extraction of polyubiquitinated proteins from cellular organelles, as described in other eukaryotes (64,157).

Given the role for VCP/Cdc48 in stress granule clearance and the fact that pathological mutations in VCP could lead to the constitutive appearance of stress granules (111), we questioned if *Li*VCP could be found in RNA or stress granules. The granular pattern observed by immunofluorescence studies using an anti-VCP antibody also prompted us to investigate this possibility. In the trypanosomatid *T. cruzi*, the DEAD-box DHH1 protein co-localizes with RNA granules (158) and the poly(A) binding protein 2 (PAB2) with RNP granules (159). We therefore carried out co-localization experiments of *Li*VCP with *Li*DHH1 (Appendix 6) or *Li*PAB2 (Appendices 7 and 8). Preliminary data suggest a partial co-localization of *Li*VCP with RNA and or RNP granules (Appendices 7 and 8). However, more work is required, also under conditions of stress, to assess the function of the *Leishmania* VCP protein in RNA or stress granules. These additional studies would bring valuable insights into new functions of this multifaceted protein.

*Li*VCP acts as an ubiquitin-selective chaperone

VCP functions as an ubiquitin-selective chaperone in other eukaryotes that uses energy through ATP hydrolysis to extract or “segregate” ubiquitylated target proteins from membranes or stable protein assemblies and present them for proteasomal degradation and as such itis central to multiple protein quality control pathways mediated by the Ubiquitin Proteasome System (UPS) (102,104). Polypeptides modified with K48-linked polyubiquitin chains, which also serve as a major targeting signal for the proteasome (160), are physiological substrates for VCP. Our previous studies revealed *Li*VCP association with several proteasome subunits (149). Here, we investigated whether decreased *Li*VCP expression in the heterozygous *Li*VCP$^{(NEO/+)}$ mutant or impaired *Li*VCP function in the

presence of dominant negative mutants VCP^{Q2} or VCP^{QQ} targeting the ATPase D2 domain of VCP has an effect on cellular levels of polyubiquitinated proteins by western blot analysis using a FK2 antibody recognizing K29-, K48-, and K63-linked mono- and polyubiquitilated proteins. Interestingly, our results indicate that a ~50% decrease in the expression of *Li*VCP in *Li*VCP$^{NEO/+}$ was sufficient to increase accumulation of polyubiquitinated proteins although to a lesser extent than in the VCP^{Q2} or VCP^{QQ} dominant negative mutants. Accumulation of polyubiquitinated proteins was indeed much higher upon expression of the VCP^{Q2} or VCP^{QQ} dominant negative mutants, especially into the *Li*VCP$^{NEO/+}$ background, suggesting that ATP hydrolysis mediated through the ATPase D2 domain is very important for the ubiquitin-selective chaperone function of *Li*VCP. Increased polyubiquitination had no significant effect on promastigote growth. However, in amastigotes where heat stress promotes proteotoxicity, the requirement for VCP becomes more critical in ensuring cellular proteostasis.

The association of *Li*VCP with the ER and to a lesser extent the mitochondrion as suggested by co-localization studies is in line with *Li*VCP being involved in the extraction of polyubiquitinated proteins from cellular organelles, as described in other eukaryotes (64,84). Thus, our data suggest a direct link between *Li*VCP function and the removal of polyubiquitinated substrates for subsequent proteasomal degradation in *Leishmania*. The higher sensitivity of the heterozygous *Li*VCP$^{NEO/+}$ and the *Li*VCP$^{(NEO/HYG)}$+VCP^{HA} mutant strains to the proteasome inhibitor MG-132 further supports such a role for *Li*VCP.

The *Li*VCP protein network: key *Li*VCP co-factors and interacting partners

VCP/p97 is a hexameric protein that interacts with a large number of protein co-factors and interacting partners that are key for its activity and functional diversity (135). Most cofactors whether they have a substrate-recruiting, processing or regulatory function interact with the Nn or Nc subdomains of VCP via a small number of conserved VCP binding modules, such as UBX (ubiquitin regulatory X with a similar three-dimensional structure described for ubiquitin) or UBX-like or UBA (ubiquitin associated) or a SHP motif or a VIM (VCP-interacting motif) or VBM (VCP-binding motif) motif, while a lower number binds to the unstructured C-terminal tail [PUB (PNGase/UBA or UBX-containing proteins) or a PUL (PLAP, Ufd3p, and Lub1p) domain)] formed by the last 7 amino acids (98,100). The *L. infantum Li*VCP homolog

is highly conserved among its eukaryotic counterparts and encodes a protein of 784 amino acids that harbors all the characteristic domains of eukaryotic VCP homologs (156).

Based on the BioGrid database and according to the e-value similarity accessed by protein BLAST (or blastP), most proteins from the human VCP network have a homolog in *Leishmania.* To unveil the *Leishmania* VCP protein network, both its major *Li*VCP co-factors and their interacting partners, we used combined datasets from multiple co-immunoprecipitation and mass spectrometry studies coupled with *in silico* analysis. Globally, our data indicate that the *Li*VCP interactome comprises more than 80 proteins with 24 exclusively interacting with *Li*VCP. Based on the similarities with the human VCP partners and the predicted domains presented for each protein, we selected several proteins as potential *Li*VCP core cofactors for further investigation. Coupled with *in silico* studies to predict conserved domains and its 3D docking within *Li*VCP, we have identified the ubiquitin-associated (UBA) and ubiquitin regulatory X (UBX) containing cofactors p47 and FAF2, the heterodimer UFD1-NPL4, and a PUB (PNGase/UBA or UBX) containing protein as the core cofactors of the *Leishmania* VCP network. The interaction of the p47, UFD1, FAF2 and PUB1 cofactors with the *Leishmania* VCP homolog was further confirmed by immunoprecipitation studies. Interestingly, we found that several proteins are shared between more than two or three *Leishmania* VCP cofactors. The only class of known VCP cofactors not identified in any of our experiments are those harboring the VIM (VCP-interacting motif)/VBM (VCP-binding motif) motifs (95). Additional IP-MS/MS experiments under different growth conditions such as promastigotes vs. amastigotes or exposure to oxidative stress or temperature stress were carried out but no significant changes in the *Li*VCP proteome were observed (data not shown).

Several of the *Li*VCP interacting partners have homologs that are known to interact with VCP in other eukaryotic systems but others do not and may be relevant to study further as part of distinct *Leishmania* VCP complexes. Overall, our data support similarities but also important differences between the *Li*VCP protein network and those characterized in other eukaryotes. Gene Ontology analysis of each VCP co-factor proteome combined with digitonin fractionation and immunofluorescence studies indicated specific compartment-association for each cofactor. Interestingly, an enrichment of a 19-fold for vacuolar proteins was seen in the *Li*UFD1 proteome, nuclear proteins were exclusively enriched within the

*Li*p47 proteome and endoplasmic reticulum-related proteins were enriched only within the *Li*FAF2 and *Li*PUB1 proteomes.

Lip47

The *Leishmania* p47 homolog presents the same domain composition than its human counterpart. It harbors the UBA and UBX domains and two SHP motifs (SHP1 and SHP2) that are known to be key for the interaction with VCP. The *Li*p47 SHP1 and SHP2 sites were identified here as FYGRGQRL and FQGHGHRL, respectively, which is similar to the consensus sequence $FxGxGx_2h$ (h, hydrophobic residue; x, any amino acid) (98). p47 interacts simultaneously with the same VCP/p97 monomer via its SHP motif and UBX domain (101). Interestingly, the *Li*p47 also contains the sequence GMPP in the UBX domain that docks *in silico* into the Nn-Nc pocket of *Li*VCP similarly to the human p47 (161). In addition to the bipartite mechanism of *Li*p47 for VCP binding, our data support an association of *Li*p47 but also of *Li*VCP with the serine/threonine phosphatase type 1 (PP1) complex consisting of the PP1 catalytic subunit Glc7/PP1-B, the SDS22 regulator-like protein, and the protein phosphatase PP1 inhibitor YPI1. In *S. cerevisiae*, it has been shown recently that these proteins form a ternary complex that is important for the nuclear localization of PP1 and that this complex and its quality control is positively regulated by the AAA-ATPase Cdc48 and its adaptor p47 (162). Interestingly, we found that *Li*p47 interacts with a large number of nuclear proteins and that is partly localized to the nucleus. From an evolutionary point of view, it is interesting that *Li*VCP in cooperation with its *Li*p47 co-factor may regulate the assembly of the Glc7-Sds22-Ypi1 complex like it is the case in yeast.

LiUFD1-LiNPL4L heterodimer

Our studies depicted important differences for the hierarchical p97-UFD1-NPL4 complex. The heterodimer UFD1-NPL4 (UN) is one of the most studied VCP co-factor linked to the (ER)-associated protein degradation (ERAD) (95,113,118) and ribosome quality control (RQC) (70). VCP recruits substrates through binding of the UFD1-NPL4 cofactor to the ubiquitin moieties and then threads the substrate through its central channel to mobilize and unfold them for subsequent degradation by the proteasome (103,163). In general, NPL4L proteins from all eukaryotes are composed by a UBX-like domain, a zinc-finger domain, an enzymatically inactive Mpr1–Pad1 N-terminal (MPN) domain and a C-terminal domain (CTD) (116). Recent structural studies on the Cdc48-Ufd1-Npl4 complex in yeast

demonstrated that NPL4 interacts through its UBX-like domain with one of the N domains of Cdc48 hexamer, and uses its two Zn^{2+}-finger domains to anchor its MPN domain to the top of the D1 ATPase ring (116). On the other hand, UFD1 interacts through a short and poorly conserved segment of its UT6 domain with NPL4, and through the two conserved flanking SHP motifs with other N domains of Cdc48 (116).

Our studies showed that similarly to its yeast counterpart, *Li*UFD1 interacts with the N-terminus of *Li*VCP through its conserved SHP motif and also harbors a UT6 domain that may be used for binding to NPL4. *Li*NPL4, however, lacks an UBX-like domain and the Zn^{2+}-finger domains for binding to VCP. Multiple sequence alignment along with different eukaryotic homologs followed by phylogenetic trees allowed us to appreciate that the *L. infantum Li*NPL4-like(L) protein is evolutionary far from other eukaryotes but contains conserved regions that potentially act as specific domains for *Li*VCP interaction. Our 3D modeling and docking experiments predict binding to *Li*VCP through the C-terminus GMPP motif of *Li*NPL4. This represents a unique feature for NPL4 binding to VCP. Indeed, the GMPP motif in NPL4 homologs was found in the genus *Leishmania*, *Leptomonas* and *Phytomonas* and a variant of this motif, GM-[EDS]-PP, is present in *Trypanosoma*. This major difference of NPL4 binding to VCP paves the way for the design of a specific inhibitor of NPL4-VCP interactions in Trypanosomatidae. Despite the NPL4 binding differences, some characteristics still remain. UFD1/NPL4 and p47 are substrate-recruiting cofactors shown to bind to VCP in a mutually exclusive manner as they compete for the same binding modules (100,101). This seems also to be the case in the *Li*VCP interaction network as *Li*p47 was neither found in the *Li*UFD1 proteome nor *Li*UFD1 in the *Li*p47 proteome.

LiFAF2

The *Leishmania* FAF2 homolog lacks the ubiquitin-associated (UBA) domain as opposed to its eukaryotic counterparts and interacts with *Li*VCP through the GFPP motif present in the UBX domain as suggested by 3D modeling and docking predictions. The UBA domain that is present in the human FAF1 and FAF2 proteins is fundamental for interacting with ubiquitinated substrates (164). In the absence of the UBA domain, *Li*FAF2 should in princible be unable to bind ubiquitinated substrates. Whether or how the *Leishmania* FAF2-VCP complex binds to ubiquitinated substrates remains to be determined. Interestingly, our data indicate association of *Li*FAF2 with the peroxisomal biogenesis factors PEX2, PEX10 and PEX11. Recent data in trypanosomatids support *de novo* biogenesis of peroxisomes

(glycosomes) from the endoplasmic reticulum (165). In higher eukaryotes PEX2, PEX10 and PEX12 are required for degrading ubiquitinated peroxisomes, a pathway that involves an AAA ATPase complex with a striking similarity to p97 (166). In *Leishmania,* VCP possibly through its FAF2 cofactor, may contribute to the control of glycosome homeostasis and turnover.

*Li**PUB1*

VCP co-factors harboring a PUB (PNGase/UBA or UBX-containing proteins) or a PUL (PLAP, Ufd3p, and Lub1p) domain form a hydrophobic pocket for interactions with the C-terminal tail of VCP (117) following association of key amino acids such as Leu^{804} and the aromatic side chain of the penultimate $tyrosine^{805}$ residue (98,100,101). The *Leishmania* *Li*PUB1 protein has no human homolog but yet interacts with the C-terminal region of *Li*VCP similarly to what was described for the human p97/VCP-PUB complex. Our *in silico* analysis indicate that *Li*PUB1 contains a conserved region that interacts with the last five amino acids ^{780}DDLYS^{784} of the *Li*VCP C-terminus tail, similarly to other PUB domain proteins (167). Our analysis led us to identify the first PUB domain proteins in *Leishmania* and to unveil *Li*PUB1 as one of the major *Li*VCP cofactors. In addition, two other PUB domain proteins were identified in our study. *Li*PUB2 was found associated with *Li*VCP in immunoprecipitation studies and it may be a putative *Li*VCP co-factor. A third UBX and PUB domain-containing protein (*Li*PUB3) was retrieved by searching the *L. infantum* genome database. Furthermore, we found that a serine palmitoyltransferase-like protein was associated solely with the *Li*PUB1 proteome. Interestingly, a homolog of this protein in yeast is required for resistance to heat shock and plays an essential role in the removal or refolding of denatured or aggregated cytoplasmic proteins (168). We have recently reported a temperature sensitive VCP mutant in *Leishmania* (156). Thus, we hypothesize that PUB proteins together with the serine palmitoyltransferase and its biosynthesis pathway may play an important role in the resistance of *Leishmania* to heat stress inside the macrophages.

Essentiality of *Li*UFD1, *Li*p47, *Li*FAF2, *Li*NPL4L and *Li*PUB1 *Li*VCP co-factors

To assess the cellular function of the key *Li*UVCP cofactors, *Li*UFD1, *Li*p47, *Li*FAF2, *Li*NPL4L and *Li*PUB1, we applied a targeted gene replacement strategy based on homologous recombination using the CRISPR-Cas9 system for depleting the genes coding for these co-factors. In the case of the *L. infantum* *Li*UFD1 gene, two independent drug resistant selection cassettes harboring either the *PURO* or *NEO* drug resistance genes

flanked by the *Li*UFD1 5'- and or 3'-UTR regions were constructed by a single PCR amplification for a sequential target and inactivation of the *LiUFD1* locus (Appendix 2). After transfecting the PCR amplified 5'YPURO3' targeting cassette into *L. infantum* expressing a Cas9 plasmid together with a single gRNA (Appendix 2, panel A), we have replaced successfully one of the two *Li*UFD1 alleles, generating a heterozygous *Li*UFD1$^{(PURO/+)}$ mutant. However, two attempts to generate a homozygous knockout mutant by introducing the 5'YNEO3' targeting cassette into *Li*UFD1$^{(PURO/+)}$ failed. Instead, we have obtained mutants harboring the *PURO* (2.8 kb) and *NEO* (3.0 kb) gene replacement cassettes but also an additional wild type *Li*UFD1 copy, as shown by PCR analysis (Appendix 2, panel B, lanes 4 and 5). Genetic inactivation of *LiUFD1* was only possible by first ectopically expressing into *LiUFD1*$^{(PURO/+)}$ an HA epitope-tagged *Li*UFD1^{HA} and then simultaneously transfecting its gRNA. This led to the generation of a facilitated *Li*UFD1 homozygous knockout (dKO) mutant (Appendix 2, panel B, right panel, lines 2 and 4). Only the presence of UFD1 and the second targeting cassette, but without the addition of the designed UFD1 gRNA was not sufficient for the generation of the dKO mutant. Altogether, these results demonstrate that *UFD1* is an essential gene in *L. infantum.*

A similar approach using CRISPR-Cas9 was applied for the inactivation of the *Li*p47, *Li*FAF2, *Li*NPL4L and *Li*Pub1 genes. The two alleles of each gene in the wild type (WT) strain (*Li*VCP$^{(+/+)}$) were submitted to subsequent replacement by the *PURO* and *NEO* targeting cassettes to generate the (PURO/+) and (PURO/NEO) mutants. No growth was observed following transfection and selection for the *Li*p47 inactivation mutants, and these experiments were not pursued any further. For the other genes, double insertion could be observed by PCR analysis of total genomic DNA using specific primers (external primers for the gene and internal primers for NEO, PURO and each co-factor ORF) (Appendix 3). Despite double insertion of the genetic markers PURO and NEO, the ORF amplification for *Li*NPL4 and *Li*Pub1 (as well inconclusive fragments for the *Li*FAF2) was also detected. The generation of a third genomic allele upon targeting of the two genomic alleles, possibly through gene amplification leading to intrachromosomal tandem duplication (169), suggest that the genes coding for *Li*NPL4, *Li*Pub1 and *Li*FAF2 are essential for *Leishmania* survival (Appendix 3). As the binding of some VCP co-factors decreases the potency of some drugs targeting VCP and increases the potency of other compounds (170), it would be interesting to evaluate the effect of VCP-related drugs (targeting VCP, or a VCP complex or a VCP co-factor) on the wild type vs. these co-factor deficient strains. These results would shed light

into the physiological role(s) of VCP and its co- factors in trypanosomatids and would pave the way for the discovery of new anti-parasitic drugs targeting the VCP protein quality control system.

Other new *Li*VCP co-factors

Using the "Identify Genes based on Text (product name, notes, etc.)" tool on the TriTrypDB database (April 2016 TriTrypDB 9.0 released), we have also identified two other putative VCP co-factors in the *L. infantum* database based on the presence of the UBX or the PUB domain known to specifically bind VCP. These are the UBX domain-containing protein LinJ.29.0350/LINF_290008400 and the PUB domain-containing protein LinJ.36.0140/LINF_360006300. To investigate further their role as putative *Li*VCP co-factors, we performed co-immunoprecipitation studies using C- and N- terminally HA-tagged versions for both proteins followed by *Li*VCP detection by Western blot using a specific anti-TbVCP antibody (93,156) and mass spectrometry analysis. The LinJ.29.0350/LINF_290008400 protein was not detected by western blotting and the studies were interrupted. On the other side, preliminary results with the new PUB domain protein – here called *Li*PUB3 (LinJ.36.0140) seem quite promising (Appendix 4).

The putative link with Mitochondria Associated Degradation – *Li*PLAA/Doa1/Lub1 protein.

Although most of co-factors bind to the VCP N-terminus, some interact to the C-terminus of the protein. These proteins are known to contain a PUB domain or a PUL domain of PLAA (phospholipase A2- activating protein or PLAP - the ortholog of yeast Doa1/Ufd3) proteins (112).

The *Li*PUB3 gene (LinJ.36.0140) was expressed in pSPαZEOα vector, cloned and transfected into *L. infantum* promastigotes. Its expression was verified by western blot (data not shown) and its interaction with VCP was assessed by immunoprecipitation studies (Appendix 4). Although the *Li*PUB3 interaction with VCP by western blot analysis was not clear, the mass spectrometry data for *Li*PUB3 revealed VCP association (although only two peptides). But more interesting, a new putative protein from the PLAA family ubiquitin binding (LinJ.24.1970) was identified within the *Li*Pub3 proteome (Appendix 4). The identified *Li*PLAA/Doa1/Lub1 (LinJ.24.1970/ LINF_240025100) protein contains a WD domain and a PLAA family ubiquitin binding domain. It was detected with 28 Exclusive

Unique Peptide Count exclusively in *Li*Pub3 (LinJ.36.0140) proteome. This is the first interacting partner from the PLAA family identified here. None of our dozen immunoprecipitation experiments has identified this protein before. Interestingly, this protein is a homologous of the Doa1 protein which was recently revealed as a critical mediator of the mitochondria-associated degradation pathway (MAD) (86). The *Leishmania* protein contains similar structure as the yeast protein that includes a PUL (PLAA) VCP binding site and two ubiquitin binding sites (WD40 and PFU). It was also shown that Doa1 is critical to the mitochondrial proteostasis as it mediates the recruitment of the ubiquitinated substrates and facilitates substrate interaction with the Cdc48-Ufd1-Npl4 complex in the outer mitochondrial membrane (OMM) (86).

Effect of VCP-targeting drugs on *Leishmania infantum* growth.

Since the first demonstration of a drug targeting the human VCP (136), multiple compounds have emerged as potential VCP inhibitors. These include DBeQ, NMS, ML240/ML241, Eerl, and more recently the dissulfiran, to name some of them. Here we accessed the effect of DBeQ, NMS-874 and ML240 on *Leishmania* promastigote and amastigote rowth. All three drugs were demonstrated to be effective against promastigote forms of *L. infantum* wild type (WT). DBeQ appears to be the most effective with IC50 < 0.5 μM, followed by ML240 with IC50 < 1.0 μM and NMS873 with IC50 < 2.0 μM (Appendix 10). So far, only DBeQ was tested in amastigote forms (Appendix 10). Axenic amastigotes seem to be less sensitive to DBeQ (Appendix 10). We showed that *Li*VCP expression is at least 3-fold higher in amastigotes than in promastigotes (156) and it is therefore possible that more drug is needed to impair the VCP activity to the point of cellular death. Yet, it remains to be disclosed if DBeQ targets only VCP in *Leishmania* or other proteins as well (e.g., other AAA+ ATPases). Another variable to consider is the association of *Li*VCP with its different adaptors/co-factors. The presence of some co-factors can interfere with drug binding and consequently the effect of the drug (142,171). A higher expression of a specific *Li*VCP co-factor in amastigotes may also explain the lower efficacy of DBeQ in amastigotes. Overexpressing different key *Li*VCP co-factors into WT promastigotes and assessing the susceptibility of known VCP-targeting drugs would be an interesting experiment to do. Moreover, it would be essential to unveil if macrophages are equally sensitive to those drugs (toxicity) and, as a consequence, to evaluate in animal models if some of these VCP-targeting drugs could be prospected as new drugs for *Leishmania* treatment. Another

interesting perspective is based on the alcohol-abuse drug disulfiram. This drug was recently considered as a repurposing drug to target cancer cells via the VCP segregase adaptor NPL4 (146). Due to our findings regarding some unique aspects of the VCP-NPL4 complex in *Leishmania* (Chapter 3), the use of disulfiram as an anti-parasitic drug should be considered in future studies.

Conclusion

Altogether, our studies led to the molecular and cellular characterization of the conserved Valosin-containing protein (VCP) AAA+ ATPase in *Leishmania,* which is associated with many ubiquitin-dependent cellular pathways that are central to protein quality control in all eukaryotic systems studied to date. We provided experimental evidence of the essential role of *Li*VCP in the intracellular development of the parasite and its capacity to respond to heat and also proteotoxic stress. We also characterized the *Li*VCP interaction network, the first in parasitic protozoa, through the identification of known co-factors and novel interacting partners potentially associated with distinct VCP quality control pathways. Our proteomics datasets identified biologically relevant functions for the *Leishmania* VCP adaptors/cofactors and provide a rich resource for further evaluation of VCP function in several cellular processes related to protein quality control in these parasites.

References

1. Lukeš J, Lys Guilbride D, Votýpka J, Zíková A, Benne R, Englund PT. Kinetoplast DNA Network: Evolution of an Improbable Structure. Eukaryot Cell. 2002 Aug;1(4):495–502.
2. Aphasizheva I, Aphasizhev R. U-Insertion/Deletion mRNA-Editing Holoenzyme: Definition in Sight. Trends Parasitol. 2016 Feb;32(2):144–56.
3. Simpson L, Thiemann OH, Savill NJ, Alfonzo JD, Maslov DA. Evolution of RNA editing in trypanosome mitochondria. Proc Natl Acad Sci U S A. 2000 Jun;97(13):6986–93.
4. Jackson AP, Otto TD, Aslett M, Armstrong SD, Bringaud F, Schlacht A, et al. Kinetoplastid Phylogenomics Reveals the Evolutionary Innovations Associated with the Origins of Parasitism. Curr Biol. 2016;26(2):161–72.
5. Lukeš J, Butenko A, Hashimi H, Maslov DA, Votýpka J, Yurchenko V. Trypanosomatids Are Much More than Just Trypanosomes: Clues from the Expanded Family Tree. Trends Parasitol. 2018;34(6):466–80.
6. Jaskowska E, Butler C, Preston G, Kelly S. Phytomonas: Trypanosomatids Adapted to Plant Environments. PLoS Pathog. 2015;11(1):1–17.
7. Campos M, Penha H, Noyma M, Santos RL, Luiza A, Vieira S. Veterinary Parasitology Naturally acquired visceral leishmaniasis in non-human primates in Brazil. Vet Parasitol. 2010;169(1–2):193–7.
8. Ribeiro RR, Suzan M, Michalick M, Da Silva ME, Peixoto CC, Santos D, et al. Canine Leishmaniasis: An Overview of the Current Status and Strategies for Control. Biomed Res Int. 2018;2018(CI).
9. Mendonça IL, Batista JF, Ribeiro IMM, Rocha FSB, Silva SO, Melo MN. Leishmania infantum in domestic cats from the municipality of Teresina, state of Piauí, Brazil. Parasitol Open. 2017;3:e1.
10. Pereira AAS, De Castro Ferreira E, Da Rocha Lima ACVM, Tonelli GB, Rêgo FD, Paglia AP, et al. Detection of Leishmania spp in silvatic mammals and isolation of Leishmania (Viannia) braziliensis from Rattus rattus in an endemic area for leishmaniasis in Minas Gerais State, Brazil. PLoS One. 2017;12(11):1–9.
11. Insinga RP, Dasbach EJ, Elbasha EH, Liaw K-L, Barr E. Leishmaniasis in high-burden countries: an epidemiological update based on data reported in 2014. Relev Epidemiol Hebd. 2016 Jun;91(22):287–96.
12. Alvar J, Vélez ID, Bern C, Herrero M, Desjeux P, Cano J, et al. Leishmaniasis worldwide and global estimates of its incidence. PLoS One. 2012 Jan;7(5):e35671.
13. Karimkhani C, Wanga V, Coffeng LE, Naghavi P, Dellavalle RP, Naghavi M. Global burden of cutaneous leishmaniasis: A cross-sectional analysis from the Global Burden of Disease Study 2013. Lancet Infect Dis. 2016;16(5):584–91.
14. França A de O, Pompilio MA, Pontes ERJC, de Oliveira MP, Pereira LOR, Lima RB, et al. Leishmania infection in blood donors: A new challenge in leishmaniasis transmission? PLoS One. 2018;13(6):e0198199.
15. Cohnenares M, Kar S, Goldsmith-pestana K, Mcmahon-pratt D. Mechanisms genetics of pathogenesis : differences amongst feishmania species. Trans R Soc Trop Med Hyg. 2002;96.

16. Costa DL, Rocha RL, de Brito Ferreira Chaves E, de Vasconcelos Batista VG, Costa HL, Nery Costa CH. Predicting death from kala-azar: Construction, development, and validation of a score set and accompanying software. Rev Soc Bras Med Trop. 2016;49(6):728–40.

17. Burza S, Croft SLL, Boelaert M, Lugo ARR, Burza S, Croft SLL, et al. Leishmaniasis. Lancet. 2018 Sep;392(10151):951–70.

18. Mock DJ, Hollenbaugh JA, Daddacha W, Overstreet MG, Lazarski CA, Fowell DJ, et al. Leishmania Induces Survival , Proliferation and Elevated Cellular dNTP Levels in Human Monocytes Promoting Acceleration of HIV Co-Infection. 2012;8(4).

19. Akhoundi M, Downing T, Votýpka J, Kuhls K, Lukeš J, Cannet A, et al. Leishmania infections: Molecular targets and diagnosis. Mol Aspects Med. 2017;57:1–29.

20. Werneck GL, Batista MSA, Gomes JRB, Costa DL, Costa CHN. Prognostic Factors for Death from Visceral Leishmaniasis in Teresina , Brazil. Ann Intern Med. 2003;(3):174–7.

21. Koltas IS, Eroglu F, Uzun S, Alabaz D. A comparative analysis of different molecular targets using PCR for diagnosis of old world leishmaniasis. Exp Parasitol. 2016;164:43–8.

22. Moreira OC, Yadon ZE, Cupolillo E. The applicability of real-time PCR in the diagnostic of cutaneous leishmaniasis and parasite quantification for clinical management: Current status and perspectives. Acta Trop. 2018;184(April):29–37.

23. Carnielli JBT, Crouch K, Forrester S, Silva VC, Carvalho SFG, Damasceno JD, et al. A Leishmania infantum genetic marker associated with miltefosine treatment failure for visceral leishmaniasis. EBioMedicine. 2018;

24. de Morais RCS, da Costa Oliveira CN, de Albuquerque S da CG, Mendonça Trajano Silva LA, Pessoa-e-Silva R, Alves da Cruz HL, et al. Real-time PCR for Leishmania species identification: Evaluation and comparison with classical techniques. Exp Parasitol. 2016 Jun;165:43–50.

25. Romero GAS, Costa DL, Costa CHN, de Almeida RP, de Melo EV, de Carvalho SFG, et al. Efficacy and safety of available treatments for visceral leishmaniasis in Brazil: A multicenter, randomized, open label trial. Reithinger R, editor. PLoS Negl Trop Dis. 2017 Jun 29;11(6):e0005706.

26. Ponte-Sucre A, Gamarro F, Dujardin J-C, Barrett MP, López-Vélez R, García-Hernández R, et al. Drug resistance and treatment failure in leishmaniasis: A 21st century challenge. PLoS Negl Trop Dis. 2017;11(12):e0006052.

27. Ouellette M, Drummelsmith J, Papadopoulou B. Leishmaniasis: Drugs in the clinic, resistance and new developments. Drug Resist Updat. 2004;7(4–5):257–66.

28. Khamesipour A, Dowlati Y, Asilian A, Hashemi-Fesharki R, Javadi A, Noazin S, et al. Leishmanization: Use of an old method for evaluation of candidate vaccines against leishmaniasis. Vaccine. 2005;23(28):3642–8.

29. McCall LI, Zhang WW, Ranasinghe S, Matlashewski G. Leishmanization revisited: Immunization with a naturally attenuated cutaneous Leishmania donovani isolate from Sri Lanka protects against visceral leishmaniasis. Vaccine. 2013;31(10):1420–5.

30. Noazin S, Khamesipour A, Moulton LH, Tanner M, Nasseri K, Modabber F, et al.

Efficacy of killed whole-parasite vaccines in the prevention of leishmaniasis-A meta-analysis. Vaccine. 2009;27(35):4747–53.

31. De Luca PM, Mayrink W, Alves CR, Coutinho SG, Oliveira MP, Bertho AL, et al. Evaluation of the stability and immunogenicity of autoclaved and nonautoclaved preparations of a vaccine against American tegumentary leishmaniasis. Vaccine. 1999;17(9–10):1179–85.

32. Srivastava S, Shankar P, Mishra J, Singh S. Possibilities and challenges for developing a successful vaccine for leishmaniasis. Parasites and Vectors. 2016;9(1):1–15.

33. Papadopoulou B, Roy G, Breton M, Kündig C, Dumas C, Fillion I, et al. Reduced infectivity of a Leishmania donovani biopterin transporter genetic mutant and its use as an attenuated strain for vaccination. Infect Immun. 2002;70(1):62–8.

34. Avishek K, Kaushal H, Gannavaram S, Dey R, Selvapandiyan A, Ramesh V, et al. Gene deleted live attenuated Leishmania vaccine candidates against visceral leishmaniasis elicit pro-inflammatory cytokines response in human PBMCs. Sci Rep. 2016;6(August):4–13.

35. Chakravarty J, Kumar S, Trivedi S, Rai VK, Singh A, Ashman JA, et al. A clinical trial to evaluate the safety and immunogenicity of the LEISH-F1+MPL-SE vaccine for use in the prevention of visceral leishmaniasis. Vaccine. 2011;29(19):3531–7.

36. Gillespie PM, Beaumier CM, Strych U, Hayward T, Hotez PJ, Bottazzi ME. Status of vaccine research and development of vaccines for leishmaniasis. Vaccine. 2016 Jun;34(26):2992–5.

37. Gradoni L. Canine Leishmania vaccines: Still a long way to go. Vet Parasitol. 2015;208(1–2):94–100.

38. Khan KH. DNA vaccines: Roles against diseases. Germs. 2013;3(1):26–35.

39. Reithinger R, Dujardin J-C, Louzir H, Pirmez C, Alexander B, Brooker S. Cutaneous leishmaniasis. Jaffe C, editor. Lancet Infect Dis. 2007 Sep 28;7(9):581–96.

40. Lehane MJ. PERITROPHIC MATRIX STRUCTURE AND FUNCTION. Annu Rev Entomol. 1997 Jan;42(1):525–50.

41. Lawyer P, Turco SJ, Secundino N, Sacks D, Capul AA, Peters NC, et al. Proteophosphoglycan confers resistance of Leishmania major to midgut digestive enzymes induced by blood feeding in vector sand flies. Cell Microbiol. 2010;12(7):906–18.

42. Rogers ME. The role of Leishmania proteophosphoglycans in sand fly transmission and infection of the mammalian host. Front Microbiol. 2012;3(JUN):1–13.

43. Atayde VD, Aslan H, Townsend S, Hassani K, Kamhawi S, Olivier M. Exosome Secretion by the Parasitic Protozoan Leishmania within the Sand Fly Midgut. Cell Rep. 2015;13(5):957–67.

44. Atayde VD, Hassani K, da Silva Lira Filho A, Borges AR, Adhikari A, Martel C, et al. Leishmania exosomes and other virulence factors: Impact on innate immune response and macrophage functions. Cell Immunol. 2016;309:7–18.

45. Olivier M, Fernandez-Prada C. Leishmania and its exosomal pathway: A novel direction for vaccine development. Future Microbiol. 2019;14(7):559–61.

46. Pruzinova K, Sadlova J, Seblova V, Homola M, Votypka J, Volf P. Comparison of bloodmeal digestion and the peritrophic matrix in four sand fly species differing in susceptibility to leishmania donovani. PLoS One. 2015;10(6):1–15.

47. Mendonça SCF. Differences in immune responses against Leishmania induced by infection and by immunization with killed parasite antigen: Implications for vaccine discovery. Parasites and Vectors. 2016;9(1):1–9.

48. Nagill R, Kaur S. Vaccine candidates for leishmaniasis: A review. Int Immunopharmacol. 2011;11(10):1464–88.

49. John B, Hunter CA. IMMUNOLOGY: Neutrophil Soldiers or Trojan Horses? Science (80-). 2008 Aug 15;321(5891):917–8.

50. Laskay T, van Zandbergen G, Solbach W. Neutrophil granulocytes – Trojan horses for Leishmania major and other intracellular microbes? Trends Microbiol. 2003 May;11(5):210–4.

51. Ribeiro-Gomes FL, Romano A, Lee S, Roffê E, Peters NC, Debrabant A, et al. Apoptotic cell clearance of Leishmania major-infected neutrophils by dendritic cells inhibits CD8+ T-cell priming in vitro by Mer tyrosine kinase-dependent signaling. Cell Death Dis. 2015;6(12):1–12.

52. Chagas AC, Oliveira F, Debrabant A, Valenzuela JG, Calvo E. Lundep , a Sand Fly Salivary Endonuclease Increases Leishmania Parasite Survival in Neutrophils and Inhibits XIIa Contact Activation in Human Plasma. 2014;10(2).

53. Gabriel C, Mcmaster WR, Girard D, Descoteaux A. Leishmania donovani Promastigotes Evade the Antimicrobial Activity of Neutrophil Extracellular Traps. 2019;

54. Abhishek K, Sardar AH, Das S, Kumar A, Ghosh AK, Singh R, et al. Phosphorylation of Translation Initiation Factor 2-Alpha in Leishmania donovani under Stress Is Necessary for Parasite Survival. Mol Cell Biol. 2017 Jan 1;37(1):e00344-16.

55. Barthelme D, Sauer RT. Origin and Functional Evolution of the Cdc48/p97/VCP AAA + Protein Unfolding and Remodeling Machine. J Mol Biol. 2016 May;428(9):1861–9.

56. Podinovskaia M, Descoteaux A. Leishmania and the macrophage: A multifaceted interaction. Future Microbiol. 2015;10(1):111–29.

57. Samali A, Pakos-Zebrucka K, Mnich K, Gorman AM, Koryga I, Ljujic M, et al. The integrated stress response. EMBO Rep. 2016;17(10):1374–95.

58. Axten JM. Protein kinase R(PKR)–like endoplasmic reticulum kinase (PERK) inhibitors: a patent review (2010-2015). Expert Opin Ther Pat. 2017;27(1):37–48.

59. Baird TD, Wek RC. Eukaryotic Initiation Factor 2 Phosphorylation and Translational Control in Metabolism. Adv Nutr. 2012 May 1;3(3):307–21.

60. Chow C, Cloutier S, Dumas C, Chou M-N, Papadopoulou B. Promastigote to amastigote differentiation of Leishmania is markedly delayed in the absence of PERK eIF2alpha kinase-dependent eIF2alpha phosphorylation. Cell Microbiol. 2011 Jul;13(7):1059–77.

61. Cloutier S, Laverdière M, Chou M-N, Boilard N, Chow C, Papadopoulou B. Translational Control through eIF2alpha Phosphorylation during the Leishmania

Differentiation Process. Moreno SN, editor. PLoS One. 2012 May 31;7(5):e35085.

62. Ciechanover A, Kwon YT. Protein quality control by molecular chaperones in neurodegeneration. Front Neurosci. 2017;11(APR):1–18.

63. Pilla E, Schneider K, Bertolotti A. Coping with Protein Quality Control Failure. Annu Rev Cell Dev Biol. 2017 Oct 6;33(1):439–65.

64. Qi L, Tsai B, Arvan P. New Insights into the Physiological Role of Endoplasmic Reticulum-Associated Degradation. Trends Cell Biol. 2017 Jun;27(6):430–40.

65. Lavie J, De Belvalet H, Sonon S, Ion AM, Dumon E, Melser S, et al. Ubiquitin-Dependent Degradation of Mitochondrial Proteins Regulates Energy Metabolism. Cell Rep. 2018;23(10):2852–63.

66. Braun RJ, Westermann B. With the Help of MOM: Mitochondrial Contributions to Cellular Quality Control. Trends Cell Biol. 2017;27(6):441–52.

67. Schmidt M, Finley D. Regulation of proteasome activity in health and disease. Biochim Biophys Acta - Mol Cell Res. 2014;1843(1):13–25.

68. Wolff S, Weissman JS, Dillin A. Differential scales of protein quality control. Cell. 2014;157(1):52–64.

69. Brandman O, Hegde RS. Ribosome-associated protein quality control. Nat Struct Mol Biol. 2016 Jan 6;23(1):7–15.

70. Defenouillère Q, Racine MF, Fromont-Racine M, Racine MF. The ribosome-bound quality control complex: from aberrant peptide clearance to proteostasis maintenance. Curr Genet. 2017;63(6):997–1005.

71. Verma R, Oania RS, Kolawa NJ, Deshaies RJ. Cdc48/p97 promotes degradation of aberrant nascent polypeptides bound to the ribosome. Elife. 2013 Jan 22;2(2):1–17.

72. Hwang J, Qi L. Quality Control in the Endoplasmic Reticulum: Crosstalk between ERAD and UPR pathways. Trends Biochem Sci. 2018 Aug;43(8):593–605.

73. Braakman I, Hebert D. Protein Folding in the Endoplasmic Reticulum. The Endoplasmic Reticulum. 2013;63–79.

74. Van Der Zand A, Gent J, Braakman I, Tabak HF. Biochemically distinct vesicles from the endoplasmic reticulum fuse to form peroxisomes. Cell. 2012;149(2):397–409.

75. Jarosch E, Taxis C, Volkwein C, Bordallo J, Finley D, Wolf DH, et al. Protein dislocation from the ER requires polyubiquitination and the AAA-ATPase Cdc48. Nat Cell Biol. 2002;4(2):134–9.

76. Christianson JC, Ye Y. Cleaning up in the endoplasmic reticulum: ubiquitin in charge. Nat Struct Mol Biol. 2014 Apr 4;21(4):325–35.

77. Olzmann JA, Kopito RR, Christianson JC. The Mammalian Endoplasmic Reticulum-Associated Degradation System. Cold Spring Harb Perspect Biol. 2013 Sep 1;5(9):a013185–a013185.

78. Wu X, Rapoport TA. Mechanistic insights into ER-associated protein degradation. Curr Opin Cell Biol. 2018 Aug;53:22–8.

79. Senft D, Ronai ZAZAZA. UPR, autophagy, and mitochondria crosstalk underlies the ER stress response. Trends Biochem Sci. 2015 Mar;40(3):141–8.

80. Glynn SE. Multifunctional Mitochondrial AAA Proteases. Front Mol Biosci. 2017;4(May).

81. Van Der Bliek AM, Sedensky MM, Morgan PG. Cell biology of the mitochondrion. Genetics. 2017;207(3):843–71.

82. Scheibye-Knudsen M, Fang EF, Croteau DL, Wilson DM, Bohr VA. Protecting the mitochondrial powerhouse. Trends Cell Biol. 2015;25(3):158–70.

83. Heo J-M, Livnat-Levanon N, Taylor EB, Jones KT, Dephoure N, Ring J, et al. A Stress-Responsive System for Mitochondrial Protein Degradation. Mol Cell. 2010 Nov;40(3):465–80.

84. Taylor EB, Rutter J. Mitochondrial quality control by the ubiquitin–proteasome system. Biochem Soc Trans. 2011 Oct 1;39(5):1509–13.

85. Xu S, Peng G, Wang Y, Fang S, Karbowski M. The AAA-ATPase p97 is essential for outer mitochondrial membrane protein turnover. Mol Biol Cell. 2011;22(3):291–300.

86. Wu X, Li L, Jiang H. Doa1 targets ubiquitinated substrates for mitochondria-associated degradation. J Cell Biol. 2016;213(1):49–63.

87. Heo J-MM, Rutter J. Ubiquitin-dependent mitochondrial protein degradation. Int J Biochem Cell Biol. 2011;43(10):1422–6.

88. Jin SM, Youle RJ. The accumulation of misfolded proteins in the mitochondrial matrix is sensed by PINK1 to induce PARK2/Parkin-mediated mitophagy of polarized mitochondria. Autophagy. 2013;9(11):1750–7.

89. Ravanan P, Srikumar IF, Talwar P. Autophagy: The spotlight for cellular stress responses. Life Sci. 2017;188(June):53–67.

90. Collins GA, Goldberg AL. The Logic of the 26S Proteasome. Cell. 2017;169(5):792–806.

91. Finley D, Chen X, Walters KJ. Gates, Channels, and Switches: Elements of the Proteasome Machine. Trends Biochem Sci. 2016;41(1):77–93.

92. Yedidi RS, Wendler P, Enenkel C. AAA-ATPases in Protein Degradation. Front Mol Biosci. 2017 Jun 20;4(June):1–14.

93. Roggy JL, Bangs JD. Molecular cloning and biochemical characterization of a VCP homolog in African trypanosomes. Mol Biochem Parasitol. 1999 Jan 5;98(1):1–15.

94. Lamb JR, Fu V, Wirtz E, Bangs JD. Functional Analysis of the Trypanosomal AAA Protein Tb VCP with trans -Dominant ATP Hydrolysis Mutants. J Biol Chem. 2001 Jun 15;276(24):21512–20.

95. Stach L, Freemont PS. The AAA+ ATPase p97, a cellular multitool. Biochem J. 2017 Sep 1;474(17):2953–76.

96. Bodnar NO, Rapoport TA. Toward an understanding of the Cdc48/p97 ATPase. F1000Research. 2017 Aug 3;6(0):1318.

97. Bulfer SL, Chou TF, Arkin MR. P97 Disease Mutations Modulate Nucleotide-Induced Conformation to Alter Protein-Protein Interactions. ACS Chem Biol. 2016;11(8):2112–6.

98. Hänzelmann P, Schindelin H. The Interplay of Cofactor Interactions and Post-

translational Modifications in the Regulation of the AAA+ ATPase p97. Front Mol Biosci. 2017 Apr 13;4(April):1–22.

99. Xia D, Tang WK, Ye Y. Structure and function of the AAA+ ATPase p97/Cdc48p. Gene. 2016 May;583(1):64–77.

100. Buchberger A, Schindelin H, Hänzelmann P. Control of p97 function by cofactor binding. FEBS Lett. 2015 Sep 14;589(19PartA):2578–89.

101. Hänzelmann P, Schindelin H, H??nzelmann P, Schindelin H, Hänzelmann P, Schindelin H. Characterization of an Additional Binding Surface on the p97 N-Terminal Domain Involved in Bipartite Cofactor Interactions. Structure. 2016 Jan;24(1):140–7.

102. van den Boom J, Meyer H. VCP/p97-Mediated Unfolding as a Principle in Protein Homeostasis and Signaling. Mol Cell. 2018 Jan;69(2):182–94.

103. Bodnar NO, Rapoport TA. Molecular Mechanism of Substrate Processing by the Cdc48 ATPase Complex. Cell. 2017 May;169(4):722-735.e9.

104. Meyer H, Bug M, Bremer S. Emerging functions of the VCP/p97 AAA-ATPase in the ubiquitin system. Nat Cell Biol. 2012 Feb 2;14(2):117–23.

105. Franz A, Ackermann L, Hoppe T. Create and preserve: Proteostasis in development and aging is governed by Cdc48/p97/VCP. Vol. 1843, Biochimica et Biophysica Acta - Molecular Cell Research. 2014. p. 205–15.

106. Wolf DH, Stolz A. The Cdc48 machine in endoplasmic reticulum associated protein degradation. Biochim Biophys Acta - Mol Cell Res. 2012 Jan;1823(1):117–24.

107. Hemion C, Flammer J, Neutzner A. Quality control of oxidatively damaged mitochondrial proteins is mediated by p97 and the proteasome. Free Radic Biol Med. 2014 Oct;75:121–8.

108. Brandman O, Stewart-Ornstein J, Wong D, Larson A, Williams CC, Li G-W, et al. A Ribosome-Bound Quality Control Complex Triggers Degradation of Nascent Peptides and Signals Translation Stress. Cell. 2012 Nov;151(5):1042–54.

109. Franz A, Ackermann L, Hoppe T. Ring of Change: CDC48/p97 Drives Protein Dynamics at Chromatin. Front Genet. 2016 May 3;7(MAY):1–14.

110. Vaz B, Halder S, Ramadan K. Role of p97/VCP (Cdc48) in genome stability. Front Genet. 2013;4(April):60.

111. Buchan JR, Kolaitis R-M, Taylor JP, Parker R. Eukaryotic Stress Granules Are Cleared by Autophagy and Cdc48/VCP Function. Cell. 2013 Jun 20;153(7):1461–74.

112. Papadopoulos C, Kirchner P, Bug M, Grum D, Koerver L, Schulze N, et al. VCP/p97 cooperates with YOD1, UBXD1 and PLAA to drive clearance of ruptured lysosomes by autophagy. EMBO J. 2017 Jan 17;36(2):135–50.

113. Ye Y, Tang WK, Zhang T, Xia D. A Mighty “Protein Extractor” of the Cell: Structure and Function of the p97/CDC48 ATPase. Front Mol Biosci. 2017 Jun 13;4(June):1–20.

114. Weith M, Seiler J, van den Boom J, Kracht M, Hülsmann J, Primorac I, et al. Ubiquitin-Independent Disassembly by a p97 AAA-ATPase Complex Drives PP1 Holoenzyme Formation. Mol Cell. 2018 Nov;72(4):766-777.e6.

115. Rezvani K. UBXD Proteins: A Family of Proteins with Diverse Functions in Cancer. Int J Mol Sci. 2016 Oct 14;17(10):1724.

116. Bodnar NO, Kim KH, Ji Z, Wales TE, Svetlov V, Nudler E, et al. Structure of the Cdc48 ATPase with its ubiquitin-binding cofactor Ufd1–Npl4. Nat Struct Mol Biol. 2018 Jul 2;25(7):616–22.

117. Zhao G, Zhou X, Wang L, Li G, Schindelin H, Lennarz WJ. Studies on peptide:N-glycanase-p97 interaction suggest that p97 phosphorylation modulates endoplasmic reticulum-associated degradation. Proc Natl Acad Sci. 2007 May 22;104(21):8785–90.

118. Stolz A, Hilt W, Buchberger A, Wolf DH. Cdc48: a power machine in protein degradation. Trends Biochem Sci. 2011 Oct;36(10):515–23.

119. Pappin D, Rabouille C, Newman R, Freemont P, Kondo H, Warren G, et al. P47 Is a Cofactor for P97-Mediated Membrane Fusion. Nature. 1997;388(6637):75–8.

120. Beuron F, Dreveny I, Yuan X, Pye VE, Mckeown C, Briggs LC, et al. Conformational changes in the AAA ATPase p97-p47 adaptor complex. EMBO J. 2006;25(9):1967–76.

121. Uchiyama K, Kondo H. p97/p47-mediated biogenesis of Golgi and ER. J Biochem. 2005;137(2):115–9.

122. Shibata Y, Oyama M, Kozuka-Hata H, Han X, Tanaka Y, Gohda J, et al. P47 negatively regulates IKK activation by inducing the lysosomal degradation of polyubiquitinated NEMO. Nat Commun. 2012;3:1013–61.

123. Uchiyama K, Jokitalo E, Lindman M, Jackman M, Kano F, Murata M, et al. The localization and phosphorylation of p47 are important for Golgi disassembly-assembly during the cell cycle. J Cell Biol. 2003;161(6):1067–79.

124. Park ES, Yoo YJ, Elangovan M. The opposite role of two UBA–UBX containing proteins, p47 and SAKS1 in the degradation of a single ERAD substrate, α-TCR. Mol Cell Biochem. 2017;425(1–2):37–45.

125. Ewens CA, Panico S, Kloppsteck P, McKeown C, Ebong I-O, Robinson C, et al. The p97-FAF1 Protein Complex Reveals a Common Mode of p97 Adaptor Binding. J Biol Chem. 2014 Apr 25;289(17):12077–84.

126. Lee J-J, Park JK, Jeong J, Jeon H, Yoon J, Kim EE, et al. Complex of Fas-associated Factor 1 (FAF1) with Valosin-containing Protein (VCP)-Npl4-Ufd1 and Polyubiquitinated Proteins Promotes Endoplasmic Reticulum-associated Degradation (ERAD). J Biol Chem. 2013 Mar 8;288(10):6998–7011.

127. Franz A, Pirson PA, Pilger D, Halder S, Achuthankutty D, Kashkar H, et al. Chromatin-associated degradation is defined by UBXN-3/FAF1 to safeguard DNA replication fork progression. Nat Commun. 2016;7.

128. Sonneville R, Moreno SP, Knebel A, Johnson C, Hastie CJ, Gartner A, et al. CUL-2LRR-1and UBXN-3 drive replisome disassembly during DNA replication termination and mitosis. Nat Cell Biol. 2017;19(5):468–79.

129. Lee JNNN, Kim H, Yao H, Chen Y, Weng K, Ye J, et al. Identification of Ubxd8 protein as a sensor for unsaturated fatty acids and regulator of triglyceride synthesis. Proc Natl Acad Sci U S A. 2010;107(50):21424–9.

130. Joon NL, Zhang X, Feramisco JD, Gong Y, Ye J. Unsaturated fatty acids inhibit

proteasomal degradation of insig-1 at a postubiquitination step. J Biol Chem. 2008;283(48):33772–83.

131. Olzmann JA, Richter CM, Kopito RR. Spatial regulation of UBXD8 and p97/VCP controls ATGL-mediated lipid droplet turnover. Proc Natl Acad Sci. 2013;110(4):1345–50.

132. Li G, Zhao G, Schindelin H, Lennarz WJ. Tyrosine phosphorylation of ATPase p97 regulates its activity during ERAD. Biochem Biophys Res Commun. 2008;375(2):247–51.

133. Zhang X, Gui L, Zhang X, Bulfer SL, Sanghez V, Wong DE, et al. Altered cofactor regulation with disease-associated p97/VCP mutations. Proc Natl Acad Sci. 2015 Apr 7;112(14):E1705–14.

134. Fessart D, Marza E, Taouji S, Delom F, Chevet E. P97/CDC-48: Proteostasis control in tumor cell biology. Cancer Lett. 2013 Aug;337(1):26–34.

135. Meyer H, Weihl CC. The VCP/p97 system at a glance: connecting cellular function to disease pathogenesis. J Cell Sci. 2014 Sep 15;127(18):3877–83.

136. Tang WK, Xia D. Mutations in the Human AAA+ Chaperone p97 and Related Diseases. Front Mol Biosci. 2016 Dec 1;3(December):1–12.

137. Chapman E, Maksim N, De La Cruz F, Clair J, La Clair JJ. Inhibitors of the AAA+ Chaperone p97. Molecules. 2015 Feb 12;20(2):3027–49.

138. Chou T-F, Brown SJ, Minond D, Nordin BE, Li K, Jones AC, et al. Reversible inhibitor of p97, DBeQ, impairs both ubiquitin-dependent and autophagic protein clearance pathways. Proc Natl Acad Sci U S A. 2011;108:4834–9.

139. Harbut MB, Patel BA, Yeung BKS, McNamara CW, Bright AT, Ballard J, et al. Targeting the ERAD pathway via inhibition of signal peptide peptidase for antiparasitic therapeutic design. Proc Natl Acad Sci. 2012 Dec 26;109(52):21486–91.

140. Zhang Y, Li W, Chu M, Chen H, Yu H, Fang C, et al. The AAA ATPase Vps4 Plays Important Roles in Candida albicans Hyphal Formation and is Inhibited by DBeQ. Mycopathologia. 2016;181(5–6):329–39.

141. Xiao Y, Jackson PK, Magnaghi P, D'Alessio R, Cozzi L, Perrera C, et al. Covalent and allosteric inhibitors of the ATPase VCP/p97 induce cancer cell death. Nat Chem Biol. 2013;9(9):548–56.

142. Xue L, Blythe EE, Freiberger EC, Mamrosh JL, Hebert AS, Reitsma JM, et al. Valosin-containing protein (VCP)–Adaptor Interactions are Exceptionally Dynamic and Subject to Differential Modulation by a VCP Inhibitor. Mol Cell Proteomics. 2016;15(9):2970–86.

143. Her N-GG, Toth JII, Ma C-TT, Wei Y, Motamedchaboki K, Sergienko E, et al. p97 Composition Changes Caused by Allosteric Inhibition Are Suppressed by an On-Target Mechanism that Increases the Enzyme's ATPase Activity. Cell Chem Biol. 2016;23(4):517–28.

144. Chou TF, Li K, Frankowski KJ, Schoenen FJ, Deshaies RJ. Structure-Activity Relationship Study Reveals ML240 and ML241 as Potent and Selective Inhibitors of p97 ATPase. ChemMedChem. 2013;8(2):297–312.

145. Anderson DJJ, Le Moigne R, Djakovic S, Kumar B, Rice J, Wong S, et al. Targeting

the AAA ATPase p97 as an Approach to Treat Cancer through Disruption of Protein Homeostasis. Cancer Cell. 2015 Nov;28(5):653–65.

146. Skrott Z, Mistrik M, Andersen KK, Friis S, Majera D, Gursky J, et al. Alcohol-abuse drug disulfiram targets cancer via p97 segregase adaptor NPL4. Nature. 2017;552(7684):194–9.

147. Gugliotta G, Sudo M, Cao Q, Lin DC, Sun H, Takao S, et al. Valosin-Containing Protein/p97 as a Novel Therapeutic Target in Acute Lymphoblastic Leukemia. Neoplasia (United States). 2017;19(10):750–61.

148. Vekaria PH, Home T, Weir S, Schoenen FJ, Rao R. Targeting p97 to Disrupt Protein Homeostasis in Cancer. Front Oncol. 2016 Aug 3;6(August):181.

149. Padmanabhan PK, Zghidi-abouzid O, Samant M, Dumas C, Papadopoulou B, Aguiar BG, et al. DDX3 DEAD-box RNA helicase plays a central role in mitochondrial protein quality control in Leishmania. Nat Publ Gr. 2016;(418).

150. Rouiller I, DeLaBarre B, May AP, Weis WI, Brunger AT, Milligan RA, et al. Conformational changes of the multifunction p97 AAA ATPase during its ATPase cycle. Nat Struct Biol. 2002 Dec 18;9(12):950–7.

151. Beuron F, Dreveny I, Yuan X, Pye VE, Mckeown C, Briggs LC, et al. Conformational changes in the AAA ATPase p97–p47 adaptor complex. EMBO J. 2006 May 3;25(9):1967–76.

152. Pye VE, Dreveny I, Briggs LC, Sands C, Beuron F, Zhang X, et al. Going through the motions: The ATPase cycle of p97. J Struct Biol. 2006 Oct;156(1):12–28.

153. Richly H, Rape M, Braun S, Rumpf S, Hoege C, Jentsch S. A series of ubiquitin binding factors connects CDC48/p97 to substrate multiubiquitylation and proteasomal targeting. Cell. 2005 Jan;120(1):73–84.

154. Marinova IN, Engelbrecht J, Ewald A, Langholm LL, Holmberg C, Kragelund BB, et al. Single Site Suppressors of a Fission Yeast Temperature-Sensitive Mutant in cdc48 Identified by Whole Genome Sequencing. Mata J, editor. PLoS One. 2015 Feb 6;10(2):e0117779.

155. Niwa H, Ewens CA, Tsang C, Yeung HO, Zhang X, Freemont PS. The role of the N-domain in the atpase activity of the mammalian AAA ATPase p97/VCP. J Biol Chem. 2012 Mar 9;287(11):8561–70.

156. Aguiar BG, Padmanabhan PK, Dumas C, Papadopoulou B. Valosin-containing protein VCP/p97 is essential for the intracellular development of Leishmania and its survival under heat stress. Cell Microbiol. 2018 Oct;20(10):e12867.

157. Taylor EBB, Rutter J. Mitochondrial quality control by the ubiquitin–proteasome system: Figure 1. Biochem Soc Trans. 2011 Oct 1;39(5):1509–13.

158. Cassola A, De Gaudenzi JG, Frasch AC. Recruitment of mRNAs to cytoplasmic ribonucleoprotein granules in trypanosomes. Mol Microbiol. 2007;65(3):655–70.

159. Kramer S, Bannerman-Chukualim B, Ellis L, Boulden EA, Kelly S, Field MC, et al. Figure S3 - Differential Localization of the Two T. brucei Poly(A) Binding Proteins to the Nucleus and RNP Granules Suggests Binding to Distinct mRNA Pools. PLoS One. 2013;8(1):2009–2009.

160. Chau V, Tobias JW, Bachmair A, Marriott D, Ecker DJ, Gonda DK, et al. A Multiubiquitin Chain is Confined to Specific Lysine in a Targeted Short-Lived

Protein. Sci New Ser. 1989;243(4898):1576–83.

161. Dreveny I, Kondo H, Uchiyama K, Shaw A, Zhang X, Freemont PS. Structural basis of the interaction between the AAA ATPase p97/VCP and its adaptor protein p47. EMBO J. 2004 Mar 10;23(5):1030–9.

162. Cheng Y-L, Chen R-H. The AAA-ATPase Cdc48 and cofactor Shp1 promote chromosome bi-orientation by balancing Aurora B activity. J Cell Sci. 2010 Jun 15;123(12):2025–34.

163. Blythe EE, Olson KC, Chau V, Deshaies RJ. Ubiquitin- and ATP-dependent unfoldase activity of P97/VCP•NPLOC4•UFD1L is enhanced by a mutation that causes multisystem proteinopathy. Proc Natl Acad Sci. 2017 May 30;114(22):E4380–8.

164. Song EJ, Yim S-H, Kim E, Kim N-S, Lee K-J. Human Fas-Associated Factor 1, Interacting with Ubiquitinated Proteins and Valosin-Containing Protein, Is Involved in the Ubiquitin-Proteasome Pathway. Mol Cell Biol. 2005 Mar 15;25(6):2511–24.

165. Bauer S, Morris MT. Glycosome biogenesis in trypanosomes and the de novo dilemma. Tschudi C, editor. PLoS Negl Trop Dis. 2017 Apr 20;11(4):e0005333.

166. Cho D-H, Kim YS, Jo DS, Choe S-K, Jo E-K. Pexophagy: Molecular Mechanisms and Implications for Health and Diseases. Mol Cells. 2018 Jan 31;41(1):55–64.

167. Zhao G, Li G, Schindelin H, Lennarz WJ. An Armadillo motif in Ufd3 interacts with Cdc48 and is involved in ubiquitin homeostasis and protein degradation. Proc Natl Acad Sci. 2009 Sep 22;106(38):16197–202.

168. Friant S. Increased ubiquitin-dependent degradation can replace the essential requirement for heat shock protein induction. EMBO J. 2003 Aug 1;22(15):3783–91.

169. Laffitte M-CN, Leprohon P, Papadopoulou B, Ouellette M. Plasticity of the Leishmania genome leading to gene copy number variations and drug resistance. F1000Research. 2016 Sep 20;5:2350.

170. Fang C-JJ, Gui L, Zhang X, Moen DR, Li K, Frankowski KJ, et al. Evaluating p97 Inhibitor Analogues for Their Domain Selectivity and Potency against the p97-p47 Complex. ChemMedChem. 2015 Jan;10(1):52–6.

171. Chou T-FF, Bulfer SL, Weihl CC, Li K, Lis LG, Walters MA, et al. Specific Inhibition of p97/VCP ATPase and Kinetic Analysis Demonstrate Interaction between D1 and D2 ATPase Domains. J Mol Biol. 2014 Jul;426(15):2886–99.

Appendices

Appendix 1 - DDX3 DEAD-box RNA helicase plays a central role in mitochondrial protein quality control in *Leishmania*

This appendix includes a scientific paper entitled “DDX3 DEAD-box RNA helicase plays a central role in mitochondrial protein quality control in *Leishmania*” by Padmanabhan, P. K., Zghidi-Abouzid, O., Samant, M., Dumas, C., Aguiar, B. G., Estaquier, J., & Papadopoulou, B. published on October 13, 2016 (*7*(10), e2406. https://doi.org/10.1038/cddis.2016.315) in *Cell Death and Disease* on which I am co-author. I perfomed immunoprecipitation and mass-spectrometry studies that revealed potential interactions of the DEAD-box RNA helicase DDX3 with key components of the cellular stress response, particularly the antioxidant response, the unfolded protein response, and the AAA+ ATPase p97/VCP/Cdc48, which is essential in protein quality control by driving proteosomal degradation of polyubiquitinated proteins. Our findings that DDX3 interacts with the valosin-containing protein p97/VCP/Cdc48 in this article (Table 1) formed the basis for my PhD thesis.

The published version of the full article is included below.

OPEN

Citation: Cell Death and Disease (2016) 7, e2406; doi:10.1038/cddis.2016.315
Official journal of the Cell Death Differentiation Association
www.nature.com/cddis

DDX3 DEAD-box RNA helicase plays a central role in mitochondrial protein quality control in *Leishmania*

Prasad Kottayil Padmanabhan[1,4], Ouafa Zghidi-Abouzid[1,4], Mukesh Samant[2], Carole Dumas[1], Bruno Guedes Aguiar[1], Jerome Estaquier[1,3] and Barbara Papadopoulou*[,1]

DDX3 is a highly conserved member of ATP-dependent DEAD-box RNA helicases with multiple functions in RNA metabolism and cellular signaling. Here, we describe a novel function for DDX3 in regulating the mitochondrial stress response in the parasitic protozoan *Leishmania*. We show that genetic inactivation of DDX3 leads to the accumulation of mitochondrial reactive oxygen species (ROS) associated with a defect in hydrogen peroxide detoxification. Upon stress, ROS production is greatly enhanced, causing mitochondrial membrane potential loss, mitochondrial fragmentation, and cell death. Importantly, this phenotype is exacerbated upon oxidative stress in parasites forced to use the mitochondrial oxidative respiratory machinery. Furthermore, we show that in the absence of DDX3, levels of major components of the unfolded protein response as well as of polyubiquitinated proteins increase in the parasite, particularly in the mitochondrion, as an indicator of mitochondrial protein damage. Consistent with these findings, immunoprecipitation and mass-spectrometry studies revealed potential interactions of DDX3 with key components of the cellular stress response, particularly the antioxidant response, the unfolded protein response, and the AAA-ATPase p97/VCP/Cdc48, which is essential in mitochondrial protein quality control by driving proteosomal degradation of polyubiquitinated proteins. Complementation studies using DDX3 deletion mutants lacking conserved motifs within the helicase core support that binding of DDX3 to ATP is essential for DDX3's function in mitochondrial proteostasis. As a result of the inability of DDX3-depleted *Leishmania* to recover from ROS damage and to survive various stresses in the host macrophage, parasite intracellular development was impaired. Collectively, these observations support a central role for the *Leishmania* DDX3 homolog in preventing ROS-mediated damage and in maintaining mitochondrial protein quality control.
Cell Death and Disease (2016) **7,** e2406; doi:10.1038/cddis.2016.315; published online 13 October 2016

DEAD-box proteins form the largest family of RNA helicases and are conserved from bacteria to humans. They belong to superfamily 2 (SF2) of RNA helicases which harbor an Asp-Glu-Ala-Asp (DEAD) motif that defines the family.[1] DEAD-box RNA helicases are central players in RNA biology and function in essentially all aspects of RNA metabolism. With few exceptions, little is known about how these enzymes physically perform multiple cellular tasks.[1] *Leishmania* and other Trypanosomatidae encode 48-50 DEAD-box RNA helicases[2] as opposed to 25 in yeast and 37 in humans.[1] Similar to other eukaryotes, many biological functions have been attributed to trypanosomatid RNA helicases, including RNA degradation,[3] translation regulation,[4] and RNA editing.[5] We recently characterized a DEAD-box RNA helicase of 67 kDa (HEL67) in *Leishmania* and demonstrated that it prevents ribosomal RNA degradation through an antisense rRNA-mediated pathway and translational arrest triggered by apoptotic stimuli.[6]

Unlike higher eukaryotes, the protozoan *Leishmania* has a single mitochondrion[7] that not only serves as the major site of ATP production through oxidative phosphorylation but also plays important roles in maintaining cell survival, apoptosis, and metabolic homeostasis.[8] Thus, mitochondrion is a central sensor of stress-induced cell death in several *Leishmania* species.[9–12] It has been shown that reactive oxygen species (ROS) represent a host cell defense in inducing the parasite death.[13–15] Excessive levels of mitochondria-derived ROS promote mitochondrial dysfunction, resulting in loss of many cellular functions and in multicellular organisms, the onset of disease.[16] Consequently, there are several quality control systems that monitor mitochondrial protein degradation to maintain mitochondrial homeostasis, including mitophagy, protease-mediated turnover and the ubiquitin–proteasome system (UPS).[17–19] Recently, it has been reported that mitochondrial stress in

[1]Research Center in Infectious Diseases, CHU de Quebec Research Center-University Laval and Department of Microbiology, Infectious Disease and Immunology, Faculty of Medicine, University Laval, Quebec, QC, Canada; [2]Department of Zoology, Kumaun University, Almora, Uttarakhand, India and [3]CNRS FR3636, Université Paris Descartes, Paris, France
*Corresponding author: B Papadopoulou, Department of Microbiology, Infectious Disease and Immunology, University Laval, Research Center in Infectious Diseases, CHU de Quebec Research Center-University Laval, 2705 Laurier Blvd, Quebec, QC, G1V 4G2, Canada. Tel: +1 4185254444 Ext. 47608; Fax: +1 4186542715; E-mail: barbara.papadopoulou@crchul.ulaval.ca
[4]These authors contributed equally to this work.
Abbreviations: ROS, reactive oxygen species; $\Delta\psi_m$, mitochondrial membrane potential; UPS, ubiquitin–proteasome system; UPR, unfolded protein response; HSP, heat-shock protein; VCP, valosin-containing protein; AAA+, ATPases associated with diverse cellular activities; SOD, superoxide dismutase; $DiOC_6$, 3,3′-dihexyloxacarbocyanine iodide; PI, propidium iodide; DHE, dihydroethidium; IP, immunoprecipitation; LC-MS/MS, liquid chromatography-tandem mass spectrometry; WT, wild type
Received 08.6.16; revised 07.9.16; accepted 08.9.16; Edited by C Munoz-Pinedo

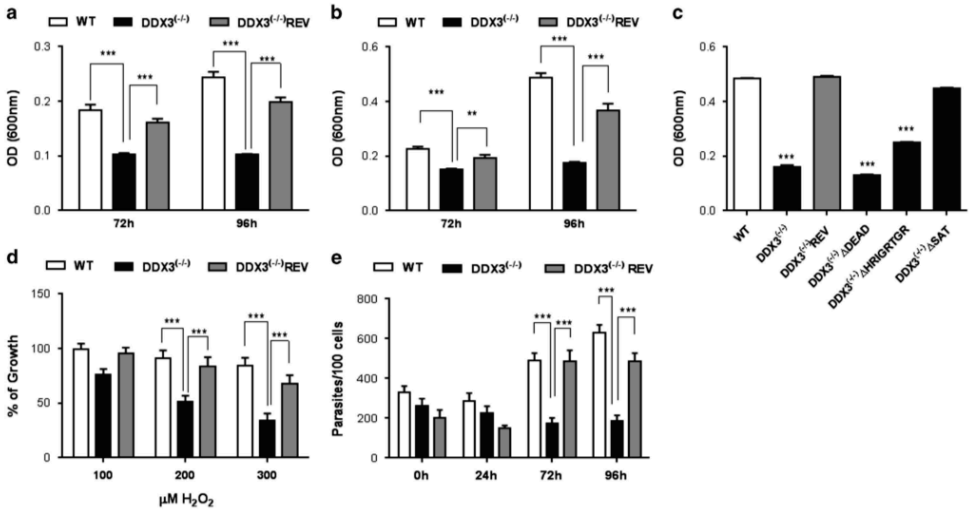

Figure 1 DDX3 is crucial to *Leishmania* intracellular growth and differentiation triggered by stress sensors. *L. infantum* promastigotes wild type (WT), DDX3$^{(-/-)}$ knockout and the add-back mutant DDX3$^{(-/-)}$REV were grown under temperature stress (37 °C) (**a**) or acidic pH (5.5) at 25 °C (**b**) or a combined heat and acidic pH stress triggering differentiation into amastigote forms (**c**). The DDX3$^{(-/-)}$ knockout was complemented with DDX3-HA (DDX3$^{(-/-)}$REV) or DDX3 deletion mutant proteins lacking either the LDEADRM motif (DDX3ΔDEAD) or the HRIGRTGR motif (DDX3ΔHRIGRTGR) participating in ATP binding and hydrolysis and/or the SAT motif (DDX3ΔSAT) involved in RNA binding (Supplementary Figure S1a). The parasite density was measured at 600 nm at 24 h intervals. (**d**) Parasites exposed to increasing concentrations of H_2O_2 (100–300 μM) for up to 72 h. (**e**) Intracellular survival of WT, DDX3$^{(-/-)}$ and DDX3$^{(-/-)}$REV strains was evaluated following infection of mouse-derived bone marrow-derived macrophages. The results shown here are the mean and standard deviation of 3–5 independent experiments performed in triplicates. Statistical significance was assessed by two-tailed paired Student's *t*-test. Asterisks indicate significant differences between WT, DDX3$^{(-/-)}$ and DDX3$^{(-/-)}$REV strains (**$P \leqslant 0.01$, ***$P \leqslant 0.001$)

Caenorhabditis elegans affects UPS.[20] However, the role of UPS is largely unknown in protozoa.

In this study, we have investigated the impact of the DEAD-box RNA helicase HEL67, the DDX3 homolog in *Leishmania,* in regulating cell death under conditions of cellular stress impacting on mitochondrial function. We show that *Leishmania* genetically depleted for DDX3 is highly susceptible to various stress stimuli encountered in the mammalian host and is thus unable to undergo intracellular development. Furthermore, we demonstrate that inactivation of DDX3 increases mitochondrial ROS production concomitantly with the levels of polyubiquitinated proteins, leading to mitochondrial membrane potential collapse, mitochondrial fragmentation and cell death. Consistent to these findings, we report potential interactions of DDX3 with key components of the stress cellular response, in particular p97/VCP/Cdc48, which is essential in clearing oxidatively damaged mitochondrial proteins.[21–23] This is the first demonstration, to our knowledge, of a central role for a DEAD-box RNA helicase of the DDX3 subfamily in mitochondrial proteostasis.

Results

DDX3 is crucial to *Leishmania* intracellular growth and differentiation triggered by stress sensors. Phylogenetic analysis of the alignment of the *Leishmania* RNA helicase HEL67[6] with members of the helicase SF2 superfamily (Supplementary Figure S1a) revealed that HEL67 is part of the Ded1/DDX3 cluster, which is closely related to DDX4, DDX5, and DDX46 and also includes the *Saccharomyces cerevisiae* Ded1 and Dbp1, the *Homo sapiens* DDX3X and DDX3Y, the *C. elegans* VBH-1, the *Drosophila melanogaster* Belle, and the *Xenopus laevis* An3 proteins[24] (Supplementary Figure S1b). HEL67 harbors all 12 signature motifs found in the highly conserved helicase core of Ded1/DDX3 subfamily members that are involved in ATP binding and hydrolysis, RNA binding, and the link of ATPase and helicase activities[1,24,25] (Supplementary Figure S1a) and hereinafter we will refer to as DDX3.

Our prior studies have established an important role for the *Leishmania* DDX3 in protecting parasites from stress-inducing cell death by preventing translational arrest.[6] As an intracellular pathogen, *Leishmania* has to overcome various stresses in order to survive in the phagolysosome of mammalian macrophages. First, we investigated whether DDX3 impacts the parasite response to stress signals triggering promastigote to amastigote differentiation inside macrophages such as higher temperature (37 °C) and low pH (~5.5).[26] *Leishmania infantum* genetically depleted for DDX3 (DDX3$^{(-/-)}$)[6] were sensitive to heat stress (Figure 1a) and acidic pH (Figure 1b) compared with the wild type (WT) and add-back mutant (DDX3$^{(-/-)}$REV). Accordingly, DDX3$^{(-/-)}$ parasites were unable to undergo amastigote differentiation upon exposure

to a combined heat and acidic stress (Figure 1c). Complementation of DDX3$^{(-/-)}$ parasites with DDX3 mutant proteins lacking either the LDEADRM motif (motif II) (DDX3ΔDEAD) or the HRIGRTGR motif (motif VI) (DDX3ΔHRIGRTGR) (Supplementary Figure 1Sa) participating in ATP binding and hydrolysis[24] failed to restore amastigote differentiation (Figure 1c). On the other hand, the SAT motif (motif III; Supplementary Figure 1Sa) facilitating ssRNA binding[24,27] was dispensable (Figure 1c). These data suggest that DDX3's critical role in amastigote differentiation requires the ATPase and not the RNA helicase activity. Because *Leishmania* has also to cope with oxidative burst in macrophages and is susceptible to exogenous ROS,[28] we assessed the effect of hydrogen peroxide (H_2O_2) on *Leishmania* growth and showed that parasites lacking DDX3 were more sensitive to oxidative stress than control strains (Figure 1d). Thus, these results explain the failure of DDX3$^{(-/-)}$ *Leishmania* to replicate within bone marrow-derived murine macrophages (72–96 h post-infection) compared with the controls (Figure 1e).

Overall, these results indicate that growth of DDX3-depleted parasites is drastically impaired in the presence of stress signals encountered in the mammalian host.

Inactivation of DDX3 leads to mitochondrial ROS accumulation associated with a defect in hydrogen peroxide detoxification. The high sensitivity of DDX3$^{(-/-)}$ *Leishmania* to heat and oxidative stresses prompted us to evaluate ROS production. First, we measured general cellular ROS using the 2′,7′-dichlorodihydrofluorescein diacetate (H_2DCFDA) dye that once oxidized, mostly by peroxyl radicals and peroxides, emits fluorescence directly proportional to the amount of ROS. DDX3$^{(-/-)}$ parasites produced 2.3-fold higher levels of oxidative species compared with the controls (Figure 2a). Superoxide production was measured by flow cytometry using the dihydroethidium (DHE) dye. Unstressed DDX3$^{(-/-)}$ parasites demonstrated a slight increase in superoxide levels but upon heat stress (24 h), 80% of DDX3$^{(-/-)}$ accumulated superoxide compared with 3 and 12% for the WT and DDX3$^{(-/-)}$REV, respectively (Figure 2b). Oxidant levels in DDX3$^{(-/-)}$ were similar to H_2O_2-treated WT parasites (Figure 2b, right panel). Mitochondrial superoxide levels measured by flow cytometry using MitoSOX were 2.7-fold higher in DDX3$^{(-/-)}$ than in controls upon heat stress (Figure 2c), indicating an outburst of mitochondrial ROS in the absence of DDX3.

Increased ROS accumulation in DDX3$^{(-/-)}$ may be attributed to a default in their detoxification. *Leishmania* encodes a mitochondrial iron superoxide dismutase (FeSODA) that detoxifies superoxide radicals into oxygen and hydrogen peroxide,[29] which are further reduced by peroxidases.[30] DDX3$^{(-/-)}$ parasites showed a slight but significant increase in SOD activity that was higher in the presence of menadione, a known inducer of intracellular superoxide production (Figure 2d). On the other hand, peroxidase activity was decreased by 4-fold in DDX3$^{(-/-)}$ cells upon induction with 0.6 mM H_2O_2 for 10 min compared with the controls (Figure 2e), indicating that *Leishmania* lacking DDX3 exhibit a defect in hydrogen peroxide detoxification.

Inactivation of DDX3 causes mitochondrial membrane depolarization under stress leading to mitochondrial fragmentation and cell death. In *Leishmania* as well as in higher eukaryotes, increased ROS production results in inner mitochondrial membrane potential ($\Delta\psi_m$) loss, mitochondrial dysfunction, and cell death.[8,31] By flow cytometry, we measured $\Delta\psi_m$ loss using $DiOC_6$ (3,3′-dihexyloxacarbocyanine iodide) and membrane permeability and cell death using propidium iodide (PI) under conditions of mitochondrial insults like prolonged heat-shock or oxidative stress. Even in the absence of stress, 9% of DDX3$^{(-/-)}$ parasites exhibited a $\Delta\psi_m$ loss compared with 0.6 and 1% for WT and DDX3$^{(-/-)}$REV, respectively (Figures 3a and b). Upon heat stress, the percentage of DDX3$^{(-/-)}$ parasites with reduced $\Delta\psi_m$ increased up to 45% in comparison with 20% for WT and 5% for DDX3$^{(-/-)}$REV (Figures 3a and b). Prolonged heat stress (24 h) elicited a significant decrease in the size of DDX3$^{(-/-)}$ cells (Figure 3c). The shrinkage and granularity of DDX3$^{(-/-)}$ parasites further infer that a population is subjected to necrosis or late apoptosis. As a positive control, WT parasites were treated (24 h) with H_2O_2, inducing massive mitochondrial membrane depolarization and cell death (Figures 3a and b).

A short exposure of DDX3$^{(-/-)}$ parasites to H_2O_2 (0.6 mM for 10 min) induced $\Delta\psi_m$ loss (32.4% $DiOC_6^{low}$ parasites) and exacerbated cell death (10.4% $DiOC_6^{low}PI^+$) (Figures 4a and c). To further investigate the impact of DDX3 on mitochondrial function, DDX3$^{(-/-)}$ parasites were grown in glucose-free medium, hence forced to use the mitochondrial oxidative respiratory machinery (OXPHOS). Interestingly, $\Delta\psi_m$ loss was greatly increased in DDX3$^{(-/-)}$ (64.5%) upon H_2O_2 stress resulting in a much higher percentage of dying cells (49% PI^+) (Figures 4b and d) compared with parasites grown in glucose-rich medium (10.4% PI^+) (Figures 4a and c). In DDX3$^{(-/-)}$REV, despite a higher (2-fold) $\Delta\psi_m$ loss as compared with WT, the percentage of dying cells (PI^+) remained similar to that of WT (13.4% *versus* 12.5%) (Figures 4b and d), suggesting that the add-back mutant is able to overcome mitochondrial stress in contrast to DDX3$^{(-/-)}$ parasites (49% PI^+ cells).

Because mitochondrial shaping and morphogenesis can be altered by apoptotic signals,[8] we evaluated the mitochondrial network in DDX3$^{(-/-)}$ and control parasites by fluorescence microscopy using the MitoTracker CMX Red dye. An antibody recognizing the mitochondrial matrix HSP70 protein was also used as a control. In the absence of DDX3, the mitochondrion appeared fragmented 24 h post-exposure to H_2O_2 (0.6 mM for 10 min) (Figure 5b, lower panel). In contrast, the WT (Figure 5a) and DDX3$^{(-/-)}$REV (Figure 5c) strains recovered rapidly from oxidant stress, demonstrating a tubular mitochondrial shaping. These observations indicate that parasites lacking DDX3 display abnormal mitochondrial morphology upon oxidative stress in line with dissipation of the mitochondrial membrane potential and higher percentage of dead cells in stressed DDX3$^{(-/-)}$ parasites (Figure 4).

Taken together, our results support a crucial role of DDX3 in mitochondrial morphogenesis and function, especially under conditions of mitochondrial stress.

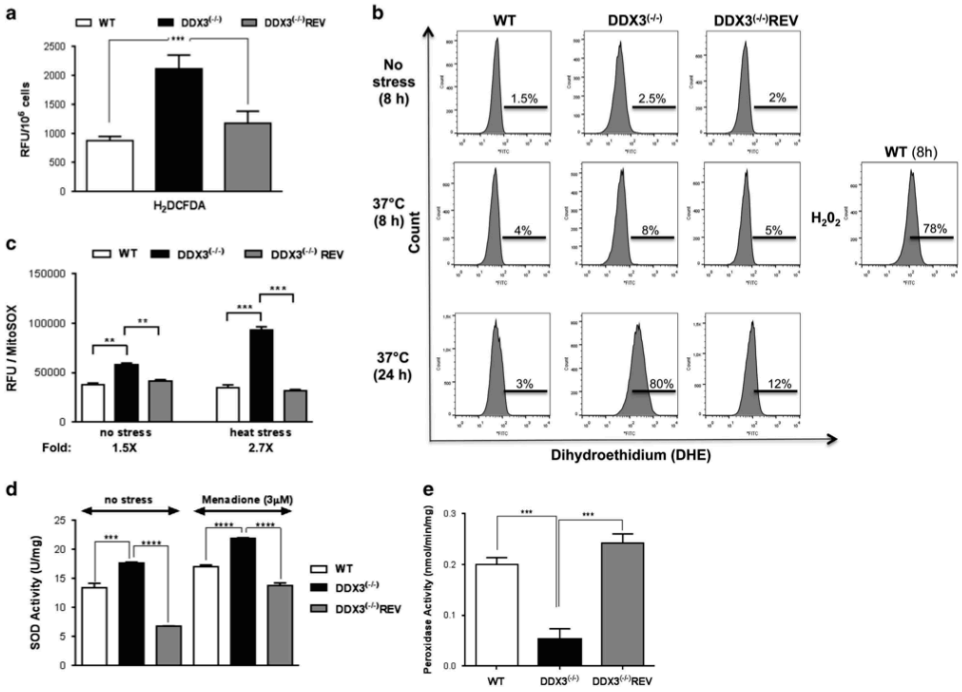

Figure 2 Inactivation of DDX3 leads to an increased production of mitochondrial ROS associated with a defect in hydrogen peroxide detoxification. (**a**) Production of peroxyl radicals and peroxides in WT, DDX3$^{(-/-)}$ and DDX3$^{(-/-)}$REV strains was measured using the 2′,7′-dichlorodihydrofluorescein diacetate (H_2DCFDA) probe. Results shown here are expressed in relative fluorescence units. (**b**) Superoxide production in the above strains cultured at RT (no stress) or at 37 °C for 8 and 24 h. Parasites were stained with the dihydroethidium (DHE) probe and analyzed by flow cytometry. WT parasites exposed to H_2O_2 for 8 h were used as a control. The experiment was repeated three times in duplicate with similar results. (**c**) Mitochondrial superoxide accumulation was measured using the MitoSOX Red probe. Parasites (2–4 ×10^7) were treated with 5 μM MitoSOX for 2 h at 25 °C and analyzed with a Victor fluorometer. The fluorescence was measured at 510 nm excitation and 580 emission wavelengths. Fluorescence was normalized with protein concentration measured using Bio-Rad protein assay. (**d**) SOD activity and (**e**) peroxidase activity were measured as indicated in the Materials and Methods. The results shown here are the mean and standard deviation of three independent experiments performed in triplicates. Statistical analysis was performed using the two-way ANOVA. Asterisks indicate significance, $^{**}P \leqslant 0.01$, $^{***}P \leqslant 0.001$, and **** $P < 0.0001$

Depletion of DDX3 activates key components of the mitochondrial unfolded protein response. Excessive ROS within mitochondria could disturb protein folding and trigger the mitochondrial unfolded protein response (UPR^{mt}) to re-establish protein homeostasis.[18] Mitochondria contain a dedicated repertoire of molecular chaperones in the matrix (e.g., mtHSP60 and mtHSP70) to facilitate protein folding and quality control proteases to degrade unfolded proteins.[18] We examined baseline levels of mitochondrial HSP60 (Figure 6a) and HSP70 (Figure 6b) proteins by western blotting and found that they were 2.6- and 2.7-fold higher in DDX3$^{(-/-)}$ cells, respectively compared with the WT and DDX3$^{(-/-)}$REV. While WT parasites showed a time-dependent HSP60/HSP70 induction upon heat stress, no further increase was observed in DDX3$^{(-/-)}$ cells under the same conditions (Figures 6a and b). A similar induction of mtHSPs was also observed in DDX3$^{(-/-)}$ upon H_2O_2 stress (Supplementary Figure S2). Interestingly, the cytosolic HSP70, one of the most studied chaperones contributing to the cytosolic UPR,[32] was also induced by 2.4/2.6-fold in DDX3$^{(-/-)}$ in the absence of heat stress (Figure 6c). A mutant lacking the DEAD motif failed to restore HSP70 cytosolic and mitochondrial levels in DDX3$^{(-/-)}$ whereas complementation with the DDX3ΔSAT mutant allowed a heat-stress-induced HSP70 response (Figure 6d) comparable to WT (Figure 6b). These results indicate that the UPR is activated in DDX3$^{(-/-)}$ parasites, most likely in response to the increased load of mitochondrial ROS.

DDX3 associates with major components of the cellular stress response and the mitochondrial protein quality control. To further dissect the role of DDX3 in mitochondrial function, we looked for potential DDX3-interacting proteins by immunoprecipitation (IP) studies followed by liquid chromatography-tandem mass spectrometry (LC-MS/MS). To assess reproducibility, IP experiments were repeated at

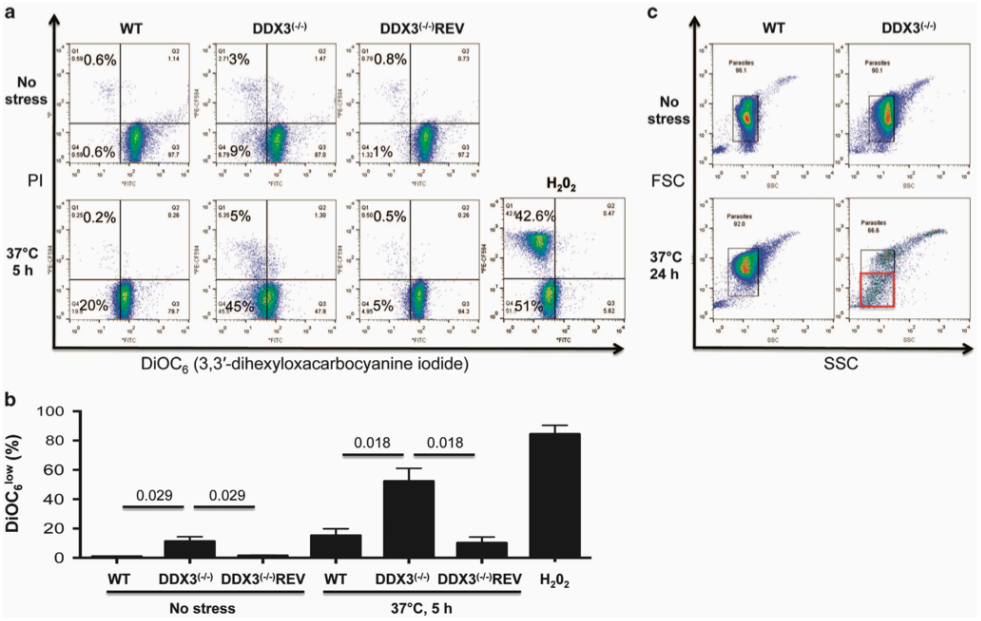

Figure 3 Heat stress induces mitochondrial membrane potential loss in *Leishmania* lacking DDX3. (**a**) 10^6 parasites from WT, DDX3$^{(-/-)}$, and DDX3$^{(-/-)}$REV strains grown in RPMI medium were exposed or not to heat stress, double-stained with $DiOC_6(3)$ and propidium iodide (PI), and analyzed by flow cytometry to measure $\Delta\psi_m$ loss and membrane permeability and cell death, respectively. H_2O_2 treatment was used as a control inducing mitochondrial depolarization and death in ~50% of WT parasites after 8 h. (**b**) The results are means+S.E.M. of three independent experiments with duplicates and statistical significance was assessed using paired Student's *t*-test Prism version 6.0 (GraphPad Software, San Diego, CA, USA). The numbers over the lines correspond to *P*-values. (**c**) Cell morphology was assessed by flow cytometry on FSC and SSC parameters. WT and DDX3$^{(-/-)}$ parasites were cultured either at room temperature or at 37 °C for 24 h. After O/N exposure to heat stress, most of the DDX3$^{(-/-)}$ parasites demonstrated shrinkage (red square) and cell death

least five times using two different methods, in gel digestion and on bead digestion, as indicated in Materials and Methods (Table 1 and Supplementary Table S1). In order to exclude nonspecific binders, we carried out two IP negative controls with total lysates from WT parasites (Supplementary Table S2) or recombinant *L. infantum* expressing GFP-HA (Supplementary Table S3) using an anti-HA antibody. A compilation from these experiments revealed potential interactions of DDX3 with key components of the cellular stress response. These include major antioxidant enzymes such as the iron superoxide dismutase (SODB1/SODB2) catalyzing the conversion of $O_2^{\bullet-}$ to H_2O_2,[33] tryparedoxin peroxidases involved in hydroperoxide detoxification[34] and a member of the sestrin family (LinJ.18.0660) known to be central to ROS suppression in mammals.[35] Also, several cytoplasmic and mitochondrial molecular chaperones and chaperonins (e.g., HSP40, HSP60, HSP70, HSP83, HSP110, and chaperonins containing T-complex protein 1) known to prevent nonspecific protein aggregates under stress[32] were co-immunoprecipitated with DDX3.

Furthermore, DDX3 IP studies depicted p97 also called valosin-containing protein (VCP) in mammals and Cdc48 in yeast (p97/VCP/Cdc48; LinJ.36.1420) as a potential DDX3-interacting partner (Table 1). p97/VCP/Cdc48 is one of the best-characterized type II AAA+ (ATPases associated with various cellular activities) ATPases[36,37] shown to play an essential role in mitochondrial quality control by clearing oxidatively damaged mitochondrial membrane proteins through ubiquitination and proteasomal degradation.[21–23] The interaction of DDX3 with p97/VCP/Cdc48 was confirmed by inverse co-IP studies using lysates from *L. infantum* expressing an HA epitope-tagged p97/VCP/Cdc48 (Table 1). Similarly to other eukaryotes,[38] the *Leishmania* p97/VCP/Cdc48 homolog interacts with ubiquitin-activating and -degrading co-factors and adaptors (e.g., UFD1-NPL4, UBX- and UBA- or PUB-domain proteins) (Table 1 and Supplementary Table S4). In line with p97/VCP/Cdc48's role in the UPS, IP studies revealed potential interactions with proteasome subunits (RPT5, RPN1, RPN2, RPN5, RPN6, RPN8, RPN9), the AAA+ proteases FtsH and ClpB-type chaperone HSP78 known to selectively degrade damaged mitochondrial

proteins,[18] and prohibitins involved in stress tolerance and mitochondrial quality control[39] (Table 1 and Supplementary Table S4). Thus, these data indicate that DDX3 associates with major components of the mitochondrial protein quality control in relationship with the UPS.

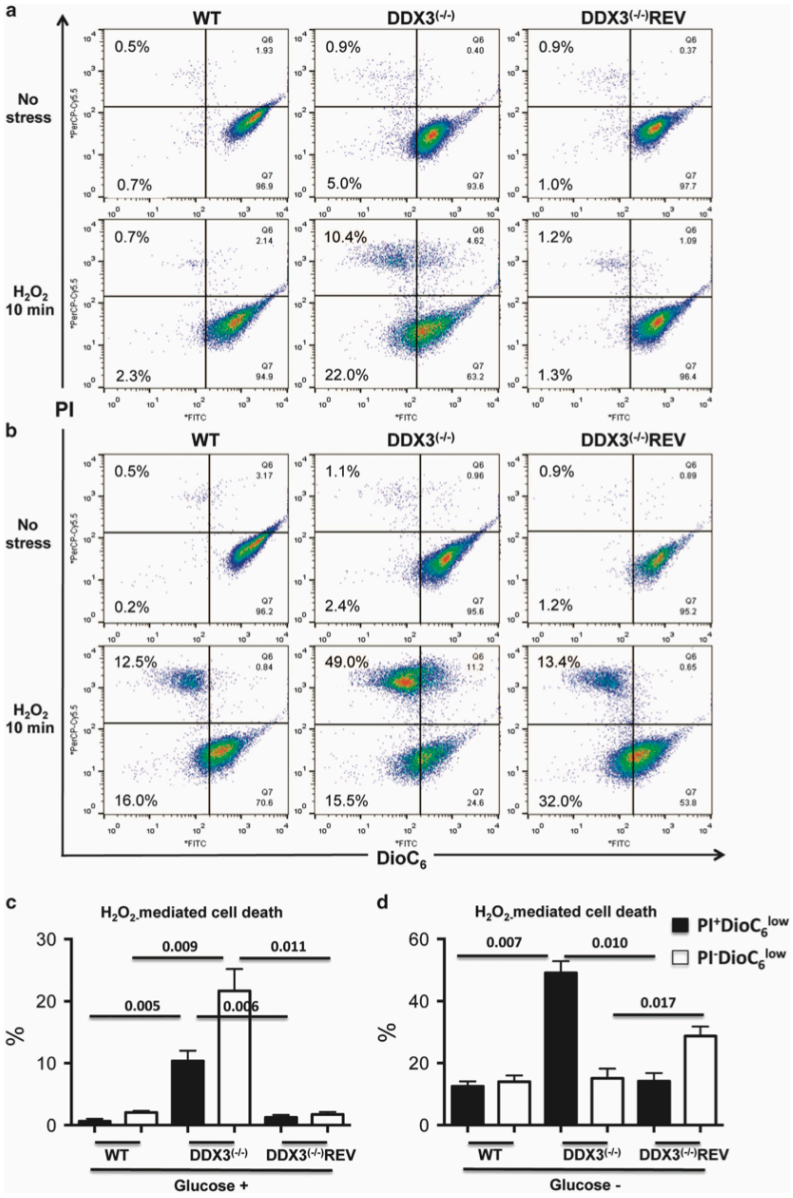

DDX3 inactivation results in the accumulation of mitochondrial polyubiquitinated proteins. The interaction of DDX3 with p97/VCP/Cdc48 prompted us to examine ubiquitinated protein levels in the mitochondrion of DDX3$^{(-/-)}$ parasites as a measure of mitochondrial proteostasis. Mitochondrial proteins were enriched either by digitonin fractionation or by mitochondrial isolation using a 20–35% Percoll gradient. LC-MS/MS analysis confirmed a high enrichment of mitochondrial proteins in these fractions (data not shown). Western blotting using a monoclonal mono- and polyubiquitinated conjugates antibody (FK2) revealed higher levels of polyubiquitinated proteins in mitochondrial (lane 3) but also in cytosolic fractions (lanes 1 and 2) from DDX3$^{(-/-)}$ compared with WT (lanes 1–3) and DDX3$^{(-/-)}$REV (lanes 1 and 3) (Figure 7a). Increased levels of polyubiquitinated proteins were also observed in purified mitochondria from DDX3$^{(-/-)}$ (Figure 7b). Similar results were obtained with DDX3$^{(-/-)}$ parasites complemented with a DDX3 mutant lacking the DEAD motif (Figure 7b), indicating that altering the efficiency of DDX3 for binding to ATP is sufficient to induce accumulation of ubiquitinated proteins in the mitochondrion. As a control for protein ubiquitination, WT parasites were treated with 10 μM of MG-132, a known proteasome inhibitor (Figure 7c). DDX3$^{(-/-)}$ parasites were more sensitive to MG-132 compared with WT and DDX3$^{(-/-)}$REV controls (Figure 7d).

Discussion

DDX3 is a highly conserved member of the Ded1/DDX3 subfamily of DEAD-box RNA helicases that harbors ATPase and RNA helicase activities.[24] Functionally, DDX3 appears to be one of the most multifaceted helicases with various roles in all steps of RNA metabolism.[24] DDX3 is also implicated in cell cycle regulation, apoptosis, cell signaling, tumor progression or suppression, and viral infection.[40,41] Few reports demonstrated a role of DDX3 members in the response to stress and apoptosis. DDX3 was found in stress granules[42] and shown to be involved in the response to hypoxia and radiation.[41,43] The *S. cerevisiae* ortholog Ded1 was found implicated in the response to nitrogen or glucose depletion, heat-shock, and low temperature.[44] VBH-1 in *C. elegans* protects nematodes from heat-shock and oxidative stress.[45]

In this study, we describe a novel function for DDX3 in regulating the mitochondrial stress response and protein quality control. We show that *Leishmania* lacking DDX3 accumulate high levels of mitochondrial ROS and, upon stress, display mitochondrial membrane potential collapse associated with fragmentation. DDX3$^{(-/-)}$ parasites are unable to recover from oxidative stress and experience cell death. Also, in the absence of DDX3, polyubiquitinated proteins accumulate in the cell, particularly in the mitochondrion, as an indicator of increased mitochondrial protein damage. In addition, we report potential interactions of DDX3 with key components of the mitochondrial stress response and particularly the AAA+ ATPase ubiquitin-selective chaperone p97/VCP/Cdc48, an essential component of mitochondrial protein quality control.

Our data support that DDX3 protects mitochondrial integrity from the damaged effects of ROS. Indeed, in the absence of DDX3, superoxide and hydrogen peroxide radicals accumulate in the mitochondrion upon the induction of various stresses due to a defect in their detoxification. Despite a slight increase in SOD activity, superoxide detoxification was largely impaired in DDX3$^{(-/-)}$ parasites. Additionally, the dramatic decrease of peroxidase activity in this knockout strain further contributed to H_2O_2 accumulation and aggravated ROS-induced stress. In line with DDX3's role in the antioxidant stress response, immunoprecipitation studies revealed potential interactions of DDX3 with the mitochondrial iron superoxide dismutase SODB1/SODB2 and tryparedoxin peroxidases involved in the detoxification of superoxide and H_2O_2 radicals, respectively.[33,34] Mitochondrial tryparedoxin peroxidases have also been attributed a chaperone activity to ensure the integrity of mitochondrial functions.[46] The association of DDX3 with proteins of the sestrin family sustains the idea that DDX3 can regulate ROS-induced mitochondrial stress. Sestrins are stress-inducible proteins known to suppress oxidative stress[35] and their inactivation in invertebrates resulted in diverse metabolic pathologies and mitochondrial dysfunction.[47]

ROS accumulation can damage mitochondria inducing the collapse of mitochondrial membrane potential ($\Delta\psi_m$), mitochondrial dysfunction, and cell death.[48] This is exactly what we have observed in DDX3$^{(-/-)}$ *Leishmania* under conditions inducing mitochondrial stress and to a lesser degree in unstressed parasites. The mitochondrion was indeed severely damaged in DDX3$^{(-/-)}$ parasites and appeared fragmented following oxidative stress. Shaping of mitochondria is essential for maintaining cellular bioenergetics by stabilizing the OXPHOS machinery and for regulating apoptosis.[8,49] The fact that DDX3$^{(-/-)}$ parasites grown in glucose-free medium where cellular ATP is produced predominantly through OXPHOS exhibited a dramatic increase in mitochondrial depolarization and sensitivity to cell death upon oxidative stress, further supports a critical role of DDX3 in maintaining mitochondrial integrity. Increased ROS-mediated damage in DDX3$^{(-/-)}$ parasites activated also the mitochondrial unfolded protein response[18] through the induction of HSP70 and HSP60 levels in order to repair misfolded/damaged proteins. In line with these findings, our IP studies revealed DDX3 interactions with chaperones and chaperonins that are essential for mitochondrial function. HSPs were also found to facilitate protein degradation by the UPS, thus playing a role in the so-called 'protein triage'.[50]

Figure 4 Mitochondrial membrane potential loss and cell death are greatly enhanced upon oxidative stress in DDX3$^{(-/-)}$ *Leishmania* forced to use the mitochondrial oxidative respiratory machinery. (**a**) Flow cytometric analysis of $DiOC_6(3)$- and PI-labeled *L. infantum* WT, DDX3$^{(-/-)}$, and DDX3$^{(-/-)}$REV grown in RPMI glucose-rich medium. Parasites were treated or not with 0.6 mM of hydrogen peroxide (H_2O_2) for 10 min, washed out, and further incubated in a fresh medium for 5 h prior to their analysis by flow cytometry. (**b**) As in (**a**) but parasites were cultured in DMEM glucose-free medium. The experiment was repeated three times with duplicates and statistical analysis of these results performed as in Figures 3b. (**c**) Glucose (+) medium) and (**d**) glucose (−) medium. The numbers over the lines correspond to *P*-values

Consistent with these results is our finding that DDX3$^{(-/-)}$ parasites accumulate polyubiquitinated proteins in the mitochondrion. Increased levels of polyubiquitinated proteins corroborate our IP studies revealing a potential interaction of DDX3 with the ubiquitin-selective chaperone p97/VCP/Cdc48. p97/VCP/Cdc48 is a cytosolic essential AAA+ chaperone that

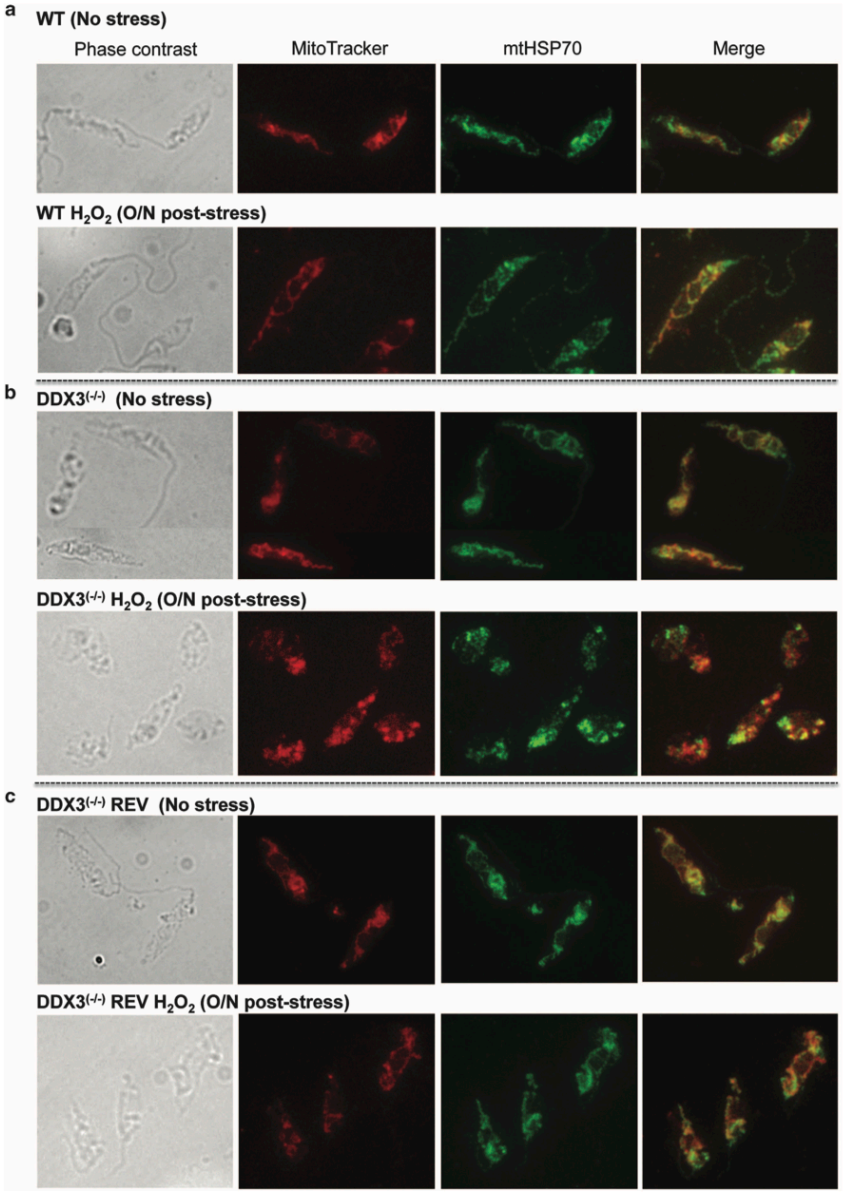

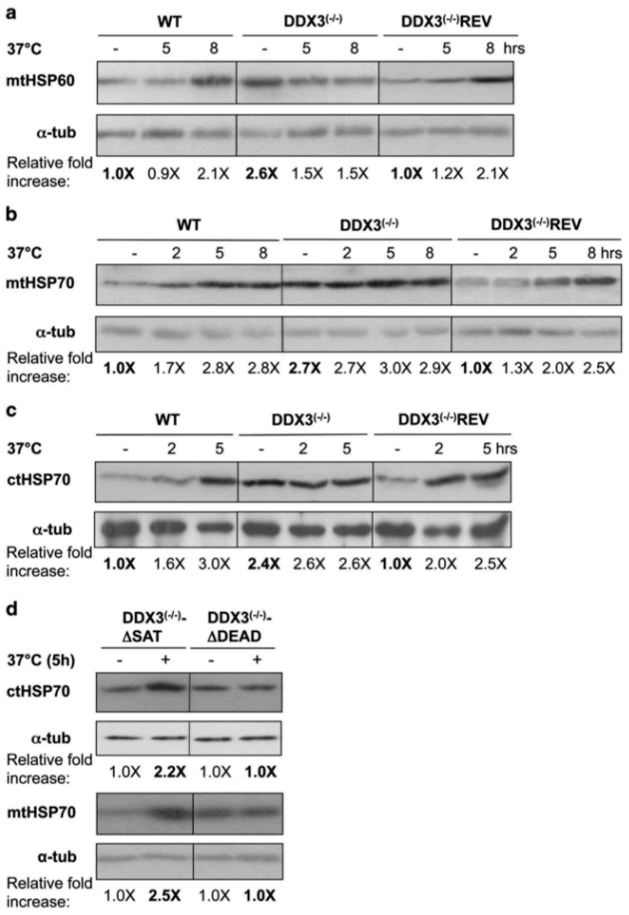

Figure 6 Inactivation of DDX3 activates key components of the mitochondrial unfolded protein response. Western blot analysis of total lysates from *L. infantum* WT, DDX3$^{(-/-)}$ and DDX3$^{(-/-)}$REV strains exposed to heat stress (37 °C) at different time points using an antibody recognizing the mitochondrial (mt) HSP60 (**a**) or mtHSP70 (**b**) or the cytoplasmic (ct) HSP70 (**c**) proteins (the same number of cells were loaded). Conditions of heat stress were compared with parasites grown at 25 °C. The same membrane was blotted with an anti-α-tubulin antibody (loading control). (**d**) Western blot analysis of total lysates from DDX3$^{(-/-)}$ parasites complemented either with the DDX3ΔDEAD or the DDX3ΔSAT mutant proteins and subjected or not to heat stress (5 h) using an anti-ctHSP70 antibody. Data shown here are representative of three independent experiments yielding similar results. Relative fold increase was calculated from three experiments and within each strain (e.g., WT, DDX3$^{(-/-)}$ and DDX3$^{(-/-)}$REV) values correspond to the ratio of heat-stressed *versus* unstressed parasites normalized with the α-tubulin protein. Values in bold represent steady-state levels of mtHSPs in DDX3$^{(-/-)}$ and DDX3$^{(-/-)}$REV relative to WT levels (**a**–**c**). In panel (**d**), values in bold are relative to the unstressed control

Figure 5 Inactivation of DDX3 impacts on mitochondrial morphogenesis upon exposure to oxidative stress. 2×10^7 *L. infantum* WT (**a**), DDX3$^{(-/-)}$ (**b**), and DDX3$^{(-/-)}$REV (**c**) grown under standard conditions (no stress) or treated for 10 min with 0.6 mM H_2O_2, washed out and further incubated O/N were stained with the MitoTracker CMX Red dye at a final concentration of 20 nM for 30 min at 26 °C. The mitochondrial network was visualized on 2% paraformaldehyde-fixed cells using a Nikon epifluorescence microscope. Immunolocalization studies were also performed using an anti-rabbit antibody against the mitochondrial matrix HSP70 protein. The data shown here are representative of three independent experiments that generated similar results

Table 1 Potentially interacting proteins with the *Leishmania infantum* DDX3 DEAD-box RNA helicase and the AAA-ATPase valosin-containing protein homolog p97/VCP/Cdc48 as determined by immunoprecipitation and LC-MS/MS studies

TriTrypDB ID	*Annotation*	*Peptide no.*[a] *(probability score >95%)*	
		WT	
		DDX3-HA	*p97/VCP/Cdc48-HA*
LinJ.32.0410	**ATP-dependent RNA helicase HEL67 (DDX3)**	**21–41**	**5–22**
Cell redox homeostasis/antioxidant activity			
LinJ.32.1910/1920	Iron superoxide dismutase, putative (SODB1/SODB2) (mitochondrial)	3–7	2–4
LinJ.08.0300	Iron superoxide dismutase, putative (FESODA) (mitochondrial)		2–3
LinJ.15.1140	Tryparedoxin peroxidase (TRYP)	2–10	6–7
LinJ.23.0050	Peroxidoxin, tryparedoxin peroxidase	2–6	1–6
LinJ.18.0660	PA26 p53-induced protein (sestrin), putative	2–2	
LinJ.05.0350	Trypanothione reductase (TRYR)		6–8
LinJ.27.1770	Trypanothione synthetase (TRYS)		7–10
Protein folding–refolding			
LinJ.28.2960	Heat-shock protein HSP70, putative	7–42	34–40
LinJ.30.2480	Heat-shock 70-related protein 1, mitochondrial precursor, putative	10–36	22–24
LinJ.26.1220	Heat-shock protein 70-related protein (HSP70.4)	2–9	18–23
LinJ.33.0360	Heat-shock proteins HSP83-2	3–38	30–31
LinJ.18.1350	Heat-shock protein HSP110, putative	1–30	14–20
LinJ.27.2350	Heat-shock protein DnaJ (HSP40), putative	2–8	9–10
LinJ.36.2130	Chaperonin HSP60, mitochondrial precursor	2–28	14–21
LinJ.23.1460	T-complex protein 1, gamma subunit (TCP-1-gamma), putative	1–13	4–14
LinJ.21.1330	T-complex protein 1, delta subunit (TCP-1-delta, putative	1–11	2–12
LinJ.35.3900	T-complex protein 1, eta subunit (TCP-1-eta), putative	3–9	4–11
LinJ.13.1400	Chaperonin TCP20, putative (TCP-1-zeta)	3–9	2–8
Ubiquitin-dependent protein catabolic process/proteasome			
LinJ.36.1420	**Valosin-containing protein, putative (p97/VCP/Cdc48)**	**4–8**	**37–59**
LinJ.35.1960	UBX domain containing protein, putative[b]		6–9
LinJ.22.0200	SEP domain containing protein, putative (NSFL1 p97 ATPase cofactor p47)[b]		7–13
LinJ.24.1650	Hypothetical protein, conserved (UBA-like, putative mitochondrial)[b]		3–8
LinJ.25.1320	NPL4 family, putative[b]		3–6
LinJ.09.1060	PUB domain containing protein, putative[b]		3–4
LinJ.11.0920	Short C-terminal domain/PUB domain containing protein, putative[b]		2–6
LinJ.36.6280	Hypothetical protein, conserved (ubiquitin thioesterase OTU1)[b]		1–4
LinJ.36.6780	Ubiquitin fusion degradation protein 1 (UFD1), putative[b]		7–12
LinJ.35.3110	Ubiquitin-activating enzyme E1, putative[b]		3–4
LinJ.09.0950	Polyubiquitin, putative		4–5
LinJ.12.0190	Proteasome regulatory ATPase subunittcc1l8.3 (AAA-ATPase)	3–6	
LinJ.22.0490	Proteasome regulatory ATPase subunit 5 (RPT5), putative (AAA-ATPase)		1–3
LinJ.29.0120	Proteasome regulatory non-ATPase subunit (RPN1), putative		5–6
LinJ.28.1850	Proteasome regulatory non-ATPase subunit 2 (RPN2), putative	2–2	3–6
LinJ.21.0840	Proteasome regulatory non-ATPase subunit 5 (RPN5), putative	2–3	2–7
LinJ.02.0340	Proteasome regulatory non-ATPase subunit 6 (RPN6), putative	3–4	2–6
LinJ.32.0400	19 S proteasome regulatory non-ATPase subunit 8 (RPN8), putative		1–2
LinJ.19.1100	Proteasome regulatory non-ATPase subunit 9 (RPN9), putative	1–4	2–5
Mitochondrial integrity and stress response			
LinJ.36.2850	ATP-dependent metallo-peptidase, Clan MA(E) (FtsH protease domain; AAA mitochondrial)[c]		12–19
LinJ.02.0680	ATP-dependent Clp protease subunit, HSP78, putative (AAA domain)[c]		3–3
LinJ.36.2850	ATP-dependent metallo-peptidase, Clan MA(E) (AAA/FtsH, mitochondrial)[c]		12–18
LinJ.35.1390	Mitochondrial metallo-peptidase, Clan ME		6–12
LinJ.05.1040	Stomatin-like protein, PHB prohibitin homolog[d]		14–20
LinJ.16.1710	Prohibitin (PHB1) (mitochondrial putative)[d]		5–8
LinJ.35.0070	Prohibitin (PHB2), putative (mitochondrial putative) (TM domains)[d]		7–12

[a]The proteins listed here co-immunoprecipitated with either the *Leishmania infantum* DDX3 homolog or the valosin-containing protein homolog p97/VCP/Cdc48 in 3–5 independent experiments with *L. infantum* DDX3-HA or p97/VCP/Cdc48-HA lysates. On bead or in gel digestion was followed by LC-MS/MS analysis (see the Materials and Methods). Proteins identified with a minimum of two peptides and a probability of >95.0% to correspond to the correct protein were included here. Identified proteins were grouped into different GO categories based on their predicted function. Only selected proteins related to the cellular stress response, the ubiquitin–proteasome system (UPS), and the mitochondrial protein quality control are indicated here. A detailed list of all co-immunoprecipitated proteins for more than three independent experiments with the protein, peptide, and spectrum reports is shown in Supplementary Tables S1 and S4. [b]p97/VCP/Cdc48 co-factors/adaptors.[38] [c]AAA+ mitochondrial proteases FtsH and ClpB-type chaperone HSP78 that selectively degrade misfolded and/or damaged mitochondrial proteins.[18] [d]Prohibitins are inner mitochondrial membrane proteins that maintain mitochondrial functional integrity and protect cells from various stresses.[39] Bold characters indicate the two major proteins used for the immunoprecipitation studies

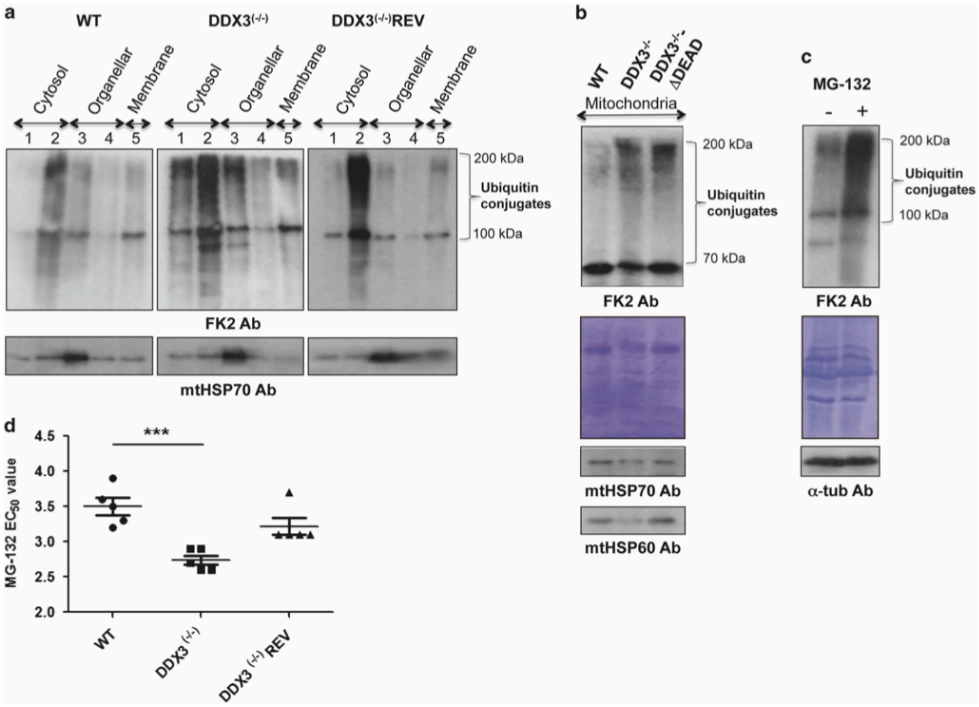

Figure 7 DDX3 inactivation results in the accumulation of mitochondrial polyubiquitinated proteins. (**a**) Digitonin (20 μM–10 mM) fractions (equal volume) isolated from the same number of WT, DDX3$^{(-/-)}$, and DDX3$^{(-/-)}$REV parasites were analyzed by western blotting using the FK2 antibody recognizing K^{29}-, K^{48}-, and K^{63}-linked mono- and polyubiquitinated proteins. As also determined by our previous experiments,[59] digitonin fractions 1 and 2 are enriched with cytosolic proteins, fractions 3 and 4 with organellar material, and fraction 5 with membrane-associated proteins. An antibody directed against the mtHSP70 protein was used as a control to confirm mitochondrial enrichment in fraction 3. (**b**) Mitochondria purified from the same number of WT, DDX3$^{(-/-)}$, and DDX3$^{(-/-)}$-ΔDEAD (DDX3$^{(-/-)}$ rescued with the DDX3ΔDEAD mutant) parasites using a 20–35% Percoll gradient centrifugation were analyzed by western blotting using the FK2 antibody. An equal amount of proteins was loaded on the gel. Shown here is one representative experiment out of three yielding similar results. (**c**) Western blot of total lysates from *L. infantum* WT treated with the proteasome inhibitor MG-132 (10 μM) using the FK2 antibody. The anti-α-tubulin antibody and Coomassie blue staining were used as loading controls. (**d**) Susceptibility of WT, DDX3$^{(-/-)}$, and DDX3$^{(-/-)}$REV strains to MG-132.

governs critical steps in ubiquitin-dependent protein quality control driving the turnover of misfolded polyubiquitinated proteins in different cellular compartments (e.g., ER, mitochondria, nucleus) by the 26 S proteasome.[22,36,37] It has been shown recently that p97/VCP/Cdc48 is essential for the turnover of oxidatively damaged outer mitochondrial membrane (OMM) proteins.[21–23] p97/VCP/Cdc48 is recruited to stressed mitochondria and upon ATP hydrolysis extracts ubiquitinated proteins from the OMM via its interaction with the UPS and presents them to the proteasome for degradation.[36,51] The interaction of DDX3 with p97/VCP/Cdc48 together with the increased accumulation of mitochondrial polyubiquitinated proteins in DDX3$^{(-/-)}$ parasites support a role for DDX3 in mitochondrial protein quality control. Our finding that complementation of DDX3$^{(-/-)}$ with a DDX3 mutant protein lacking the DEAD motif involved in the binding of the α and β phosphates of ATP[24,52] did not prevent accumulation of mitochondrial polyubiquitinated proteins suggests that the ATPase activity of DDX3 drives its function on mitochondrial proteostasis. It is possible that the interaction of DDX3 with p97/VCP/Cdc48 requires DDX3 binding to ATP and that this step is important for removing polyubiquitinated proteins out of the mitochondrion for proteosomal degradation. DDX3 does not seem to affect p97/VCP/Cdc48 binding to its co-factors or adaptors as IP studies against p97/VCP/Cdc48 in the DDX3$^{(-/-)}$ background did not reveal any major changes in p97/VCP/Cdc48 interacting partners (Supplementary Table S5). Additional studies are needed, however, to fully address the impact of DDX3-p97/VCP/Cdc48 interaction on mitochondrial protein quality control.

Taken together, our data support a central role for the *Leishmania* DDX3 homolog in mitochondrial protein quality control under normal growth conditions and particularly upon stress by preventing ROS-mediated damage and polyubiquitinated protein accumulation in the mitochondrion. Because of its important role in tumorigenesis and viral infection,[40] DDX3

represents a potent novel therapeutic target.[21] On the other hand, defects in p97/VCP/Cdc48 activity have been linked to several human pathologies.[37,53] Accordingly, a comprehensive understanding of how DDX3 monitors mitochondrial quality control would possibly inform the prevention and treatment not only of parasitic but also of other human diseases.

Materials and Methods

Parasite strains and cell culture. *L. infantum* MHOM/MA/67/ITMAP-263 was used in this study. *L. infantum* promastigotes were cultured in SDM-79 medium supplemented with 10% heat-inactivated FCS (Multicell Wisent Inc., Canada) and 5 μg/ml hemin at pH 7.0 and 25 °C. *L. infantum* axenic amastigotes were grown in MAA-20 medium supplemented with 20% FCS in 5% CO_2 atmosphere at pH 5.5 and 37 °C.[54] Bone marrow-derived murine macrophages were seeded in a 16-well chamber and infected with *L. infantum* as described previously.[55]

Plasmid constructs and transfections. The *L. infantum DDX3* gene (LinJ.32.0410, http://tritrypdb.org) knockout and the rescue mutant DDX3$^{(-/-)}$REV have been described previously.[6] To engineer DDX3 deletion mutant proteins lacking either the DEAD-box (motif II) (DDX3ΔDEAD) or the SAT (motif III) (DDX3ΔSAT) or the HRIGRTGR motif (motif VI) (DDX3ΔHRIGRTGR), the Phusion DNA polymerase (NEB)-based PCR strategy was used. The HA-tagged DDX3 wild type and DDX3 mutant proteins were cloned into the *Xba*I and *Hin*dIII sites of vector pSPαZEOα.[56] To generate the p97/VCP/Cdc48-HA construct, the *p97/VCP/Cdc48* ORF (LinJ.36.1420) was PCR-amplified from *L. infantum* and cloned into the *Hin*dIII and *Xba*I sites of pSPαZEOα. Primer sequences or all constructs described here are indicated in Supplementary Table S6. Stable transfections of the above DNA constructs into *Leishmania* were carried out by electroporation as described previously.[57]

Protein lysate preparations and western blots. Western blots were performed following standard procedures. The anti-mouse α-tubulin antibody (1:10 000 dilution; Sigma, Canada), the anti-mouse hemagglutinin (HA) tag monoclonal antibody (1:3000; ABM, Canada), the anti-HSP70 (cytosolic) monoclonal antibody universal (1:1000, (5A5)-Alexis Biochemicals, Canada), the anti-rabbit HSP70 (mitochondrial) antibody (1:2000, kindly provided by Dr Osvaldo de Melo Neto, Recife, Brazil), the anti-mouse HSP60 (mitochondrial) antibody (1:400; Acris, USA), and the anti-mouse mono- and polyubiquitinated conjugates monoclonal antibody (FK2) (1:5000 and blocking in 1% BSA; Enzo, Canada) were used in this study. FK2 Ab was used on total and digitonin-fractionated extracts as well as on purified mitochondria in the presence or absence of the proteasome inhibitor MG-132 (10 μM; Enzo). Mitochondria were purified from 5 to 10 $\times 10^9$ log-phase *L. infantum* promastigotes using a 20–35% Percoll gradient, as described previously.[58] Digitonin fractionation was carried out as described before.[59]

ROS measurement. Intracellular oxidant species from *L. infantum* promastigotes were measured using 25 μg/ml H_2DCFDA flCFDA fluor probe (Invitrogen, Canada) and incubated at 25 °C for 30 min. Fluorescence was measured with a Victor fluorometer (Perkin-Elmer, USA), cells were counted, and RFU was normalized to 10^6 cells. To monitor superoxide production, 10^6 parasites grown in RPMI medium (Wisent, Canada) were stained for 20 min with the DHE (Life Technologies, Canada) probe and analyzed by flow cytometry. Mitochondrial superoxide was detected in live parasites using the fluorescent MitoSOX Red dye (Invitrogen). 2–4 $\times 10^7$ parasites were incubated with 5 μM MitoSOX Red for 2 h at 25 °C and the fluorescence assessed by a Victor fluorometer (Perkin-Elmer, USA).

Peroxidase activity. To measure peroxidase activity, we used the Peroxidase Activity Assay Kit (Sigma-Aldrich, Canada; MAK092) with some modifications. Briefly, stationary phase *L. infantum* promastigotes were treated with H_2O_2 (0.6 mM for 10 min), washed twice in PBS, and harvested by centrifugation at 6000 *g* for 10 min. The pellets were resuspended in 100 μl of Assay Buffer, disrupted by several passages through a 30-gauge needle, and the lysate was centrifuged at 15 000 *g* for 10 min. Protein concentrations of parasite extracts were determined using the BCA protein assay system (Pierce, Canada). Peroxidase activity was measured via its coupling to H_2O_2 reduction and a fluorescent probe, resulting in a colorimetric (570 nm) product. Peroxidase activity reported as nmole/min/mg where one unit of peroxidase is defined as the amount of enzyme that reduces 1.0 mmol of H_2O_2 per minute at 37 °C.

Superoxide dismutase activity. SOD activity was measured using OxiSelect Superoxide Dismutase Activity Assay (Cellbiolabs, USA; STA-340) according to the manufacturer's protocol. Stationary phase *L. infantum* promastigotes (10^9) were treated or not with 3 μM menadione (Sigma) O/N, washed twice in PBS and harvested by centrifugation at 6000 *g* for 5 min. The pellets were resuspended in 100 μl of cold 1 × Lysis Buffer (10 mM Tris, pH 7.5, 150 mM NaCl, 0.1 mM EDTA, protease inhibitor). Cells were lysed by three freeze–thaw cycles alternating liquid nitrogen and a 37 °C bath. The lysates were centrifuged at 15 000 *g* for 10 min at 4 °C, and protein contents were determined using a BCA protein assay system. The SOD assay system utilizes the xanthine oxidase, which oxidizes its substrate xanthine to produce superoxide anions. The included chromagen produces a water-soluble formazan dye upon reduction by superoxide anions. Inhibition of yellow formazan after the addition of whole-cell extracts to the SOD assay mix was determined as a measure of SOD activity. One unit of SOD will inhibit by 50% the rate of reduction of chromagen.

Mitochondrial membrane potential measurement. The 3,3′-dihexyloxacarbocyanine iodide ($DiOC_6$(3) (Molecular Probes, Eugenes, OR, USA) was used to measure mitochondrial membrane potential ($\Delta\Psi_m$) by flow cytometry. *L. infantum* promastigotes grown either in RPMI medium or in glucose-free medium (11966-DMEM; Life Technologies) were exposed or not to H_2O_2 treatment (0.6 mM for 10 min and further incubation in a fresh medium in the absence of oxidants), washed twice in PBS, and double-stained (10^6 cells) with 40 nM $DiOC_6$(3) for 20 min at RT and with l μg/ml of PI (Life Technologies) for 5 min on ice prior to flow cytometry analyses. $DiOC_6$(3)/PI double-stained cells were analyzed on BD Influx (Becton Dickinson, Canada). Analyses were performed using FlowJo software (Tree Star, Inc., OR, USA), as well as GraphPad prism (GraphPad Software, Inc., San Diego, CA, USA) for statistics.

MitoTracker staining and immunofluorescence. Parasites (2–4 $\times 10^7$/ml) were centrifuged and washed once with 1 × PBS and stained with MitoTracker CMX Red (Life Technologies) at a final concentration of 20 nM for 30 min at 26 °C. For immunofluorescence, cells were spotted on a slide (spread 5 μl), air dried at RT, washed twice in 1 × PBS and then fixed in 2% paraformaldehyde for 10 min. Following washings (3 ×) in 1 × PBS, cells were permeabilized in 1 × PBS, 0.2% Triton X-100, and 5% FCS at RT for 30 min and blocked in 1 × PBS, 2% milk, 0.02% Tween 20, and 0.1% Triton X-100 for 1 h at RT. The hybridization was performed with the anti-rabbit mitochondrial HSP70 (1:300, 1 h) followed by the secondary antibody, Alexa fluor 488 anti-rabbit (Life Technologies) (1:1000, 1 h). After washing, the cells were observed under a Nikon epifluorescence microscope.

Immunoprecipitation studies and mass spectrometry analysis. For immunoprecipitation studies, *L. infantum* promastigotes expressing DDX3-HA or p97/VCP/Cdc48-HA proteins were lysed in ice-cold 1 × lysis buffer (10 mM Tris-HCl (pH 7.5), 50 mM KCl, 2 mM $MgCl_2$, 1% Triton X-100, 10 μl/ml of protease inhibitors (Sigma), protease inhibitor cocktail (Roche Applied Science, Canada), 1 mM DTT, 0.1 mM Na_9VO_4, 1 mM phenylmethylsulfonyl fluoride and 20 nM okadaic acid (Sigma)), passed through a 30-gauge needle and centrifuged at 10 000 *g* for 10 min at 4 °C. Soluble proteins (750 μg) were mixed with Pierce Anti-HA Magnetic Beads (Thermo Scientific, Canada) as per the manufacturer's protocol. Proteins on beads were washed 3 × with 50 mM ammonium bicarbonate buffer and kept at − 20 °C until mass spectrometry analysis. Alternatively, proteins eluted from beads were resolved only up to 1 cm in a 10% SDS PAGE followed by Coomassie blue staining. Then, 1 × 1 cm^2 gel slice was excised, trypsin-digested, and analyzed by mass spectrometry. Peptide separation and elution, mass spectra acquisition, database searching, and peptide identification were performed as described previously.[60] In order to exclude nonspecific binders to DDX3-HA or to p97/VCP/Cdc48-HA proteins, we carried out IP studies under the same experimental conditions with total lysates from either *L. infantum* wild type (Supplementary Table S2) or recombinant parasites expressing an HA-tagged GFP (Supplementary Table S3) as part of an episomal vector. Contaminant proteins present in the two IP negative controls were excluded from Table 1.

Statistics. All analyses were performed using GraphPad Prism software (version 6.04; GraphPad, La Jolla, CA, USA). Results were expressed as means ± S.D. or

±S.E.M. of at least three independent experiments in triplicates or in duplicates. Statistical significance was assessed by two-tailed paired Student's-*t*-test or the two-way ANOVA. Statistical significance was set at $P \leqslant 0.05$ (**$P \leqslant 0.01$, ***$P \leqslant 0.001$, and ****$P \leqslant 0.0001$).

Conflict of Interest

The authors declare no conflict of interest.

Acknowledgements. We are grateful to the Proteomics platform of the CHU de Quebec Research Center. We also thank Gina Racine and Félicien Moukambi for helping in analyzing flow cytometry data. PP was a recipient of a postdoctoral fellowship from the Canadian Institutes of Health Research (CIHR) Strategic Training Program STP-53924 and the Centre for Host-Parasite Interactions (CHPI) funded by the Fonds de Recherche du Québec-Nature et Technologies. BA is a recipient of doctoral fellowships from the CAPES 'Frontiers without Borders' program. JE thanks the Canada Research Chair program for financial assistance and the Canadian Foundation of Innovation for infrastructure grants. This work was supported by the CIHR operating grant MOP-12182 and the Natural Sciences and Engineering Research Council of Canada (NSERC) Discovery Grant GC100741 (418444) awarded to BP.

1. Linder P, Fuller-Pace F. Happy birthday: 25 years of DEAD-box proteins. *Methods Mol Biol* 2015; **1259**: 17–33.
2. Gargantini PR, Lujan HD, Pereira CA. *In silico* analysis of trypanosomatids' helicases. *FEMS Microbiol Lett* 2012; **335**: 123–129.
3. Delhi P, Queiroz R, Inchaustegui D, Carrington M, Clayton C. Is there a classical nonsense-mediated decay pathway in trypanosomes? *PLoS One* 2011; **6**: e25112.
4. Kramer S, Queiroz R, Ellis L, Hoheisel JD, Clayton C, Carrington M. The RNA helicase DHH1 is central to the correct expression of many developmentally regulated mRNAs in trypanosomes. *J Cell Sci* 2010; **123**(Pt 5): 699–711.
5. Li F, Herrera J, Zhou S, Maslov DA, Simpson L. Trypanosome REH1 is an RNA helicase involved with the 3'-5' polarity of multiple gRNA-guided uridine insertion/deletion RNA editing. *Proc Natl Acad Sci USA* 2011; **108**: 3542–3547.
6. Padmanabhan PK, Samant M, Cloutier S, Simard MJ, Papadopoulou B. Apoptosis-like programmed cell death induces antisense ribosomal RNA (rRNA) fragmentation and rRNA degradation in Leishmania. *Cell Death Differ* 2012; **19**: 1972–1982.
7. Menna-Barreto RF, de Castro SL. The double-edged sword in pathogenic trypanosomatids: the pivotal role of mitochondria in oxidative stress and bioenergetics. *Biomed Res Int* 2014; **2014**: 614014.
8. Estaquier J, Vallette F, Vayssiere JL, Mignotte B. The mitochondrial pathways of apoptosis. *Adv Exp Med Biol* 2012; **942**: 157–183.
9. Arnoult D, Akarid K, Grodet A, Petit PX, Estaquier J, Ameisen JC. On the evolution of programmed cell death: apoptosis of the unicellular eukaryote Leishmania major involves cysteine proteinase activation and mitochondrion permeabilization. *Cell Death Differ* 2002; **9**: 65–81.
10. Lee N, Bertholet S, Debrabant A, Muller J, Duncan R, Nakhasi HL. Programmed cell death in the unicellular protozoan parasite Leishmania. *Cell Death Differ* 2002; **9**: 53–64.
11. Sen N, Das BB, Ganguly A, Mukherjee T, Tripathi G, Bandyopadhyay S *et al.* Camptothecin induced mitochondrial dysfunction leading to programmed cell death in unicellular hemoflagellate Leishmania donovani. *Cell Death Differ* 2004; **11**: 924–936.
12. Getachew F, Gedamu L. Leishmania donovani mitochondrial iron superoxide dismutase A is released into the cytosol during miltefosine induced programmed cell death. *Mol Biochem Parasitol* 2012; **183**: 42–51.
13. Roy A, Ganguly A, BoseDasgupta S, Das BB, Pal C, Jaisankar P *et al.* Mitochondria-dependent reactive oxygen species-mediated programmed cell death induced by 3,3'-diindolylmethane through inhibition of F0F1-ATP synthase in unicellular protozoan parasite Leishmania donovani. *Mol Pharmacol* 2008; **74**: 1292–1307.
14. Kathuria M, Bhattacharjee A, Sashidhara KV, Singh SP, Mitra K. Induction of mitochondrial dysfunction and oxidative stress in Leishmania donovani by orally active clerodane diterpene. *Antimicrob Agents Chemother* 2014; **58**: 5916–5928.
15. Mandal A, Das S, Roy S, Ghosh AK, Sardar AH, Verma S *et al.* Deprivation of L-arginine induces oxidative stress mediated apoptosis in Leishmania donovani promastigotes: contribution of the polyamine pathway. *PLoS Negl Trop Dis* 2016; **10**: e0004373.
16. Baker MJ, Palmer CS, Stojanovski D. Mitochondrial protein quality control in health and disease. *Br J Pharmacol* 2014; **171**: 1870–1889.
17. Baker MJ, Tatsuta T, Langer T. Quality control of mitochondrial proteostasis. *Cold Spring Harb Perspect Biol* 2011; **3**: a007559.
18. Voos W. Chaperone-protease networks in mitochondrial protein homeostasis. *Biochim Biophys Acta* 2013; **1833**: 388–399.
19. Ni HM, Williams JA, Ding WX. Mitochondrial dynamics and mitochondrial quality control. *Redox Biol* 2015; **4**: 6–13.
20. Segref A, Kevei E, Pokrzywa W, Schmeisser K, Mansfeld J, Livnat-Levanon N *et al.* Pathogenesis of human mitochondrial diseases is modulated by reduced activity of the ubiquitin/proteasome system. *Cell Metab* 2014; **19**: 642–652.
21. Xu S, Peng G, Wang Y, Fang S, Karbowski M. The AAA-ATPase p97 is essential for outer mitochondrial membrane protein turnover. *Mol Biol Cell* 2011; **22**: 291–300.
22. Hemion C, Flammer J, Neutzner A. Quality control of oxidatively damaged mitochondrial proteins is mediated by p97 and the proteasome. *Free Radic Biol Med* 2014; **75**: 121–128.
23. Fang L, Hemion C, Pinho Ferreira Bento AC, Bippes CC, Flammer J, Neutzner A. Mitochondrial function in neuronal cells depends on p97/VCP/Cdc48-mediated quality control. *Front Cell Neurosci* 2015; **9**: 16.
24. Sharma D, Jankowsky E. The Ded1/DDX3 subfamily of DEAD-box RNA helicases. *Crit Rev Biochem Mol Biol* 2014; **49**: 343–360.
25. Fairman-Williams ME, Guenther UP, Jankowsky E. SF1 and SF2 helicases: family matters. *Curr Opin Struct Biol* 2010; **20**: 313–324.
26. Zilberstein D, Shapira M. The role of pH and temperature in the development of Leishmania parasites. *Annu Rev Microbiol* 1994; **48**: 449–470.
27. Banroques J, Doere M, Dreyfus M, Linder P, Tanner NK. Motif III in superfamily 2 "helicases" helps convert the binding energy of ATP into a high-affinity RNA binding site in the yeast DEAD-box protein Ded1. *J Mol Biol* 2010; **396**: 949–966.
28. Van Assche T, Deschacht M, da Luz RA, Maes L, Cos P. Leishmania-macrophage interactions: insights into the redox biology. *Free Radic Biol Med* 2011; **51**: 337–351.
29. Getachew F, Gedamu L. Leishmania donovani iron superoxide dismutase A is targeted to the mitochondria by its N-terminal positively charged amino acids. *Mol Biochem Parasitol* 2007; **154**: 62–69.
30. Castro H, Tomas AM. Peroxidases of trypanosomatids. *Antioxid Redox Signal* 2008; **10**: 1593–1606.
31. Venditti P, Di Stefano L, Di Meo S. Mitochondrial metabolism of reactive oxygen species. *Mitochondrion* 2013; **13**: 71–82.
32. Richter K, Haslbeck M, Buchner J. The heat shock response: life on the verge of death. *Mol Cell* 2010; **40**: 253–266.
33. Buettner GR. Superoxide dismutase in redox biology: the roles of superoxide and hydrogen peroxide. *Anticancer Agents Med Chem* 2011; **11**: 341–346.
34. Poynton RA, Hampton MB. Peroxiredoxins as biomarkers of oxidative stress. *Biochim Biophys Acta* 2014; **1840**: 906–912.
35. Budanov AV, Sablina AA, Feinstein E, Koonin EV, Chumakov PM. Regeneration of peroxiredoxins by p53-regulated sestrins, homologs of bacterial AhpD. *Science* 2004; **304**: 596–600.
36. Taylor EB, Rutter J. Mitochondrial quality control by the ubiquitin-proteasome system. *Biochem Soc Trans* 2011; **39**: 1509–1513.
37. Yamanaka K, Sasagawa Y, Ogura T. Recent advances in p97/VCP/Cdc48 cellular functions. *Biochim Biophys Acta* 2012; **1823**: 130–137.
38. Buchberger A, Schindelin H, Hanzelmann P. Control of p97 function by cofactor binding. *FEBS Lett* 2015; **589**: 2578–2589.
39. Van Aken O, Whelan J, Van Breusegem F. Prohibitins: mitochondrial partners in development and stress response. *Trends Plant Sci* 2010; **15**: 275–282.
40. Ariumi Y. Multiple functions of DDX3 RNA helicase in gene regulation, tumorigenesis, and viral infection. *Front Genet* 2014; **5**: 423.
41. Bol GM, Xie M, Raman V. DDX3, a potential target for cancer treatment. *Mol Cancer* 2015; **14**: 188.
42. Shih JW, Wang WT, Tsai TY, Kuo CY, Li HK, Wu Lee YH. Critical roles of RNA helicase DDX3 and its interactions with eIF4E/PABP1 in stress granule assembly and stress response. *Biochem J* 2012; **441**: 119–129.
43. Bol GM, Raman V, van der Groep P, Vermeulen JF, Patel AH, van der Wall E *et al.* Expression of the RNA helicase DDX3 and the hypoxia response in breast cancer. *PLoS One* 2013; **8**: e63548.
44. Tarn WY, Chang TH. The current understanding of Ded1p/DDX3 homologs from yeast to human. *RNA Biol* 2009; **6**: 17–20.
45. Paz-Gomez D, Villanueva-Chimal E, Navarro RE. The DEAD Box RNA helicase VBH-1 is a new player in the stress response in C. elegans. *PLoS One* 2014; **9**: e97924.
46. Castro H, Teixeira F, Romao S, Santos M, Cruz T, Florido M *et al.* Leishmania mitochondrial peroxiredoxin plays a crucial peroxidase-unrelated role during infection: insight into its novel chaperone activity. *PLoS Pathog* 2011; **7**: e1002325.
47. Lee JH, Budanov AV, Karin M. Sestrins orchestrate cellular metabolism to attenuate aging. *Cell Metab* 2013; **18**: 792–801.
48. Ray PD, Huang BW, Tsuji Y. Reactive oxygen species (ROS) homeostasis and redox regulation in cellular signaling. *Cell Signal* 2012; **24**: 981–990.
49. Cogliati S, Frezza C, Soriano ME, Varanita T, Quintana-Cabrera R, Corrado M *et al.* Mitochondrial cristae shape determines respiratory chain supercomplexes assembly and respiratory efficiency. *Cell* 2013; **155**: 160–171.
50. Lanneau D, Wettstein G, Bonniaud P, Garrido C. Heat shock proteins: cell protection through protein triage. *Scientific World J* 2010; **10**: 1543–1552.
51. Heo JM, Livnat-Levanon N, Taylor EB, Jones KT, Dephoure N, Ring J *et al.* A stress-responsive system for mitochondrial protein degradation. *Mol Cell* 2010; **40**: 465–480.
52. Pause A, Sonenberg N. Mutational analysis of a DEAD box RNA helicase: the mammalian translation initiation factor eIF-4 A. *EMBO J* 1992; **11**: 2643–2654.

53. Meyer H, Weihl CC. The VCP/p97 system at a glance: connecting cellular function to disease pathogenesis. *J Cell Sci* 2014; **127**(Pt 18): 3877–3883.
54. Sereno D, Roy G, Lemesre JL, Papadopoulou B, Ouellette M. DNA transformation of Leishmania infantum axenic amastigotes and their use in drug screening. *Antimicrob Agents Chemother* 2001; **45**: 1168–1173.
55. Chow C, Cloutier S, Dumas C, Chou MN, Papadopoulou B. Promastigote to amastigote differentiation of Leishmania is markedly delayed in the absence of PERK eIF2alpha kinase-dependent eIF2alpha phosphorylation. *Cell Microbiol* 2011; **13**: 1059–1077.
56. Richard D, Leprohon P, Drummelsmith J, Ouellette M. Growth phase regulation of the main folate transporter of Leishmania infantum and its role in methotrexate resistance. *J Biol Chem* 2004; **279**: 54494–54501.
57. Papadopoulou B, Roy G, Ouellette M. A novel antifolate resistance gene on the amplified H circle of Leishmania. *EMBO J* 1992; **11**: 3601–3608.
58. Mukherjee A, Padmanabhan PK, Sahani MH, Barrett MP, Madhubala R. Roles for mitochondria in pentamidine susceptibility and resistance in Leishmania donovani. *Mol Biochem Parasitol* 2006; **145**: 1–10.
59. Padmanabhan PK, Dumas C, Samant M, Rochette A, Simard MJ, Papadopoulou B. Novel features of a PIWI-like protein homolog in the parasitic protozoan Leishmania. *PLoS One* 2012; **7**: e52612.
60. Dupe A, Dumas C, Papadopoulou B. Differential subcellular localization of Leishmania Alba-Domain proteins throughout the parasite development. *PLoS One* 2015; **10**: e0137243.

Supplementary Information accompanies this paper on Cell Death and Disease website (http://www.nature.com/cddis)

Appendix 2 – Inactivation of the *L. infantum Li*Ufd1 gene by knockout strategy using CRISPR-Cas9.

The puromycin N-acetyl-transferase gene (PURO) and neomycin phosphotransferase gene (*NEO*) targeting cassettes were used to replace both copies of the endogenous *L. infantum UFD1* gene (LinJ.36.6780; http://tritrypdb.org) through homologous recombination using the 5'- and 3'-flanking sequences of UFD1 in the presence of UFD1 gRNA and the CAS9-expressing plasmid.

PCR of total genomic DNA. The two *LiUFD1* alleles in the wild type (WT) strain (*Li*VCP$^{(+/+)}$) were subsequently replaced by the *PURO* and *NEO* targeting cassettes to generate the *Li*VCP$^{(PURO/+)}$ and *Li*VCP$^{(PURO/NEO)}$ mutants, respectively. Following *PURO* gene replacement, double inactivation in *Li*VCP$^{(NEO/+)}$ was only possible by ectopically providing a pSPαZEOα vector expressing HA-tagged *Li*UFD1(+Ufd1-HA (N) or +HA-Ufd1 (C)) and using the gRNA (g) for CRISPR strategy. These results suggest that the *Li*Ufd1 gene is essential for parasite growth.

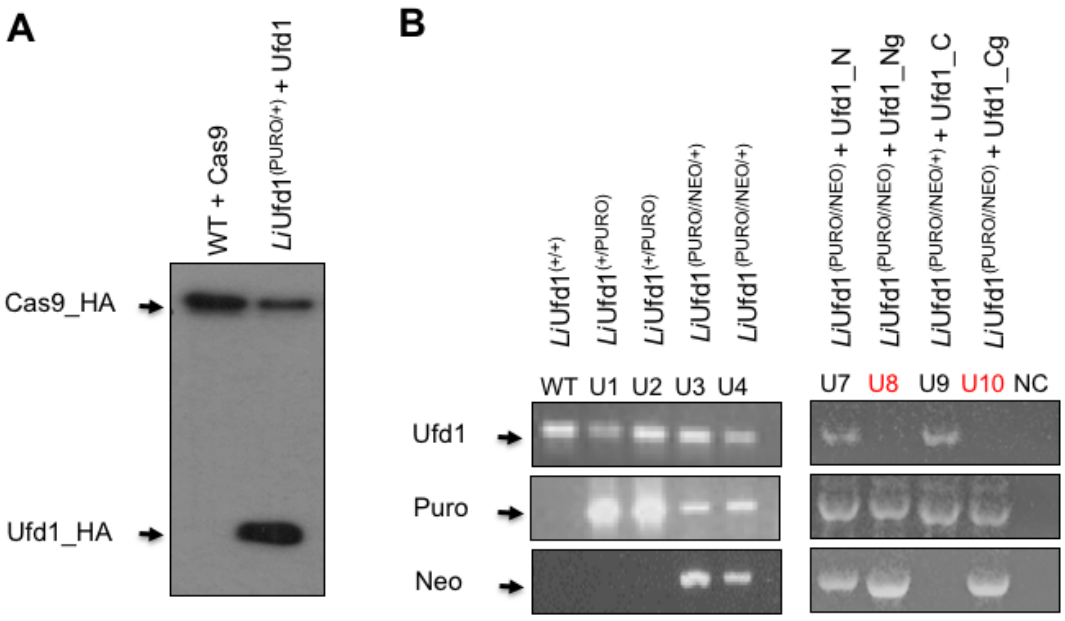

Appendix 3. Inactivation of the *L. infantum Li*Faf, *Li*NPL4 and *Li*Pub1 genes by knockout strategy using CRISPR-Cas9.

PCR of total genomic DNA using specific primers for detecting possible replacement of *Li*FAF or *Li*NPL4L and or *Li*Pub1 genes by the PURO or NEO targeting expression cassettes using CRISPR-Cas9. The two alleles of *Li*FAF, *Li*NPL4L and *Li*Pub1 in the wild type (WT) strain (*Li*VCP$^{(+/+)}$) were subsequently targeted for replacement by the *PURO* and *NEO* cassettes to generate the (PURO/+) and (PURO/NEO) mutants. Double insertion was detected by using primers external to each gene and internal for NEO and PURO. Despite the double insertion of the resistance selectable markers, we were still able to amplify the *Li*NPL4 and *Li*Pub1 genes (as well inconclusive fragments for the *Li*FAF gene), suggesting an essentiali role for these genes.

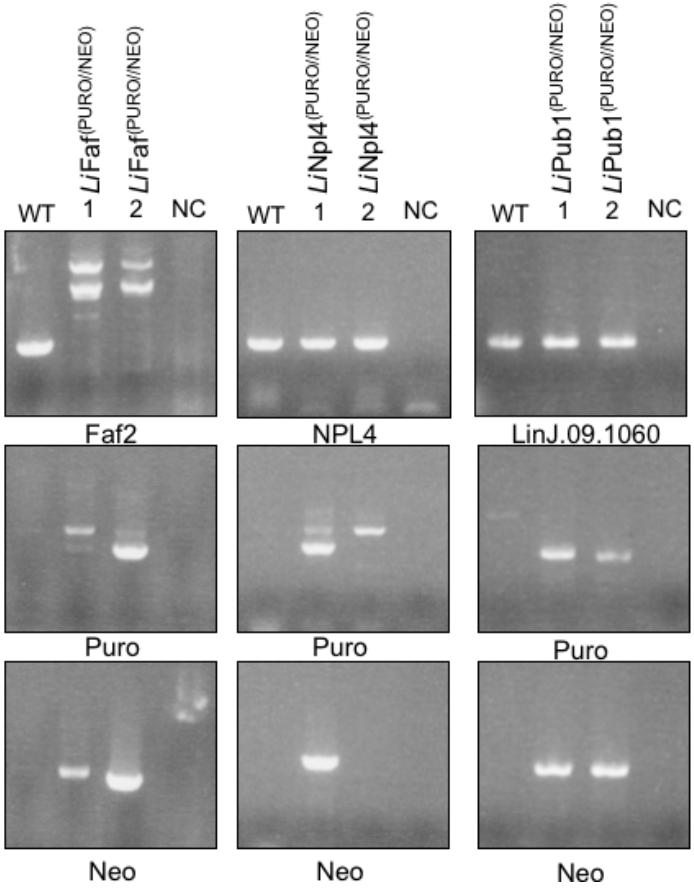

Appendix 4 - *Li*PLAA/Doa1/Lub1 protein - The putative link with Mitochondria Associated Degradation (MAD)

BLAST analysis on the *L. infantum* genome in TriTrypDB using the yeast Doa1 gene as bait depicted LinJ.24.1970, a WD domain, G-beta repeat/PFU (PLAA family ubiquitin binding protein) as the putative Doa1 homolog in *Leishmania* as well as a PUB domain containing protein (LinJ.36.0140), both identified to interact with VCP by co-immunoprecipitation and LC-MS/MS studies.

TriTryp ID	Name	EUPC
LinJ.36.1700	clathrin heavy chain, putative	64
LinJ.24.1970	**WD domain, G-beta repeat/PFU (PLAA family ubiquitin binding)**	28
LinJ.28.2960	heat-shock protein hsp70, putative	25
LinJ.17.0090	elongation factor 1-alpha	18
LinJ.36.0140	**PUB domain containing protein, putative**	18
LinJ.34.0210	Antimony resistance marker of 56 kDa	18
LinJ.08.1280	beta tubulin	14
LinJ.10.0490	GP63, leishmanolysin	11
LinJ.33.0360	heat shock protein 83	9
LinJ.30.2480	heat shock 70-related protein 1, mitochondrial precursor, putative	9
LinJ.36.7280	protein disulfide isomerase 2	9
LinJ.19.1590	inosine-5'-monophosphate dehydrogenase	8
LinJ.36.4100	S-adenosylhomocysteine hydrolase	8
LinJ.36.1320	fructose-1,6-bisphosphate aldolase	7
LinJ.21.0300	hexokinase	6
LinJ.19.0190	ADP/ATP translocase 1, putative	6
LinJ.05.0500	ATP synthase F1, alpha subunit, putative	6
LinJ.32.0410	ATP-dependent RNA helicase HEL67	6
LinJ.27.1710	Phosphoenolpyruvate carboxykinase [ATP], glycosomal	5
LinJ.32.3100	nucleoside diphosphate kinase b	5
LinJ.25.1210	ATP synthase subunit beta, mitochondrial, putative	5
LinJ.01.0790	Eukaryotic initiation factor 4A-1	5
LinJ.03.0220	long chain fatty Acyl CoA synthetase, putative	5
LinJ.35.0370	ATP-dependent DEAD-box RNA helicase, putative	5
LinJ.36.2140	chaperonin HSP60, mitochondrial precursor	5
LinJ.14.1240	enolase	5
LinJ.18.1350	heat shock protein 110, putative	5
LinJ.15.1140	tryparedoxin peroxidase	5

LinJ.13.0330	alpha tubulin	4
LinJ.26.1220	heat shock protein 70-related protein	4
LinJ.30.2990	glyceraldehyde 3-phosphate dehydrogenase, glycosomal	4
LinJ.18.0690	citrate synthase, putative	4
LinJ.03.0190	delta-1-pyrroline-5-carboxylate dehydrogenase, putative	4
LinJ.25.1850	3-oxo-5-alpha-steroid 4-dehydrogenase, putative	4
LinJ.27.2350	heat shock protein DNAJ, putative	4
LinJ.03.0960	Eukaryotic translation initiation factor 2 subunit alpha	4
LinJ.25.1460	GTP-binding protein, putative	4
LinJ.36.0190	elongation factor 2	3
LinJ.29.1160	ribosomal protein L1a, putative	3
LinJ.28.1310	luminal binding protein 1 (BiP), putative	3
LinJ.04.0750	60S ribosomal protein L10, putative	3
LinJ.30.3560	S-adenosylmethionine synthetase	3
LinJ.13.0090	metallo-peptidase, Clan MA(E) Family M32	3
LinJ.22.1370	60S ribosomal protein L14, putative	3
LinJ.01.0430	ribosomal protein S7, putative	3
LinJ.15.1060	60S ribosomal protein L6, putative	3
LinJ.02.0430	Mitochondrial outer membrane protein porin, putative	3
LinJ.09.1020	elongation factor-1 gamma	3
LinJ.04.1250	actin	3
LinJ.31.2890	ADP-ribosylation factor, putative	3
LinJ.17.0980	hypothetical protein, conserved	3
LinJ.28.1050	40S ribosomal protein S14	3
LinJ.36.1420	**Valosin-containing protein, putative**	2
LinJ.13.1120	40S ribosomal protein S4, putative	2
LinJ.21.1820	ATP-dependent RNA helicase SUB2, putative	2
LinJ.18.1500	P-type H+-ATPase, putative	2
LinJ.17.0010	eukaryotic translation initiation factor 3 subunit a	2
LinJ.18.0740	Elongation factor Tu, mitochondrial, putative	2
LinJ.32.1910	iron superoxide dismutase, putative	2
LinJ.36.2130	chaperonin HSP60, mitochondrial precursor	2
LinJ.18.0510	aconitase, putative	2
LinJ.32.0790	nuclear RNA binding domain	2
LinJ.24.2200	3-hydroxy-3-methylglutaryl-CoA synthase, putative	2
LinJ.29.2570	60S ribosomal protein L13, putative	2
LinJ.16.1510	paraflagellar rod protein 2C	2
LinJ.34.2410	ALBA-domain protein 3	2
LinJ.21.1290	60S ribosomal protein L9, putative	2
LinJ.10.0310	isocitrate dehydrogenase [NADP], mitochondrial precursor, putative	2

LinJ.09.0950	polyubiquitin	2
LinJ.26.0150	60S ribosomal protein L7, putative	2
LinJ.32.4050	60S ribosomal protein L8, putative	2
LinJ.20.1620	ribosomal protein S11 homolog	2
LinJ.32.3510	dihydrolipoamide dehydrogenase, putative	2
LinJ.35.1870	60S ribosomal protein L5, putative	2
LinJ.19.0390	40S ribosomal protein S13, putative	2
LinJ.19.0050	40S ribosomal protein S2	2
LinJ.25.1220	ribosomal protein S25	2
LinJ.06.0590	60S ribosomal protein L23a, putative	2
LinJ.19.0100	hypothetical protein, conserved	2
LinJ.27.2020	RNA-binding protein, putative	2
LinJ.36.3100	succinyl-CoA ligase [GDP-forming] beta-chain, putative	2
LinJ.20.1320	calpain-like cysteine peptidase, putative	2
LinJ.32.2830	ribosomal protein L27, putative	2
LinJ.27.1630	hypothetical protein, conserved	2
LinJ.31.1240	Pyrophosphate-energized vacuolar membrane proton pump 1, putative	2
LinJ.35.3810	60S ribosomal protein L27A/L29, putative	2
LinJ.06.0950	hypothetical protein, conserved	2
LinJ.36.2370	Gamma-tubulin complex component 3-like protein	2
LinJ.19.0240	centrosomal protein of 104 kDa	2
LinJ.14.1450	myo-inositol-1-phosphate synthase	2
LinJ.03.0180	U2 splicing auxiliary factor, putative	2

Appendix 5 - *Li*VCP localization in *Leishmania infantum* by different approaches

Immunofluorescence analysis showing *Li*VCP (green) localization in *L. infantum* promastigote forms. Nucleus and kinetoplast DNA were stained with DAPI (blue). On panel **a)** an anti-*Trypanosoma brucei* VCP antibody was used as primary antibody. On **b**) and **c)** anti-HA was used as first antibody to identify *Li*VCP-HA overexpressed and *Li*VCP-HA integrated constructs, respectively. For all conditions, Alexa Fluor® 488 anti-mouse was used as secondary antibody. These experiments suggest that *Li*VCP is mostly localized to the cytoplasm.

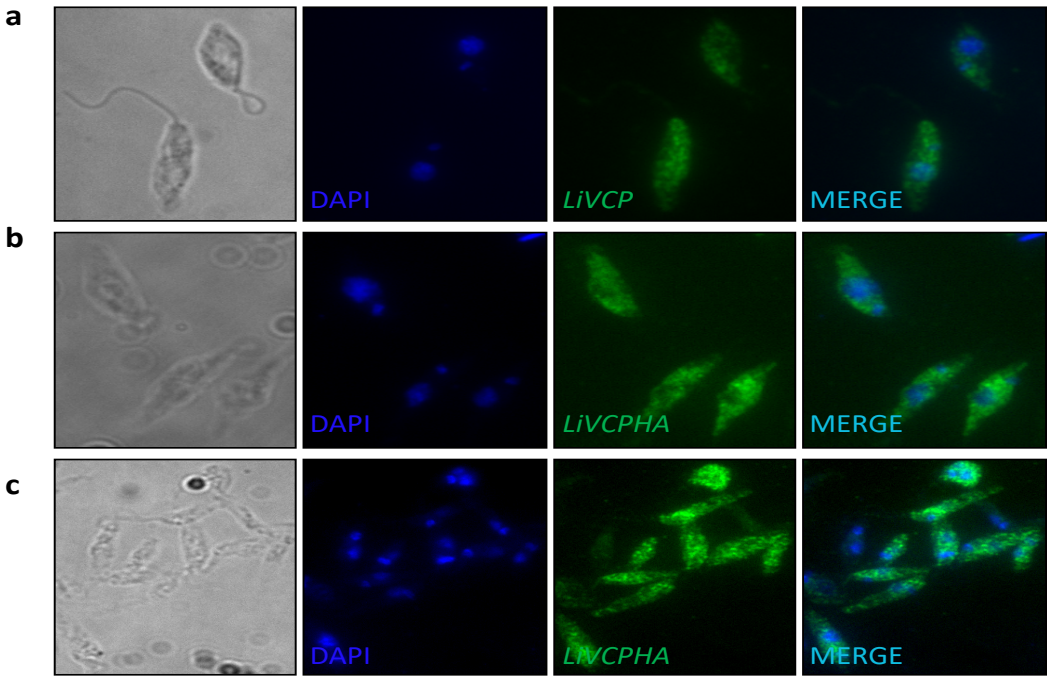

Appendix 6 - *Li*VCP co-localization with DHH1 protein in *Leishmania infantum*.

Schematic representation and immunofluorescence analysis of *LiVCP*-GFP and DHH1-mCherry constructs used for localization studies in *L. infantum*. The *LiVCP*-GFP construct was made by placing the *Li*VCP gene in frame with the eGFP protein and then cloned it into pGEM-αZEOα-vector and transfected into *L. infantum* promastigotes. DHH1 has been localized in stress granules and these co-localization studies suggest that *Li*VCP may also associate with these RNA foci.

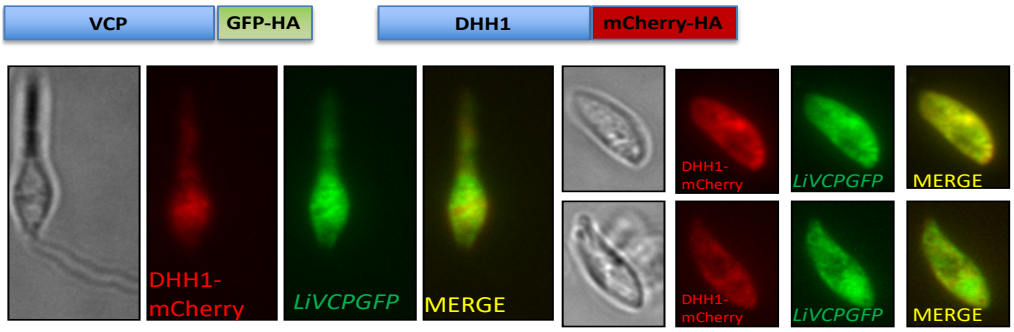

Appendix 7 - PABP2 as a marker of stress granules in *Leishmania infantum* and *Trypanosoma brucei*.

We carried out immunofluorescence analysis both in *Leishmania* (upper panel) and *Trypanosoma brucei* (middle and lower panels) using an antibody directed against the poly(A) binding protein 2 (PABP2) (red) to visualize stress granule formation in these parasites. Nucleus and kinetoplast DNA were stained with DAPI (blue). An anti-rabbit antibody against *Li*PABP2 (kindly provided by Dr. Osvaldo de Melo Neto, Recife, Brazil) followed by Alexa Fluor® 555 was used. Poly-A binding protein (PABP2) was accessed on methanol-fixed cells.

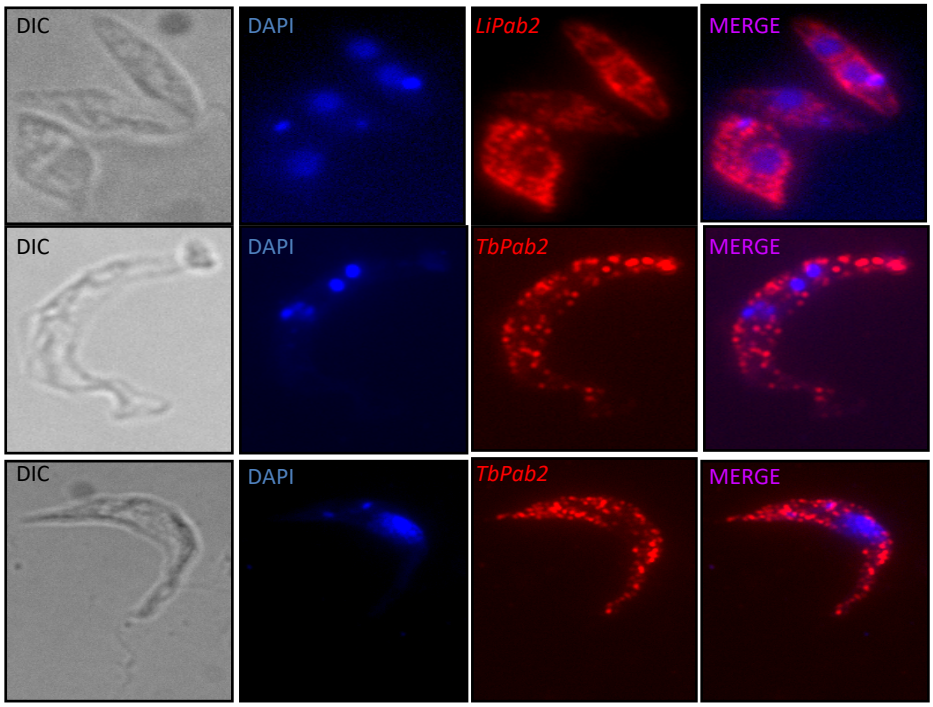

Appendix 8 - *Li*VCP partly co-localizes with PABP2 protein in *Leishmania infantum.*

Immunofluorescence analysis showing *Li*VCP (green) localization in *L. infantum* promastigote (a) and axenic amastigote (b) forms. Nucleus and kinetoplast DNA were stained with DAPI (blue). An anti-*Trypanosoma brucei* VCP antibody was used as primary antibody followed by Alexa Fluor® 488 anti-mouse as secondary antibody. For co-localization studies, an anti-rabbit antibody against *Li*PABP2 (red) followed by Alexa Fluor® 555 was used. Poly-A binding protein (PABP2) was accessed on methanol-fixed cells (a,b). Images are maximal Z-projections of 30 to 35 contiguous stacks separated by 0.1 µ m and were acquired with a 63x objective, using a LEICA SP5II confocal microscope. These experiments suggest a partial co-localization of *Li*VCP with PABP2, known to associate with stress granules.

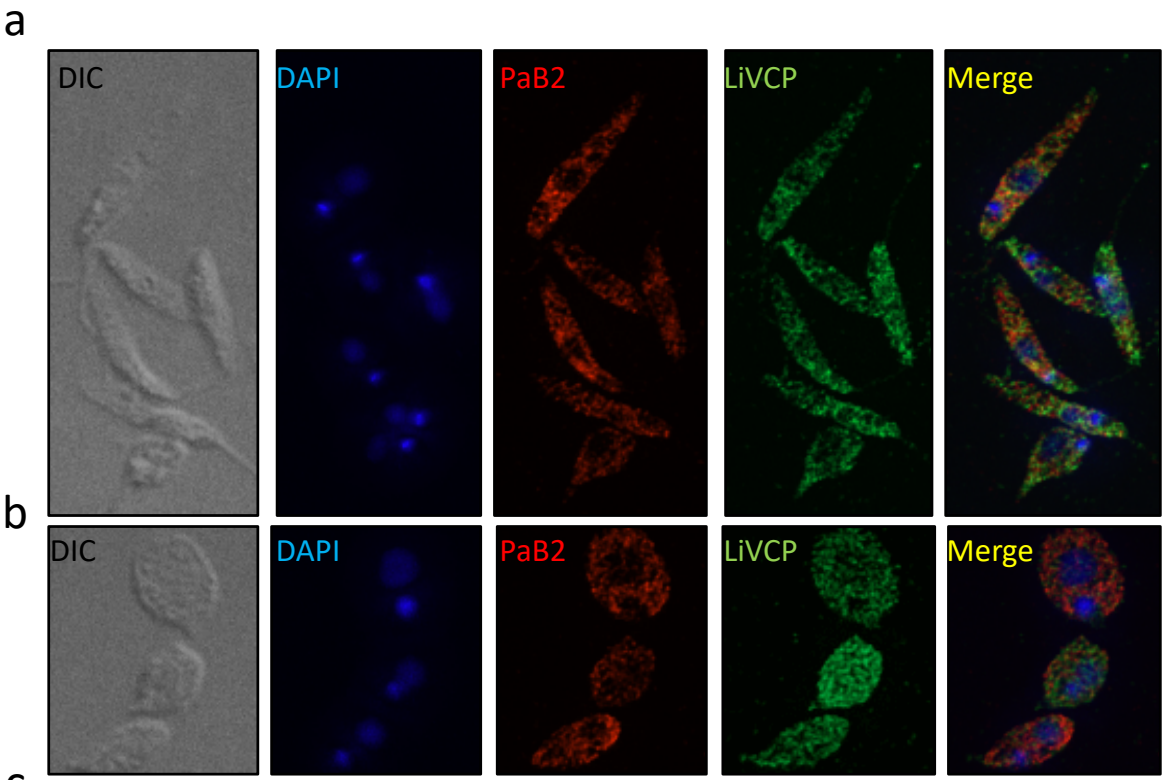

Appendix 9 - Production of mitochondrial ROS is increased in *Leishmania* mutants exhibiting less VCP activity

Mitochondrial superoxide accumulation was measured using the MitoSOX Red probe. Parasites (2–4 $\times 10^7$) were treated with 5 µM MitoSOX for 2 h at 25 °C and analyzed with a Victor fluorometer. The fluorescence was measured at 510 nm excitation and 580 emission wavelengths. Fluorescence was normalized with protein concentration measured using Bio-Rad protein assay. Mitochondrial superoxide accumulation was assessed also in the presence of miltefosine (25 µM) and Menadione (50 µM) treatment. Wild type (WT) expressing an empty vector and *Li*VCP$^{NEO/+}$ haploid mutant (sKO) expressing either a VCP-HA (C-terminal tagging of VCP affects its activity) or the VCP^{QQ} dominant negative mutant. Results shown here are expressed in relative fluorescence units. These results indicate that miltefosine treatment results in more mitochondrial ROS accumulation in parasites mutants exhibiting less VCP activity, like the sKO+VCP-HA and sKO+ VCP^{QQ} strains, which is in line with the role of VCP in maintain proteostasis.

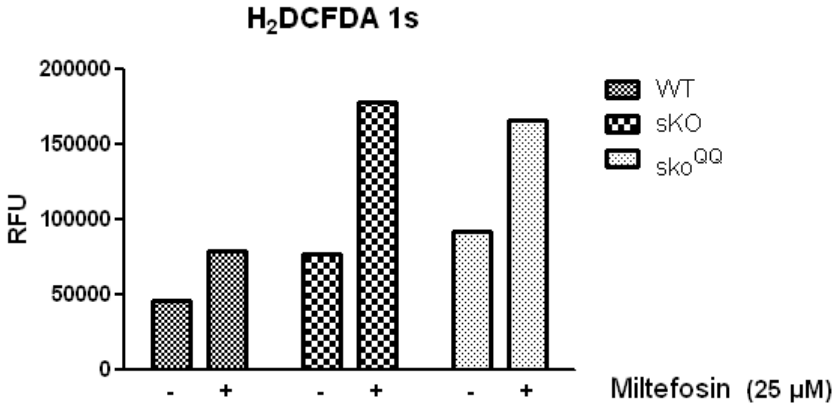

Production of peroxyl radicals and peroxides in Wild type (WT), *Li*VCP(NEO/+) (sKO), and sKO expressing the WT VCP or the dominant negative mutant VCP^{QQ} strains in the presence of miltefosine (25 µM) was measured using the 2′,7′-dichlorodihydrofluorescein diacetate (H2DCFDA) probe. Results shown here are expressed in relative fluorescence units. These results indicate that more ROS accumulate in parasite mutants exhibiting less VCP activity, like the sKO+VCP-HA and sKO+ VCP^{QQ} strains.

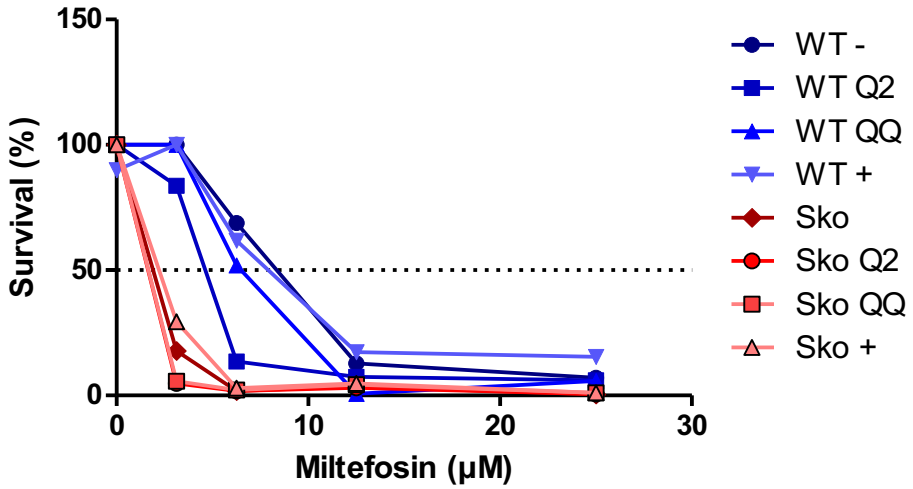

	WT -	WT Q2	WT QQ	WT +	Sko	Sko Q2	Sko QQ	Sko +
IC50	7.698	4.339	6.311	7.624	1.870	0.3837	0.3834	2.399

The sensitivity of *Leishmania* with impaired VCP to oxidative stress was also observed upon Miltefosine treatment. Promastigote forms of *Leishmania infantum* wild type (WT) or sKO

(*Li*VCP(NEO/+)) expressing or not the dominant negative mutants VCPQ1 or VCPQ2 or the double mutant VCPQQ were used. The proportion of surviving parasites was assessed by optical density measured at 600 nm after 72h following miltefosine treatment. Data were analyzed by GraphPad prism and the EC_{50} was calculated from those plots.

Appendix 10 – Effect of drugs targeting VCP on *Leishmania infantum* growth.

The efficacy of DBeQ on promastigote forms of *Leishmania infantum* wild type (WT) was first evaluated here. The proportion of surviving parasites was assessed by measuring optical density at 600 nm after 72h following treatment. Data were analyzed by GraphPad prism and the EC50 was calculated from those plots. Among the three drugs tested, DBeQ, NMS873 and ML240, DBeQ was the one shown the better efficacy in killing *Leishmania* with an IC50 = 0.38 µM vs. 0.6 µM for ML240 and 1.8 µM for NMS873.

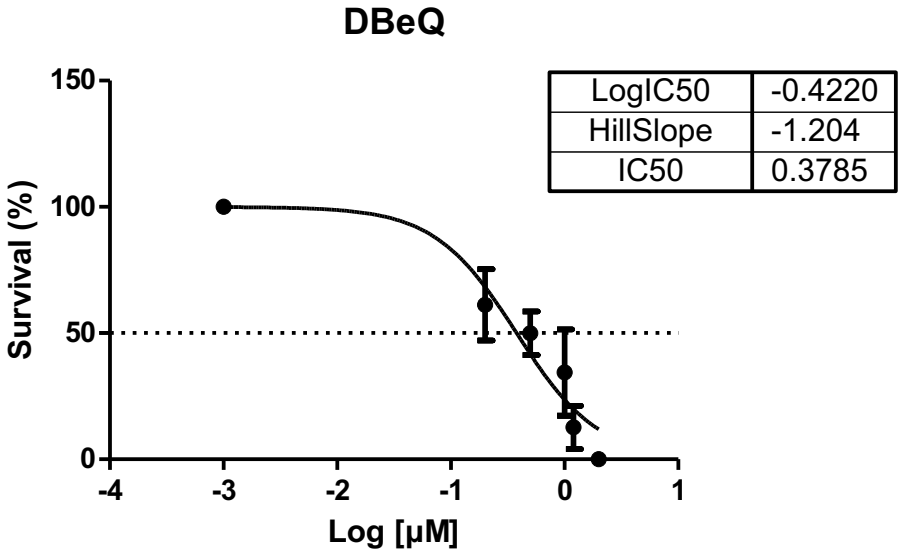

The efficacy of NMS on promastigote forms of *Leishmania infantum* wild type (WT) was also evaluated. The percentage of surviving parasites was assessed by measuring optical density at 600 nm after 72h following treatment. Data were analyzed by GraphPad prism and the IC50 was calculated from those plots.

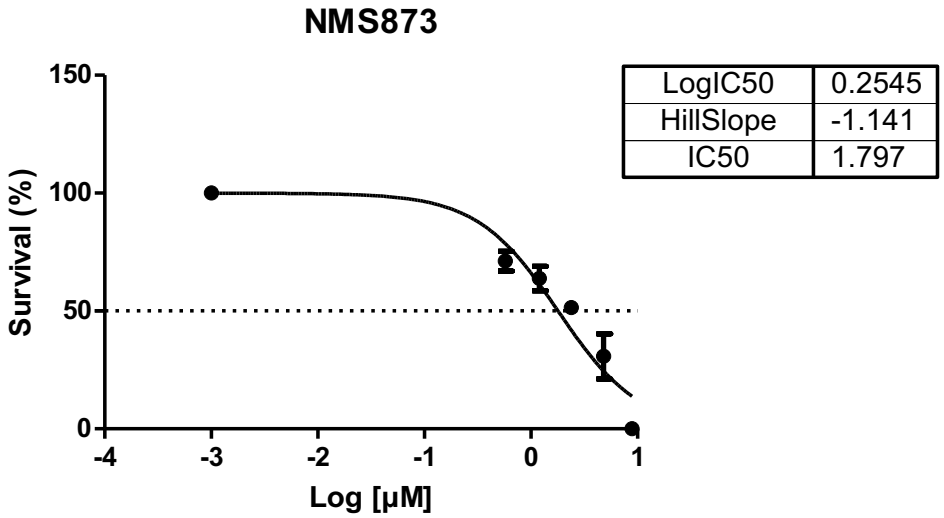

The efficacy of ML240 on promastigote forms of *Leishmania infantum* wild type (WT) was evaluated as well. The percentage of surviving parasites was assessed by measuring optical density at 600 nm after 72h following treatment. Data were analyzed by GraphPad prism and the IC50 was calculated from those plots.

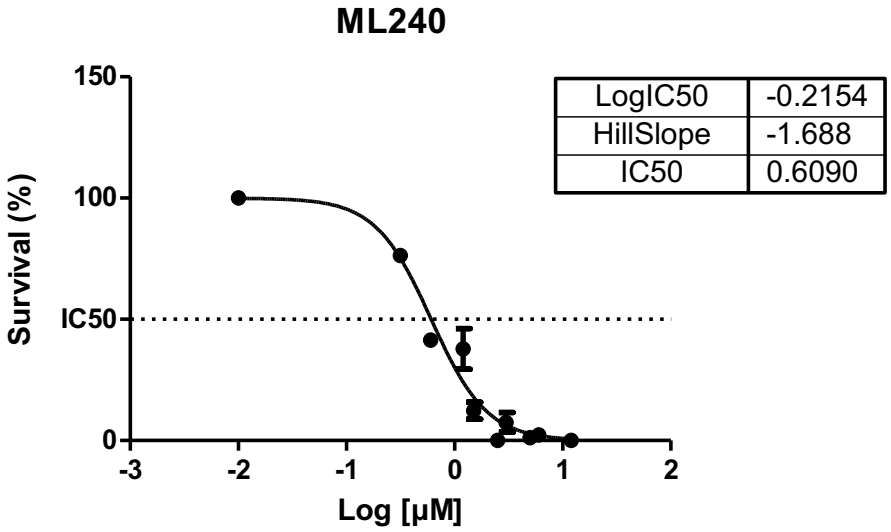

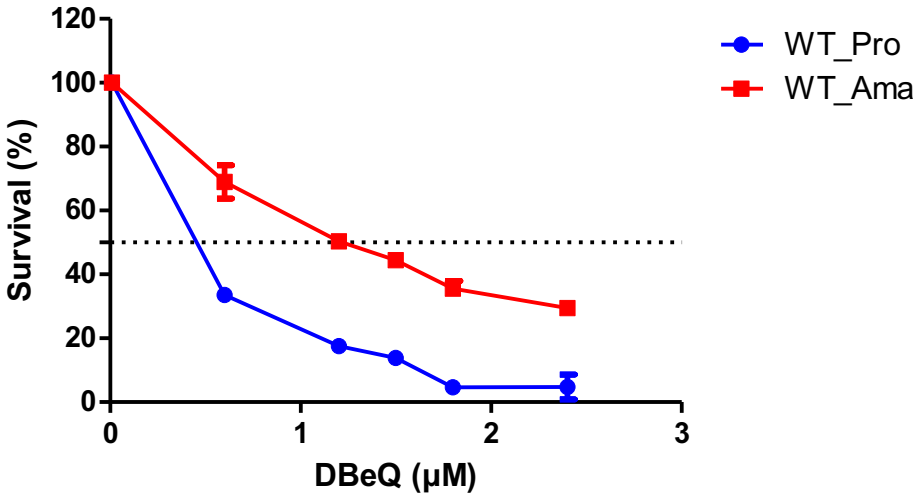

	WT_Pro	WT_Ama
LogIC50	-0.4043	0.07272
HillSlope	-1.543	-1.225
IC50	0.3942	1.182

The efficacy of DBeQ on axenic amastigote forms of *Leishmania infantum* wild type (WT) was also evaluated here. The percentage of surviving parasites was assessed by measuring optical density at 600 nm after 72h following treatment. Data were analyzed by GraphPad prism and the IC50 was calculated from those plots.

These preliminary studies suggest that DBeQ is also active on amastigotes although approximately 3-times less than on promastigotes (IC50 = 1.18 µM for amastigotes vs. IC50 = 0.3 µM for promastigotes).